FATIGUE OF GLASS REINFORCED PLASTICS

UNDER COMPLEX STRESSES

by

John R. Griffiths B.Sc.

Thesis submitted to the University of Nottingham for the degree of Doctor of Philosophy.

OCTOBER 1974.

VOLUME CONTAINS CLEAR OVERLAYS

OVERLAYS HAVE BEEN SCANNED SEPERATELY AND THEN AGAIN OVER THE RELEVANT PAGE

LIST OF CONTENTS.

ABSTRACT.

Many failure theories have been postulated to predict the behaviour of glass reinforced plastics (GRP) under complex stresses. However, the efficient use of these theories for design purposes is inhibited because the experimental complex stress data needed to verify and discriminate between them is not available. This thesis presents some of the experimental data required.

Uniaxial stress test results from flat laminates, and biaxial stress test results from thin-walled tubes under combined internal pressure and axial force, are presented for various damage states under both static and fatigue loading for a plane isotropic material and an orthotropic material. The data were then used to establish which failure theory provided the most acceptable prediction of the observed behaviour. For ultimate strength, the Norris Failure theory gave adequate predictions, but not for resin cracking. The most generally acceptable predictions, for both materials, were given by those theories whose equations contain a constant which is derived from complex stress data, these being the modified Marin and the strength tensor theories.

For the orthotropic material, three-dimensional representations of the plane stress ultimate strength and damage failure surfaces are presented for both static and fatigue loading. However, even though a considerable number of specimens were tested, only very few failure surface sec-

tions were experimentally established.

It was found for both materials that fatigue loading was more damaging than static loading, for both uniaxial and biaxial stress conditions, and that the behaviour of the materials was dependent upon the ratio of the biaxial stresses.

Jointed reinforcement layers severely affect the zero-tension fatigue behaviour of the plane isotropic material, but the effect on the orthotropic material decreases with increasing fatigue life.

The effect of macro-voids on crack initiation should be acknowledged if damage is used as a design criterion.

ACKNOWLEDGEMENTS.

The author gratefully acknowledges :-

The Science Research Council for funding the research and for the award of a Research Studentship.

Dr. M.J. Owen for his assistance and guidance.

Mr. G.F. Budd for preparing specimens and for his engineering expertise.

Mr. J. Unwin for his continual encouragement and advice.

Mr. J.R. Harrison for photographic work.

His colleagues, past and present, for many useful discussions.

Mrs. P.A. Found for her excellent typing.

His wife for her unselfishness.

NOMENCLATURE.

GRP	Glass reinforced plastic.
1,2,3	Principal material axes.
σ_1	Normal stress in '1' principal material direction.
σ_2	Normal stress in '2' principal material direction.
σ_6	In-plane shear stress associated with σ_1 and σ_2.
X	Tensile strength in the '1' direction.
X'	Compressive strength in the '1' direction.
Y	Tensile strength in the '2' direction.
Y'	Compressive strength in the '2' direction.
Z	Tensile strength in the '3' direction.
Z'	Compressive strength in the '3' direction.
S	In-plane shear strength.
σ_x	Cylinder hoop stress.
σ_y	Cylinder axial stress.
R	Biaxial stress ratio (σ_y/σ_x)
p	Internal pressure.
F	Axial force.
t	Cylinder wall thickness.
d	Cylinder inside diameter.
S	Compliance.
F	Strength tensor.

F_{12}	Tensor component characterising σ_1, σ_2 interaction.
K_2	Modified Marin theory floating constant.
θ	Angle between the loading axis and the principal material axis.

Chapter 1.

Introduction.

Glass reinforced plastics (GRP) have gained engineering acceptance through desirable characteristics such as high strength, low density and chemical inertness. At the present time, the full potential of these materials cannot be utilised since a generally acceptable design procedure has not been established. A programme of research directed by Dr. M.J. Owen in the Department of Mechanical Engineering, University of Nottingham is aimed at establishing such a procedure. The part of the programme described in this thesis is a continuation of the research previously conducted by Dr. M.S. Found (1).

The behaviour of GRP's under simple uniaxial loading has been extensively studied but the information obtained is of limited use for efficient structural design. Most stress environments are complex in nature. Many theories of failure have been postulated that attempt to predict the complex stress behaviour of orthotropic and anisotropic materials. The lack of experimental verification of these theories, especially for fatigue loading, leaves the designer without full confidence in their use. Further problems arise because GRP's exhibit various damage stages prior to catastrophic failure. In some design situations it is impossible to tolerate any composite damage, in others some damage may be acceptable. Thus, a useful failure criterion must be able to predict the onset of all damage stages, including catastrophic

failure. In addition, if the failure mode is dependent upon the nature of the complex stresses then different failure criteria may have to be used to predict different complex stress conditions. From the above brief introduction it will be realised that the presentation of experimental data and the verification of, and discrimination between, failure theories is of the utmost importance.

Found (1) designed apparatus and investigated the behaviour of chopped strand mat (C.S.M.)/Polyester resin cylinders over a range of biaxial stress ratios (R). He investigated three damage states, adhesive failure of the glass/resin interface (debonding), local cohesive failure of the resin matrix (resin cracking), and catastrophic failure, under static and fatigue loading. He also studied the off-axis loading behaviour of flat orthotropic plates. In Found's work on C.S.M. cylinders there were some unexplained discrepancies in the test data and the initial part of the present work was directed towards solving these. Further investigations were directed towards studying the biaxial stress behaviour of glass-fabric reinforced cylinders. Two cases of special orthotropy were chosen and results were obtained for various damage states under static and fatigue loading. The experimental evidence was then used to assess the two and three-dimensional plane stress failure fields predicted by the various failure theories.

Chapter 2.

Literature Survey.

The following sections discuss the significance of and differences between failure theories, the testing required to experimentally determine a failure surface, and the published experimental data. Thus, in addition to providing a literature survey, this chapter is a guide to the understanding of failure conditions in geometric terms.

2.1 Failure Theories.

2.1.1 General Introduction.

A failure theory or criterion is a mathematical function relating stress to strength that attempts to predict material behaviour under complex loading conditions from uniaxial properties.

Found (1) presented the failure theories proposed for orthotropic and generally anisotropic materials. In section 2.1 these theories and their geometric representations are discussed and the influence of uniaxial strengths and other parameters on the relationship between the stress reference axes and the principal axes of the failure envelopes and surfaces is explained.

A biaxial stress state σ_x, σ_y, τ_{xy} can be transformed into two principal stresses and an angle θ. For an isotropic material, the material properties do not vary with θ and failure can be described in terms of the two principal stresses (2). Hence, for isotropy, using principal stresses eliminates shear.

For an orthotropic or anisotropic material, the material properties at a point in a body change as the co-ordinate system is rotated i.e. they are orientation dependent. The stresses must be referred to the principal axes of the material, i.e. the axes of orthotropy or anisotropy, and principal stresses have no real significance. The orthotropic axes are designated 1, 2 and 3, and using contracted notation (4) the stresses associated with the 1, 2 axes in plane stress are normal stresses σ_1 and σ_2 and the in-plane shear stress σ_6, ($\sigma_3=\sigma_4=\sigma_5=0$). Hereafter, σ_1, σ_2 and σ_6 are designated the principal material direction stresses or the stresses referred to the principal material axes. Applying principal stresses σ_x and σ_y to a material yields the stress state $\sigma_1=\sigma_x, \sigma_2=\sigma_y$, and $\sigma_6=0$, if the loading axes and the orthotropic axes coincide. For off-axis cases, i.e. where the loading is applied at angle θ to the orthotropic axes, the applied stresses have to be transformed and σ_1, σ_2 and σ_6 can all be operative. Thus, a three-dimensional (3-D) failure surface with reference axes σ_1, σ_2 and σ_6 is required to represent the plane stress behaviour of an orthotropic material. These reference axes are not necessarily the principal failure surface axes. For an orthotropic material not in plane stress the fracture condition is represented by a failure surface in six-dimensional space.

Reviews of failure theories are given in (1, 3-10). Failure theory relationships are shown for plane stress in Tables 1, 2 and for general cases in Tables A1, A2. The theories shown in Table 1 only require uniaxial strengths, whereas those in Table 2 also require complex stress data.

When comparing failure theories in the absence of experimental data it seems general practice to normalise the axes i.e. to express stresses as functions of principal strengths i.e. σ_1/X, σ_2/Y etc., where X and Y are normal strengths in the 1 and 2 directions respectively (see Tables 1, 2). This practice indicates that failure envelopes are smooth and continuous which is not always true. In the following analysis, theories are compared by selecting various degrees of strength anisotropy.

It should be noted that when a laminated composite such as an angle ply is evaluated, the failure envelope for the total laminate can be obtained by superimposing the envelopes described by each lamina (2). Care is required because normal and shear stresses can be induced by lamina interactions and the actual lamina stresses must be analytically determined (2, 16, 17).

2.1.2 Discussion of Theories in a two-dimensional state ($\sigma_6 = 0$)

2.1.2.1 Maximum Stress Theory.

This states that failure occurs when one of the principal strengths is reached and hence no strength interaction is considered. Off-axis cases are accounted for (11) by transforming applied stresses to the principal material axes. When $\sigma_6 = 0$ and X=Y=X'=Y', the geometric representation is a square with its centre coincident with the origin of the reference axes.

2.1.2.2 Distortional Energy Theories.

Many theories (8, 9, 12-15) are based on the Hencky-Von Mises distortional energy criterion for isotropic materials which assumes that the distortional energy is

constant irrespective of the applied stresses. The theories developed from this to account for some degree of anisotropy reduce to the original condition when isotropy is assumed. Yielding and failure are considered synonymous.

Hill's Theory (12) was postulated to account for anisotropy seen in metals after working. No account for different strengths in tension or compression was made and Table 1 shows that the normal strength in the 3 direction, Z, is included in the equation. For composites, this produces a dilemma since the failure envelope region where Z should assume its compressive value is unknown. Hence, this is limited to cases where $Z = Z'$. The effect of Z on the failure envelope for $\sigma_6 = 0$ and $X=Y=X'=Y'$ is shown in Fig. 1. The envelope is circular if $Z = X/\sqrt{2}$ since the cross-term in $\sigma_1 \sigma_2$ becomes zero (see Table 1). If $Z > X/\sqrt{2}$ an ellipse is formed with its' major axis lying along the symmetry line $\sigma_1 = \sigma_2$, and its tip passes through the point $\sigma_1 = Z$. If $Z < X/\sqrt{2}$ the ellipse rotates about the origin, its major axis lies along the symmetry line $\sigma_1 = -\sigma_2$, and the minor part of the ellipse in the first and third quadrants cuts $\sigma_1 = \sigma_2$ at $\sigma_1 = Z$.

The use of Hill's theory was extended for composites by Azzi and Tsai (14). They assumed transverse isotropy, i.e. $Y = Z$, and introduced the stress transformation relationships (4) into the theory to account for off-axis cases. The geometric representation is an ellipse similar to Hill's but it cannot attain a circular state. If $X=Y=X'=Y'$ the ellipse is smooth, but for other cases the theory can describe different elliptical sections in each quadrant because no account is made for differences

in tensile and compressive principal strengths.

The Norris Interaction theory (18) is empirical and was postulated to fit experimental data from plywood, an orthotropic material. The equation (Table 1) is similar to the distortional energy type except that there is no cross-term in $\sigma_1 \sigma_2$. If X=Y=X'=Y' and $\sigma_6 = 0$ the envelope is a circle of radius X. If this strength symmetry is untrue, a different arc is generated in each quadrant and the failure condition is the outer boundary formed by a set of intersecting arcs whose radii are principal strength dependent (Fig. 2).

The Norris Failure theory (13) for orthotropic materials consists of a set of distortional energy failure conditions (Table A1). For plane stress, two of these conditions simplify, as shown in Table 1. Geometrically (Fig. 3), the failure envelope for $\sigma_6 = 0$ is an ellipse with the maximum stress theory superimposed, the criterion being that any stress condition lying outside the inner boundary formed by the combination of the two envelopes is unacceptable. The theory is similar to the maximum stress in the first and third quadrants but is elliptical in the second and fourth quadrants.

Fischer (19) attempted to extend the Norris Failure theory to predict failure of any laminate layer by introducing a constant derived from elastic moduli into the $\sigma_1 \sigma_2$ cross-term. However, by using elastic constants, linear elasticity is implied which is seldom the case in composites.

Hoffman (15) extended Hill's theory to account for differences in tensile and compressive strengths by

introducing linear terms in σ_1, σ_2 and σ_3 into Hill's equation (see Table A1). There is no physical significance attached to the failure condition. The first of the Hoffman equations shown in Table 1 is restricted to transverse isotropy hence eliminating strengths Z and Z'. For other cases, Z needs to be known as in Hill's theory but this time both tensile and compressive Z values are included in the condition. The Hoffman equation always describes a smooth ellipse irrespective of principal strengths because of the inclusion of linear terms.

Caddell et al (20) recently developed a yield criterion for oriented polymers. The Hill theory is assumed as a basis, linear terms are included and the resulting equation is identical to Hoffman's. A novel technique is shown for predicting off-axis uniaxial strengths which eliminates experimental determination of Z, Z' and shear strength S. Table A1 shows that 2(N-H) is unique since it depends only on material strengths. However, from equation (2) in Table A1, which includes the stress transformation relationships, two values of 2(N-H) are possible due to the inclusion of linear terms. This unique value occurs when the linear terms equal zero i.e.

$$\sigma [k_1 \cos^2\theta + k_2 \sin^2\theta] = 0 \text{ , or } \tan^2\theta = -k_1/k_2$$

where θ = off-axis angle and k_1, k_2 are the strength dependent constants of the linear terms. If experimental data is available at the θ value given from above then 2(N-H) can be evaluated. Strengths Z and Z' are eliminated from constants F, G and H by addition. The technique is one of curve fitting, i.e. the predicted curve is made to

pass through the experimental data at angle θ, but there is an implicit condition. At the value of θ used, the absolute values of tensile and compressive strength must be the same.

Marin (9) proposed a distortional energy failure condition for orthotropic materials but this is limited to principal stresses.

Franklin (8) modified Marin's theory to include a constant, k_2, whose determination was directly dependent upon experimental complex stress data. The equation (Table 2) can be re-arranged to provide a k_2 value. By determining k_2 values for each quadrant, the failure envelope is made to pass through the data chosen to determine it and hence a curve fitting parameter is introduced to obtain better correlation between experimental and predicted values. The equation is identical to Hoffman's when $k_2 = 1$. The theory describes an ellipse, but if different k_2 values are chosen for each quadrant then the overall envelope is not necessarily smooth. The use of a floating constant such as k_2 can be especially useful in cases where the failure mode is dependent upon the nature of the complex stresses since k_2 can be determined for different failure modes.

2.1.2.3 Strength Tensor Theories.

The concept of a strength tensor analogous to that for elastic constants was introduced by Gol'denblat and Kopnov (21), Ashkenazi (22), and later by Tsai and Wu (23), to provide a failure criterion for generally anisotropic materials that could account for differences in tensile and compressive strengths and the dependence of

shear strength on the sign of the shear stress.

Most failure criteria are limited to special orthotropy and for general cases stresses are transformed to principal material axes. Since strength tensors follow established tensor mathematics then rotation of the material axes can be performed i.e. strength tensor components can be transformed. Most of the theories discussed earlier are contained in the tensor theories as special cases. Interactions amongst stress components are considered to be independent material properties which is different from earlier theories where interactions are either fixed or unacceptable.

The Gol'denblat and Kopnov and Tsai and Wu theories consist of second and fourth rank tensors (see Table A2), higher order terms, e.g. sixth rank, can be included but this creates difficulty in mathematical operation and failure envelope instability can occur. The major difference between these two theories is the ease of use, the square root in the Gol'denblat and Kopnov equation tending to introduce operational complexity. Both theories produce a similar failure condition which for plane stress with $\sigma_6 = 0$ is an ellipse and with $\sigma_6 \neq 0$ is an ellipsoid.

Table 2 shows the equations for plane stress where the tensor components F_i and F_{ij} when $i = j$ are expressed in terms of engineering strengths. Contained in these equations is tensor component F_{12} which characterises the interaction of the normal stresses for plane stress and it's significance must be understood. F_{12} is a constant, similar to k_2 in the Modified Marin equation, whose magnitude is determined from complex stress data, that attempts to provide better correlation between experimental and

theoretical results. Only one F_{12} value is necessary to define the failure surface but since its magnitude determines the inclination and semi-axes of the ellipse then care is required in its use. Fig. 4 shows the effect of F_{12} on the Tsai and Wu, Gol'denblat and Kopnov failure envelopes for $\sigma_6 = 0$ and X=Y=X'=Y'. (The effect of k_2 on the Modified Marin theory is similar if k_2 assumes equivalent values to F_{12}). Tsai and Wu included a stability condition into their equation constraining the magnitude of F_{ij} interaction components. This is :-

$$F_{ij} < \pm \sqrt{F_{ii}\, F_{jj}} \qquad \text{e.g.} \quad F_{12} < \pm \sqrt{F_{11}\, F_{22}}$$

If $F_{12} \geqslant L$, where L is the stability limit, the failure envelope becomes hyperbolic. The Gol'denblat and Kopnov equation has no constraint but Ashkenazi (22) has shown that using an unconstrained F_{12} produces instability. Fig. 4 shows that when $F_{12} = 0$, and X=Y=X'=Y', the envelope is circular similar to the Norris Interaction theory. When $F_{12} = -0.5L$ the envelope is an ellipse with its major axis lying along the symmetry line $\sigma_1 = \sigma_2$. As F_{12} approaches - L the ellipse ellongates but minor axis changes are small due to the constraint imposed by the ellipse having to intersect the reference axes σ_1, σ_2 at the principal strengths. If F_{12} is positive the ellipse rotates and its major axis lies along the line $\sigma_1 = -\sigma_2$. For anisotropic materials such as graphite/epoxy, Collins and Crane (24) observed that as F_{12} increases the semi-axes of the ellipse increase, its centre translates in the 1 - 2 plane and its principal axes rotate about the 3 axis. An example of this is shown in Fig. 5 where envelopes are drawn at various F_{12} values for a unidirectional GRP having

$X = 500$, $Y = 60$, $X' = 300$, $Y' = 180$ MNm^{-2}. From the above it can be appreciated that F_{12} has a marked influence on the failure envelope shape.

The magnitude of F_{12} can be determined from any test that produces a complex stress state in the principal material directions such as off-axis uniaxial stress tests and biaxial stress tests. Since the influence of F_{12} on the failure envelope is large then the most accurate method of F_{12} evaluation must be selected. F_{12} should be unique for a particular material but due to material property scatter and testing methods and since the theories are phenomological then in practice this is not necessarily true. Numerous F_{12} values can be obtained for the same material from different tests and hence a technique is required to discriminate between determination methods. By re-arranging Tsai and Wu equation shown in Tables 2, A2, the variation of F_{12} with failure strength can be determined for various test modes e.g. for the uniaxial tension of a 45^{o} off-axis specimen, $\sigma_1 = \sigma_2 = \sigma_6 = U/2$, where U= failure strength, hence substituting U into the equation in Table 2 and re-arranging yields F_{12} variation with U. The above analysis shows the most sensitive determination method i.e. that method which produces the least F_{12} change with change in experimental strength. Fig. 6 shows F_{12} variation with strength, in the four stress quadrants, for different test methods and for two materials having different degrees of strength anisotropy. For the first material ($X = Y = 100$, $X' = Y' = 200$ MNm^{-2}) biaxial stress tests at $R = +1$ in the first quadrant yield relatively insensitive F_{12} values within the stability band. In the same quadrant, the 45^{o}

off-axis tensile test yields greater insensitivity and when the shear strength S = 70 MNm^{-2} the maximum strength deviation required to span the stability band is only 20 MNm^{-2}. Composite materials exhibit an appreciable scatter in experimental strength. Different laboratories evaluating the same material could easily produce off-axis strengths completely spanning the F_{12} stability band and hence predicting totally different failure envelopes. Thus, the off-axis test must be used with caution. The second quadrant shows that R = -1 or 45° off-axis shear tests yield more sensitive F_{12} values but R = +1 tests in the third quadrant would yield the greatest sensitivity.

For the second material (X = 100, Y = 50, X' = 250, Y' = 125 MNm^{-2}), similar results to above are obtained. Biaxial stress tests in the second and third quadrants yield the most sensitivity.

Wu (25) and Pipes and Cole (34) concluded that uniaxial off-axis tests yield poor F_{12} sensitivity. Wu (25) attempted to optimise F_{12} by accounting for experimental scatter and concludes it is best determined from biaxial stress tests on cylinders. However, the biaxial stress ratio which optimises F_{12} is usually difficult to achieve experimentally.

2.1.3 Comparison of failure envelopes for $\sigma_6 = 0$.

Figs. 7-9 compare failure envelopes for different degrees of strength anisotropy, the letters denoting failure theories are defined in Tables 1, 2.

When X=Y=X'=Y' (Fig. 7), the distortional energy theories are similar to the tensor theories with $F_{12} = -0.5L$, because the linear terms become zero and the $\sigma_1 \sigma_2$ cross-terms

have a coefficient of 1. All theories lie within the Maximum Stress boundary in the second and fourth quadrants, the Norris Interaction theory, and the tensor theories with $F_{12} = 0$, being contained within this boundary in all quadrants.

Fig.8 represents a case where tensile and compressive strengths are different but X = Y and X' = Y'. The Hoffman envelope is similar to the Modified Marin and tensor theories with $F_{12} = -0.5L$ because the cross-term coefficients are the same. For Hoffman's theory X.X' is assumed equal to ZZ' to eliminate Z. The ellipse falls within the Maximum Stress boundary in three quadrants and it's origin has moved along the symmetry axis $\sigma_1 = \sigma_2$. The Norris Failure theory deviates from Hoffman's in the second and fourth quadrants because of the linear terms in the latter equation.

Fig. 9 represents a fair degree of strength anisotropy. This time the Hoffman and Tsai and Wu envelopes with $F_{12} = -0.5L$ are dissimilar since the cross-term coefficient of the latter equation is twice that of Hoffman's but differences only become marked in the third quadrant due to the constraints of the principal strengths. Some theories have lost their smoothness and the origins of the elliptical envelopes have been translated in the 1 - 2 plane.

2.1.4 Three-dimensional representations.

The case of $\sigma_6 = 0$ is seldom the loading condition in practice. For an orthotropic material in plane stress a three-dimensional surface with reference axes σ_1, σ_2 and σ_6 is required to represent the failure condition.

Fig. 10 shows predicted surfaces for the hypothetical but simple case where X = Y = X' = Y' = S. All the distortional energy and tensor theories, with the exception of the Norris Failure theory, produce the same ellipsoid. The Maximum Stress boundary is presented to show where and to what extent it contains the ellipsoid. For clarification, the surface will be sectioned and viewed in two dimensions.

Consider the surface to be cut in half along MNQ'POR. An observer standing at P, looking towards S, sees a profile as shown in Fig. 11. The sections shown intersect the Maximum Stress boundary at $\sigma_1 > X$. A similar view is seen by standing on the $+\sigma_2$ axis looking towards S, the $-\sigma_2$ axis looking towards T, and the $-\sigma_1$ axis looking towards T.

Fig. 12 shows the effect of F_{12} on the $\sigma_1 = \sigma_2$ surface section in σ_1, σ_6 space i.e. the section along line OS in Fig. 10. When $F_{12} = 0$ the profile is the same as for $\sigma_1 = 0$ or $\sigma_2 = 0$ since the cross-term coefficient in the equation is zero. As F_{12} approaches -L, the profile moves outwards along the $\sigma_1 = \sigma_2$ symmetry axis. At point W the effect of F_{12} is only small compared with it's effect further along the $\sigma_1 = \sigma_2$ axis.

The Norris Failure theory with $\sigma_6 = 0$ consisted of an ellipse with the Maximum Stress theory superimposed (see Fig. 3). With $\sigma_6 \neq 0$ the above is still true and the 3 - D surface is an ellipsoid that has been sliced away along planes Q'PSU and VUSQ in Fig. 10 in the first quadrant and along equivalent planes in the fourth quadrant. Fig. 13 illustrates the profile seen by standing on line OP in

Fig. 10 and looking towards S. Fig. 14 shows the view seen standing on line PS in Fig. 10 looking towards the $+\sigma_2$ axis.

2.2 Experimental determination of failure surfaces.

Off-axis uniaxial and biaxial stress testing produces a complex stress state in the principal material directions. By transforming applied stresses to principal material axes, as shown in Table 3, σ_1, σ_2 and σ_6 can be determined and the results can be plotted in three-dimensional space.

Fig. 15 shows the first two quadrants of a failure surface having reference axes σ_1, σ_2 and σ_6. Table 4 shows the sections of the surface determined by off-axis uniaxial tests and by tests on thin cylinders subjected to combined internal pressure and axial force. The surface section determined by off-axis uniaxial compression tests is not shown in Fig. 15 but the results lie in the $-\sigma_1$, $-\sigma_2$ quadrant. Curve JKI in Fig. 15 represents cylinder tests at a biaxial stress ratio (R) of + 0.5 with varying off-axis angle θ. At J, $\theta = 0^\circ$, at k, $\theta = 45^\circ$, and at I, $\theta = 90^\circ$. Tests at R = - 0.5 yield the curve LMNP. At points M and P the curve cuts the $\sigma_2 = 0$ and $\sigma_1 = 0$ planes respectively at θ values of 35° and 54° respectively. Similarly, for tests at R ratios between 0 and -1, θ values exist that allow data to be obtained in the $\sigma_2 = 0$ and $\sigma_1 = 0$ planes. Tests at R = -1 and pure shear tests on thin cylinders are analytically equivalent and yield the curve EB. Point E corresponds to R = -1 with $\theta = 0^\circ$ and pure shear with $\theta = 45^\circ$ and point B corresponds to R = -1 with $\theta = 45^\circ$ and pure shear with $\theta = 0^\circ$.

2.3 Prediction of Uniaxial off-axis strength.

By substituting the stress transformation equations, as shown in Table 3, into the failure theories the uniaxial strength variation with off-axis angle can be predicted. Many workers have attempted to verify their failure theories by this approach.

Schneider (33) has shown that for boron/epoxy composites the off-axis test does not provide sufficient discrimination between failure theories. In section 2.2 and Fig. 15 it was shown that the off-axis test only investigates a narrow segment (DGA) of the failure surface and Schneider concludes that all theories predict similar results along this segment. However, it must not be inferred that the predicted failure envelopes with $\sigma_6 = 0$ or the complete failure surfaces will be similar.

Pipes and Cole (34) showed that when predicting off-axis uniaxial strengths by the Tsai and Wu theory the value of F_{12} only produced second order changes in the predicted curve even when F_{12} was taken well outside it's stability limit. This is very different from the biaxial stress predictions discussed in section 2.1.2.3 where F_{12} had a marked effect on the failure envelope shape and an unconstrained F_{12} caused instability.

2.4 Complex stress test data.

There is a grave lack of published experimental complex stress data on GRP.

Jones (26) performed biaxial tension static failure tests on glass/epoxy filament wound tubes. Experimental data was compared with predictions by the Azzi and Tsai and Norris Failure theories and the latter was found

to be more satisfactory. It is the view of the author that the Modified Marin or tensor theories would have provided a more accurate prediction.

Protasov and Kopnov (27) studied the static failure of satin and linen weave glass/epoxy cylinders under combined internal pressure and axial force. They performed tests for $\sigma_6 = 0$ in four stress quadrants for the materials. In addition, for the satin weave cloth, they studied static failure in the first stress quadrant with $\sigma_6 \neq 0$ by adding a torque. Their results show good correlation with the Gol'denblat and Kopnov failure theory.

Owen and Found (6) studied the biaxial stress static behaviour of chopped strand mat (C.S.M.)/polyester resin cylinders in the first and second quadrants for debonding, resin cracking and failure. The Modified Marin and tensor theories provided the most accurate predictions.

Franklin (8) presented results by Ely (28) on type G graphite to verify the Modified Marin theory in the first and second quadrants showing the advantage of using a k_2 value for each quadrant.

Sultan and McGarry (30) studied the static biaxial stress behaviour, over two stress quadrants, of epoxy resin containing rubber particles. They showed that by increasing the particle size, the failure mechanism in each stress quadrant differed, and the behaviour was best described by two Von Mises type equations, one for each quadrant, having different coefficients.

Other biaxial stress static data is given in (29, 31, 32) where no comparison with failure theories is shown or where it appears incorrect use of failure theories has been made.

The literature in the complex stress fatigue behaviour of GRP is very limited indeed and a summary of that available is given in (1). Most of the work is limited to R = 0 or + 0.5 on filament wound pressure vessels at very low cyclic rates or at very short fatigue lives. Owen and Found (6) studied the biaxial stress fatigue behaviour of C.S.M./polyester resin cylinders in the first and second quadrants at various damage states. They concluded that biaxial loading was more damaging than uniaxial loading and that the Modified Marin and tensor theories provided the most accurate data prediction.

Chapter 3.

Test Equipment, Modifications and Calibrations.

3.1 Uniaxial Stress Fatigue Machines.

These were specially designed by Owen (36) for use with GRP. A full discussion of the machines and of the test procedure is given by Smith (37).

Five independent axial loading frames are fed from a hydraulic pulsator pump. The machines are of the constant displacement type and as specimen damage progresses its stiffness reduces and displacement adjustments have to be made to maintain constant load. Specimen alignment adjustments are incorporated and a variety of grips are available, all of the fixed non-rotating type. Due to the hysteresis and low thermal conductivity of GRP, the test frequency has to be low (37) and 100c/min, consistent with other workers in the research group (1, 37, 38, 39, 40, 41), was used in all investigations.

3.2 Biaxial Stress Test Machines.

3.2.1 General description.

To obtain a biaxial stress condition thin-walled cylinders under combined internal pressure and axial force were used. Found (1) designed a biaxial stress test machine for cylinders which is briefly discussed below.

This consists of one static loading frame, four fatigue loading frames, and a pulsator pump similar but larger to that used for the uniaxial stress fatigue machines. A variable speed motor drives a multi-output

pulsator pump which supplies oil pulsating at 100c/min. to the fatigue frames. The specimen in the loading frame is mounted on top of a ram/cylinder unit to and through which pulsating oil is passed (Fig. 16). A loading rod, connected to a reaction plate, holds the top of the specimen in position. The ram/cylinder unit is mounted on a load cell, the axial load being transmitted through this to the lower reaction plate of the loading frame. Oil passed through the ram unit provides the internal pressure which is monitored by a pressure transducer, while oil passed to the ram unit provides the in-phase axial load. Transducer outputs are fed into a strain gauge balancing/ amplifying/recording system where they are displayed on a D.V.M. A trip circuit consisting of pressure switches, solenoid valves and associated electronics is incorporated into the machine to divert the oil back to the tank when specimen burst occurs.

The ratio of axial/hoop stress (R) in the cylinder walls is fixed by the ram unit. A range of these are available providing nominal R ratios of 1, 0.75, 0.5, 0.25, 0, -0.25, -0.5, -0.75, -1.0, thus enabling testing over a limited range in the first two stress quadrants.

Internal pressure adjustment is achieved by varying the oil volume entering the specimen and thus the maximum obtainable pressure of 13.8 MN_m^{-2} (2000 p.s.i.) is only available to specimens exhibiting small strains. Due to stiffness changes, pressure adjustment is required as specimen damage progresses.

For static loading, oil is fed from a hand pump to the specimen via a ram/cylinder unit. Transducer output

is displayed upon X - Y recorders.

3.2.2 Calibrations.

Prior to commencing a test programme it was thought desirable to re-calibrate all load cells and pressure transducers. Calibrations were performed in a similar manner to (1). Transducer supply voltage is the controlling calibration factor. Instead of measuring transducer output at a standard supply or excitation voltage, the transducer supply voltage is adjusted to yield a standard output at maximum load or pressure. This technique results in increased sensitivity.

3.2.2.1 Pressure Transducers.

A Budenberg deadweight pressure tester was used. For 'fatigue' purposes, transducer output was monitored by the recording frame D.V.M. This was zeroed for zero applied pressure. The maximum pressure (13.8 MN_m^{-2}) was applied and the transducer supply voltage adjusted until the D.V.M. displayed 10·000 volts (amplified transducer output). Incremental loading techniques (1.38 MN_m^{-2} steps) were then used to determine the calibration curve. Three attempts were made for both increasing and decreasing pressure for each transducer. Mean output values were computed and calibration graphs plotted, an example of which is shown in Fig. 18.

For 'static' calibration the maximum applied pressure was 17.3 MN_m^{-2} (2500p.s.i.), this being the transducer limit. Similar techniques to above were used but the output was displayed on an X - Y plotter and calibrations made in terms of X - Y plotter deflection against pressure.

3.2.2.2 Load cells

Calibrations were performed on a Denison 500KN test machine. The various load cells and their capacities are given in (1). The calibration technique was very similar to that for pressure transducers.

3.2.3 Machine Modifications.

3.2.3.1 Electrical modifications.

As shown in section 3.2.2., transducer supply voltage is the controlling calibration factor. Before a test can be performed on the machines, individual transducer supply voltages have to be set up with the aid of the recording frame D.V.M. This procedure was initially time consuming since one had to crawl underneath the recording frame to disconnect the D.V.M. input and re-connect it across each transducer supply voltage in turn. To overcome these problems switching circuits (Fig. 17) were built into the recording frame by the author to allow easy supply voltage monitoring. The switch wafers S_a and S_b are carried on one shaft and allow any loading frame to be selected. Switch S1 controls whether load cell or pressure transducer supply voltage is being monitored. S2 is a 3 position rotary switch and acts as a D.V.M. function control. Position 1 short-circuits the D.V.M. input enabling its zero to be set. Position 2 allows setting up of transducer supply voltage. Position 3 monitors transducer output during a test and S_a, S_b, S1 all become inoperative in this position.

3.2.3.2 End cap modifications.

Full details of specimen end caps used for cylinder testing are given in (1).

Due to difficulties experienced with biaxial tensile stress specimens pulling out of their threaded end caps under high axial loads, two pairs of these were modified. A taper was machined in place of the threads (Fig. 22) to allow a large epoxy resin taper to be cast onto the specimen before test.

A compression end cap has been modified by temporarily blocking off the oil feed hole and hence allowing uniaxial compression tests on cylinders subject to suitable specimen design.

3.3 Torsion Fatigue Machine.

3.3.1 General description and modifications.

This machine is described in (42). A motor drives a large flywheel connected to an eccentric whose output arm applies torque to one end of the specimen. It is a constant strain machine with a wide range of throw. The specimen is located in grips, at the moving head, which are mounted in bearings, hence eliminating superimposed bending stresses. The torque is transmitted from the other end of the specimen to a calibrated strain gauged torsion bar whose output is fed into a D.C. bridge/amplifier and then into an oscilloscope. The machine can accommodate a wide range of specimen lengths.

The only machine modification required was to replace the motor with a variable speed type and hence to reduce the speed from 500 r.p.m. to a maximum of 100 r.p.m.

3.3.2 Torsion fatigue end caps.

The screw threaded end caps used for biaxial tension tests (Fig. 21) proved adequate for static torsion

testing but of no use for fatigue work due to slip between the cast screw thread on the specimen and the split end cap housing. This slip was prevented by milling slots into the split housings (Fig. 23) so that the casting resin (see section 4.3.2.) filled the slots and on cure securely located the specimen. In addition, dowel pins were placed between the split housing and the inserts to prevent slip between these two.

3.3.3 Trip circuit.

A trip device was required to switch off the machine when the specimen failed. The drop in output from the torsion bar strain gauges at specimen failure could have been used but this had the disadvantage of requiring a continuous strain gauge power supply. Specimen failure did not occur around the complete circumference, hence bending occurred which was transferred to the torsion bar. This fact was utilised in a trip circuit designed by the author. The torsion bar bending activates a micro-switch controlling an electronic circuit which operates a mains solenoid acting as an electronic finger to push the machine 'stop' button. The electronics (Fig. 19) consist of a Schmitt Trigger, a monostable multivibrator and a simple transistor switch operating a relay which controls the solenoid. When the micro-switch contacts close, i.e. on specimen failure, the Schmitt Trigger turns on sending a sharp positive-going pulse to the monostable. This switches to its unstable state turning on the transistor switch, hence operating the relay and solenoid which switches off the machine. After approximately 2 seconds, the monostable reverts to its stable state, turning off

the transistor switch and hence the relay and solenoid, thus eliminating risks due to power being continuously drawn through the solenoid winding.

3.3.4 Torsion bar calibration.

This was performed by attaching a pivoted lever arm to the torsion bar and hanging weights 36 inches from the pivot.

The torsion bar strain gauge output was fed into a D.C. bridge/amplifier and into an oscilloscope to balance the resistance change. Incremental loading techniques were used in 20lb steps upto a 200lb maximum, yielding a maximum applied moment of 7200lb. in (810 N m). The calibration graph is shown in Fig. 20.

Chapter 4.

Specimen Manufacture and Preparation.

4.1 Materials.

4.1.1 Reinforcement.

Two reinforcements were used, one a random chopped strand mat (C.S.M.), the other a balanced plain weave fabric having two orthogonal fibre directions.

The C.S.M. was SuprEmat, supplied by Fibreglass Ltd., and was similar but of a different batch to Found's (1). It has a 600g $/m^2$ nominal weight and consists of 51mm strands bonded by a P.V.A. binder. When laminated the product is macroscopically homogeneous and plane isotropic.

The fabric was Tyglass Y449, supplied by Fothergill and Harvey, and has equal fibre counts in both fibre directions, a nominal weight of 375grm/m^2 and type T5 finish. When laminated the product is orthotropic.

4.1.2 Resin.

This was a low viscosity, high reactivity polyester resin (L2615) supplied by B.I.P Chemicals Ltd., and is made by reacting propylene glycol with an unsaturated dibasic acid (maleic anhydride) producing long-chain highly reactive polyester groups which can be cross-linked by a monomer (styrene) (65).

Resin components are :-

Maleic anhydride	2 mol.
Phtalic anhydride	1 mol.
Propylene glycol	3 mol.
Alkyd/styrene ratio	65/35
Hydroquinone	0.008% on blended resin.

The cure agents used were a methyl ethyl Ketone peroxide (M.E.K.P.) catalyst and a cobalt accelerator (ACC.B) promoting high catalyst reactivity.

4.2 Cylinder manufacture.

The majority of cylinders manufactured were produced by the author, cylinder preparation prior to testing being performed by Mr. G.F. Budd.

4.2.1 C.S.M./Polyester resin cylinders.

Hand lay-up methods were employed similar to (1).

To overcome the slight anisotropy of the mat the reinforcement was cut from the roll as shown in Fig. 24. Two layers were used for specimens to be tested under tensile axial loads and 3 layers used for specimens to be tested under compressive axial loads.

An aluminium mandrel was coated with silicone grease and a layer of Melanex release film wrapped around its circumference. The reinforcement was weighed and a quantity of resin twice its weight was prepared using 1% M.E.K.P. and 1% ACC.B. The release film was coated with resin and the first reinforcement layer was wrapped onto the mandrel and resin stippled in with a brush. A roller was used to remove entrapped air and to assist in fibre wetting out. The batch of mat used had poor wetting out

qualities. A butt joint was made to complete the layer, any excess reinforcement being cut off. Care was taken when making the joint to avoid resin rich areas. The other layers were wound on in similar fashion, the layer join lines being spaced at 120° and 180° for 3 and 2 layered specimens respectively. After lay-up completion, a final resin coat was applied and a Melanex release film wrapped around the lay-up aided by an aluminium roller which removed excess resin and air. The ends of the lay-up were sealed to prevent air being drawn in and the mandrel was allowed to rotate. The cure cycle was 18 hours at room temperature followed by 3 hours at 80°C.

4.2.2 Y449/Polyester resin cylinders.

The techniques were similar to those used for C.S.M. cylinders. The reinforcement, which was a continuous length sufficient to produce a 5 layered cylinder, was cut from the roll as shown in Figs. 25, 26, and its leading edge was marked before lay-up so that its location could be identified after manufacture. The reinforcement was soaked in a resin bath prior to lay-up to ensure adequate fibre wetting out. Care was taken during manufacture to ensure fibre alignment. The cure cycle was as for C.S.M. cylinders.

A special technique was developed due to the problem of Y449 cylinders pulling out of their threaded end caps under high tensile axial load. In addition to the modified end caps described in section 3.2.3.2. a technique had to be devised to improve the bond between the cast epoxy and the GRP cylinder. For C.S.M. the axial loads

were small enough to allow a roughening of the cylinder surface to be a sufficient key but for Y449 this proved inadequate.

Instead of winding a mandrel length sheet of Melanex onto the lay-up, two 125mm wide Melanex strips were wound around two portions of the lay-up. These covered portions became the specimen gauge length. The final resin layer was then wiped off the exposed regions, lying either side of and between the covered regions, and cure allowed to take place. This produced regions of a knurled nature since the final layer fibres were now exposed and an ideal bonding surface after further preparation.

Similar testing problems were found under torsion fatigue and a similar technique to above was employed but 3 pieces of melanex, 65mm wide, were used to enable 3 short specimens to be obtained from a mandrel.

4.3 Specimen Preparation.

After removal from the mandrel the cylinders were in general cut into two 185mm lengths for tension and compression type specimens and into three 125mm lengths for torsion.

4.3.1 Compression cylinders.

End strengthening pieces made by winding a 40mm wide, 60cm long, piece of Y449 soaked in polyester resin around the circumference at each cylinder end were applied to prevent end splay-out under high compressive axial loads. After the end sections had cured (room temperature only), the specimens were faced on a lathe producing a cylinder with 180mm overall length and 100mm gauge length (see Fig.27).

Liners were applied as shown in section 4.3.4. if required.

4.3.2 Tension cylinders.

The 185mm lengths were faced to 180mm on a lathe. Before casting the specimens with epoxy resin into their end caps, surface preparation of the final 25mm sections of the specimen length was carried out to ensure a good GRP/epoxy bond and liners were applied as shown in section 4.3.4 if required. For C.S.M. and Y449 specimens to be tested under low tensile axial loads the end sections were grooved and roughened. For Y449 specimens to be tested under high tensile axial load, specimens of the 'wiped end' variety as described in section 4.2.2. were used and the 'knurled' end sections roughened using a wire brush. All specimen types had their end sections thoroughly washed in acetone and were allowed to dry.

During the initial phases of the work, a similar resin type and cure cycle was employed for casting purposes as used by Found (1). This consisted of Epikote 828 epoxy resin, Epikure NMA catalyst, BDMA accelerator in proportions given in (1). A hot cure cycle had to be used for this system and the final product proved to have insufficient strength for Y449 work. This was replaced by a cold cure formulation consisting of Epikote 828, and DX116 amine curing agent, in weight proportions 1:0.6, which produced a resin with a gel time of approximately 30 minutes and sufficient strength. A 20lb weight was applied to the top of the specimen during the casting operation to ensure specimen alignment after resin cure. For cases of high tensile axial load the taper type end caps as described in section 3.2.3.2. along with 'wiped end'

specimens were used.

4.3.3 Torsion specimens.

These we faced to 120mm length on a lathe before casting. A similar preparation and casting resin were used as for the tension case. For static torsion work the specimen end sections were grooved and roughened but for the fatigue case the 'wiped end' specimen was used. No liners were required in this work.

4.3.4 Liner preparation and application.

To prevent possible adverse effects of mineral oil on GRP and to prevent pressurising medium seepage, a liner was applied to the inside surfaces of specimens tested to failure.

The cold-cure silicone rubber liner and primer used by Found (1) had insufficient bonding strength to ensure liner adhesion under fatigue loading. A modified technique was developed. The specimen inside surface were thoroughly cleaned using acetone. For specimens required to withstand cyclic loads, I.C.I. Primer O.P. was applied to the inside surface and allowed to dry for approximately ½ hour. For static test specimens Midlands Silicones MS2650 primer was used to enable easy liner removal after test.

Found (1) suggested that a dark pigment should be added to the liner formulation to enable easier detection of progressive specimen damage. A 2 layered liner was developed by the author using I.C.I. Silcoset type 105 cold cure silicone rubber. The first layer was carbon black filled. This was allowed to dry before the application of a layer of unfilled rubber which was required because the

carbon filled layer tended to have a high pin hole density. The liner layers were applied using a small brush.

4.4 Flat laminates.

4.4.1 Manufacturing details.

All laminates were prepared in the laboratory by the hand lay-up technique as used by other workers in the research group (1, 37, 38, 39, 40, 41). They were prepared on a glass plate, having a thin surface film of silicone release agent, covered by a Melanex sheet. Care was taken to avoid silicone contamination of the resin since it can inhibit surface cure. The polyester resin (L2615) was prepared using 1% M.E.K.P. and ½% ACC.B. The cure cycle was as used for cylinders.

In addition to normal C.S.M. and Y449/Polyester resin laminates, laminates were also prepared containing a jointed reinforcement layer to simulate cylinder construction. Preparation techniques were similar to above.

4.4.2 Specimen preparation and geometry.

Blanks were machined from laminates using a diamond cutter.

Specimen types are shown in Fig. 28. For contoured specimens (types A,B,C) the shaping was done using a pantograph and tungsten carbide cutter. Specimen (A), the compression specimen, was designed to prevent buckling failures (1). The static tensile specimen, type (B), complies with BS2782 Part 3 1965 and ASTM D2150-63T. Specimens (C) and (D) are zero-tension fatigue specimens, type (C) is consistent with (1), type (D) is a parallel sided strip.

Chapter 5.

Test Programme.

5.1 Flat laminate test programme.

5.1.1 General Introduction.

For material characterisation, and for correlation with cylinder data, flat laminate results under uniaxial static and fatigue loading were required.

Static tests were performed on an 'E' type Tensometer at a cross-head speed of 1.27 mm/min. using wedge type non-rotating grips. An extensometer operating over a 50.8 mm gauge length measured deflections up to resin cracking. Specimens of types A and B (Fig. 28) were used for compression and tensile tests respectively.

Fatigue tests were performed on the machines described in section 3.1 in both 'normal' and 'oil' test environments. A 'normal' environment was laboratory conditions of 20°C, 50% R.H. For 'oil' environment tests the specimen gauge length was enclosed in a polyethylene jacket containing Shell 'Tellus 15' mineral oil i.e. the oil used as the pressurising medium in the biaxial stress test machine described in section 3.2.1. Specimens of types C and D (Fig. 28) were used along with pin and button (47) and flat faced grips respectively.

5.1.2 C.S.M./polyester resin laminates.

Large discrepancies were revealed by Found (1) and Owen and Found (6) in fatigue loading, but not in static loading, between the analytically equivalent cases of R = 0 for cylinders and flat laminates under uniaxial

tension as shown in Fig. 40. Explanations offered (1) were (a) an adverse size effect, (b) that cylinder radial stresses could not be neglected, (c) that the pressurising medium affected fatigue behaviour. The above were not evaluated by Found and thus, in addition to characterisation tests, a test programme was initiated to solve the anomaly. A brief discussion of the possible causes listed above and others is given below :-

(a) Size effect - there are two possibilities here. Firstly, there are more initial defects in a cylinder than a flat specimen and hence more crack initiation sites. Secondly, as shown by Bishop (38), the larger the specimen and crack length, the smaller the effect of the crack tip plastic zone, hence the smaller the effect of the crack tip energy absorbance after damage and hence the lower the fracture toughness.

(b) Radial stresses. The cylinders complied with isotropic theory, i.e. the ratio of internal diameter to wall thickness $(d/t) \geqslant 20$, and hence radial stresses can be neglected if the material is considered isotropic.

(c) Chemical effect of the pressurising medium. This has been found to affect metal cylinders in fatigue loading (44).

(d) Cylinder construction. An inherent failure site is incorporated into the cylinders during manufacture, since by using a separate reinforcement piece for each layer a discontinuity exists at the joint terminating each layer.

It was thought possibilities (a) and (b) would

yield noticeable static loading effects whereas (c) and (d) would yield maximum effects in fatigue loading. Hence (c) and (d) were evaluated.

5.1.2.1 Simulation of cylinder construction.

To investigate (d), laminates having similar discontinuities to cylinders were manufactured. Fig. 29 shows reinforcement joint regions in cylinders and flat specimens. For consistency with cylinders, the butt joint was usually in the first reinforcement layer i.e. the first layer during laminate manufacture.

5.1.2.2 Test Programme.

The ultimate strength of GRP varies with glass content. Test data can only be directly compared at a specific glass content and hence the strength variation with glass content needs to be known. As stated in sections 4.1.1 and 4.2.1 the C.S.M. used was similar but of a different batch to that used by Found (1) and it had poor wetting out qualities. Thus, the variation of static tensile and compressive strength with glass content was evaluated, using 3 and 6 layered laminates respectively.

All other testing was tensile, the test programme being shown in Table 5. Specimens of type C (Fig. 28) were used for all the fatigue testing. The effect of an oil environment was only studied in fatigue loading. Oil under pressure was not used because of, (i) difficulty in applying external pulsating pressure, (ii) lack of time to develop the technique.

Under biaxial loading, stresses are present at both 0° and 90° to the cylinder joints and thus joint effects in flat laminates were evaluated for both 0° and

90° joint orientations. For specimens with a 0° joint orientation, the joint ran along the full specimen length and the loading axis, whereas for a 90° joint orientation the joint ran across the full specimen width and along the transverse axis (see Fig. 28). Joint effects in uniaxial compression loading were not evaluated because, (i) 6 layered specimens were necessary to avoid buckling failures thus introducing possible thickness effects, (ii) joint effects were thought to be small in this loading mode.

5.1.3 Y449-Fabric reinforced laminates.

5.1.3.1 Simulation of cylinder construction.

To attempt to account for any discrepancies arising between uniaxial and biaxial stress test results, as found for C.S.M., the lap-joint and overlap construction of 0°off-axis cylinders was simulated by using similarly constructed flat specimens (Fig. 30).

5.1.3.2 Test Programme.

All testing was tensile, the test programme being shown in Table 5. Joint effects were evaluated in fatigue using type D specimens (Fig. 28) because these allowed a similar applied stress condition to exist in both the joint and overlap regions for consistency with cylinders. The joint lay at 90° to the load and ran across the full specimen width and along the transverse axis. The 0° joint orientation case was not studied since a wide specimen is required to simulate cylinder conditions hence introducing possible width effects. To eliminate effects due to specimen shape, 0° off-axis plain specimens of type D were fatigue tested for comparison with joint results.

Static and fatigue tests were performed on 45°

off-axis plain laminates using specimens of types B and D (Fig. 28) respectively. Laminate construction difficulties prevented the investigation of joint effects in 45^{o} off-axis specimens where the joint must lie at 45^{o} to the fibre directions.

5.2 Cylinder test programme.

5.2.1 General introduction.

The main research topic was to study the biaxial stress behaviour of various GRP's by subjecting thin-walled cylinders to combined internal pressure and axial force. Biaxial stress tests were performed on the machines described in section 3.2. Setting-up and general test precedure was described by Found (1) and is not discussed here.

In-plane shear results were obtained from torsion of thin cylinders. Static tests were performed on an Avery test machine, and fatigue tests on the machine described in section 3.3. at 100 C/min.

Biaxial stress and torsion results were computed from the equations shown in Table A3.

Static uniaxial compression tests ($R = -\infty$) were performed on a Denison 500 kN test machine for C.S.M. cylinders, and on the biaxial stress test machine using the modified end caps described in section 3.2.3.2 for fabric-reinforced cylinders, to see whether flat laminates and cylinders had similar strengths. Practical difficulties prevented uniaxial tensile tests being performed.

5.2.2 C.S.M./polyester resin cylinders.

The author extended the work performed by Found (1) in order to determine a more complete experimental

failure envelope and to see if results were operator dependent. Found investigated R ratios of 1, 0.5, 0, -0.5, -1.0 under static and fatigue loading for debonding resin cracking and ultimate failure. The work performed by the author is shown in Table 6, failure being the only damage state studied. Cylinder dimensions are shown in Fig. 27 and Table 6, the (d/t) ratio complying with isotropic theory. For consistency with Found, 't' was computed from the equation :-

$$t = \frac{\text{minimum O.D. - nominal I.D. (65 mm)}}{2}$$

where O.D and I.D are outside and insider cylinder diameters respectively.

To help clarify the discrepancies discussed in section 5.1.2 the local glass content in the section containing the failure line was determined for static test cylinders in addition to the average glass content in the remainder of the gauge length to indicate whether or not failure occurred in a low glass content region. The failure lines were cut from the cylinders and the resin burnt off at 625°C.

5.2.3 Y449-Fabric reinforced polyester resin cylinders.

5.2.3.1 Introduction.

Section 2.2 described the sections of the plane stress failure surface that are evaluated by tests on thin cylinders. Complete surface evaluation for static and fatigue loading is time consuming and uneconomic. Hence, a compromise has to be made and tests selected that determine important surface sections. For the main programme of study, off-axis angles of 0° and 45° were investigated. Section 2.2 and Table 4 showed that testing 0° and 45° off-

axis thin cylinders, over a range of applied biaxial stress ratios (R), investigated sections ADC and FB respectively in Fig. 15, i.e. the above represent cases where $\sigma_6 = 0$, and $\sigma_1 = \sigma_2$ but $\sigma_6 \neq 0$ respectively. For a balanced weave fabric material, such as Y449, both 0^o and 45^o off-axis angles represent cases of special orthotropy since the normal - shear coupling compliances S_{16} and S_{26} and their transformed values S_{16}' and S_{26}' are zero (see Table A4).

Initially, experiments were performed to determine the number of reinforcement layers required from a test view point. Tests were made on 4 - layered 0^o off-axis angle cylinders at R = -1, the most severe condition, to see if buckling occurred. No buckling was apparent but premature failure occurred due to delamination and unwinding of the final reinforcement layer. After further investigation, 5 - layered cylinders were chosen with the outer reinforcement layer overlapping the inner starting edge as shown in Fig. 30. This proved successful experimentally and allowed consistency with design recommendations by Pagano and Whitney (49) who suggest that a high internal diameter to wall thickness ratio (d/t) is required to neglect radial stresses. The specimen dimensions (Fig. 27) yield a (d/t) ratio of about 35 which was considered adequate. Correct cylinder design is important but in practise a compromise has to be made between test machine capabilities, the prevention of premature failure and an acceptable stress distribution. Further information on this topic is given in (56 - 64).

Inside and outside cylinder diameters were

measured using internal and standard micrometers. Three and five readings were taken for inside and outside diameters respectively and mean values used to compute 't'.

5.2.3.2 Test programme.

The tests performed and the damage states studied are shown in Table 6. Static tests at R = -1 at off-axis angles of 15° and 30° were performed in addition to those of 0° and 45°, to further evaluate section EB in Fig. 15. For all biaxial stress tests, separate specimens were used for damage and ultimate failure studies.

Chapter 6.

Results

6.1 C.S.M./polyester resin composites.

6.1.1 Uniaxial static results.

Fig. 31 shows the ultimate tensile strength (U.T.S.) and ultimate compressive strength (U.C.S.) variation with glass content, for the reinforcement batch used, along with Found's (1) data. All curves are Least Squares linear regression lines, ultimate strength being considered the dependent variable, and the standard errors of estimate and linear correlation coefficients are shown. Discrepancies exist between Found's and the author's data. These differences are attributed to the poor wetting-out qualities of the reinforcement used by the author. A poor glass-resin bond would produce premature failure since failure is preceded by progressive damage, an initial stage of which is debonding. The suppliers of the reinforcement, Fibreglass Ltd., discovered that the wetting out problem stemmed from a manufacturing fault at their Birkenhead factory which occurred during the shift of the manufacturing process from Birkenhead to Wrexham.

Fig. 31 shows there is a high linear correlation between U.T.S. and glass content but a low correlation between U.C.S. and glass content for both reinforcement batches. A possible reason for this is that compressive failure occurs when resin support fails (67), and hence compressive failure is failure mode rather than glass content dependent.

Table 7 summarises the other uniaxial static tensile test data, individual results being tabulated in progress reports submitted to Dr. M.J. Owen. Maximum, minimum and mean values are presented for each laminate type and it should be noted that values along a line do not necessarily correspond. Specimen thickness is given to show that glass content within and between specimen, groups was not constant and allowance has to be made for this when comparing results. In the majority of cases, actual glass content was not determined since it was desired to retain the specimens for examination purposes and hence an estimate was derived from Fig. 32. A strength estimate (N) based on mean thickness was derived from Fig. 33 for each specimen group. Laminate G3, a non-jointed laminate, was considered as the norm i.e. estimated strength = 103.5 MN_m-2. Each group was corrected to the norm by multiplying the experimental strength by P where P = norm strength/N i.e. 103.5/N. These values are shown in column 11 of Table 7 and provide a basis for direct comparison.

Column 11 of Table 7 indicated that joints have only a small effect on U.T.S. Laminates G11 and G17 have corrected U.T.S. values either similar to or above the norm whereas G6 and G8 have values below the norm. Laminate G6 has the lowest value of the 3-layered laminates but this laminate was made by Mr. R. Harrison and hence operator error was introduced. Fig. 34 shows photographs, taken using transmitted light, of untested samples of plain and jointed laminates prepared by grinding-off the resin rich layer, etching the glass with hydrofluoric acid for 1.75 minutes and then staining the surface with black ink. For plain

laminate G3 the fibre orientation is quite random and no discontinuities exist. For laminate G6 the joint discontinuity is very noticeable and few fibres cross the resin rich joint zone. For G8, which was manufactured by the author, the joint discontinuity is not as marked as in G6 but is still discernible whereas for G10 the joint is difficult to locate. G8 and G10 are considered to have well made joints. Consideration of column 5 in Table 7 shows that G6, G8 and G10 produce relatively low minimum strengths. This could be attributed to a poor joint, similar to the untested sample of G6 in Fig. 34, and if so indicates that joints incorrectly made have an adverse effect on U.T.S. Conclusions similar to the above extend to 'strain to resin cracking' as shown in column 9 of Table 7.

Fig. 35 shows photographs of 25mm wide parallel sided strips of G6, G8 and G10 tested until joint cracking occurred under static tension. For G6 the only crack present is in the resin rich joint zone whereas for G8 and G10 joint cracking was preceeded by resin cracking in other sections of the specimen. This shows how the onset of resin cracking can be initiated in poor joints having large resin rich zones possibly leading to premature failure.

Fig. 36 shows ground, etched and stained samples of laminate G17, a 3-layered laminate containing a centre reinforcement layer butt-joint, photographed using transmitted light. The top set of photographs show untested material and show that the joint is invisible near to the laminate surface but becomes discernible as the specimen is progressively ground. This reveals the difficulty in

detecting jointed layers. The bottom set of photographs are of a 25mm wide parallel strip of G17 tested under static tension until joint cracking occurred. The specimen has been progressively ground similar to the untested sample and shows how the joint cracks are revealed in the resin rich joint zone. There are more cracks in the joint zone than elsewhere showing the effect of the joint stress concentrator and resin rich zone on damage intensity.

Fig. 37 shows that joints have little effect on initial tensile modulus which is not surprising since the joint is a local defect. Similar correlation is obtained for secondary modulus variation with glass content although this figure has not been presented. After debonding C.S.M. shows a loss in stiffness denoted by a knee on the load v displacement plot and secondary modulus is the tangent modulus after debonding.

6.1.2 Biaxial stress static test results.

Table 8 gives a summary of the biaxial stress static failure data, individual results being presented in Fig. 38 and in progress reports submitted to Dr. M.J. Owen.

The axes of Fig. 38 are axial stress and hoop stress which are principal stresses. There is a difference between actual and nominal biaxial stress ratio due to friction in the ram units (1). Scatter is quite marked, as much as $\pm$20% of the mean in some cases but this is consistent with uniaxial flat laminate data. No correction has been made for glass content variation between results at different stress ratios, or by different operators, since it is not known if the relationship between strength and glass content is stress ratio dependent. The mean glass content of Found's

cylinders was below that of the author's as shown in Table 8. From consideration of Fig. 31 glass content differences between the two cylinder sets account for strength discrepancies due to reinforcement batch problems and hence both the author's and Found's data were plotted on Fig. 38 without further correction. Correlation between data obtained by the two operators is acceptable.

Table 8 shows that the local glass content in the region of failure for the author's specimens was in general below the specimen average. Prior to failure the glass content in this region would have been lower than shown since at failure some of the matrix was expelled, indicating that failures probably occurred at a joint. This cannot be substantiated since the majority of the specimens were destroyed during the burn-off programme. However, uniaxial flat laminate data indicate that joints have little effect under static loading and hence cylinder joint effects were considered to be negligible in this loading mode. The R = 0 results obtained by the author, having a mean failure line glass content of 33.18%, correlate well with corrected U.T.S. values from G8 flat laminates (see Table. 7, column 11). This indicates the absence of a width effect as suggested by Found (1) and is substantiated by uniaxial compression results from cylinders as shown in Table 8. These compression results were invalid since failure occurred prematurely at the specimen ends but the strength values obtained correlate well with U.C.S. data given in Fig. 31.

Comparison between predicted and mean experimental static data is given in Fig. 39. The letters denoting the

various failure theories are defined in Tables 1 and 2. For failure prediction the hoop strength X, was taken as the mean of R = O data by Found and the author. The compressive strength Y' was obtained by multiplying the flat laminate ultimate compressive strength by P where P is the ratio of hoop strength to uniaxial tensile strength. For C.S.M., Y = X and Y' = X', the shear strength S is not required for failure prediction since $\sigma_6 = 0$. In the first stress quadrant data are plotted between R = ∞ and R = +1, these results being a reflection about the $\sigma_1 = \sigma_2$ (R = +1) symmetry axis of data plotted between R = O and R = +1. It was considered acceptable to do this since C.S.M. is plane isotropic and joint effects are a minimum under static loading conditions. The data follow a similar pattern to that presented by Jones (26) on filament wound cylinders. The maximum stress theory (A) is inadequate in defining failure. The Norris Interaction theory (C) is conservative in the first quadrant but wildly optimistic in the second quadrant due to it's circular form. Hoffman's theory (F, unidirectional case) is conservative in the first quadrant but slightly optimistic in the second. The Tsai and Wu (I), Gol'denblat and Kopnov (H), and the Modified Marin (G) theories provide the most accurate overall prediction. The constants F_{12} and k_2 were determined from the mean of Found's and the author's data at R = +1 and the failure envelope passes between the two data sets. The Norris Failure theory (D) is slightly optimistic in the first quadrant but provides a good approximation to the data and would be acceptable for strength predictions in cases where no complex stress data is available to compute F_{12} and k_2.

6.1.3. Uniaxial zero-tension fatigue results.

Section 5.1.2. discussed the discrepency revealed by Found (1), and Owen and Found (6), between R = 0 results from cylinders and zero-tension fatigue results from flat laminates, as shown in Fig. 40, and the course of action embarked upon by the author to solve the anomaly. Figs. A1 - A9 show individual fatigue results for a variety of C.S.M. laminates tested in different environments or containing jointed reinforcement layers. All curves are Least Squares linear regression lines with strength being considered the dependent variable and the equations are shown on the individual figures. Static data along with scatter bands are presented at the $\frac{1}{4}$ cycle position. The fatigue results are summarised in Table 9, individual results being tabulated in progress reports submitted to Dr. M.J. Owen.

Fig. 41 presents results from laminate G3 in normal and oil environments. At 10^3 cycles a difference exists between the two curves which is due to glass content as shown in Table 9. At 10^6 cycles the oil environment results indicate a slight increase in fatigue strength over the norm. If this effect is real it could be due to moisture exclusion (51) or to a lubricating effect at the glass-resin interface after the onset of damage. Oil effects are expected to be less for cylinders than for flat specimens since they have no exposed edges and hence oil penetration is limited to diffusion through the resin until resin cracking occurs. The chemical effect of oil would be greatest on specimens containing a reinforcement joint since an easy oil penetration path is present after the onset of joint cracking. Results from laminate G8, as shown in Fig. 41, indicate no

adverse effect of oil but a slight increase in fatigue strength at 10^6 cycles as seen for G3. It is concluded that oil effects on C.S.M./polyester resin laminates are negligible.

Comparison of Figs. A1 - A9 show that scatter in fatigue results is considerably reduced when a joint is present since a failure initiation site is introduced into the specimens. Even though care was taken in jointed laminate manufacture, a resin rich zone exists in the joint region as shown in Figs. 34 - 36. The fatigue failure mechanism of G6 and G8 specimens having joints lying perpendicular to the tensile stress axis and across the full specimen width in one outer reinforcement layer is detailed below and in Fig. 42. Firstly, a joint crack appeared across the full specimen width. This joint crack was usually the first crack to appear in the specimen. As the test progressed the damage intensity at the joint increased, as shown in photograph 2 of Fig. 42, and the crack appeared to propagate along the resin rich zone of the overlap. This produced some bending of the specimen due to a shift of the neutral axis with respect to the loading points. Final failure occurred across the plane of the joint as shown in photograph 3 of Fig. 42. Photograph 4 of Fig. 42 is a view of the specimen edge after failure and shows how the crack propagated along the resin rich overlap zone prior to failure.

Fig. 43 shows the effect of joints when comparing results on a stress basis. Curve 1, i.e. laminate G3 in a normal environment, is considered the norm for comparison purposes. Curves 1 and 4 show that the effect of an outer layer reinforcement joint lying perpendicular to the applied stress in a 3 - layered laminate is considerable, the strength

reduction due to the joint being 38% at 10^3 cycles and 58% at 10^6 cycles. Curves 4 and 5 compare favourably indicating that joints were the cause of the fatigue anomaly shown by Found (1). Curve 6 is for plain 2 - layered specimens from laminate G9. There is a discrepancy between curves 1 and 6 at 10^3 cycles which is due to glass content, as shown in Table 9, but at 10^6 cycles where glass content is considered to have negligible effect (37) the two curves are comparable. The effect of a reinforcement joint at 90^o to the loading axis in 2 - layered laminates is shown by curves 6 and 4 and is of similar magnitude to the 3 - layered case. Curve 3 is for a 3 - layered laminate (G17) with a joint, at 90^o to the tensile stress, in the middle reinforcement layer. In this case no significant bending occurs due to neutral axis shifts because of symmetry about the loading axis. Comparison of curves 1 and 3 shows the effect of the joint and although it is not as marked as in previous cases it increases with fatigue life and the trend indicates that beyond 10^6 cycles middle layer and outer layer joints may have similar effects.

For reasons given in section 5.1.2.2 the effect of joints lying parallel to the tensile stress was evaluated for 2 and 3 - layered specimens, curves 7 and 2 in Fig. 43 denoting these cases respectively. No joint effect was expected here but quite a marked one appeared indicating that cylinders under biaxial tension fatigue loading would be more affected by joints than at R = 0. Examination of the flat specimens after test yielded no explanation of the behaviour. No differences were observed in the type of damage, damage intensity or failure appearance between these

and G3 specimens and no cracks were observed parallel to the loading axis.

One question arising from these results was whether or not a 3 - layered jointed specimen was equivalent to a 2 - layered plain specimen i.e. could the jointed layer simply be considered as non-load bearing. Fig. 44 shows a similar set of curves to Fig. 43 but the ordinate is the tensile axial force applied to the specimens during test. Mean static data are shown at the $\frac{1}{4}$ cycle position and under this loading mode 3 - layered jointed specimens from laminate G8 require a 26% greater force to fail them than 2 - layered plain specimens from laminate G9. At 10^3 cycles however, G8 (curve 4) and G9 (curve 6) are equivalent. As the life increases G8 requires a lower force to cause failure than does G9 and at 10^6 cycles the effect is very marked, i.e. the failure force of G8 is 37% below that of G9. Hence, the jointed layer cannot simply be considered as non-load bearing possibly because of joint crack propagation into the remaining laminate layers. Comparison of curves 3 and 6 indicates that at 10^3 cycles the force required for failure of the middle layer jointed laminate, G17, is well above that of G9 but between 10^5 and 10^6 cycles the two become comparable indicating a joint crack propagation failure mode. The results of G17 are above those of G8 which is expected since joint crack propagation along the resin rich overlap zone would be aided by the bending of G8 specimens caused by a neutral axis shift. The effect of joints lying parallel to the loading axis is quite marked as shown by curves 1 and 2, and 6 and 7 especially for the 2 - layered case (curve 7). An interesting point is that

G8 (curve 4), and G10 with a 0^{o} joint orientation (curve 7), yield similar results. The implications of the above results are very disturbing since reinforcement joints in structures are inevitable due to there being a finite reinforcement roll width and hence joints must be located in very low stress regions to avoid premature catostrophic failure.

Fig. 45 presents further indication that joints caused the fatigue anomaly (1) and shows R = 0 data from cylinders by the author along with uniaxial zero-tension results from laminates having outer layer reinforcement joints lying perpendicular to the loading axis. Correlation between all data sets is excellent.

6.1.4 Biaxial stress fatigue results.

Biaxial stress total failure fatigue results obtained from C.S.M./polyester resin cylinders by the author and by Found (1) are summarised in Table 8. Individual results by the author are given in Figs. A10 - A14 and in progress reports submitted to Dr. M.J. Owen.

The fatigue anomaly shown in Fig. 40 was also present in the R = 0 results obtained by the author as shown in Fig. 46. A discrepancy exists between R = 0 fatigue data by Found and the author the magnitude of which is not present in the zero tension flat laminate data or in the R = 0 static data. It was shown in sections 6.1.1 and 6.1.3 that joints have little static loading effect but a devastating fatigue effect and hence it is possible that this discrepancy is due to slight differences in cylinder manufacturing technique and hence slight differences in the width of the resin rich joint zone or in the number of fibres crossing it. It could also be due to the reinforcement

wetting-out problem experienced by the author. The similarity between the zero-tension fatigue curves is due to glass content differences, the mean of Found's flat specimens was 33.18% whereas the author's was 37.42%. Scatter in the author's R = 0 fatigue results is low and more resembles that of jointed flat laminate G8 (Fig. A4) than plain laminate G3 (Fig. A1) hence substantiating the 'joint' theory. Fig. 48 shows the inner reinforcement layer joint region in an untested cylinder along with a joint crack and a joint failure occurring under R = 0 fatigue loading. Comparison of Figs. 34 - 36 with photograph 1 of Fig. 48 shows that joints are more difficult to detect in cylinders than in flat specimens. This is because the mandrel upon which the cylinders are manufactured aids joint formation. Photograph 3 of Fig. 48 shows that joint damage or failure extends beyond the gauge length into the over-wrapped regions and almost traverses the full length of the cylinder bore indicating the severity of damage occurring in joint regions.

Biaxial stress fatigue curves at five R ratios are shown in Fig. 47. Only small differences exist between these which indicates no biaxial stress effect but the results cover too narrow a section of σ_1, σ_2 stress space to infer that the maximum stress theory would be suitable.

Fig. 49 shows fatigue results by the author and by Found (1) covering a range of R ratios from +1 to -1. Due to differences between R = 0 fatigue strengths as shown in Fig. 46, the author's data was corrected to Found's by multiplying each curve at 10^3 and 10^6 cycles by T, where T is the ratio of the R = 0 fatigue strength determined by Found

to that determined by the author. At 10^3 cycles very little difference exists between the curves, except at R = +0.5 and +1, whereas at 10^6 cycles other slight deviations are seen. A very marked biaxial tension effect is indicated in Found's data at R = +0.5 and +1 but not in the author's data at R = +0.25 and +0.75. Section 6.1.3 showed that joints lying parallel to the loading axis in 2 - layered laminates affected the fatigue performance and hence joint effects could be greater in cylinders under biaxial tension than R = 0. This coupled with possible glass content differences may explain Found's results but the argument is contradicted by the author's data. No real explanation can be forwarded for this discrepancy. Some unsuccessful attempts were made at correcting cylinder fatigue results to plain laminate results and hence predicting true failure strengths. However, this is difficult because it is not known if biaxial stresses produce independent or interactive joint effects.

Fig. 50 compares data at 10^6 cycles obtained from Fig. 49 with predicted failure envelopes. In the second quadrant the correlation between both data sets is acceptable. However, useful failure theory prediction is inhibited because the first quadrant shows a severe lack of data correlation. In the second quadrant the Norris Failure (D) and the Tsai and Wu (I), Gol'denblat and Kopnov(H), and modified Marin (G) theories, with F_{12} and k_2 determined from R = -1 data, provide useful predictions. The most useful overall prediction for inconsistent data of this type is provided by the modified Marin theory with a k_2 value determined from each stress quadrant. Constant F_{12} in the tensor theories was not deter-

mined from R = +1 data as for the static loading case since the value obtained would violate the F_{12} stability condition and hence cause the envelope to become hyperbolic as shown in Fig. 50.

6.1.5 Appearance of failures under biaxial stresses.

Typical static failures are shown in Fig. 51. The card against each cylinder denotes the biaxial stress ratio. Failures at R = 0 and R =-0.25 occurred parallel to the cylinder axis, i.e. at 90^{o} to the hoop stress, and were similar to failures observed in flat laminates tested under uniaxial tension. At R = -0.75 combined hoop tensile and axial compressive failures were observed. The tensile fracture was at 90^{o} to the hoop stress with a fork at one end showing the influence of axial compression. The compressive axial failure almost spanned the full specimen circumference and there were no signs of macro-buckling. Comparison of failures at R = +0.25, +0.75 and +1 shows the increasing influence of the axial tensile stress, as R approaches +1, by the size of the forks at the end of the hoop tensile failure. At R = +1 the fracture orientation was somewhat arbitrary as expected since all directions are principal stress directions. At R = 0 and +1 joint influenced failures appeared to predominate but at R = +0.25, +0.75, -0.25 and -0.75 this was not the case.

For fatigue loading the failure appearance of the author's specimens was similar to the static case except for R = -0.75. Here, combined fractures as shown in Fig. 51 were not seen but typical joint failures occurred similar to that shown for R = 0 in Fig. 48. Examination of Found's specimens showed that at R = +1 the

failures ceased to be at arbitrary orientations and were straight fractures at 90° to the hoop stress, and at R = -1 even though combined failures occurred in some cases the hoop tensile failure appeared to be a joint failure. It was found that joint failures predominated at all R ratios under fatigue loading.

Photographs 1 - 6 in Fig. 52 show the difference between static and fatigue damage at R = +1, 0 and -1. Samples were cut from Found's ultimate failure specimens and the cylinder bores were examined, using transmitted light, on the macro setting of a Vickers M41 microscope. All magnifications were X10. In all cases the resin cracking is far more severe in fatigue loading and the cracks are generally shorter and of a finer nature. At R = +1 cracks occur at arbitrary orientations, since all directions are principal stress directions, producing a mosaic type effect. At R = -1 the nature of the damage is similar to that at R = 0 i.e. most cracks are at 90° to the hoop stress, none being caused by the axial compression. This was expected since C.S.M. is twice as strong under uniaxial compression as under uniaxial tension as shown in Fig. 31 and resin cracking does not occur in the compression mode until 80% of the failure load is reached (1).

Photograph 7 of Fig. 52 shows cracks radiating from voids in the resin rich layer of a cylinder bore tested under static loading at R = 0. The high fatigue crack intensity shown in photographs 2, 4 and 6 of Fig. 52 is probably caused by the growth of cracks from such stress concentrators.

6.1.6 Discussion of C.S.M. results.

The effect of reinforcement joints on the static tensile strength of flat laminates is only small. This is substantiated by biaxial stress static failure results from cylinders where joint failures were not predominant. It is concluded that true cylinder failure strengths were reached and that confidence can be put in the results. The static flat laminate results suggested a joint effect on the onset of resin cracking which agrees with Bishop (38) who indicated that stress concentrators were more effective at initiating damage than catastrophic failure. Owen and Found (6) have shown that the static resin cracking stress of $38MNm^{-2}$ for cylinders under R = 0 was 25% below that for flat laminates under uniaxial tension. It appears that this effect was caused by joints since the value of $38MNm^{-2}$ compares well with G8 flat laminate results shown in Table 7. Joint effects on the initial and secondary tensile modulii of flat laminates were negligible because the joint is a local defect.

Maximum joint effects were seen in fatigue loading. The magnitude of the effect on flat laminates under zero-tension fatigue loading varied with joint position and joint orientation but in all cases it was severe. Examination of Figs 34 - 36, 42 and 48 shows that only very few fibres cross the resin rich joint zone, hence joint crack propagation has no barrier in the jointed layer and hence premature catastrophic failure occurs. Bishop (38) has shown that a 20mm length butt joint in one layer of a 3 - layered laminate under fatigue loading is equivalent to an initial defect size of 8 - 10mm length passing completely

through the thickness. Extrapolating this result to a larger scale reveals that a 1m width joint is equivalent to a 400 - 500mm through the thickness crack. Bishop (38) concludes that a crack of this length in a large plate subjected to a zero-tension fatigue stress level equivalent to that required to produce debonding in a plain specimen would produce failure after only 1800 cycles. Joints lying parallel to the loading axis also produced fatigue strength reductions. No real explanation can be forwarded for this although Ashbaugh (52) indicates that a broken layer in a composite severely affects the stress distribution in other layers for a material such as C.S.M. and hence this should be an initial consideration in further investigations of parallel joint effects. The effect of joints in zero-compression fatigue loading was not determined but it should be negligible because the onset of resin cracking occurs very close to ultimate failure (1, 6) and this, coupled with the crack closing mode of compression loading, indicates that joint crack propagation would be insignificant. The fatigue results on jointed laminates have real significance especially if designers specify a heavier gauge mat to reduce the number of layers and keep the same component size. Reinforcement joints in structures are inevitable since there is a finite reinforcement width and hence careful thought must be given to the positioning of joints if premature catastrophic failure is to be avoided. The above results are substantiated by biaxial stress fatigue tests on cylinders where joint failures were found to predominate. The fatigue anomaly shown by Found (1) has thus been explained.

A mineral oil environment appears to improve the fatigue strength slightly at 10^6 cycles possibly because of moisture exclusion (51) or because of a lubricating effect at the glass-resin interface after the onset of damage.

The significance of stress concentrators in crack initiation was shown by cracks radiating from voids in resin rich cylinder bores which could propagate under fatigue loading. This void effect was not seen in flat laminates since the outermost laminate regions are not as resin rich as in cylinders because excess resin can be easily 'rolled out' during the flat laminate manufacturing process.

The biaxial stress static failure behaviour of C.S.M. is best described by those failure theories containing a floating constant, i.e. the modified Marin, the Tsai and Wu and the Gol'denblat and Kopnov theories, as shown by Owen and Found (6). However, the Norris Failure theory would be acceptable in the absence of complex stress data. Joint effects were found to be negligible under static loading and hence the results are considered valid.

For fatigue loading at 10^6 cycles, biaxial stress test results by different operators did not correlate in the tension-tension stress quadrant. Examination of Found's and the author's biaxial tension fatigue specimens suggested no reason for this discrepancy, the damage intensity of all specimens being very high in the fatigue loading mode. Correlation between data is acceptable in the tension-compression quadrant and with due allowance for joint effects confidence can be put in the results. Since

the data in the first quadrant are suspect then useful failure theory prediction is severely restricted and the modified Marin theory, using a k_2 value from each stress quadrant, produces the only generally acceptable data fit.

6.2 Y449 Fabric-reinforced polyester resin test results $\alpha = 0^{o}$

The results presented in this section are for an orthotropic composite with an off-axis angle (α) of 0^{o}, i.e. the loading axes and material axes coincide, and the in-plane shear stress, σ_6, associated with principal material direction stresses σ_1 and σ_2 is zero. The composite is specially orthotropic since the normal - shear coupling compliances are zero (see Table A4).

Tables 10 - 13 summarise the test data, individual results are presented in progress reports submitted to Dr. M.J. Owen.

6.2.1 Uniaxial static flat laminate results.

Uniaxial tension was the only static loading mode investigated and the results are summarised in Table 10. Maximum, minimum and mean values are presented for the author's data from 5-layered laminates (G12) and results along a line do not necessarily correspond. Five-layered laminates were used for consistency with cylinders. Data by Found (1) and Bishop (38) from 7-layered laminates are also presented for comparison purposes. A glass content estimate for the author's specimens is given in Table 10. This was derived from Fig. 53 showing the glass content variation with thickness for 5-layered laminates. A comparison of the damage stress levels, shown in Table 10, determined by the author, Found and Bishop reveals discrepancies. These are probably due to differences between resin batches, operator differences in laminating technique and in damage observation. A comparison of the failure strength shows that the author's data is below Found's and

Bishop's but this is due to glass content.

Table 10 shows that a lap-joint has a small effect on static tensile strength. This is because 4 of the 6 reinforcement layers were continuous, as shown in Fig. 30, and just prior to failure the 'overlap' layer delaminated and hence the load was redistributed over the remaining layers causing premature failure. There is no joint effect on the static tensile moduli. Fig. 54 shows untested and tested samples of laminate G13 which have been surface ground, etched in hydrofluoric acid for 1.75 minutes, and stained with black ink. The lap-joint region is clearly visible and shows the resin rich zone at the end of the reinforcement. The tested sample was loaded in static tension until joint cracking occurred and the long joint crack is readily discernible. Table 10 shows that joint cracking occurred after the onset of resin cracking and Fig. 54 substantiates this by showing that the joint crack is not the only crack in the specimen. It is concluded that lap-joints have a negligible effect on uniaxial static tensile properties.

6.2.2 Biaxial stress static test results.

Results were obtained in the first and second stress quadrants, from R = +1 to R = -1, for resin cracking and ultimate failure and they are summarised in Table 11. When the off-axis angle (Θ) is 0° then σ_1 and σ_2 are equal to the hoop and axial stresses σ_x and σ_y respectively.

A comparison of Tables 10 and 11 shows that cylinders tested at R = 0 yield 20% higher ultimate strengths than non-jointed 5 - layered flat specimens tested under the equivalent loading conditions of uniaxial tension. This

is probably due to the absence of edge effects in cylinders (49) even though a joint is present. By such considerations the cylinder is considered to be the ideal characterisation specimen (2, 49). Similarly, the resin cracking stress at R = 0 and the ratio of resin cracking stress to ultimate failure stress was higher than for flat specimens. Again this could be due to the absence of edge effects since damage in flat specimens is edge initiating.

Fig. 55 presents the static biaxial stress test data. There is a slight difference between actual and nominal R ratio due to friction in the ram units (1) and subsequent references to the magnitude of R refer to nominal values unless otherwise stated. Scatter in the data is low apart from resin cracking results at R = -1. The ultimate strength decreases quite markedly in the tension-compression quadrant as the axial stress is increased, whereas in the first quadrant only a small biaxial stress effect is suggested. The resin cracking results indicate the reverse effect to failure although scrutinisation of the data shows little correlation between R = 0 and results at other stress ratios. This suggests that the R = 0 results are suspect although no reason can be forwarded and the scatter in results at this stress ratio is very low.

Fig. 56 shows the relationship between mean resin cracking stress and the stress levels at which joint cracking occurred. Mean resin cracking stress is presented in preference to the individual results shown in Fig. 55 to avoid confusion since in some cases joint cracking and resin cracking occurred simultaneously. It appears from the

results that joint cracking is more hoop stress level than stress ratio dependent. Joint cracking occurred at similar stress levels to resin cracking and it is thus concluded that the effect of joints on static strength is expected to be small, as for flat laminates, and of a similar magnitude at all stress ratios. Fig. 57 shows the lap-joint region on the bore of an untested cylinder that has been internally ground, etched with hydrofluoric acid and stained with black ink. Comparison of Figs. 54 and 57 shows the excellent simulation of cylinder joints obtained in jointed flat laminates. Fig. 57 also shows a joint crack, occurring in a cylinder tested at R = 0 under static loading, which spans the full specimen gauge length. Joint cracks always occurred along the resin rich joint seam i.e. at 90^{o} to the hoop stress.

As shown in Tables 1 and 2, the prediction of behaviour by failure theories for $\sigma_6 = 0$ requires a knowledge of the principal tensile strengths X and Y and the principal compressive strengths X' and Y'. Found (1), and Owen and Found (35), have shown that Y449/polyester resin laminates have equal uniaxial tensile and compressive ultimate failure strengths in both fibre directions. This was not confirmed by the author although an attempt was made to determine the ultimate compressive strength of 5-layered cylinders, as shown in Table 11, but the results were invalid due to premature failure at the specimen ends. Thus, for failure theory prediction, strengths at R = ∞ and $-\infty$, i.e. at $\sigma_1 = 0$, have been assumed equivalent to the R = 0 ultimate strength i.e. X=Y=X'=Y' = (R = 0 strength). Comparison between mean ultimate strength test

data and predicted failure envelopes is given in Fig. 58. The letters denoting the various failure theories are defined in Tables 1 and 2. The maximum stress theory (A) is inadequate in predicting the failure behaviour over two stress quadrants of an orthotropic material. The most acceptable prediction of static failure is by the Norris Failure theory (D), which in the first quadrant shows a maximum deviation between theoretical and experimental data of 8% at R = +1 and in the second quadrant yields a conservative prediction although not conservative enough to inhibit a designer from realising the full material potential. The Tsai and Wu (I), Gol'denblat and Kopnov (H), and modified Marin (G) theories also provide a good prediction. The modified Marin envelope deviates from that of the tensor theories in the second quadrant because two values of the floating constant k_2 were determined, one for each quadrant, and hence the envelope is discontinuous.

The magnitude of the interaction tensor component F_{12} was determined from experimental data at R = +1, (actual value R = +0.96). Fig. 59 shows the variation of F_{12} with experimentally measured hoop strength for each actual R ratio. Over the range of strengths obtained, and R ratios investigated, data at R = +0.96 yields the most sensitive F_{12} determination method, i.e. that method producing the least change in F_{12} with change in strength, and hence yields the most accurate prediction possible by the tensor theories from the data available. Constant k_2 of the modified Marin theory was selected by a similar procedure to F_{12}, data at R = +0.96 and -0.43 being chosen to determine k_2 for the first and second quadrants respectively.

Fig. 61 compares mean experimental static resin cracking data with the behaviour predicted by failure theories. For prediction purposes the R = ∞ resin cracking strength, i.e. Y, was assumed to be equivalent to that at R = 0, i.e. X, since Found (1) has shown that flat laminates with off-axis angles of 0° and 90° have similar resin cracking stress levels under uniaxial tensile loading. The R = - 0 and R = $-\infty$ resin cracking strengths, i.e. X' and Y', were assumed to be equivalent to the ultimate compressive strength because in the test on cylinders under uniaxial compression loading, as shown in Table 11, no resin cracking was seen prior to failure. Furthermore, if the resin cracking strength at R = $-\infty$ is estimated from flat laminate data and correction factors applied to account for the higher cylinder strengths then the resulting stress level is greater than the expected ultimate compressive strength. It could be that true compressive failure strengths have not yet been obtained or that the damage and ultimate failure envelopes intersect, i.e. that failure occurs before damage over a limited region of the second stress quadrant and hence the resin cracking 'failure' envelope would not necessarily cross the reference axes at R = $-\infty$. Fig. 61 shows that the modified Marin theory provides the most acceptable prediction by using a k_2 value determined from each stress quadrant. However, none of the theories are really adequate because no acceptable correlation exists between the data at R = 0 and that at other stress ratios. Assuming that the R = 0 data is optimistic indicates that the maximum stress boundary may well provide a good data fit although there is no reason

to suspect this data since the scatter in individaul results was very low.

F_{12} for the tensor theories was determined from data at R = -1, (actual value R = -0.87). Fig. 60 shows the F_{12} variation with hoop strength for resin cracking, similar to Fig. 59 for ultimate failure, and indicates that within the stability boundary data from R = -0.87 or R = +0.95 yield similar F_{12} sensitivity. Constant k_2 for the modified Marin theory was determined from data at R = +0.95 and -0.87 for the first and second quadrants respectively.

6.2.3 Uniaxial zero-tension fatigue results.

For reasons discussed in section 5.1.3.2 fatigue tests were performed on 5-layered laminates in normal and oil environments and on specimens containing lap-joints. A summary of the ultimate failure fatigue data is given in Table 12. Individual results are shown in Figs. 63, A15 and A16.

Fig. 62 compares ultimate failure fatigue results from type C contoured specimens (see Fig. 28). An oil environment has no adverse effect on the fatigue behaviour and at long lives a strengthening effect is indicated, as seen for C.S.M, which could be due to either moisture exclusion or to a lubricating effect at the glass-resin interface. There is a discrepancy between Found's results from 7-layered specimens and the author's data which could be due to glass content differences although the effect of glass content on the fatigue behaviour of this material is unknown. Another possibility is based on a statistical argument similar to that discussed by Scop and Argon (54).

They have shown that laminate strength is above that of a single lamina because of the shear action of the resin between laminae and that the laminate strength increases and the strength distribution decreases with an increasing number of laminate layers.

Fig. 63 shows ultimate failure fatigue results from parallel sided specimens utilising the lap-joint construction. This specimen type was used to allow a similar applied stress condition to exist in both the joint and overlap regions. Scatter in the results is very low because the failure site was similar for most specimens i.e. in general specimens failed through the thickness in the jointed region i.e. at X-X in specimen D of Fig. 28. Fig. 63 also shows results from plain parallel sided specimens for comparison with jointed laminate results, and R = 0 cylinder data which is presented in more detail in Fig. 65. Jointed laminate results and R = 0 cylinder results correlate exceptionally well indicating that the jointed laminates provide a good simulation of the R = 0 cylinder condition. A discrepancy exists between plain and jointed laminate results at 10^3 cycles which reduces to zero at 10^6 cycles. This indicates that lap-joint effects in composites utilising continuous reinforcements are stress level dependent i.e. at low stress levels and long fatigue lives joint effects tend to zero. This is the reverse of the C.S.M. case where no barrier to joint crack propagation exists.

A comparison of resin cracking fatigue data from 5 and 7-layered laminates is given in Fig. 64. The criterion of 'onset of damage' used by Bishop (38) was the

first sign of resin cracking occurring at the specimen edge, these cracks generally being the first to appear in the specimen. The criterion used by Found (1) and the author was resin cracking occurring away from the specimen edge. A difference exists between results from 5 and 7-layered laminates. It should be remembered that damage results are influenced to some extent by operator expertise and technique and this could account for some of the discrepancy. Other possible reasons are differences in resin batch, and statistical strength distributions (54). Fig. 64 shows that the discrepancy between the data sets decreases at long fatigue lives. Owen and Rose (68) have shown that resin flexibiliser additions delay the onset of resin cracking in fatigue loading at 10^3 cycles but at fatigue lives of 10^5 and 10^6 cycles the effect is insignificant and hence slight resin batch differences may have caused the discrepancy in Fig. 64. Due to an increasing strength distribution with a decreasing number of laminate layers (54) then there is a possibility that resin cracking would initiate from a particular layer earlier in the 5-layered case. It was noticed that damage tended to initiate from the first reinforcement layer, i.e. the first layer during the manufacturing process, which tends to substantiate the above argument.

6.2.4 Biaxial stress fatigue test results.

Results were obtained for resin cracking and ultimate failure at five biaxial stress ratios (R). A summary of the data is given in Tables 13 and 14, individual results being shown in Figs. 65, 66 and A17 - A19.

Typical fatigue curves are presented in Figs. 65

and 66. Static data and scatter bands are plotted at the ¼ cycle position. The scatter in fatigue results is very low considering that there are approximately 15 individual results associated with each fatigue curve. All ultimate failure curves are Least Squares regression lines with strength considered the dependent variable, whereas the damage curves were fitted by eye.

Fig. 67 compares ultimate failure fatigue results at various R ratios. The R = +1 curve has a severe gradient which is difficult to explain. All the specimens tested under biaxial tension and at R = 0 were joint failures, i.e. failure occurred at 90^{o} to the hoop stress along the lap-joint seam. Examination of the R = +1 specimens showed that, apart from in the region of fracture, none of the 'opaque damage' associated with the fibre cross-over points in woven fabric materials, seen under zero-tension fatigue loading of flat laminates and R = 0 fatigue loading of cylinders, occurred. Hence, it appears that the lap-joint has a more severe effect under equal biaxial tension than R = 0 and this could explain the severity of the fatigue curve.

Fig. 68 shows a constant life diagram for ultimate failure. In the tension-compression quadrant the results show a great similarity to the static behaviour, i.e. a marked decrease in hoop strength with increasing axial compression, at all fatigue lives up to 10^{6} cycles. In the tension-tension quadrant similarity with static behaviour is seen at 10^{3} and 10^{4} cycles but at longer fatigue lives the results indicate that biaxial tension loading at R = +0.5 enhances the fatigue strength. If this behaviour change is

a consequence of lap-joint effects then it indicates that joint effects under biaxial tension are stress level and not necessarily stress ratio dependent and that the true strength of specimens at R = +0.5 is being approached at long fatigue lives. A failure mechanism change could produce a similar result but failures up to 10^6 cycles were joint failures.

A comparison of experimental data at 10^6 cycles with predicted behaviour from failure theories is given in Fig. 69. The letters denoting the failure theories are defined in Tables 1 and 2. As discussed in section 6.2.2, and shown in Tables 1 and 2, the principal strengths X, X', Y and Y' need to be known for failure theory prediction. Principal tensile strengths X and Y were assumed to be equivalent to the R = 0 hoop strength at 10^6 cycles since Found (1) has shown that flat laminates with off-axis angles of 0^o and 90^o have equivalent zero-tension fatigue strengths. Since no cylinder tests were performed at R = $-\infty$ then the principal compressive strengths X' and Y' were estimated from Found's zero-compression flat laminate fatigue results by the following equation :-

$$X' = Y' = \left(\frac{A}{B} \cdot X \right) \text{ at } 10^6 \text{ cycles}$$

where A and B refer to the zero-compression and zero-tension fatigue strengths respectively. Fig. 69 shows that the tensor theories (H, I) provide the most useful overall prediction of behaviour. The interaction tensor component, F_{12}, was determined from data at R = +1. The modified Marin (G) envelope is discontinuous since two k_2 values were determined, one from data at R = +1 and one from data at R = -0.5, and the prediction in the second quadrant is not as accurate

as that of the tensor theories. If only one k_2 value, from R = +1 data, was determined for the complete failure envelope then the prediction would be similar to that provided by the tensor theories. Choosing R = -1 data to determine the second quadrant k_2 value would have resulted in a most acceptable overall prediction but this would have violated the k_2 and F_{12} selection procedure discussed in sections 2.1.2.3 and 6.2.2. Of those theories not requiring complex stress data for prediction purposes the Norris Failure theory provides a good mean data fit.

A comparison of resin cracking results is given in Fig. 70. All biaxial stress ratios yield very similar results considering the amplified ordinate. The most disturbing factor is the very low stresses at which damage occurs, e.g. R = 0 results show a fatigue strength of only 25% and 8.5% of the static resin cracking strength at 10^3 and 10^6 cycles respectively. The stresses are too low for design purposes and this suggests that an intermediate damage state or an acceptance of a certain amount of resin cracking would have to be the design criterion. A discrepancy exists between R = 0 data and zero-tension flat laminate data as shown in Fig. 70. However, an explanation can be forwarded. The internal pressure cycle applied to the cylinders is not between zero and maximum pressure but is between a fairly constant low magnitude base pressure and maximum. The hoop stresses are computed as range stresses i.e. the difference between base and maximum stress. For resin cracking, the internal pressures and hence hoop stresses are very low and thus the base pressure is a significant percentage of the maximum pressure, i.e. for R = 0

this percentage is approximately 15% and 35% at 10^3 and 10^6 cycles respectively. Increasing the R = 0 results by above percentages yields good correlation with the zero-tension fatigue data.

The criterion of 'onset of resin cracking' was not joint cracking but cracking occurring in other regions of the specimen. Joint cracking occurred at 90^o to the hoop stress along the joint seam as discussed in section 6.2.2. As the axial stress became more compressive there was a decreasing tendency for the first crack to appear to be a joint crack. At R = 0, the first crack to appear was always a joint crack, whereas at R = +0.5 and +1 this was not always the case. It appears that joint cracking is stress level and not necessarily stress ratio dependent as found for static loading.

A constant life diagram for the onset of resin cracking is shown in Fig. 71. The behaviour is similar to that in static loading as shown in Fig. 61 especially if the R = 0 static results are considered to be suspect as discussed in section 6.2.2. Since the stresses are so small and since (a) the fatigue curves of Fig. 70 show only a small biaxial stress effect and (b) the curves were fitted by eye then it is possible that the behaviour could be described at all fatigue lives by a straight line parallel to the σ_2 axis. This has not been shown on Fig. 71 because the behaviour between R = -1 and R = $-\infty$ is unknown and curves predicting a more conservative trend in the tension-compression quadrant were chosen.

A comparison between mean experimental resin cracking data at 10^6 cycles with predicted failure envelopes

is given in Fig. 72, the letters denoting the failure theories being defined in Tables 1 and 2. For prediction purposes, the principal tensile strengths X and Y were assumed to be equivalent to the R = 0 strength. The compressive strengths X' and Y' were computed from the equation given earlier for ultimate failure, but in this instance factors A and B refer to the zero-compression and zero-tension resin cracking fatigue strengths respectively. The tensor theories (H, I), modified Marin (G) and Norris Failure (D) theories all provide an acceptable prediction. Constant k_2 for the modified Marin theory was evaluated from R = +1 and R = -1 data for the first and second quadrants respectively, and constant F_{12} was derived from R = +1 data since R = -1 data, as used for the static case, violated the F_{12} stability condition. However, the virtually negligible biaxial stress effect, increased to some extent by the amplified axes, indicates that the maximum stress theory (A) would provide an acceptable prediction over the range of data obtained.

6.2.5 Appearance of biaxial stress failures.

Typical static failures are shown in Fig. 73, the card against each cylinder denoting the biaxial stress ratio. The failures at R = 0, +0.5 and +1.0 were hoop tensile failures i.e. the fracture path was along the cylinder axis and at 90° to the hoop stress.

Failures at R = -0.5 and -1.0 were combined hoop tensile and axial compressive failures. The axial compressive failure became more marked and the hoop tensile failure became shorter as the axial stress increased as shown in Fig. 73, indicating that between R = -1.0 and

R = -∞ the axial compressive mode would be the dominant failure. Since combined failures were seen at R = -1.0 this gives confidence to the assumption of section 6.2.2 that the R = 0 and R = -∞ ultimate failure strengths were equivalent.

The hoop tensile failures at R = 0, +0.5, +1.0 and -0.5 were joint failures i.e. they occurred along the joint seam at 90° to the hoop stress. Scrutinisation of the R = 0 failure in Fig. 73 reveals a line of opaque damage, parallel to the cylinder axis, extending from the top of the failure line to the end of the gauge length. This is delamination of the lap-joint on the cylinder bore. At R = -1.0 not all of the hoop tensile failures were joint failures. For the R = -1.0 specimen shown in Fig. 73 the hoop tensile failure occurred close to the overlap region on the cylinder circumference and was not a joint failure.

All specimens show intense mushroom-shaped opaque damage regions around the hoop tensile fracture path. The narrow sections of the mushroom-shaped regions are probably where fracture initiated, which then propagated causing delamination of the reinforcement layers due to the strain energy release.

Under fatigue loading the fracture appearance was similar except at R = -1.0. Here, failures tended to be of the axial compressive type indicating that the R = 0 and R = -∞ fatigue strengths are not equivalent, i.e. that R = 0 strength > R = -∞ strength. This conflicts with the assumption of section 6.2.4. where for failure theory prediction the R = -∞ strength was estimated from flat

laminates to be slightly greater than the R = 0 strength, i.e. at 10^6cycles R = 0 strength = 60.41 MNm^{-2}, R = $-\infty$ strength = 64.8 MNm^{-2}. All failures at R = 0, +0.5 and +1.0 were joint failures whereas only some of the R = -0.5 specimens failed in this way and the R = -1.0 failures were of the axial compression type.

Fig. 74 shows the difference between static and fatigue damage at R = 0, +1.0, -1.0. Samples were machined from ultimate failure test pieces and the cylinder bores were examined, using transmitted light, on the macro setting of a Vickers M41 microscope. All magnifications were x10. At R = +1.0 cracks occur in both principal material directions, due to the axial and hoop tensile stresses, with similar intensity. The degree of resin cracking in both static and fatigue specimens is similar probably because of (a) the high stresses sustained under static loading, and (b) the fact that later damage states, such as 'opaque damage' at the fibre cross-overs, were not seen in fatigue loading at R = +1.0 because it seems that premature joint failure may have occurred. At R = 0, resin cracks can be seen at 90° to the hoop stress. The resin cracking intensity is much greater in fatigue loading although debonding damage, denoted by the fine dark lines, appears to be more intense under static loading. No explanation can be forwarded for this. At R = -1.0 the severe buckling damage at the fibre cross-overs due to the axial compressive load is clearly visible in both static and fatigue loading as dark diamond-shaped areas. The intensity of these buckled regions is greater under fatigue loading and resin cracking is more severe and of

a finer nature. Resin cracking is seen to be associated with the fibre cross-over points possibly because of the tensile stress concentrations arising in these regions due to the fibre crimp (55).

6.2.6 Discussion of Y449-fabric results, $\sigma_6 = 0$, $\Theta = 0^\circ$.

The effect of 'Tellus 15' mineral oil at atmospheric pressure on the zero-tension fatigue behaviour of flat laminates was determined in order to assess the influence of the internal pressurising medium on biaxial stress fatigue results from cylinders. No detrimental effect was observed on flat laminates, and in fact a slight enhancement of fatigue strength was indicated at long lives. The likely cause of this is a combination of (i) moisture exclusion (51), (ii) lubricating effects at (a) the glass-resin interface, and (b) the glass roving to roving contact points thus reducing the number of micro-flaws initiated and hence enhancing the fatigue strength. It is thus concluded that, although the effects of pulsating pressure have not been established, the influence of the internal pressurising medium on biaxial stress fatigue results from cylinders is negligible.

To estimate lap-joint effects in cylinders the behaviour of similarly constructed flat laminates was determined under both static and zero-tension fatigue loading. Excellent simulation of cylinder construction was achieved as shown by comparison of Figs. 54 and 57. The test results show that the lap-joint has a small effect on static ultimate tensile strength, because of the failure mode discussed in section 6.2.1 and possibly because of

joint stress concentration effects, but a negligible effect on the zero-tension fatigue strength at 10^6 cycles. Thus, the difference in fatigue behaviour between lap-jointed fabric reinforced laminates and butt-jointed C.S.M reinforced laminates is quite distinct. As shown in section 6.1.3 and Figs. 34-36, 42 and 48 very few fibres cross the resin rich joint zone in jointed C.S.M. laminates, hence joint crack propagation has no barrier and thus joint effects become more severe with increasing fatigue life. For lap-jointed fabric laminates, even though long joint cracks occur along the resin-rich lap-joint seam as shown in Fig. 54, Bishop (38) has shown that it is very difficult to propagate cracks transverse to the fibre directions in a continuous composite, and hence joint effects would have a stress level rather than cyclic dependency. This view was substantiated by the biaxial stress tests on cylinders where joints appeared to be stress level rather than stress ratio or cyclic dependent. Biaxial tensile stresses appear to produce greater fatigue joint effects than a uniaxial tensile stress but this decreases with the magnitude of the axial tensile component.

Correlation between lap-jointed flat laminates under zero-tension fatigue loading and R = 0 cylinder data is excellent and hence joints appear to explain the discrepancy shown in Fig. 63. However, under static tensile loading the jointed laminate ultimate strength is only 70% of the R = 0 cylinder strength. This discrepancy extends to resin cracking where the static tensile resin cracking stress is only 60% of the equivalent cylinder data but in fatigue loading the two specimen types yield comparable

results. Due to the absence of edge effects the cylinder is the most desirable characterisation specimen (2, 49 69) and would yield somewhat higher mean strengths than flat laminates. Since joints have only a small effect on static loading then the above argument would explain the discrepancy in this loading mode. For ultimate failure in fatigue loading joints caused the similarity between flat laminate and cylinder behaviour by inducing premature cylinder failure. This is substantiated by the fact that the intensity of later damage stages such as 'opaque damage' at the fibre cross-overs was not as great in cylinders as in flat laminates and hence true cylinder strengths were not achieved as a consequence of a predetermined failure path. This evidence suggests that non-jointed cylinders would be stronger than flat laminates in the fatigue loading mode. The similarity in fatigue behaviour for the onset of resin cracking between flat laminates and cylinders is explained on the basis that there are more initial defects in a cylinder because of the greater volume of material and these would yield a maximum effect on fatigue damage.

Differences between flat laminate and cylinder results could also be due to specimen thickness measurements. The cylinder wall thickness was computed by subtracting the mean of five circumference measurements from the mean of 3 bore measurements and dividing the result by 2. An experiment was performed to assess the accuracy of this method. A cylinder was measured by the above method using standard and internal micrometers. A ring of material was then removed from the central region of the cylinder gauge length and cut into five sections. The thickness of each section was measured

using a micrometer and the mean thickness was computed. The difference in mean thickness obtained by both methods was within 1% and it was thus concluded that the method of measuring the circumference and the cylinder bore was acceptable. However, in the joint region six reinforcement layers are present due to the overlap layer and hence the thickness in this region is approximately 10% greater than the mean. Thus, the large differences in static strength between cylinders and flat laminates could in part be due to this.

Dimensional changes would also affect cylinder results within and between specimens tested at different stress ratios. The effect here would be less than between flat laminates and cylinders because the method of thickness measurement would be constant. However, Figs. 55, 65, 66 and A17 - A19 shows that scatter in the data is very low which reflects the quality of cylinder dimension control and measurement. Internal pressure could be used as a comparator in place of hoop stress, hence eliminating errors due to dimension measurement, but before this could be done it has to be shown that failure pressure and the failure load of flat laminates, is independent of thickness over a small thickness range. However, since thickness is related to glass content this has proved impossible.

The biaxial stress test results show a marked decrease in ultimate strength in the tension-compression stress quadrant under both static and fatigue loading. The behaviour is similar to that found for a linen-weave fabric reinforcement by Protasov and Kopnov (27) under static loading. In the tension-tension stress quadrant no

real stress ratio effect was observed in static loading but the fatigue mode indicates a change in behaviour. At 10^3 and 10^4 cycles the behaviour is similar to the static mode but at 10^5 and 10^6 cycles the results indicate that R = +0.5 loading enhances the fatigue strength. It is thought that this is because the axial tensile stress has dropped below the threshold level at which biaxial tension joint effects occur at R = +0.5 and hence true failure strengths are being approached. Results at 10^7 cycles would indicate whether this effect is seen at R = +1 and if this were the case then the data would follow a pattern similar to that predicted by Von Mises type failure theories.

For the onset of resin cracking under static loading no real correlation exists between R = 0 data and data at other stress ratios although no explanation of this behaviour can be forwarded. For fatigue loading the most striking characteristic of the data is the very low stress level at which resin cracking initiated at all stress ratios. It is thus concluded that the use of the onset of resin cracking as a fatigue design criterion would be very restrictive and components would have to be unreasonably massive unless some degree of damage was acceptable. However, in certain applications such as container and pressure vessels resin cracking cannot be tolerated and hence careful thought must be given to design considerations in view of the above results.

As discussed in section 6.2.2 no resin cracking was observed in the invalid static uniaxial compression tests on cylinders and estimating the uniaxial compressive resin cracking strength from flat laminates yielded a value

above the estimated ultimate strength. It is thus possible that the failure envelopes describing damage and ultimate failure intersect i.e. that failure occurs before damage somewhere in the tension-compression quadrant between R = -1 and R = $-\infty$. Fig. 75 shows experimental failure envelopes for static damage and ultimate failure. The ultimate failure results follow a well defined pattern and thus the failure envelope shape is easily assessed. However, two out of a number of possibilities for the damage envelope are shown. The curved surface assumes that the R = 0 data is correct whereas the rectangular envelope assumes that the R = 0 data is suspect and the best line of fit has been drawn through the remaining data. Assuming that the damage envelopes intersect the $-\sigma_2$ axis then the rectangular envelope predicts that failure will occur without prior resin cracking over a small region of the tension-compression quadrant. Hence, two envelopes, i.e. the damage envelope and the region of the ultimate failure envelope between the intersection with the damage envelope and R = $-\infty$, are required to describe damage 'failure'. It is possible that no damage is observed in a valid uniaxial compression test on a cylinder prior to failure in which case the damage envelopes would be open-ended, i.e. they would not intersect the $-\sigma_2$ axis. A similar set of curves is shown for fatigue loading in Fig. 76. It is possible that the point of intersection of the curved damage envelope with the $-\sigma_2$ axis is incorrect. This value was estimated from flat laminate data as discussed in section 6.2.4, but the photograph in Fig. 74 showing the damage occurring in an ultimate failure specimen tested at

R = -1 indicates that no cracking has occurred due to the axial compressive stress. Thus, the R = $-\infty$ point is possibly suspect and damage could be described by a rectangle that intersects the ultimate failure envelope between R = -1 and R = $-\infty$. One implication of the above results is that if damage is used as a design criterion then failure could occur before resin cracking is observed. However, scrutinisation of Figs. 75 and 76 shows that the failure envelope intersection points are quite close to the $-\sigma_2$ axis and hence it seems likely that design safety factors would automatically account for this effect. The above is pure conjecture but it is possible. The behaviour of the material between R = -1 and R = $-\infty$ needs experimentally verifying because the above is only true if the threshold value of hoop stress required to initiate damage is constant at all biaxial stress ratios between these two values.

The Norris Failure theory provides the most accurate prediction of static ultimate failure behaviour. The tensor and modified Marin theories are also acceptable but the Norris Failure theory does not require data from complex stress tests before predictions can be made. It was shown in section 6.2.5 that since combined hoop tensile and axial compression failures occurred at R = -1 in static loading then confidence can be put in the assumption that the principal tensile and compressive ultimate strengths are the same. Thus, the above conclusions on failure theory predictions are considered to be valid. For ultimate failure at 10^6 cycles the tensor theories provide the most acceptable prediction but the Norris Failure theory provides

a good mean data fit. However, from earlier discussions of the R = +0.5 behaviour at 10^6 cycles it appears that the data in the biaxial tension quadrant is possibly not depicting the true behaviour because of biaxial tension joint effects. In addition as discussed in section 6.2.5, the combined hoop tensile and axial compression failures observed in static loading at R = -1 were not seen in fatigue loading where the specimens failed in the axial compression mode. Thus, it seems the assumption that the principal compressive strengths are greater than the principal tensile strengths, as discussed in section 6.2.4, is invalid and that the reverse is true. The trend in the tension-compression quadrant in Fig. 69 tends to substantiate this view although the only method of verification is by performing uniaxial compression fatigue tests on cylinders.

For static resin cracking, data correlation between R = 0 and results at other stress ratios was poor and hence failure theory prediction is somewhat inhibited. The modified Marin theory provided the only acceptable prediction by using two values of constant k_2, one determined from data in each stress quadrant. As found for C.S.M. at 10^6 cycles ultimate failure, two values of k_2 can successfully account for behaviour differences because the envelope has to pass through data points in each stress quadrant as well as intersect the reference axes at the principal strengths. Using two or more k_2 values can lead to a loss of flexibility since data is required in each stress quadrant but by doing this different failure modes can be accounted for. At 10^6 cycles, the tensor, modified

Marin and Norris Failure theories all provide good predictions of behaviour, but since the data were so similar at all stress ratios the maximum stress theory is equally acceptable over the range of data available and in the limit of human error.

As discussed in section 2.1.2.3, the tensor interaction component F_{12} and constant k_2, can be determined from any complex stress test. One such test is the 45^{o} off-axis uniaxial tensile test which produces a stress state in the fibre directions of $\sigma_1 = \sigma_2 = \sigma_6 = \sigma/2$ where σ= applied uniaxial tensile stress. Figs. 59 and 60 show that this test, denoted as '45^{o} off-axis R = O' in the figures, is a very insensitive method of determining F_{12} for this material and should be avoided because a small change in experimental strength produces a large F_{12} change, and hence the effect of experimental scatter in off-axis tensile test results would be to produce enormous changes in the predicted Tsai and Wu and Gol'denblat and Kopnov failure envelopes. Figs. 58, 59, 60 and 72 show that F_{12} can sometimes be successfully determined from data at R = +0.5. This is the easiest biaxial stress condition to obtain in thin walled tubes since it only requires internal pressure and hence is a relatively inexpensive test method which could be used by designers to estimate F_{12}.

6.3 Off-axis and in-plane shear results from Y449-fabric reinforced polyester resin composites.

6.3.1 Introduction.

As discussed in section 2.1.1, a three-dimensional (3-D) failure surface with reference axes σ_1, σ_2 and σ_6 is required to geometrically represent the plane stress

behaviour of an orthotropic material. Stresses σ_1 and σ_2 are normal stresses acting in the principal material directions, and σ_6 is the in-plane shear stress associated with σ_1 and σ_2. This 3-D failure surface is evaluated experimentally by off-axis uniaxial, biaxial and torsion tests as discussed in section 2.2 and as shown in Table 4 and Fig. 15. Complete surface evaluation for static and fatigue loading is time consuming and uneconomic, and hence a compromise has to be made and tests selected that determine important surface sections. The results described in section 6.2 were for the special case where $\sigma_6 = 0$ and these data determined segment AFJDLEC of Fig. 15. The data presented in section 6.3 are 45° off-axis uniaxial and biaxial stress static and fatigue results which determine segment FKGNB of Fig. 15, 15° and 30° off-axis biaxial stress static results at R = -1 which determine segment EB of Fig. 15, and static and fatigue torsion results for in-plane shear strength determination.

6.3.2 Uniaxial stress test results from flat laminates.

Static tensile test results from 45° off-axis 5-layered flat laminates are shown in Table 15, along with data by Found (1) and Bishop (38) from 7-layered laminates. A comparison of the 45° off-axis data determined by the three operators, using specimen type B shown in Fig. 28, reveals discrepancies similar to those observed for 0° off-axis angle specimens (see section 6.2.1). Discrepancies in damage stress are thought due to resin batch differences, operator differences in laminating technique and in damage observation. Differences between ultimate strength results are due to glass content. Hence, in

general, consistency with other workers was attained.

Found (1), and Owen and Found (35), have presented results showing the variation of uniaxial tensile and compressive strength with off-axis angle for 7-layered Y449-fabric reinforced laminates. Specimens of types A and B shown in Fig. 28 were used in the static strength investigation and the results are given in Table 15. Uniaxial off-axis test data can be used to determine certain sections of the plane stress failure surface. Thus the author wished to use the data given in (1,35) and Table 15 to supplement biaxial stress results given in sections 6.2, 6.3.3 and 6.3.4 and hence construct a more complete experimental failure surface. It was shown in section 2.2, and in Table 4, that by transforming applied uniaxial stresses to the material axes the results can be plotted in terms of σ_1, σ_2 and σ_6. Uniaxial tensile test results treated in this way describe segment AGD of the failure surface of Fig. 15 in σ_1, σ_2, σ_6 stress space, and the uniaxial compression results describe a similar segment but in $-\sigma_1$, $-\sigma_2$, $-\sigma_6$ stress space. The results given in references (1,35) are presented in terms of σ_1, σ_2 and σ_6 in Figs. 77 and 78, and the plan view of the points, on the $\sigma_6 = 0$ plane, is shown in Fig. 79. Since the principal static tensile and compressive ultimate strengths of this composite are equal, as discussed in section 6.2.2, then the failure surface for static ultimate strength is expected to be symmetrical about the reference axes and the tensile and compressive strength curves shown in Fig. 79 should be a reflection of one another. Indeed, failure theories would predict this. However, Fig. 79 shows that

this is not the case. Fig. 80 shows that under static tensile loading the ratio of damage stress to ultimate failure stress increases with off-axis angle (θ), whereas for static compression loading it is essentially constant. Found's results, shown in Table 15, indicate that the variation of resin cracking stress with θ under tensile loading is only small whereas the failure stress decreases markedly. It was observed by Found that under tensile loading the failures changed from tensile to shear types as θ increased from 0° to 45°. For compression loading the failures were inclined at an angle to the central plane of the specimens forming V or W shaped fractures and θ had little effect on the failure mode. Endo et al (70) have shown that specimen width can affect the tensile off-axis strength because of the fibre discontinuity. Table 15 shows that static tensile tests on 19mm wide fatigue type contoured specimens by Bishop (38) produced much higher off-axis strengths than the standard tensile test piece. Hence, it is thought that the failure mode coupled with specimen width effects, and not the progression of damage, are the factors controlling failure and hence the asymmetry between the tensile and compressive off-axis results. Bishop (38) did not perform uniaxial compression tests on the 19mm wide fatigue type specimens, and hence specimen width effects cannot be fully evaluated and no conclusions concerning failure surface symmetry can be drawn from his data. Due to the compression failure mode discussed earlier, it is possible that stresses in the '3' direction influence the behaviour and that a plane stress state does not exist. If this is the case then symmetry between the tensile and

compressive off-axis results is unlikely to be observed.

For resin cracking the asymmetry shown in Fig. 79 is expected because the tensile and compressive principal strengths are dissimilar.

Zero-tension fatigue ultimate failure results from 5 and 7-layered laminates determined by the author and Found (1) respectively are shown in Fig. 81 and summarised in Table 12. A discrepancy exists at 10^3 cycles but at 10^6 cycles the two data sets are comparable. Although the effect of glass content on the fatigue behaviour of this material is unknown, the discrepancy between data sets is thought to be due to this because as shown by Smith (37), for C.S.M. laminates, the effect of glass content decreases with increasing fatigue life.

Found (1), and Owen and Found (35), have shown that the tensile and compressive ultimate failure zero-tension fatigue strengths of this material are similar at 10^6 cycles, i.e. 96.5 and 103.5 MNm^{-2} respectively. However, Figs. 82 and 83 reveal that, as for static loading, the off-axis tensile and compressive fatigue strengths are dissimilar and hence the results indicate an asymmetrical failure surface. Figs. 82-85 show that tensile loading becomes more damaging than compressive loading as the fatigue life increases. These results indicate that for fatigue loading the suggested asymmetry depends on damage state and fatigue life as well as failure mode. The peaks seen in Figs. 83 and 85 at $\theta = 30^\circ$ at short fatigue lives may be due to the normal-shear coupling compliance S_{16} inducing shear and bending stresses into the specimens as a result of rigid clamping and non-rotating grips (2,56).

6.3.3 Biaxial stress static test results.

Test data are summarised in Table 16, individual results being presented in Figs. 86, 88, 89, 91 and 92, and in progress reports submitted to Dr. M.J. Owen.

It was found impossible to remove all the entrapped air from the resin during the manufacture of off-axis cylinders and hence, to determine the effect of void stress concentrators, the stress levels at which resin cracking initiated from air bubbles were noted. In addition, the stress levels at the onset of joint cracking and resin cracking at 90^{o} to the hoop stress were noted, and where possible the stresses at the onset of cracking in the principal material directions were recorded. The number of specimens used to examine each damage state at each biaxial stress ratio (R) appears to be inconsistent as shown in Table 16. This is because 4 and 5 specimens were used for damage and ultimate failure experiments respectively at each R ratio, and damage results were also noted from 'failure' test pieces. Since the damage data agreed closely from both specimen sets, mean values were taken, and hence where '9' specimens appear in Table 16 this indicates the mean of all the test pieces. Where specimen numbers of less than 9 appear this indicates that the particular damage state was not observed in all specimens.

Fig. 86 presents resin cracking and ultimate failure data plotted in terms of principal stresses σ_x and σ_y. The resin cracking data is that occurring at 90^{o} to the hoop stress. An elliptical section has been drawn through the ultimate failure results and appears to fit the data well. The points of intersection of this ellipse with

the σ_x and σ_y axes were assumed to be equivalent to the R = 0 hoop strength and the data indicate that this assumption is valid. This infers that the uniaxial tensile and compressive off-axis strengths are equivalent and that the failure surface is symmetrical which conflicts with flat laminate data presented in section 6.3.2. The ratio of the 45° off-axis cylinder strength to the 0° off-axis cylinder strength at R = 0 is 77% whereas the equivalent ratio from flat laminates is only 54%. Cylinder gauge length fibres are eight times longer than in a type B flat specimen (Fig. 28) and extend from one loading point to the other. The above facts substantiate the view suggested in section 6.3.2 that off-axis tensile test results from flat specimens are dependent upon specimen width because of fibre discontinuity (70) and thus conclusions based on this data regarding failure surface shape should be treated with caution.

Fig. 87 compares mean 0° and 45° off-axis static data from cylinders in terms of σ_x and σ_y and reveals a surprising result. The ellipse drawn through the 45° off axis ultimate failure data intersects the line drawn through the 0° off-axis ultimate failure data in the tension-tension quadrant indicating that between R = +0.5 and R = +1 there is no decrease in hoop strength with change in off-axis angle (α). At R = +1 no change in strength with α is expected because all directions are principal stress directions and the data here is in excellent agreement with this. At R = +0.5 the hoop strength at $\alpha = 45^\circ$ is marginally above that at $\alpha = 0^\circ$ which is unexpected. It has been shown by Sandhu (66) that for a unidirectional composite under a

biaxial stress condition the Azzi and Tsai failure theory (14) indicates that $\alpha = 0^{\circ}$ is not necessarily the optimum fibre direction for maximum strength. It is possible that this is also true for a balanced weave fabric material. A similar effect is also indicated for resin cracking.

The 45° off-axis results presented in Fig. 86 are shown in Fig. 88 in terms of σ_1, σ_2 and σ_6. It should be noted that for $\alpha = 45^{\circ}$, $\sigma_1 = \sigma_2$ and Fig. 88 represents results in segment OHFKGNB of the failure surface of Fig. 15. Due to ram unit friction (1) differences existed between actual and nominal R values, R = -1 became R = -0.87, R = -0.5 became R = -0.4, R = 0 became R = +0.03, and R = +1 became R = +0.96. Actual R values are given in Fig. 88 and it should be remembered that R is based on σ_x and σ_y. In following discussions nominal R is referred to for consistency with previous sections unless otherwise stated. In-plane shear results from 0° off-axis 60 mm gauge length cylinders under torsion loading are presented in Fig. 88 and in Table 17. Cylinders with $\alpha = 0^{\circ}$ under torsion yield an equivalent loading condition to R = -1 with $\alpha = 45^{\circ}$. However, the value of σ_6 at failure from the torsion test pieces was only 74% of that determined from R = -1 with $\alpha = 45^{\circ}$, and no macro-buckling was apparent under torsion loading. Table 17 shows that by increasing the specimen gauge length of 0° off-axis cylinders, the ultimate shear strength decreases and hence it seems that results are dependent upon specimen length as observed for isotropic materials (71). Similar disagreement was observed between the equivalent cases of R = -1 with $\alpha = 0^{\circ}$ and cylinders with $\alpha = 45^{\circ}$ under torsion loading as seen by

comparing Tables 11 and 17. It is concluded that true shear strengths have not yet been obtained for this material by torsion loading and a programme of work is required to establish the optimum specimen length to outside diameter, and diameter to thickness ratios.

Fig. 88 shows that the R = -1 results (actually R = -0.87) do not follow the symmetrical ellipse suggested by the data at other R ratios. If a single ellipse was to represent all the biaxial stress data given in Fig. 88 in $\sigma_1 = \sigma_2$, σ_6 stress space then its major axis would lie in 3-D space and not along the $\sigma_1 = \sigma_2$, $\sigma_6 = 0$ axis and the ellipse would be inclined upwards. This would mean that strength was dependent upon the sign of σ_6, but a balanced weave fabric composite should be independent of this. Alternatively, it is possible that a closed ellipse is not formed in this segment of the failure surface due to the influence of the axial compressive principal stress, σ_y, on the failure mode. Examination of the R = -1 failures showed that fracture occurred due to σ_y but a normal compressive failure, having fracture surfaces inclined at angles to the central plane of the material, was not obtained. The failures, as shown in Fig. 120, were local and it is thought that macro-buckling occurred causing premature failure. The resin cracking data given in Fig. 88 do not show this peculiarity and hence the above is substantiated.

Fig. 89 shows mean resin cracking data along with cracking occurring at stress concentrators, i.e. joint cracking and macro void initiated cracking. At R = 0, -0.5 and -1 the effects of stress concentrators on crack initia-

tion are more severe than under biaxial tension. There may be an explanation based on strains although no analysis has been performed. Fig. 90 shows the means of the data of Fig. 89 plotted in terms of σ_1 and σ_6 and the results indicate that stress concentration effects increase with σ_6.

Biaxial stress static data at R = -1 at various off-axis angles is shown in Fig. 91. The data at $\alpha = 30^\circ$ shows higher σ_6 values than that at $\alpha = 45^\circ$. Examination of the fractures at $\alpha = 15^\circ$ and 30° showed that compressive failures occurred which were inclined to the central plane of the material. This substantiates the view stated earlier that R = -1 data at $\alpha = 45^\circ$ is suspect due to macro-buckling. Figs. 92-93 show the effect of a stress concentrator on crack initiation and similar conclusions to the 45° off-axis case (Figs. 89-90) can be drawn although voids have almost no effect until α approaches 45°. The specimen void content appeared to decrease with α and this could explain the effect.

Figs. 91-93 contain an important approximation. The actual R ratio was only -0.87, instead of -1, due to ram friction. Thus, if the data in these figures was projected onto the $\sigma_6 = 0$ plane without regard to the magnitude of σ_6 then they would not lie along a line passing through the origin of the reference axes, as suggested by the figures, but they would lie along a line that intersects the $+\sigma_2$ axis at a small distance from the origin. For simplicity, this was not shown in Figs. 91-93.

The variation of hoop strength with α at R = -1 is given in Fig. 94 and follows the well established trend

of uniaxial off-axis results shown by Found (1).

As shown in Tables 1 and 2, failure theory prediction for $\sigma_6 \neq 0$ requires a knowledge of the in-plane shear strength, S, in addition to principal strengths X, X', Y and Y'. Due to the suspect R = -1 data at $\alpha = 45^\circ$, and the torsion data at $\alpha = 0^\circ$, a value of 110 MNm^{-2} was assumed for the ultimate failure value of S since this followed the trend indicated by the data in Figs. 88 and 91. Fig. 95 compares mean experimental biaxial stress static data with the plane stress failure surfaces predicted by the failure theories. The letters denoting the theories are defined in Tables 1 and 2. Due to the complexity of presenting all failure theories on one set of reference axes two drawings are given in Fig. 95, the top one showing Group 1 theories and the bottom one showing Group 2 theories. The data shown in the $\sigma_6 = 0$ plane is that presented in section 6.2.2 for $\alpha = 0^\circ$ and the predictions shown in this plane are identical to those given in Fig. 58. In order to determine which theories most accurately predict the behaviour in the experimentally evaluated sections where $\sigma_6 \neq 0$, Figs. 96-97 are presented. These figures show normal views onto those radial sections of the failure surface representing 45° off-axis biaxial stress data, and data at R = -1 with varying α. Figs 95-97 indicate that the Norris Failure (D), the modified Marin (G), and the tensor (H, I) theories provide adequate prediction. The magnitude of constants F_{12} and k_2 for theories (H, I) and (G) respectively were as discussed in section 6.2.2 for $\sigma_6 = 0$, i.e. F_{12} was derived from R = +1 data at $\alpha = 0^\circ$, k_2 was derived from R = +1 data at $\alpha = 0^\circ$ for the + σ_1,

+ σ_2, σ_6 segment and from R = -0.5 data at $\alpha = 0^\circ$ for the + σ_1, - σ_2, σ_6 segment. All theories produce similar results in the segments shown in Figs. 96-97 and this is the reason why the off-axis uniaxial testing of flat laminates does not adequately discriminate between failure theories (33). Fig. 95 shows that the Hoffman (F) and Norris Failure (D) theories are identical except that the ellipsoid predicted by the Norris Failure theory is sliced away along planes $\sigma_1 = X$ and $\sigma_2 = Y$ in the first quadrant due to the superimposition of the maximum stress boundary. The maximum stress theory has not been presented because it was shown to be inadequate in Fig. 58 for $\sigma_6 = 0$, and it is also inadequate for $\sigma_6 \neq 0$.

A comparison between experimental static resin cracking data and predicted failure surfaces is given in Figs. 98-99, Group 1 and Group 2 theories being represented in these figures respectively. For prediction purposes the in-plane shear strength, S, was taken as the resin cracking stress at R = -1 with $\alpha = 45^\circ$. Figs. 100 - 101 show the view normally onto those radial sections of the surface presenting 45° off-axis biaxial stress data, and R = -1 data with varying α. The modified Marin (G) and Hoffman (F) theories provide acceptable predictions in the sections given in Figs. 100-101. Fig. 99 shows that the modified Marin theory provides the best overall prediction due to using two k_2 values, one for the + σ_1, + σ_2, σ_6 segment and one for the + σ_1, - σ_2, σ_6 segment. Acceptable data correlation exists for the off-axis results as shown in Figs. 100-101 but for results in the $\sigma_6 = 0$ plane no real correlation exists, as discussed in section

6.2.2, and it was thought that the R = 0 data with $\alpha = 0^{o}$ is suspect. This R = 0 data largely controls the failure envelope shape in the $\sigma_6 = 0$ plane and hence any discrepancies here are bound to reflect adversely on failure predictions. If the R = 0 data at $\alpha = 0^{o}$ is true then it indicates the failure theories having less than two floating constants cannot accurately define behaviour as seen in the $\sigma_6 = 0$ plane.

6.3.4 Biaxial stress fatigue test results.

A summary of the biaxial stress 45^{o} off-axis ultimate failure and damage fatigue data is given in Tables 18 and 19 respectively, individual results being presented in Figs. 102-103 and A20-A22 and in progress reports submitted to Dr. M.J. Owen. No ultimate failure data was obtained at R = +1 due to testing difficulties, but damage data was determined at this stress ratio.

Individual fatigue curves are shown in Figs. 102, 103 and A20-A22. The ultimate failure curves are Least Squares regression lines, with strength considered as the dependent variable, whereas the damage curves were fitted by eye. The scatter in the fatigue data is very low considering the number of individual results associated with each fatigue curve. Static data along with scatter bands are plotted at the $\frac{1}{4}$ cycle position.

A comparison of ultimate failure fatigue data at various stress ratios is given in Fig. 104 and shows that the results are stress ratio dependent. Cylinders tested at R = 0 have a greater fatigue strength than flat laminates under zero-tension loading because of the fibre discontinuity in off-axis flat specimens. Tables 13 and 18 show

that a decrease in hoop strength is observed when α is changed from 0° to 45° at all the biaxial stress ratios evaluated. This is different from static loading, as discussed in section 6.3.3, where cylinders tested at R = +0.5 with $\alpha = 45^{\circ}$ yield slightly greater hoop strengths than those tested at R = +0.5 with $\alpha = 0^{\circ}$. In addition, Tables 13 and 18 show that at 10^6 cycles, cylinders tested at R = +0.5 with $\alpha = 45^{\circ}$ yield a slightly greater hoop strength than at R = 0 with $\alpha = 0^{\circ}$.

Fig. 105 compares torsion fatigue data at $\alpha = 0^{\circ}$ with R = -1 data at $\alpha = 45^{\circ}$. The torsion results are summarised in Table 17. In contrast to the static results discussed in section 6.3.3, the torsion and R = -1 fatigue results are comparable. This is thought to be due to the effect of the compressive principal stress, σ_y, under R = -1 fatigue loading causing premature buckling failure as shown in Fig. 119.

Resin cracking fatigue data is shown in Fig. 106. As found for the $\alpha = 0^{\circ}$ case in section 6.2.4 the low stresses are the main concern, i.e. for R = -1 the σ_x value at 10^6 cycles is only 6.5 MNm^{-2}. Tables 14 and 19 show that the R = +1 data at both $\alpha = 0^{\circ}$ and 45° are very similar and this establishes confidence in the results since these data should be independent of α. In addition, these tables show that at 10^6 cycles there is a negligible effect of α on the resin cracking stress, σ_x, at R = 0 and +0.5, whereas at 10^3 cycles an effect is indicated. This agrees with the uniaxial zero-tension flat laminate behaviour observed by Found (1). Figs. 107-111 present individual fatigue curves showing the onset of joint

cracking and macro-void initiated cracking. Since these results were recorded from resin cracking test pieces then, in general, data up to 10^6 cycles were not obtained and hence the curves were extrapolated. Figs. 112-114 indicate that these stress concentration effects are stress ratio dependent but in all cases, except at R = +1, the effect is quite large. This shows that these defects, which are likely to be present in engineering structures, cause premature crack initiation at extremely low stresses in fatigue loading.

Comparisons between experimental data at 10^6 cycles and the plane stress failure surfaces predicted by the various failure theories are given in Figs. 115 and 116 for ultimate failure and resin cracking respectively. The letters denoting the theories are defined in Tables 1 and 2. Views looking normally onto those radial sections of the surfaces of Figs. 115 and 116 representing 45° off-axis biaxial stress data are given in Figs. 117 and 118. As shown in Fig. 117 for ultimate failure, the data at R = -1 with $\alpha = 45^\circ$ does not follow the trend predicted by the data at other stress ratios similar to the static case discussed in section 6.3.3 because of premature buckling failure shown by Fig. 119. Thus, for prediction purposes a value of in-plane shear strength, S, of $25 MNm^{-2}$ was assumed since this followed the general data trend. For resin cracking no buckling problems were encountered, and hence the R=-1 with $\alpha = 45^\circ$ resin cracking stress was used for theoretical predictions. The failure theory predictions shown in the $\sigma_6=0$ plane in Figs. 115 and 116 are identical to those presented in Figs. 69 and 72 for $\alpha = 0^\circ$ for ultimate failure and resin

cracking respectively.

For ultimate failure, Figs. 115 and 117 show that data at R = +0.5 with $\alpha = 45^{\circ}$ yield high strengths in similar fashion to the $\alpha = 0^{\circ}$ case. This tends to dispute the R = +1 data with $\alpha = 0^{\circ}$ which, as discussed in section 6.2.4, is suspect due to biaxial tension joint effects. Figs. 115 and 117 show that the tensor (H, I) and modified Marin (G) theories provide a conservative prediction because constants F_{12} and k_2 were determined from the suspect R = +1 data with $\alpha = 0^{\circ}$. However, this prediction would be acceptable for design purposes without using additional safety factors. Of the simple strength theories, i.e. those designated as Group 1 theories in Table 1, the Norris Failure (D) is very acceptable as found for static ultimate failure. All theories shown in Fig. 115 predict essentially the same envelope in those segments of the surface where either σ_1 or σ_2 is zero but $\sigma_6 \neq 0$. This is because constants F_{12} and k_2 of the Group 2 theories become zero, and the linear terms in the equations become negligible because the principal strengths X, X', Y and Y' are similar.

For resin cracking, Figs. 116 and 118 show that the tensor theories (H, I) with F_{12} derived from R = -1 data with $\alpha = 0^{\circ}$ provide the most acceptable prediction of behaviour. Of the Group 1 theories, the Hoffman (F) theory provides a conservative but useful prediction in the absence of complex stress data.

6.3.5. Appearance of biaxial stress and torsion failures.

Typical biaxial stress static failures are shown in Fig. 120, the card against each cylinder denoting the

biaxial stress ratio (R). Part of the final reinforcement layers of the R = 0 test piece has been removed to show the fracture path more clearly. The R = 0 failure involves fractures in both fibre directions. The fracture type is similar to that observed by Found (1) in flat laminates under uniaxial tension loading although failure only occurred along one of the fibre directions. Failures at R = +0.5 were joint failures, i.e. they occurred along the joint seam at 90° to the hoop stress σ_x, and the fractures completely spanned the gauge length. This was the only stress ratio where joint failures were observed. The R = +1 failures were of the axial tensile variety occurring at 90° to the principal tensile stress σ_y. Failures at R = -0.5 were combined failures as shown. The compressive fracture was at 90° to the axial compressive stress, σ_y, and was inclined at an angle to the central plane of the material, and no buckling was apparent. At R = -1, the failures were at 90° to σ_y but they were not of the normal compressive type seen by Found (1) in flat laminates under uniaxial compression loading and as discussed in section 6.3.2. The material in the failed region bulged outwards and it is thought that some macro-buckling occurred.

Fatigue failures were similar except at R = -0.5 where at high stress levels the axial compressive failure mode dominated and the failures indicated a slight buckling tendency similar to that observed at R = -1 in Fig. 119.

Typical static torsion failures are shown in Fig. 121. For α = 0°, both the 60mm and 120mm gauge length specimens yielded a similar shear fracture appearance. For

$\alpha = 45^{\circ}$, the fracture path occurred along that fibre direction perpendicular to the compressive principal stress and the failure was of a compressive nature. The $\alpha = 0^{\circ}$ and $\alpha = 45^{\circ}$ cases are equivalent to R = -1 with $\alpha = 45^{\circ}$ and R = -1 with $\alpha = 0^{\circ}$ respectively. From comparison of Fig. 121 with Figs. 73 and 120 it can be seen that the intensity of later damage stages such as local compressive buckling at the fibre cross-overs was not as great under torsion loading as under the equivalent R = -1 condition.

Fig. 122 shows the difference between static and fatigue damage at different biaxial stress ratios. Samples were machined from ultimate failure test pieces and the cylinder bores were examined using transmitted light, on the macro setting of a vickers M41 microscope. All magnifications were X10. At R = +1 only the static evidence is presented because no successful fatigue ultimate failure tests were performed. Resin cracks occur in many directions since all are principal stress directions. At R = +0.5 the cracks, in both static and fatigue loading, are predominantly at 90° to the hoop tensile principal stress σ_x although cracks can be seen in the fibre directions. The cracks are shorter and of a finer nature under fatigue loading and the overall cracking is more intense. The evidence at R = 0 is somewhat similar to that at R = +0.5 except that only a very few cracks are seen in the fibre directions. At R = -1, the difference in crack intensity between static and fatigue loading is very marked. All the cracking observed here is due to the hoop tensile principal stress, σ_x, and no cracks occur along the fibre directions, i.e. no shear cracks are observed. It should be remembered

that R = -1 with $\alpha = 45^{\circ}$ yields a stress state of pure shear along the fibre directions. Fig. 123 shows the similarity in resin cracking damage between cylinders with $\alpha = 0^{\circ}$ tested under torsion and the equivalent case of R = -1 with $\alpha = 45^{\circ}$. However, for the torsion case the debonding damage, shown by the fine dark lines running in the fibre directions, is much more intense than for R = -1. In all the above cases, resin cracking mainly occurs as a result of the principal tensile stress, σ_x, and the cracks seem to initiate from the fibre cross-over points, as found for the $\alpha = 0^{\circ}$ case in section 6.2.5, probably because of the high tensile stress concentrations occurring in this region (55) and then they propagate through the resin-rich 'windows' between the fibre bundles.

6.3.6 Discussion of off-axis results.

Off-axis ultimate failure uniaxial tensile and compressive data by Found (1) were shown to reveal anomalies in both static and fatigue loading. Failure theories would predict a symmetrical failure surface for a composite whose principal strengths X, X', Y and Y' were equal and where shear stress sign did not affect shear strength magnitude, i.e. failure theories would predict that off-axis tensile and compressive strengths were identical. It has been shown that the results presented by Found (1), and Owen and Found (35), indicate that the static and fatigue failure surfaces are a symmetrical. The difference between the off-axis tensile and compressive results is thought by the author to be due to failure mode and specimen width effects. Biaxial stress tests on 45° off-axis cylinders indicate that the uniaxial tensile and compressive 45° off-axis strengths are

similar as shown by Fig. 86 and hence it is thought that the failure surface is symmetrical. However, the author does acknowledge the fact that since experimental data on off-axis cylinders under uniaxial compression loading have not been obtained, then it is possible that a change in failure mode may distort the failure surface and that more than one failure surface may be required to described fracture under plane stress conditions.

The results by Found (1), and Owen and Found (35), could not be used by the author to supplement the biaxial stress data, and hence aid the construction of the experimental failure surfaces, because of the discrepancy detailed above. A single correction factor could not be applied to the results to enable correlation with cylinder data because the discrepancy between cylinders tested at R = 0 and flat laminates tested under uniaxial tension loading increased with increasing off-axis angle (α). This in itself indicates that off-axis flat laminates under uniaxial tension yield unduly pessimistic strengths because of fibre discontinuity. It is concluded that tubular specimens, and not flat laminates, should always be used to determine failure surface segments.

The biaxial stress static off-axis results indicate that maximum ultimate and resin cracking strengths are not necessarily achieved when $\alpha = 0^{\circ}$, since 45° off-axis cylinders tested at R = +0.5 yield slightly higher strengths than with $\alpha = 0^{\circ}$. Sandhu (66) has shown that this is possible for unidirectional composites.

Ultimate failure static and fatigue biaxial stress data at R = -1 with $\alpha = 45^{\circ}$ indicates that the failure

surface is not closed and that more than one failure surface is required to represent fracture because of the effect of the compressive axial principal stress, σ_y, on the failure mode. However, even though conclusive evidence is not available, it is thought that the above is untrue because of macro-buckling causing premature failure. This is substantiated by the fact that abnormal axial compressive failures, and not shear failures along the fibre directions, were obtained. Loading of R = -1 with $\alpha = 45^{\circ}$ produces a state of pure shear along the fibre directions.

Further discrepancies were noticed between the R = -1 data with $\alpha = 45^{\circ}$ and torsion data with $\alpha = 0^{\circ}$. Found (1) determined the in-plane shear strength by testing flat laminates in 4-point bending. The mean static shear strength determined by this method was 72.5MNm^{-2} which compares favourably with the value of 72.3 MNm^{-2} determined by the author from 60mm gauge length cylinders. However, Found observed no damage prior to failure in these specimens whereas the author observed quite advanced damage states. It is thus concluded from the above that no accurate value of shear strength has yet been obtained for this material and shear strength determination methods must be evaluated and standardised.

In view of the above discrepancies, for failure theory prediction, a value of in-plane shear strength, S, had to be estimated for ultimate failure in static and fatigue loading from the trend indicated by the biaxial stress off-axis data. For ultimate failure, in both static and fatigue loading, the Norris Failure, modified Marin

and tensor theories of Tsai and Wu, and Gol'denblat and Kopnov provided adequate correlation with the available experimental data. For resin cracking, the static loading behaviour was best described by the modified Marin theory using two values of constant k_2, although the Hoffman theory could be used in the absence of complex stress data. If the data in the $\sigma_6 = 0$ plane can be relied upon then it indicates that failure theories having less than two floating constants cannot accurately define the type of behaviour seen in this plane. For fatigue loading at 10^6 cycles, the resin cracking behaviour was best described by the tensor theories, but again the Hoffman theory is useful in the absence of complex stress data. It appears that those theories containing a constant derived from complex stress data can generally describe the behaviour of an orthotropic material more accurately than the simple Group 1 theories shown in Table 1.

Chapter 7.

General discussion, conclusions, and recommendations for future work.

7.1 General discussion.

One aim of this work was to establish the cause of the discrepancy, revealed by Found (1), in the fatigue behaviour of a C.S.M.-reinforced polyester resin. Found (1) has shown that the fatigue strength of cylinders tested at R = 0 was, depending on life, between 40-60% below that of flat laminates tested under the equivalent condition of zero-tension loading, whereas under static loading no discrepancy was observed. The possible causes of the above anomoly listed in section 5.1.2. that were considered to yield maximum fatigue effects were evaluated, these being the effects of mineral oil, and reinforcement joints. As discussed in section 6.1.6, 'Tellus 15' mineral oil had no adverse effect on the zero-tension fatigue behaviour of flat laminates, and in fact an enhancement of fatigue strength at 10^6 cycles was indicated. This is thought to be due to a combination of (i) moisture exclusion (51), (ii) lubricating effects at (a) the glass-resin interface, and (b) the fibre-fibre contact points thus reducing the number of micro-flaws initiated and hence enhancing the fatigue strength. Thus, mineral oil effects did not cause the anomaly. It was demonstrated by tests on suitably constructed flat laminates, as discussed in sections 6.1.3 and 6.1.6, that the reduced cylinder fatigue strengths were due to an inherent failure initiation site, i.e. the

reinforcement butt-joint. The effect of these joints was shown to be remarkably severe in zero-tension fatigue loading, especially at long lives, although the effect on the static tensile properties was negligible. It is considered that joint effects under biaxial tension fatigue loading may be even more severe than for uniaxial loading. As shown in Figs. 34-36, 42 and 48, very few fibres cross the resin rich joint zone in jointed C.S.M. laminates, hence joint crack propagation has no barrier and premature catastrophic failure occurs. It should be noted that although the joints are in general readily discernible in Figs. 34-36, 42 and 48, no success was achieved in their detection in untested plates by examination through the plate width in the jointed region using a microscope. Joints are very difficult to detect by techniques other than that discussed in section 6.1. It has been shown in section 6.1.3 that a 3-layered laminate containing a butt-joint, in the first reinforcement layer, oriented at 90^{o} to the loading axis, and tested in zero-tension fatigue loading is not equivalent to a 2-layered non-jointed laminate, i.e. the jointed layer cannot simply be treated as non-load bearing. At fatigue lives beyond 10^{3} cycles, the 3-layered jointed laminate requires a lower axial tensile force to cause failure than does the 2-layered plain laminate because of the inherent crack initiation site and crack propagation path. The effect of joints in zero-compression fatigue loading was not determined, but it should be neglig ble because the onset of resin cracking occurs very close to ultimate failure (1,6) and this, coupled with the crack closing mode of compression loading,

indicates that joint crack propagation would be insignificant. Since reinforcement joints are inevitable in engineering structures due to there being a finite reinforcement width, and since there appears to be a tendency for designers to use heavier gauge reinforcement and hence less layers for the same component size, then the positioning of joints is of the utmost importance, in situations where tensile fatigue loading is encountered, if premature catastrophic failure is to be avoided. This view is held by Bishop (38). The problem is not solved by using lap-joints in place of butt-joints because a resin rich zone still exists between the jointed sections of reinforcement.

Joints of a different nature to the above were present in the Y449 fabric-reinforced polyester resin cylinders. Uniaxial tensile tests on lap-jointed Y449 fabric-reinforced flat laminates, as discussed in sections 6.2.1, 6.2.3 and 6.2.6, indicated that in cases where the lap-joint is situated at 90^{o} to the loading axis there is a slight effect on the static failure strength, but a negligible effect at 10^{6} cycles in zero-tension fatigue loading, i.e. the reverse of the C.S.M. case. The difference in behaviour between the discontinuous C.S.M. and the continuous fabric-reinforced composites is that, even though long joint cracks occur along the resin rich lap-joint seam for the fabric-reinforced laminates, Bisnop (38) has shown that it is very difficult to propagate cracks transverse to the fibre directions in a continuous composite, and hence joint effects would tend to be stress level dependent, i.e. at low stresses lap-joint effects in fabric

materials would tend to disappear. Fatigue tests on fabric-reinforced cylinders indicated that biaxial tension joint effects may be greater than for uniaxial loading. However, no flat laminate tests were performed to examine the effect of a lap joint lying at 0^{o} to the loading axis because of testing difficulties, i.e. a wide specimen would be needed to simulate the lap-joint and overlap cylinder condition.

The effect of 'Tellus 15' mineral oil on the zero-tension fatigue behaviour of fabric-reinforced flat laminates was evaluated and a similar trend to that found for C.S.M. was indicated, i.e. there was a slight enhancing effect on fatigue strength at 10^{6} cycles.

Voids, in 45^{o} off-axis fabric-reinforced cylinders, were found to readily initiated cracking, especially in fatigue loading, as shown in section 6.3.4. For R = 0 loading, macro-void initiated cracking occurred at 10^{6} cycles at an estimated 60% of the resin cracking stress. The effect of voids on failure are not expected to be as great as joints because it has been shown by Bishop (38) that a stress concentrator such as a hole is more effective at initiating damage than it is at causing catastrophic failure. However, if the onset of resin cracking is used as a design criterion, then the effects of inherent stress concentrators such as voids must be acknowledged.

The main aim of the research was to experimentally establish the biaxial stress behaviour of C.S.M. and Y449 fabric-reinforced polyester resins under static and fatigue loading, and then to assess the validity of various failure theories for predicting the observed data. Many anomolies

in the test data were revealed showing the complexity of the whole problem.

Initially, the work by Found (1) on the failure of C.S.M.-reinforced polyester resin cylinders was extended to provide a more complete experimental failure envelope. Variables such as reinforcement batch differences were introduced at the outset of this work, as discussed in section 6.1.1, and these did not aid correlation between data by Found (1) and by the author. In spite of these problems, static ultimate failure biaxial stress data correlation between results by the two operators was acceptable because of glass content differences as discussed in section 6.1.2. However, in fatigue loading, data correlation was acceptable in the tension-compression quadrant but in the tension-tension quadrant each data set suggested different trends, i.e. Found's data indicated a severe biaxial tension effect whereas the author's data indicated a negligable biaxial tension effect. Since correlation was good in the tension-compression quadrant, and since biaxial tensile stresses are thought to produce more severe joint effects than uniaxial tensile stresses, then it suggests that the behaviour differences in the tension-tension quadrant may in part be due to the quality of the reinforcement butt-joint. In addition, examination of failed biaxial tension fatigue specimens showed that the damage intensity was of a similar severity in both specimen sets. This suggests that resin cracking initiated earlier in Found's specimens than in the author's, and thus joint crack propagation commenced earlier leading to a difference in fatigue behaviour. This cannot be substan-

tiated because no damage test results were obtained by the author on this material.

The biaxial stress static ultimate failure behaviour of C.S.M. reinforced polyester resin is best described by those failure theories containing a floating constant, i.e. the modified Marin (8), the Tsai and Wu (23), and the Gol'denblat and Kopnov (21) theories, as shown by Found (1), and Owen and Found (6). These theories require experimental complex stress data to derive their constants k_2, and F_{12}. If this data is unavailable then the Norris Failure (13) theory would be acceptable. For fatigue loading at 10^6 cycles, useful failure theory prediction was severely restricted because of the different trends indicated by Found's and the author's data in the tension-tension quadrant. The modified Marin theory produced the only generally acceptable data fit by using a value of k_2 for each stress quadrant, and hence causing the predicted envelope to pass through a data point in each stress quadrant in addition to intersecting the reference axes at the principal strengths.

For the Y449 fabric-reinforced polyester resin both two and three-dimensional representations of the plane stress 'failure' condition were presented in sections 6.2 and 6.3, corresponding respectively to the special case where $\sigma_6 = 0$, and to the case where σ_1, σ_2 and σ_6 can all be operative. Ultimate failure under static loading and at 10^6 cycles under fatigue loading was adequately described by the tensor (21, 23), the modified Marin (8), and the Norris Failure (13) theories. The value of in-plane shear strength, S, was estimated from the general trend suggested

by the 45° off-axis biaxial stress data, for both static and fatigue ultimate failure predictions, because of the anomalies discussed in sections 6.3.3, 6.3.4 and 6.3.6. It is acknowledged by the author that if the experimental S values are reliable then ultimate failure appears to require more than one failure surface, i.e. intersecting failure surfaces, to define the fracture behaviour due to the effect of different failure modes. However, the available evidence, although inconclusive, suggests that the experimental S values are suspect and hence it was assumed that a single failure surface was adequate. Off-axis flat laminate data presented by Found (1), and Owen and Found (35), suggests an a symmetrical failure surface as discussed in section 6.1.2. This is possible because of differences in the observed failure mode of uniaxial tensile and compressive test specimens which could distort the failure surface. However, the limited evidence, based on the effects of fibre discontinuity, presented in section 6.1.2 and 6.1.3 tends to discount the degree of failure surface asymmetry suggested by Found's ultimate failure data. Since the asymmetry evidence was inconclusive, it was assumed that a single symmetrical failure surface, as would be predicted by failure theories for a composite of this type, could describe the ultimate fracture behaviour.

For resin cracking under static loading conditions the behaviour of the fabric-reinforced polyester resin was best described by the modified Marin (8) theory using a value of constant k_2 for each quadrant. In the absence of complex stress data being available, the Hoffman (15) theory may be acceptable. However, none of the

theories were completely adequate because the R = 0 data in the $\sigma_6 = 0$ plane showed little correlation with other data in this plane. If the R = 0 data is valid it suggests that failure theories containing less than two floating constants determined from complex stress experiments are unable to accurately predict the type of behaviour seen in the $\sigma_6 = 0$ plane. Under fatigue loading, the main concern was the very low stresses at which resin cracking initiated, e.g. for R = 0 at 10^6 cycles resin cracking initiated at only 8.5% of the static resin cracking stress and at 18% of the ultimate failure fatigue stress at 10^6 cycles. This tends to exclude the onset of resin cracking as a useful design criterion and some degree of damage will have to be accepted. In addition, the effect of voids on crack initiation should be acknowledged as discussed earlier. At 10^6 cycles, the behaviour was adequately described by the tensor (21, 23), and the Hoffman (15) theories. For prediction purposes the experimental values of in-plane shear strengths, S, were used because no anomolies were revealed in the data. For resin cracking, in both static and fatigue loading, the failure surface is a single a symmetrical surface. The a symmetry occurs because the principal tensile and compressive strengths are unequal.

In section 6.2.6, and Figs. 75 and 76, it was suggested that for both static and fatigue loading the damage and ultimate strength failure envelopes may intersect in the $\sigma_6 = 0$ plane, indicating that failure would occur without prior damage in a limited region of σ_1, $-\sigma_2$ stress space. The above relied to some extent on the

assumption that the resin cracking behaviour in the $\sigma_6 = 0$ plane could be represented by a rectangular envelope, i.e. by the maximum stress theory. No data were determined in those sections of σ_1, $-\sigma_2$, σ_6 stress space which would confirm the above possibility. However, the maximum stress theory is inadequate in predicting that behaviour evaluated in σ_1, σ_2, σ_6 stress space and hence this tends to discount the above unless intersecting resin cracking failure surfaces are formed. At the present time, the possibility of intersecting failure surfaces cannot be proven or disproven due to a lack of available data.

It has been shown that the Norris Failure (13) theory can adequately describe both the static and fatigue ultimate failure behaviour of an orthotropic material, but it does not predict the resin cracking behaviour so accurately. In general, the most favourable predictions for the plane isotropic and orthotropic materials that were investigated were provided by the tensor theories of Tsai and Wu (23), and Gol'denblat and Kopnov (21), and the modified Marin theory suggested by Franklin (8). This was expected because of the additional constraint of constants F_{12} and k_2 imposed on the predicted ellipsoid. However, as discussed in section 2.1.2.3, the effect that these constants have on the predicted failure surface must be understood. For a composite whose principal strengths are equal, i.e. X=Y=X'=Y'=S, a change in F_{12} from zero to almost one limit of the F_{12} stability band will change the surface from a sphere to a very elongated ellipsoid, and changing the sign of F_{12} will rotate the ellipsoid by 90° about it's principal axes. Thus, very great care is required in F_{12}

determination. The effects of k_2 on the modified Marin theory are similar if k_2 assumes equivalent values to F_{12}. The 45° off-axis uniaxial tensile test produces a stress state in the fibre directions of $\sigma_1 = \sigma_2 = \sigma_6 = \sigma/2$ where σ = applied uniaxial stress and hence F_{12} could be determined by this method. However, as discussed in section 6.2.2, this test produces very insensitive F_{12} values for this material which means that small changes in the observed 45° off-axis uniaxial tensile strength produce large F_{12} changes. Since composite materials exhibit appreciable scatter in their properties, then different operators investigating the same material may determine slightly different mean off-axis uniaxial strengths, and hence produce widely differing F_{12} values and predicted failure surfaces. The use of the off-axis uniaxial tensile test should be avoided for predicting plane stress failure surfaces for this material. However, this test can be used to determine F_{12} for predicting the variation in uniaxial strength with off-axis angle since in this case large F_{12} changes produce small changes in the predicted curve as discussed in section 2.3. If the theories containing these constants F_{12} and k_2 are to be used it is suggested that an analysis of their evaluation methods is performed as shown by Tsai and Wu (23), and section 2.1.2.3. This is a simple procedure ideally suited for computing methods and it only involves re-arranging the failure theory equations in terms of the tests considered. A more complex method of F_{12} determination from cylinders is given by Wu (25), this method being considered to be the most accurate available. However, it is realised that in many cases the

testing of thin-walled cylinders to determine F_{12} is prohibited by the cost of the test apparatus. It has been shown that in general useful failure theory predictions are obtained by determining F_{12} from tests on 0^{o} off-axis cylinders at R = +0.5. This test condition is very simple to produce, i.e. internal pressure only, and only a bare minimum of instrumentation is required.

In general, it was found that by using more than one value of k_2 in the modified Marin theory more accurate predictions were obtained. This leads to a loss of flexibility since complex stress data is required in each stress quadrant, but it does mean that different failure modes can easily be accounted for. If only one k_2 value is used then, for plane stress, the theory is identical to the tensor theories (21, 23).

A great number of fabric-reinforced cylinders and flat laminates were tested during this research but only a very small number of failure surface sections have been experimentally established, and many anomalies have been revealed in the test data. One problem is that there is virtually no published experimental evidence with which to compare the data presented in this thesis and from which a more complete failure surface may be established. To verify beyond doubt that a particular failure theory is valid for the complete plane stress failure surfaces requires many failure surface sections to be experimentally evaluated. To do this for static and fatigue loading at various damage states requires a tremendous amount of time consuming and costly research to have any real confidence in the final result. Thus, no definitive answers as to

which failure theory optimises the material properties can be presented in this thesis. The suggestions presented are guidlines from which designers can gain some much needed assistance and the justification of this research can only lie in the design of an engineering structure.

7.2 Conclusions.

1. Jointed reinforcement layers have a marked adverse effect on the zero-tension fatigue strength of C.S.M.-reinforced polyester resins when the number of reinforcement layers is small, although a negligable effect on the static tensile properties. Joints are inevitable in structures and their positioning requires careful consideration if premature catastrophic failure is to be avoided.

2. Lap-joint effects in continuous balanced weave fabric-reinforced polyester resins are stress level dependent and become negligable at 10^6 cycles under zero-tension fatigue loading, although the effects under biaxial tension loading appear to be more severe.

3. Joints and macro-voids are effective damage initiators in fabric-reinforced cylinders under both static and fatigue loading.

4. Failure may occur before damage over a limited region of σ_1, σ_2 stress space, for the fabric-reinforced material, as suggested by intersecting damage and ultimate strength failure envelopes in the $\sigma_6 = 0$ plane.

5. The Norris Failure (13) theory adequately described the static and fatigue ultimate failure behaviour of an orthotropic material, but not the resin cracking behaviour.

6. Failure theories containing a constant

determined from complex stress experiments (8, 21, 23) are generally more acceptable for GRP but the effects of these constants on the predicted failure surfaces must be understood.

7. The behaviour of both the plane isotropic and orthotropic materials investigated is in general stress ratio dependent.

8. For the orthotropic material, the resin cracking stresses under fatigue loading are too low to be used as a basis for a design criterion. Some degree of damage will have to be accepted for most design purposes.

7.3 Recommendations for future work.

To fully evaluate anisotropic failure theories a material with a high degree of anisotropy should now be investigated. A reinforcement such as Y221 satin weave fabric which has an 10:1 fibre count in the warp and weft directions would provide useful data in this respect. Uniaxial tensile and compressive flat laminate data on a polyester resin reinforced with this fabric is available in references (1, 38) and none of the principal tensile and compressive strengths are equal. As shown in this thesis, for the materials investigated, it is difficult in certain cases to readily discriminate between the failure theories, but a unidirectional material would highlight the differences. Careful consideration must be given to cylinder design to strike a compromise between an acceptable stress distribution, the prevention of buckling failures, and maximum test machine capability. In addition, the effect of jointed reinforcement layers should be established. Before any experimental biaxial stress work is

embarked upon it is recommended that those failure surface sections that are most likely to test the validity of the failure theories are decided upon and the test programme formulated around this decision. The failure surface of a unidirectional GRP will not be symmetrical about the reference axes and it will be possible, by three-dimensional representation, to see which sections are able to withstand high shear stresses.

In view of the discrepancies discussed in this thesis an evaluation of shear strength determination methods is required. If cylinders under torsion loading are decided to be the most accurate method then a programme of work to establish the optimum specimen length to outside diameter and diameter to thickness ratios should be initiated.

It is recommended that the following modifications are incorporated into the biaxial stress test machine:-

a) the fatigue test frames can be easily modified to enable static tests to be performed on them, hence saving a great deal of time in changing ram units etc. to the static frame, and also allowing residual strength tests on fatigue test specimens to be carried out quickly.

b) modify the loading frames so that a torque can be applied to the cylinders, hence enabling further sections of the failure surfaces to be established experimentally.

REFERENCES.

1. Found, M.S. — 'Biaxial Stress Fatigue of Glass Reinforced Plastics', Ph.D. Thesis University of Nottingham, 1972.

2. Ashton, J.E., Halpin, J.C., Petit, P.H. — 'Primer on Composite Materials: Analysis', Technomatic Publishing Co., Inc., Conn., U.S.A. 1969.

3. Kaminski, B.E., Lantz, R.B. — 'Strength Theories of Failure for Anisotropic Materials', Composite Materials : Testing and Design, A.S.T.M. STP 460, 1969, 160-169.

4. Tsai, S.W. — 'Mechanics of Composite Materials', Part II - Theoretical Aspects, AFML-TR-66-149.

5. Tsai, S.W. — 'Mechanics of Composite Materials', Part I - Introduction, AFML - TR-66-149.

6. Owen, M.J. Found, M.S. — 'Static and Fatigue Failure of Glass Fibre Reinforced Polyester Resin under Complex Stress Conditions', Faraday Special Discussion of the Chemical Society, 2, 1972, 77-89

7. Jones, B.H. — 'Predicting the Stiffness and Strength of Filamentary Composites for Design Applications', Plastics and Polymers, April 1968, 119-126.

8. Franklin, H.G. — 'Classic Theories of Failure of Anisotropic Materials', Fibre Science and Technology, 1, No2, 1968, 137-150.

9. Marin, J. — 'Theories of Strength for Combined Stresses and Nonisotropic Materials', J. Aeronautical Sciences, 24, No4, 1957, 265-268.

10. Puck, A., Schneider, W. — 'On Failure Mechanisms and Failure Criteria of Filament-Wound Glass Fibre-Resin Composites', Plastics and Polymers, 37, No.127, 1969, 33-44.

11. Stowell, E.Z., Liu, T.S. 'On the Mechanical Behaviour of Fibre Reinforced Crystalline Materials', J. Mech.Phys. Solids, 9, 1961, 242-260.

12. Hill, R. 'A Theory of Yielding and Plastic Flow of Anisotropic Metals', Proc. Royal Soc., Series A, 193, 1948, 281.

13. Norris, C.B. 'The Strength of Orthotropic Materials Subjected to Combined Stresses', Forest Products Lab. Rep. No.1816, May 1962.

14. Azzi, V.D., Tsai, S.W. 'Anisotropic Strength of Composites', Experimental Mechanics, 5, No 9, 165, 283-288.

15. Hoffman, O. 'The Brittle Strength of Orthotropic Materials', J. Composite Materials, 1, No 2, 1967, 200-206.

16. Tsai, S.W. 'Structural Behaviour of Composite Materials', N.A.S.A. Rpt. CR-71, July 1964.

17. Azzi, V.D. Tsai, S.W. 'Elastic Moduli of Laminated Anisotropic Composites', Experimental Mechanics, 5, 1965, 177-185.

18. Norris, C.B., McKinnon, P.F. 'Compression, Tension and Shear Tests on Pellow-Poplar Plywood Panels of Sizes that do not Buckle with Tests made at various Angles to the Face Grain', Forest Products Lab. Rpt. No 1328, 1946.

19. Fischer, L. 'Optimisation of Orthotropic Laminates', ASME Trans.J. Eng. for Industry, 89 No3, 1967 399-402.

20. Caddell, R.M., Raghava, R.S., Atkins, A.G. 'A Yield Criterion for Anisotropic and Pressure Dependent Solids such as Oriented Polymers', J. Materials Science, 8, 1973, 1641 - 1646.

21. Gol'denblat I.I., Kopnov, V.A. 'Strength of Glass Reinforced Plastics in the Complex Stress State', Mekhanika Polimerov, 1, No2, 1965, 70-78.

22. Ashkenazi, E.K. 'Problems of the Anisotropy of Strength', Mekhanika Polimerov, 1, No 2, 1965, 79-92.

23. Tsai, S.W., Wu, E.M. 'A General Theory of Strength for Anisotropic Materials', J. Composite Materials, 5.Jan. 1971. 58-80.

24. Collins, B.R., Crane, R.L. 'A Graphical Representation of a Failure Surface of a Composite', J. Composite Materials, 5. July 1971, 408-413.

25. Wu, E.M., 'Optimal Experimental Measurements of Anisotropic Failure Tensors', J. Composite Materials, 6. Oct. 1972, 472-489.

26. Jones, E.R. 'Strength of Glass Filament Reinforced Plastics in Biaxial Loading', S.P.E. 26th. Annual Tech. Conf., May 1968, 11-14.

27. Protosov, V.D., Kopnov, V.A. 'Study of the Strength of Glass-Reinforced Plastics in the Plane Stress State', Mekhanika Polimerov, 1, No.5, 1965, 39-44.

28. Ely, R.E. 'Biaxial Fracture Stresses for Graphite, Ceramic, and Filled and Reinforced Epoxy Tube Specimens', U.S. Army Missile Command, Alabama, U.S.A., Rpt. No. RR-TR-65-10, 1965.

29. 'Design Information from Analytical and Experimental Studies on Filament Wound Structures subjected to Combined Loading', Final Rpt, Project 637-35, ABL Subcontract 89, AD-451-216.

30. Sultan, J.N., McGarry, F.J. 'Effect of Rubber Particle Size on Deformation Mechanism of Glassy Epoxy', Polymer Eng. and Science, 13, No.1, 1973, 29-34.

31. Weng, Tu-Lung. 'Biaxial Fracture Strength and Mechanical Properties of Graphite-Base Refractory Composites', AIAA Journal, 7, No 5, 1969, 851-858.

32. Babell, H.W., Sines, G. 'An Improved Method of Uniaxial and Biaxial Testing of Brittle Materials', J. Materials, JMLSA, 3 No.1, 1968, 134-152.

33. Schneider, G.J. 'Evaluation of Lamina Strength Criteria by Off-Axis Tensile Coupon Tests', Fibre Science and Technology, 5, Jan. 1972, 29-35.

34. Byron Pipes R., Cole, B.W. 'On the Off-Axis Strength Test for Anisotropic Materials', J. Composite Materials, 7, April 1973, 246-256.

35. Owen, M.J., Found, M.S., To be published.

36. Owen, M.J., 'A New Fatigue Machine for Reinforced Plastics', Trans. J. Plastics Inst., Feb. 1967, 353-357.

37. Smith, T.R. 'The Fatigue of Glass Reinforced Plastics', Ph.D. Thesis, University of Nottingham, 1968.

38. Bishop, P.T. 'Failure of Reinforced Plastics caused by Stress Concentrations', Ph.D. Thesis, University of Nottingham, 1973.

39. Howe, R.J. 'Cumulative Damage of a Glass Reinforced Plastic', Ph.D. Thesis, University of Nottingham, 1971.

40. Rose, R.G. 'The Effect of Resin Flexibility on the Mechanical Properties of Glass Fibre Reinforced Polyesters', Ph.D. Thesis, University of Nottingham, 1971.

41. Dukes, R. 'Failure Mechanisms in Glass Reinforced Plastics', Ph.D. Thesis, University of Nottingham 1968.

42. Andrew, J.E. 'Mechanical Factors Affecting the Strength of Springs', Ph.D. Thesis, Sheffield University, 1949.

43. Paulus, H.J., 'Fibrous Glass Reinforcements', Modern Plastics Encyclopedia, 1968, 590-593.

44. Morrison, J.L.M., Crossland, B., Parry, J.S.C. 'Strength of Thick Walled Cylinders Subjected to Repeated Internal Pressure', Proc. Inst. Mech. Engs., 74, 1960, p95.

45. Owen, M.J., Smith, T.R. 'Some Fatigue Properties of Chopped-Strand-Mat/Polyester - Resin Laminates', Plastics and Polymers, Feb. 1968, 33-44.

46. Owen, M.J., Dukes, R., 'Failure of Glass-Reinforced Plastics Under Single and Repeated Loading', J. Strain Analysis, 2, No.4, 1967.

47. Owen, M.J., Dukes, R., Smith, T.R., 'Fatigue and Failure Mechanisms in GRP with Special Reference to Random Reinforcements', 23rd Annual Tech. and Man. Conf. SPI, Washington DC, 1968, Section 14A.

48. Owen M.J. 'Fatigue', Glass Reinforced Plastics (Chapter 18), Edited by B. Parkyn, Iliffe Books, London, 1970.

49. Pagano, N.J., Whitney, J.M. 'Geometric Design of Composite Cylindrical Characterisation Specimens', J. Composite Materials, 4, July 1970,360-378

50. Owen, M.J., Bishop, P.T. 'Critical Stress Intensity Factors Applied to Glass Reinforced Plastics', J. Composite Materials, 7,April 1973, 146-159.

*51. Steel, D.J. 'The Creep and Stress Rupture of Reinforced Plastics', Trans. J. Plastics Inst., Oct. 1965.

52. Ashbaugh, N. 'Stresses in Laminated Composites Containing a Broken Layer - Part 11, Numerical Results', AFOSR Scientific Rpt., AFOSR-TR-72-0031,Oct.1971.

53. Dew - Hughes,D., Way, J.L. 'Fatigue of Fibre Reinforced Plastics: A Review', Composites, July 1973, 167-173.

54. Sco p, P.M., Argon, A.S. 'Statistical Theory of Strength of Laminated Composites', J. Composite Materials, 1, 1967, 92-99.

55. Margetts, A.J., Bott, T.R. 'Stress Distribution in a Brittle Plastics Matrix Surrounding Woven or Crimped Reinforcing Fibres', Plastics and Polymers, 40, No 148, 1972, 219-227.

56. Pagano, N.J., Halpin, J.C. 'Influence of End Constraint in the Testing of Anisotropic Bodies', J. Composite Materials, 2, No.1, 1968, 18-31.

57. Whitney, J.M., Halpin, J.C. 'Analysis of Anisotropic Tubes under Combined Loading', J. Composite Materials, 2, No.3, 1968, 360-367.

58. Pagano, N.J., 'Stress Gradients in Laminated Composite Cylinders', J. Composite Materials, 5, April 1971, 260-265.

59. Reuter, R.C. 'Analysis of Shells under Internal Pressure' J. Composite Materials, 6, Jan. 1972, 94-113.

60. Sherrer, R.E. 'Filament-Wound Cylinders with Axial-Symmetric Loads', J. Composite Materials, 1, 1967, 344-355.

61. Vicario, A.A. Rizzo, R.R. 'Effect of Length on Laminated Thin Tubes Under Combined Loading', J. Composite Materials, 4, April 1970, 273-277.

62. Whitney, J.M. 'On the Use of Shell Theory for Determining Stresses in Composite Cylinders', J. Composite Materials, 5, July 1970, 340-352.

63. Gulati, S.T., Essenburg,F. 'Effects of Anisotropy in Axisymmetric Cylindrical Shells', J. Applied Mechanics, 34, Sept. 1967, 659-666.

64. Widera, O.E., Chung, S.W. 'A Theory of Non-Homogeneous Anisotropic Cylindrical Shells', J. Composite Materials, 6, Jan 1972, 14-29.

65. Beadle, J.D. 'Design Engineering Series, Plastics Vol. 1', Morgan-Grampian Ltd., London, 1970.

66. Sandu, R.S. 'Parametric Study of Tsai's Strength Criteria for Filamentary Composites', AFFDL-TR-68-168, AD691028, Wright Patterson Air Force Base, Ohio, May 1969.

67. McCrum, N.G. 'A Review of the Science of Fibre Reinforced Plastics, H.M. Stationary Office, London, 1971.

68. Owen, M.J., Rose, R.G. 'The Effect of Resin Flexibility on the Fatigue Behaviour of GRP', 7th Int. Reinforced Plastics Conf., B.P.F., Brighton, Oct.1970 8/1 - 8/8.

69. Lucas, J.J., Sainsbury-Carter,J.B. 'Effect of Specimen Geometry on Fatigue Strength of Boron and Glass Epoxy Composites'. J. Materials, JMLSA, 7, No.4, Dec. 1972, 586 -589.

70. Endo, K., Yano, A., Okuda, Y. 'Studies of Fatigue Strengths of Fibreglass Reinforced Plastics', 9th Japan Congress on Testing materials, 1966, 104 - 108.

71. Dieter, G.E. 'Mechanical Metallurgy', McGraw - Hill Book Company, Inc., London, 1961.

Group 1

(A) Maximum Stress

$$\sigma_1 = X, \quad \sigma_2 = Y, \quad \sigma_6 = S \quad \checkmark$$

(B) Hill

$$\left(\frac{\sigma_1}{X}\right)^2 + \left(\frac{\sigma_2}{Y}\right)^2 - \sigma_1\sigma_2\left(\frac{1}{X^2} + \frac{1}{Y^2} - \frac{1}{Z^2}\right) + \left(\frac{\sigma_6}{S}\right)^2 = 1 \quad \checkmark$$

(C) Norris Interaction

$$\left(\frac{\sigma_1}{X}\right)^2 + \left(\frac{\sigma_2}{Y}\right)^2 + \left(\frac{\sigma_6}{S}\right)^2 = 1 \quad \checkmark$$

(D) Norris Failure

$$\left(\frac{\sigma_1}{X}\right)^2 + \left(\frac{\sigma_2}{Y}\right)^2 - \frac{\sigma_1\sigma_2}{XY} + \left(\frac{\sigma_6}{S}\right)^2 = 1 \; ; \; \left(\frac{\sigma_1}{X}\right)^2 = 1 \; ; \; \left(\frac{\sigma_2}{Y}\right)^2 = 1.$$

(E) Azzi and Tsai

$$\left(\frac{\sigma_1}{X}\right)^2 + \left(\frac{\sigma_2}{Y}\right)^2 - \frac{\sigma_1\sigma_2}{X^2} + \left(\frac{\sigma_6}{S}\right)^2 = 1$$

(F) Hoffman

(1). $$\frac{\sigma_1^2 - \sigma_1\sigma_2}{XX'} + \frac{\sigma_2^2}{YY'} + \left(\frac{X'-X}{XX'}\right)\sigma_1 + \left(\frac{Y'-Y}{YY'}\right)\sigma_2 + \left(\frac{\sigma_6}{S}\right)^2 = 1$$

(2). $$\frac{\sigma_1^2}{XX'} + \frac{\sigma_2^2}{YY'} - \sigma_1\sigma_2\left(\frac{1}{XX'} + \frac{1}{YY'} - \frac{1}{ZZ'}\right) + \left(\frac{X'-X}{XX'}\right)\sigma_1 + \left(\frac{Y'-Y}{YY'}\right)\sigma_2 + \left(\frac{\sigma_6}{S}\right)^2 = 1$$

Key

X = strength in '1' direction

Y = strength in '2' direction

Z = strength in '3' direction

S = in-plane shear strength

σ_1, σ_2, σ_6 are principal material direction stresses see table 2 for X', Y' Z'

N.B. Theories E, F(1) are limited to transverse isotropy.

Table 1 Failure Theories for Plane Stress

Group 2

(G) Modified Marin

$$\frac{\sigma_1^2 - k_2\sigma_1\sigma_2}{XX'} + \frac{\sigma_2^2}{YY'} + \left(\frac{X'-X}{XX'}\right)\sigma_1 + \left(\frac{Y'-Y}{YY'}\right)\sigma_2 + \left(\frac{\sigma_1}{S}\right)^2 = 1$$

(H) Gol'denblat and Kopnov

$$\frac{1}{2}\left(\frac{1}{X}-\frac{1}{X'}\right)\sigma_1 + \frac{1}{2}\left(\frac{1}{Y}-\frac{1}{Y'}\right)\sigma_2 + \left\{\frac{1}{4}\left(\frac{1}{X}+\frac{1}{X'}\right)^2\sigma_1^2 + \frac{1}{4}\left(\frac{1}{Y}+\frac{1}{Y'}\right)^2\sigma_2^2 + 2F_{12}\sigma_1\sigma_2 + \left(\frac{\sigma_6}{S}\right)^2\right\}^{1/2} = 1$$

(I) Tsai and Wu

$$\left(\frac{1}{X}-\frac{1}{X'}\right)\sigma_1 + \left(\frac{1}{Y}-\frac{1}{Y'}\right)\sigma_2 + \frac{\sigma_1^2}{XX'} + \frac{\sigma_2^2}{YY'} + 2F_{12}\sigma_1\sigma_2 + \left(\frac{\sigma_6}{S}\right)^2 = 1$$

Key

X = tensile strength, '1' direction
X' = compressive strength, '1' direction

Y = tensile strength, '2' direction
Y' = compressive strength, '2' direction

Z = tensile strength, '3' direction
Z' = compressive strength, '3' direction

S = in-plane shear strength

σ_1, σ_2, σ_6 are principal material direction stresses

K_2 = floating constant = coefficient of normal stress cross term.

F_{12} = normal stress interaction tensor component.

Table 2 Failure Theories for Plane Stress

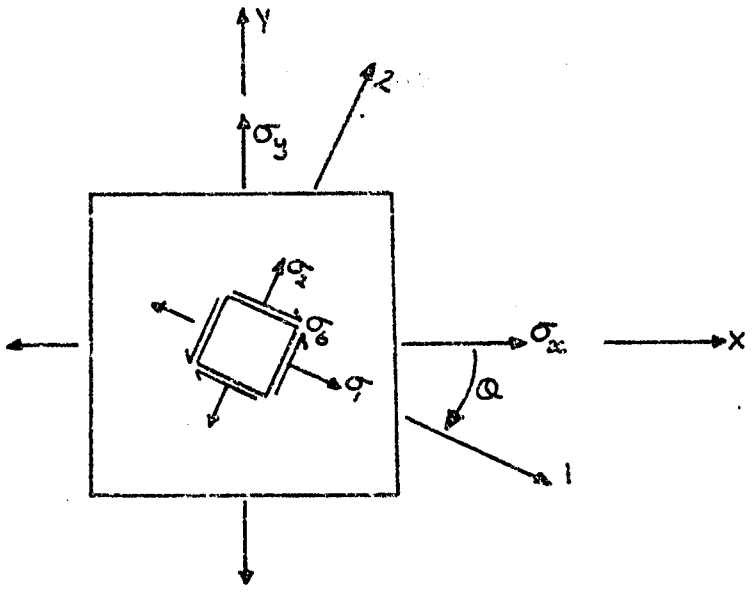

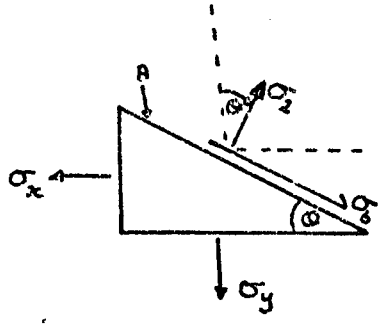

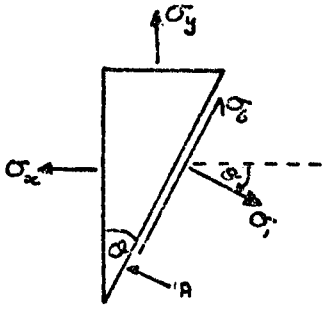

SUMMATE FORCES IN '2' DIRECTION:-

$\sigma_2 A - \sigma_x \sin\theta . A \sin\theta - \sigma_y \cos\theta . A \cos\theta = 0.$

$\therefore \sigma_2 = \sigma_x \sin^2\theta + \sigma_y \cos^2\theta$

SUMMATE FORCES IN '1' DIRECTION:-

$\sigma_1 A - \sigma_x \cos\theta . A \cos\theta - \sigma_y \sin\theta . A \sin\theta = 0$

$\therefore \sigma_1 = \sigma_x \cos^2\theta + \sigma_y \sin^2\theta$

SUMMATE FORCES IN '1' DIRECTION:-

$\sigma_b A + \sigma_y \sin\theta . A \cos\theta - \sigma_x \cos\theta . A \sin\theta = 0.$

$\therefore \sigma_b = \sin\theta . \cos\theta . (\sigma_x - \sigma_y)$

SUMMATE FORCES IN '2' DIRECTION:-

$\sigma_b A + \sigma_y \cos\theta . A \sin\theta - \sigma_x \sin\theta . A \cos\theta = 0$

$\therefore \sigma_b = \sin\theta . \cos\theta (\sigma_x - \sigma_y)$

N.B. FOR UNIAXIAL SPECIMEN, $\sigma_y = 0$. $\therefore \sigma_1 = \sigma_x \cos^2\theta$, $\sigma_2 = \sigma_x \sin^2\theta$, $\sigma_b = \sigma_x \sin\theta . \cos\theta$.

FOR CYLINDERS UNDER COMBINED INTERNAL PRESSURE AND AXIAL FORCE, σ_x = HOOP STRESS, σ_y = AXIAL STRESS.

Table 3 Stress Transformation Relationships.

OFF-AXIS ANGLE θ°	σ_1/σ_{xc}	σ_2/σ_{xc}	σ_6/σ_{xc}	SECTION OF FIG.15 EVALUATED
0	1	0	0	D
15	0·933	0·067	0·25	
30	0·75	0·25	0·433	
45	0·5	0·5	0·5	G
60	0·25	0·75	0·433	
75	0·067	0·933	0·25	
90	0	1	0	A

$\sigma_1 = \sigma_x m^2$
$\sigma_2 = \sigma_x n^2$
$\sigma_6 = \sigma_x m.n$

σ_x = UNIAXIAL TENSILE STRESS
$m = \cos\theta$
$n = \sin\theta$

UNIAXIAL SLOT SPECIMENS

$R = \sigma_y/\sigma_x$	σ_1/σ_{xc}	σ_2/σ_{xc}	σ_6/σ_{xc}
0	m^2	n^2	mn
+0·5	$m^2 + 0.5n^2$	$n^2 + 0.5m^2$	$0.5mn$
+1·0	1	1	0
−0·5	$m^2 - 0.5n^2$	$n^2 - 0.5m^2$	$1.5mn$
−1·0	$m^2 - n^2$	$n^2 - m^2$	$2mn$

$\sigma_1 = \sigma_x m^2 + \sigma_y n^2$
$\sigma_2 = \sigma_x n^2 + \sigma_y m^2$
$\sigma_6 = m.n(\sigma_x - \sigma_y)$

σ_x = HOOP STRESS
σ_y = AXIAL STRESS

TRANSFORMATION RELATIONSHIPS FOR CYLINDERS

OFF-AXIS ANGLE θ°	SECTIONS OF FIG.15 EVALUATED BY 'R' RATIOS:−				
	+1	+0·5	0	−0·5	−1
0	F	J	D	L	E
15	F				
30	F				
45	F	K	G	N	B

CYLINDERS UNDER COMBINED INTERNAL PRESSURE AND AXIAL FORCE

Table 4 Stress Transformation Relationships.

Laminate number	Material	No. Layers	Off-Axis Angle, ϕ	Joint type	Jointed *Layer No.	Joint Orientation to load	Test Environment	Loading Mode	Damage States Studied for (c).	Damage States Studied for (d).
G3	A	3	-	-	-	-	a	c,d	f,h	h
G3	A	3	-	-	-	-	b	d	-	h
G9	A	2	-	-	-	-	a	c,d	f,h	h
G6	A	3	-	m	1	90°	a	c,d	f,h	h
G8	A	3	-	m	1	90°	a	c,d	f,h	h
G8	A	3	-	m	1	90°	b	d	-	h
G10	A	2	-	m	1	90°	a	c,d	f,h	h
G10	A	2	-	m	1	0°	a	d	-	h
G11	A	3	-	m	1	0°	a	c,d	f,h	h
G17	A	3	-	m	2	90°	a	c,d	f,h	h
G12	C	5	0°	-	-	-	a	c,d	e,f,h	f,h
G12	C	5	0°	-	-	-	b	d	-	h
G13	C	5	0°	n	1	90°	a	c,d	e,f,h	h
G14	C	5	0°	-	-	-	a	d	-	h
G14	C	5	45°	-	-	-	a	d	-	h
G20	C	5	45°	-	-	-	a	c	e,f,h	f

Key :-

A - C.S.M./polyester resin
C - Y449/polyester resin
a - normal (air)
f - resin cracking
b - oil
h - failure
c - static tension
m - butt joint
d - zero-tension fatigue
n - lap joint and overlap
e - debonding
* - '1' indicates lst layer

Table 5 Summary of the Flat Laminate Test Programme.

Material	No. Layers	Off-Axis Angle, θ	Specimen gauge length mm	Stress States Studied in :-		Damage States Studied in :-	
				Static	Fatigue	Static	Fatigue
A	2	-	120	a,b,d	b,d	n	n
A	3	-	100	e,f,h	e,f,h	n	n
A	3	-	100	j	-	n	-
C	5	0°	120	a,c	a,c	m,n	m,n
C	5	0°	100	e,g,i	e,g,i	m,n	m,n
C	5	0°	50	j	-	n	-
C	5	0°	60	k	k	m,n	n
C	5	0°	120	k	-	m,n	-
C	5	45°	120	a,c	a*,c	m,n	m,n
C	5	45°	100	e,g,i	e,g,i	m,n	m,n
C	5	45°	120	k	-	m,n	-
C	5	15°	100	i	-	m,n	-
C	5	30°	100	i	-	m,n	-

Key :-

A - C.S.M./polyester resin
C - Y449/polyester resin
a - R=+1,
b - R= +0.75,
c - R= +0.5,
d - R= +0.25,
e - R = 0,
f - R= -0.25,
g - R= -0.5,
h - R= -0.75
i - R= -1
j - R= $-\infty$
k - pure shear (torsion)
m - resin cracking
n - failure
* - damage only

Table 6 Summary of the Cylinder Test Programme.

1	2	3	4	5	6	7	8	9	10	11
Laminate description	Laminate Number	No. of test coupons in group	Thickness mm	Resin cracking stress MN_m^{-2}	Total failure stress MN_m^{-2}	Ratio A	Tensile Modulus GN_m^{-2} Initial	Tensile Modulus GN_m^{-2} Secondary	% Strain to resin cracking	Glass Content WT. %	Corrected U.T.S. MN_m^{-2}
3 layered	G3	10	a) 3.24 b) 3.41 c) 3.12	a) 53.46 b) 62.90 c) 40.65	a) 103.78 b) 111.5 c) 93.0	a) 51.74 b) 60.4 c) 38.9	a) 9.65 b) 10.57 c) 8.86	a) 8.05 b) 8.94 c) 7.15	a) 0.61 b) 0.71 c) 0.42	a) 33.76† a) 33.50*	a) 103.5
2 layered	G9	8	a) 2.47 b) 2.30 c) 2.60	a) 50.92 b) 66.62 c) 35.53	a) 96.07 b) 109.11 c) 81.10	a) 52.89 b) 70.30 c) 40.51	a) 9.32 b) 10.76 c) 8.18	a) 8.02 b) 9.23 c) 6.98	a) 0.59 b) 0.74 c) 0.41	a) 33.29†	
3 layered butt joint ⊥ to tensile stress axis in one outer layer.	G6	10	a) 3.36 b) 3.39 c) 3.33	a) 46.88 b) 53.75 c) 36.50	a) 88.60 b) 109.20 c) 74.00	a) 53.15 b) 63.99 c) 43.14	a) 9.58 b) 10.70 c) 8.12	a) 8.03 b) 8.97 c) 6.83	a) 0.55 b) 0.60 c) 0.47	a) 34.56† a) 32.67*	a) 91.7
3 layered butt joint as above.	G8	9	a) 3.45 b) 3.56 c) 3.36	a) 38.86 b) 45.05 c) 28.02	a) 90.31 b) 100.07 c) 79.24	a) 43.61 b) 56.85 c) 28.00	a) 9.079 b) 9.58 c) 8.46	a) 7.43 b) 7.80 c) 6.92	a) 0.46 b) 0.57 c) 0.20	a) 32.12*	a) 95.8
3 layered butt joint // to tensile stress axis in one outer layer.	G11	9	a) 3.66 b) 3.80 c) 3.50	a) 44.59 b) 48.60 c) 39.00	a) 91.08 b) 97.28 c) 84.38	a) 49.06 b) 53.83 c) 42.43	a) 7.56 b) 9.61 c) 6.97	a) 6.58 b) 8.45 c) 5.72	a) 0.61 b) 0.70 c) 0.42	a) 30.77*	a) 103.2
3 layered butt joint ⊥ to tensile stress axis in middle layer.	G17	12	a) 3.49 b) 3.64 c) 3.30	a) 57.20 b) 74.01 c) 46.88	a) 104.33 b) 118.77 c) 96.13	a) 55.11 b) 72.92 c) 40.65	a) 8.94 b) 10.39 c) 7.58	a) 7.53 b) 8.80 c) 6.34	a) 0.71 b) 0.99 c) 0.55	a) 31.87*	a) 111.8
2 layered butt joint ⊥ to tensile stress axis in one outer layer.	G10	9	a) 2.25 b) 2.31 c) 2.13	a) 38.39 b) 44.79 c) 25.64	a) 88.03 b) 111.56 c) 70.81	a) 44.36 b) 55.97 c) 27.39	a) 8.23 b) 10.50 c) 6.73	a) 7.32 b) 9.23 c) 5.76	a) 0.50 b) 0.62 c) 0.33		

(a) = Mean Value, (b) = Max. Value, (c) = Min. Value. † = Experimental Value * = Estimated from Fig.32

Ratio (A) = (resin cracking stress ÷ total failure stress) x 100%

Table 7 Summary of Static Uniaxial Test Data for C.S.M./Polyester Resin Laminates.

Nominal Biaxial Stress Ratio(R) σ_y/σ_x	No. Test Specimen in group	Static Data: Failure Stress MN_m-2 Hoop σ_x	Static Data: Failure Stress MN_m-2 Axial σ_y	Static Data: Glass Content WT. % Spec. Ave.	Static Data: Glass Content WT. % At Failure line	No. Test Specimen in group	Fatigue Data: Maximum Failure Stress MN_m-2 at cycles:- Hoop σ_x 10^3	Fatigue Data: Maximum Failure Stress MN_m-2 at cycles:- Hoop σ_x 10^6	Fatigue Data: Maximum Failure Stress MN_m-2 at cycles:- Axial σ_y 10^3	Fatigue Data: Maximum Failure Stress MN_m-2 at cycles:- Axial σ_y 10^6	Fatigue Data: Failure Stress Range MN_m -2 at cycles:- Hoop σ_x 10^3	Fatigue Data: Failure Stress Range MN_m -2 at cycles:- Hoop σ_x 10^6	Fatigue Data: Failure Stress Range MN_m -2 at cycles:- Axial σ_y 10^3	Fatigue Data: Failure Stress Range MN_m -2 at cycles:- Axial σ_y 10^6
0	7	97.08	+1.87	34.64	33.18	10	59.53	26.06	+0.38	+0.27	55.38	22.98	+0.59	+0.34
* 0	3	100.06	+0.57	34.55		6					65.51	31.73	+0.39	+0.19
+0.25	5	99.65	+26.76	31.45	29.27	11	57.88	26.48	+14.61	+6.74	52.04	22.07	+13.01	+5.52
*+0.5	3	90.95	+45.47	28.52		7					46.89	24.14	+23.45	+12.07
+0.75	5	96.68	+69.33	32.92	30.89	9	57.92	28.23	+42.66	+21.58	52.93	23.61	+38.12	+16.90
+1.0	4	90.29	+87.03											
*+1.0	3	80.13	+78.32	30.33		5					45.51	19.95	+42.33	+17.08
-0.25	5	92.13	-19.21	32.98	32.54	10	54.63	22.06	-11.71	-5.12	50.52	19.12	-10.75	-3.89
*-0.5	3	86.96	-41.14	30.59		6					67.57	26.89	-29.74	-11.83
-0.75	7	91.68	-62.15	31.70	30.65	11	56.34	22.76	-39.51	-15.54	52.34	19.45	-35.5	-13.2
*-1.0	3	74.01	-69.55	30.84		7					66.21	20.68	-63.56	-19.86
- ∞	2		-197.5											
			Ave. (Found)	30.96										
			Ave. (Griffiths)	32.73	31.31									

* Indicates data by Found.

Table 8 Summary of Biaxial Stress Test Results from C.S.M./Polyester Resin Cylinders.

Laminate Description	Test Environment	Laminate Number	No. Test Specimens in group	Axial Force KN, (from fig 39) at cycles:-		Axial stress MN_m^{-2} (from fig 38) at cycles:-		Glass Content Wt. %
				10^3	10^6	10^3	10^6	
3 layered	normal	G3	10	3.43	2.27	90.35	59.72	37.42
3 layered	oil	G3	11	3.08	2.39	79.50	61.76	36.09
3 layered butt joint ⊥ to tensile stress axis in one outer layer	normal	G6	12	1.31	1.00	48.18	26.52	
3 layered joint as above	normal	G8	8	2.38	1.05	56.96	25.25	
3 layered joint as above	oil	G8	7	2.21	1.27	53.31	30.69	
3 layered butt joint // to tensile stress axis in one outer layer	normal	G11	10	3.17	1.92	77.93	47.17	
3 layered butt joint ⊥ to tensile stress axis in middle layer.	normal	G17	9	3.25	1.52	79.74	37.31	
2 layered	normal	G9	11	2.26	1.66	79.89	57.59	36.63
2 layered butt joint ⊥ to tensile stress axis in one layer.	normal	G10	8	1.45	0.70	54.07	26.12	
2 layered butt joint // to tensile stress axis in one layer.	normal	G10	7	2.27	1.19	76.9	41.2	

Table 9 Summary of Zero-Tension Uniaxial Stress Fatigue Data for C.S.M/Polyester Resin composites.

Laminate Type	Laminate Number	Off - Axis Angle	No. Specimens in group	Thickness mm	Uniaxial Tensile Stress MNm^{-2}				Tensile Modulus GNm^{-2}		Glass Content Wt. %
					Debonding	Resin Cracking	Joint Cracking	Ultimate Failure	Initial	Secondary	
5 layered	G12	0^{o}	9	2.08	a)64.7 b)73.8 c)53.5	a) 72.8 b) 77.4 c) 68.7		a)209.2 b)219.5 c)193.5	a)17.6 b)18.3 c)16.2	a)15.7 b)16.4 c)15.3	52.3*
5 layered joint and overlap	G13	0^{o}	10		a)73.6 b)78.9 c)56.5	a) 81.6 b) 91.8 c) 69.1	a)87.3 b)97.1 c)79.8	a)184.3 b)195.6 c)169.7	a)17.9 b)18.3 c)17.6	a)15.5 b)15.9 c)15.0	
7 layered (FOUND)		0^{o}			a)83.4	a) 83.4		a)231	a)20.9		58.0
7 layered (BISHOP)		0^{o}	5		a)93.7	a)105.0		a)229			

(a) = Mean, (b) = Max., (c) = Min. * = estimated from Fig. 53

Table 10 Uniaxial Static Test Data from Y449-Fabric/Polyester Resin Laminates.

Nominal 'R' σ_y/σ_x	No. Specimens in Group.	Joint Cracking Stress MN_m^{-2}		Resin Cracking Stress MN_m^{-2}		Failure Stress MN_m^{-2}	
		Hoop σ_x	Axial σ_y	Hoop σ_x	Axial σ_y	Hoop σ_x	Axial σ_y
0	4	120.58	+ 3.89	129.07	+ 3.79		
0	5					262.2	+ 6.4
+0.5	4	90.51	+45.26	85.35	+42.67		
+0.5	5					263.9	+131.9
+1.0	4	89.51	+85.48	82.95	+79.16		
+1.0	5					241.17	+230.57
-0.5	4	99.14	-39.14	97.42	-38.47		
-0.5	5					233.9	- 98.9
-1.0	4	96.30	-82.94	100.96	-88.25		
-1.0	5					163.4	-147.4
$-\infty$	3						-200.0

Table II Summary Table showing Mean Biaxial Stress Static Test Results from Y449/Polyester Resin Cylinders 0^o Orientation.

Laminate description	Test Environment	Laminate Number	Fibre Orientation	No. Specimens in group.	Specimen type (see Fig. 28)	Axial Stress MN_m^{-2} at cycles: 10^3	10^6
5 layered	normal	G12	0^o	13	C	174	60.00
5 layered	oil	G12	0^o	8	C	160.00	69.18
5 layered	normal	G12+ G14	0^o	10	D	183.94	60.28
5 layered joint and overlap construction	normal	G13	0^o	8	D	143.80	60.35
5 layered	normal	G14	45^o	10	D	87.23	48.72
7 layered (Found 1)	normal		0^o		C	202.7	96.5
			45^o		C	111.7	48.3
7 layered (Bishop 38)	normal		0^o		C	203	96.5
			45^o		C	112	48.2

Table 12 Summary of Uniaxial Zero-Tension Fatigue Data for Failure of Y449/Polyester Resin Laminates.

Nominal 'R' σ_y/σ_x	No. Specimens in Group	Maximum Failure Stress MN_m-2 at cycles:-				Failure Stress Range MN_m-2 at cycles :-			
		Hoop σ_x		Axial σ_y		Hoop σ_x		Axial σ_y	
		10^3	10^6	10^3	10^6	10^3	10^6	10^3	10^6
0	16	151.95	61.97	+ 2.69	+ 0.82	145.41	60.41	+ 2.18	+ 2.06
+0.5	15	146.12	80.85	+72.90	+41.03	139.11	77.18	+70.38	+39.80
+1.0	15	141.49	55.37	+138.64	+55.75	136.31	50.34	131.23	48.59
-0.5	15	130.96	63.58	-60.70	-28.38	122.20	57.35	-54.30	-24.74
-1.0	17	104.90	43.82	-97.44	-40.95	96.21	38.76	-88.29	-32.58

Table 13 Summary Table showing Mean Biaxial Stress Fatigue Test Results from Y449/Polyester Resin Cylinders 0^o Orientation.

Nominal 'R' σ_y / σ_x	No Specimens in group.	Stress Range MNm^{-2} at cycles :-			
		Hoop σ_x		Axial σ_y	
		10^3	10^6	10^3	10^6
0	15	32.0	11.0	+0.8	+0.3
+0.5	15	27.5	10.0	+13.8	+5.0
+1.0	14	29.5	10.5	+28.8	+10.3
-0.5	15	28.0	11.0	-12.9	-5.1
-1.0	15	26.6	9.0	-23.9	-8.1

Table 14 Biaxial Stress Fatigue Resin Cracking Test Results From Y449/Polyester Resin Cylinders 0^o Orientation.

Laminate Number	No. of layers	Off-axis Angle, degrees	No specimens in group.	Specimen Type	Operator	Loading Mode	Uniaxial Stress MNm^{-2} Debonding	Resin Cracking	Ultimate Failure
G12	5	0	9	K	G	T	64.7	72.8	209.2
G20	5	45	13	K	G	T	41.2	68.0	112.3
	7	0/90		K	F	T	83.4	83.4	231
	"	15		"	"	"	75.8	75.8	190.3
	"	30		"	"	"	71.0	71.0	151.7
	"	45		"	"	"	71.0	71.0	133.8
	7	0	5	K	B	T	83.7	105.0	229.0
	"	15	"	"	"	"	91.6	-	183.0
	"	30	"	"	"	"	75.9	-	132.0
	"	45	"	"	"	"	69.0	-	113.0
	7	0		M	B	T	93.7	105.0	229.0
	"	15		"	"	"	91.5	97.8	211.0
	"	30		"	"	"	92.2	92.2	192.0
	"	45		"	"	"	91.6	91.6	183.0
	7	0/90		N	F	C	191	191	226.8
	"	15		"	"	"	169.3	169.3	209.4
	"	30		"	"	"	166.2	166.2	204.9
	"	45		"	"	"	149.6	149.6	190.2

KEY:-

Specimen Types
K - type B Fig.28
N - type A Fig.28
M - fatigue type

Loading Mode
T - tension
C - compression

Operator
G - Griffiths
F - Found (1)
B - Bishop (38)

Table 15 Uniaxial Static Test Data from Y449-Fabric/ Polyester Resin Laminates.

Failure Mode.	Nominal 'R' σ_y/σ_x	Fibre Orientation degrees	No. Specimens in group.	Applied Stress MN_m^{-2} Hoop σ_x	Axial σ_y	Principal Direction Stress MN_m^{-2} σ_1	σ_2	σ_6
Resin Cracking $//\sigma_y$ from Air Bubbles.	0	45	4	71.81	2.11	36.96	36.96	34.85
	+0.5	45	4	97.96	48.98	73.47	73.47	24.49
	+1.0	45	-	-	-	-	-	-
	-0.5	45	6	70.23	-25.46	22.38	22.38	47.85
	-1.0	45	4	48.21	-41.24	3.49	3.49	44.73
	-1.0	15	-	-	-	-	-	-
	-1.0	30	3	71.83	-62.08	38.35	-28.61	57.99
Joint Cracking $//\sigma_y$	0	45	11	76.55	2.57	39.56	39.56	36.99
	+0.5	45	9	94.14	47.07	70.60	70.60	23.54
	+1.0	45	3	70.25	66.03	68.14	68.14	2.08
	-0.5	45	9	72.57	-26.78	22.89	22.89	49.68
	-1.0	45	9	59.85	-51.70	4.08	4.08	55.78
	-1.0	15	6	86.05	-75.97	75.20	-65.11	40.51
	-1.0	30	5	71.65	-61.78	38.29	-28.43	57.77
Resin Cracking $//\sigma_y$	0	45	11	93.04	3.00	48.02	48.02	45.02
	+0.5	45	9	101.10	50.56	75.83	75.83	25.28
	+1.0	45	3	91.79	88.40	90.10	90.10	1.69
	-0.5	45	8	77.29	-28.95	24.16	24.16	53.12
	-1.0	45	9	73.49	-63.98	4.88	4.88	68.74
	-1.0	15	6	73.91	-66.21	64.52	-56.82	35.03
	-1.0	30	6	78.18	-67.83	41.68	-31.33	63.22
Resin Cracking // principal direction	0	45	-	-	-	-	-	-
	+0.5	45	9	127.81	63.91	95.86	95.86	31.95
	+1.0	45	10	82.82	79.06	80.94	80.94	1.88
	-0.5	45	-	-	-	-	-	-
	-1.0	45	-	-	-	-	-	-
	-1.0	15	6	82.09	-71.84	71.77	-61.53	38.49
	-1.0	30	-	-	-	-	-	-
Failure	0	45	4	202.82	6.12	104.47	104.47	98.35
	+0.5	45	5	269.09	134.54	201.82	201.82	67.27
	+1.0	45	5	240.82	231.56	236.19	236.19	4.63
	-0.5	45	5	156.34	-63.73	46.30	46.30	110.04
	-1.0	45	5	103.89	-91.00	6.45	6.45	97.44
	-1.0	15	3	159.28	-143.42	139.00	-123.13	75.68
	-1.0	30	3	125.58	-110.14	66.66	-51.22	102.07

Table 16 Summary of Off-Axis Biaxial Stress Static Test Data From Y449/Polyester Resin Cylinders.

Off - axis angle, θ	Specimen gauge length mm.	No specimens in group.	Static Data: Resin Cracking Stress $MN\ m^{-2}$	Static Data: Failure Stress $MN\ m^{-2}$	Fatigue Data: Failure Stress $MN\ m^{-2}$ at cycles :- 10^3	Fatigue Data: Failure Stress $MN\ m^{-2}$ at cycles :- 10^6
0°	120	2	57.22	68.58		
0°	60	5	57.59	72.33		
0°	60	6			50.68	31.36
45°	120	2	60.96	104.18		

Table 17 Results from torsion tests on Y449/polyester resin cylinders.

Nominal 'R' σ_y/σ_x	No. Specimens in group.	Maximum Failure Stress MN_m^{-2} at cycles:-				Failure Stress Range MN_m^{-2} at cycles:-				Maximum Principal Direction Stress MN_m^{-2} at cycles:-				Principal Direction Stress Range MN_m^{-2} at cycles:-			
		Hoop σ_x		Axial σ_y		Hoop σ_x		Axial σ_y		σ_1		σ_6		σ_1		σ_6	
		10^3	10^6	10^3	10^6	10^3	10^6	10^3	10^6	10^3	10^6	10^3	10^6	10^3	10^6	10^3	10^6
0	15	116.03	57.72	1.28	1.01	109.48	52.67	1.55	1.17	58.65	29.36	57.37	28.35	55.51	26.92	53.96	25.75
+0.5	12	125.91	70.78	62.93	35.34	120.02	65.20	60.01	32.60	94.42	53.06	31.49	17.72	90.01	48.9	30.00	16.3
-0.5	12	78.18	38.69	-34.46	-16.77	71.68	33.12	-31.03	-13.93	21.91	10.96	56.32	27.73	20.32	9.59	51.36	23.53
-1.0	12	62.75	29.14	-57.97	-27.06	56.73	23.05	-50.52	-21.37	2.39	1.04	60.36	28.10	3.10	0.84	53.62	22.21

N.B. $\sigma_2 = \sigma_1$ for $\Theta = 45^\circ$

Table 18 Summary of 45° off-axis Biaxial Stress Fatigue Data from Y449/Polyester Resin Cylinders.

Nominal 'R' σ_y / σ_x	No Specimens in group	Stress Range MNm^{-2} at cycles :-				Principal Direction Stress Range MNm^{-2} at cycles :-			
		Hoop σ_x		Axial σ_y		σ_1(+ve)		σ_6(-ve)	
		10^3	10^6	10^3	10^6	10^3	10^6	10^3	10^6
0	10	26.5	10.0	+0.5	+0.2	13.3	5.1	13.3	4.9
+0.5	11	26.0	9.5	+13.5	+4.9	19.8	7.2	6.3	2.3
+1.0	10	26.0	9.5	+23.6	+8.7	24.8	9.1	1.2	0.42
-0.5	11	23.0	7.5	-8.1	-2.6	7.4	2.4	15.6	5.1
-1.0	11	23.5	6.5	-20.2	-5.8	1.7	0.4	21.8	6.1

N.B. $\sigma_2 = \sigma_1$ for $\Theta = 45^\circ$

Table 19 Biaxial Stress Fatigue Resin Cracking Results from Y449-Fabric/Polyester Resin Cylinders 45° Orientation.

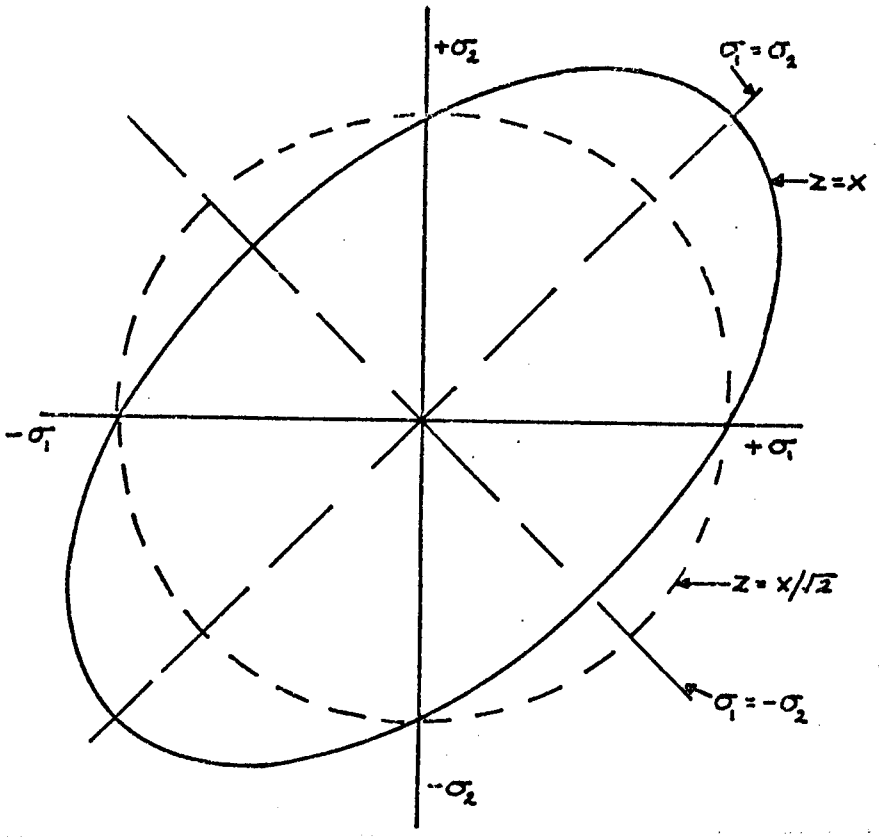

Fig. 1 The effect of Z on the Hill failure envelope, $X=X'=Y=Y'$, $\sigma_6=0$.

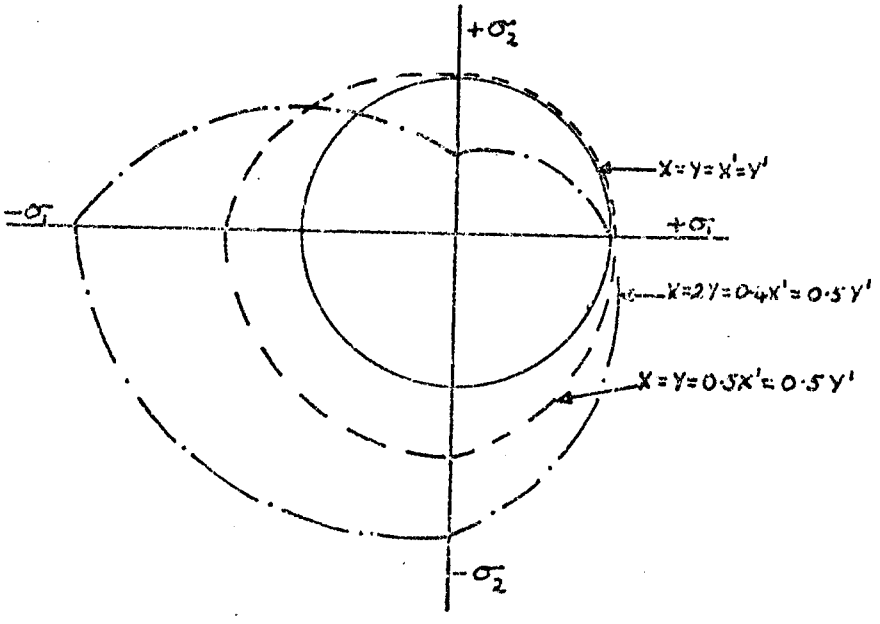

Fig. 2 The effect of principal strength variation on the Norris interaction failure envelope, $\sigma_6=0$.

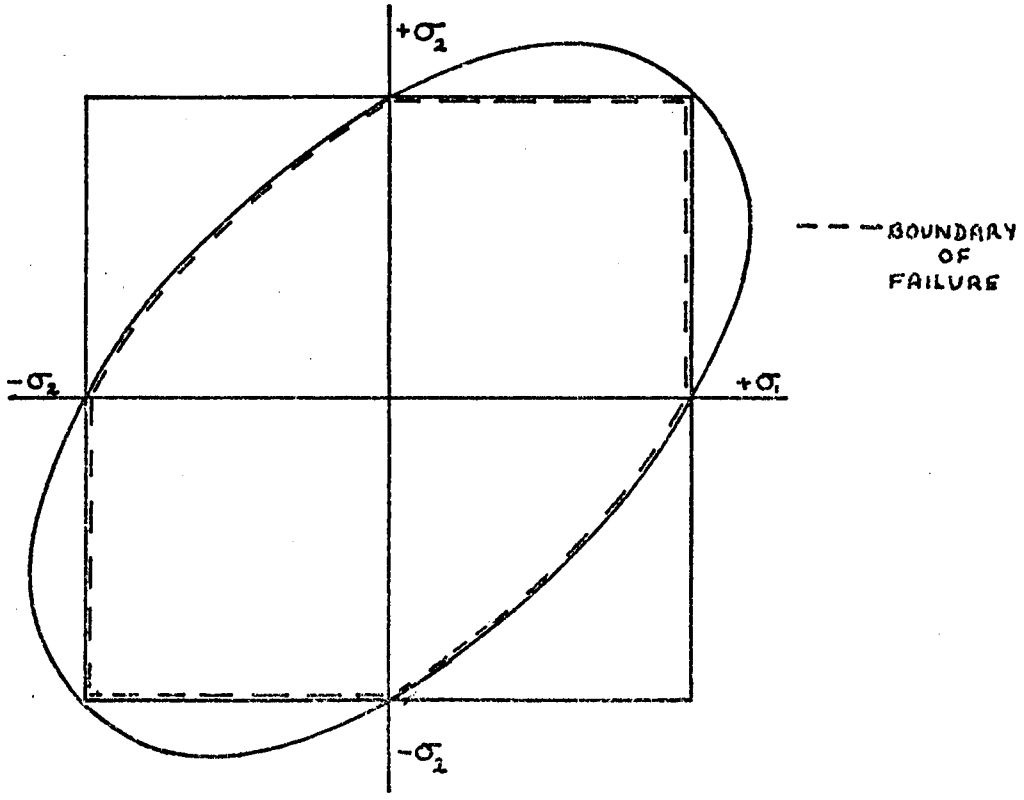

Fig. 3 The Norris failure condition, $X=X'=Y=Y'$, $\sigma_0=0$.

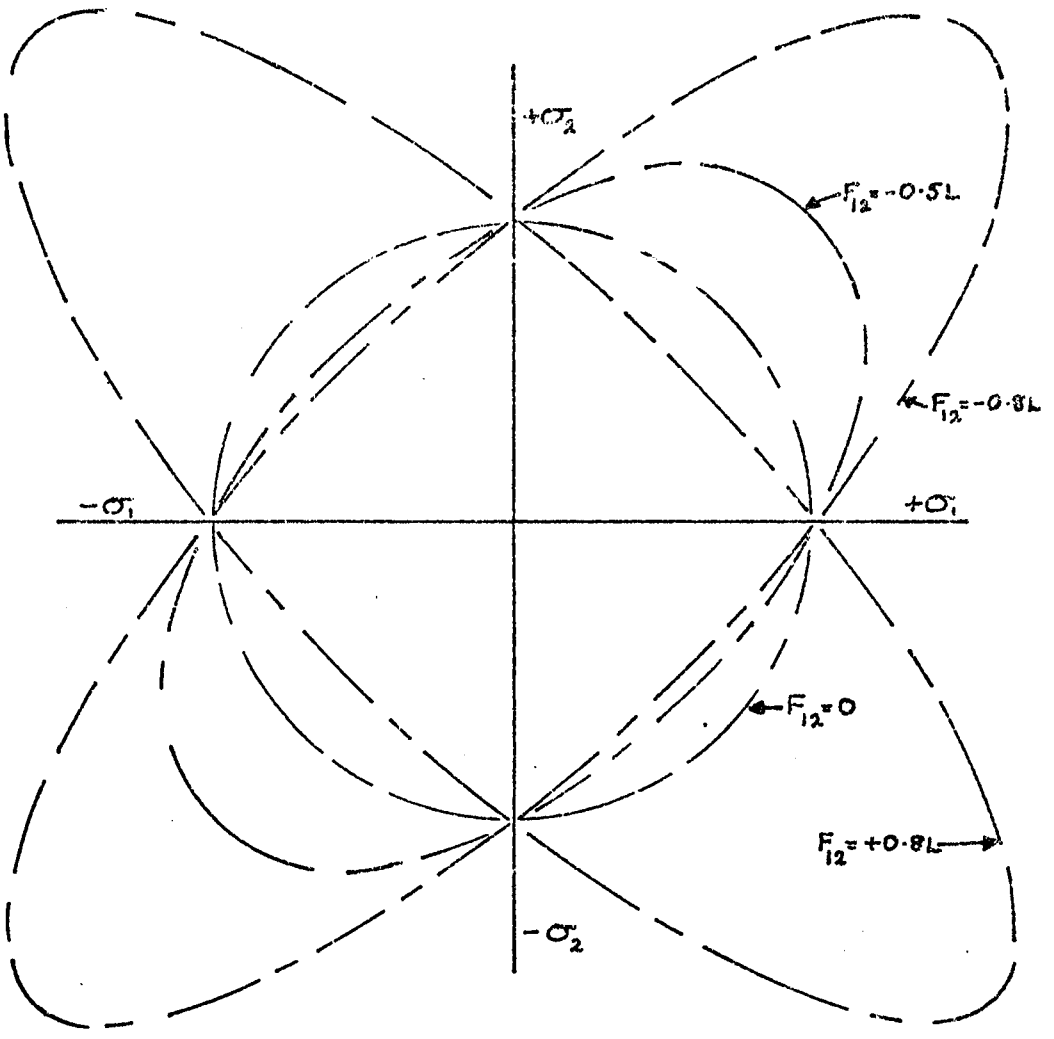

Fig. 4 The effect of F_{12} on the Tsai and Wu failure envelope, $X=X'=Y=Y'$ $\sigma_6=0$.

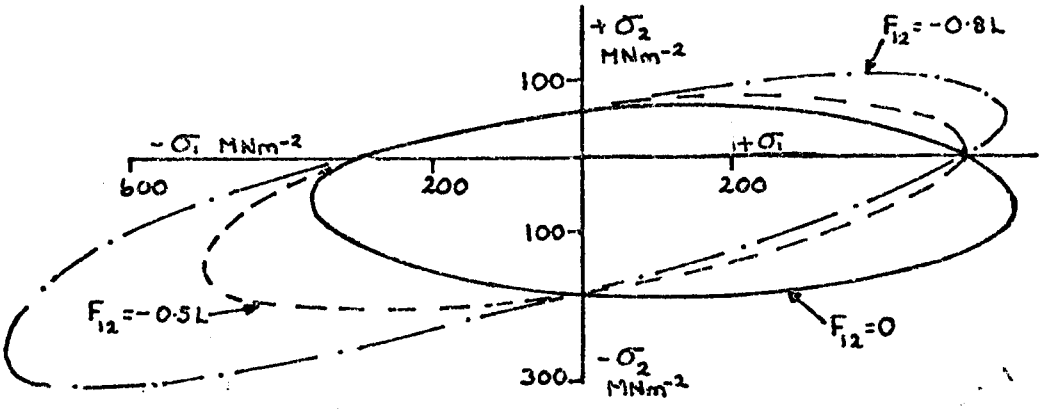

Fig. 5 The effect of F_{12} on the Tsai and Wu failure envelope for a unidirectional GRP with X=500, X'=300, Y=60, Y'=160 MNm^{-2}, $\sigma_6=0$.

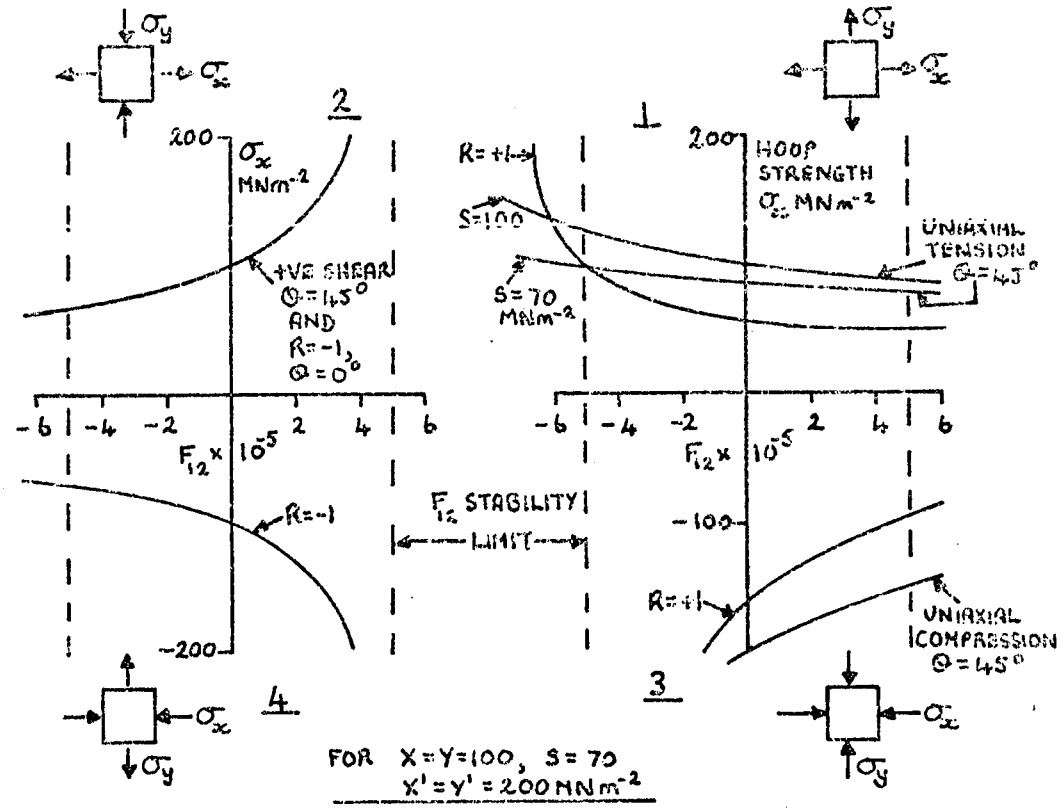

N.B. $R = \sigma_y / \sigma_x$. THE 'R' VALUES SHOWN ARE FOR Θ=0° i.e. $R = \sigma_2/\sigma_1$, $\sigma_2 = 0$.
Θ = OFF-AXIS ANGLE.

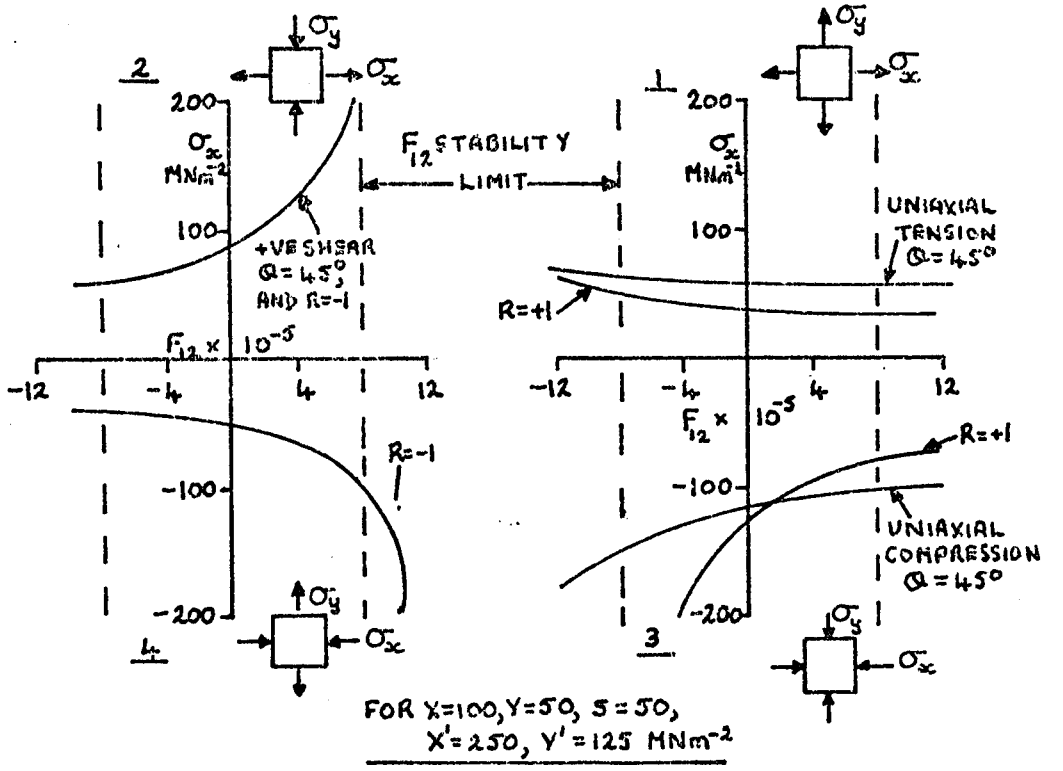

Fig. 6 F_{12} variation with strength for different degrees of strength anisotropy.

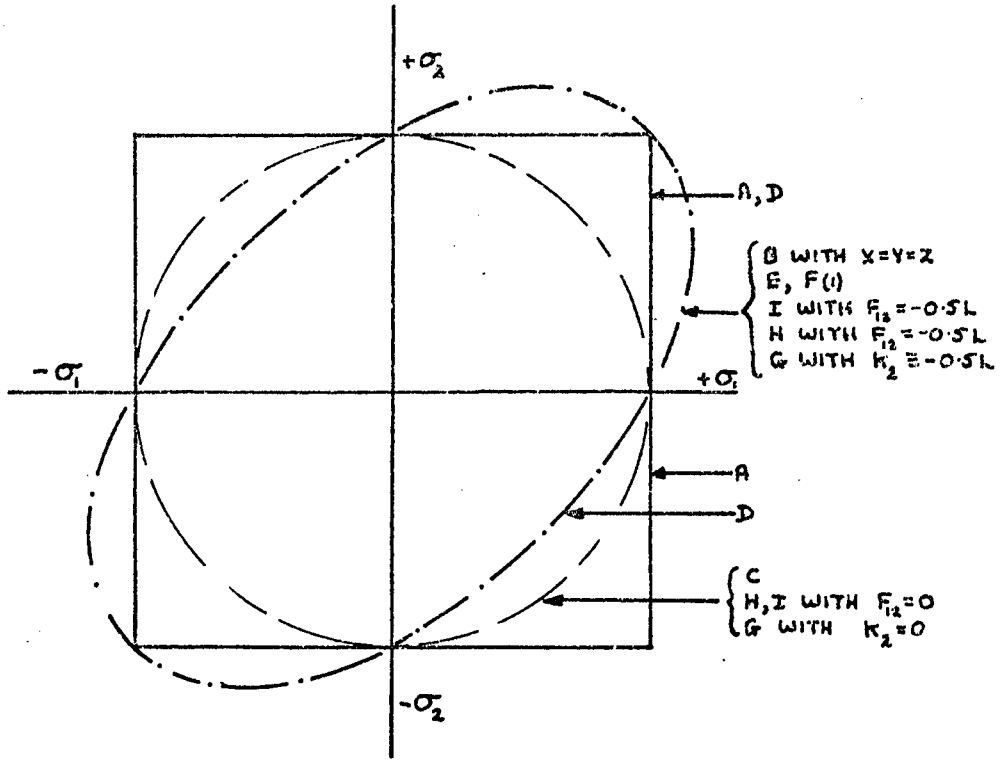

Fig. 7 Comparison of failure envelopes for X=Y=X'=Y' and $\sigma_6=0$.

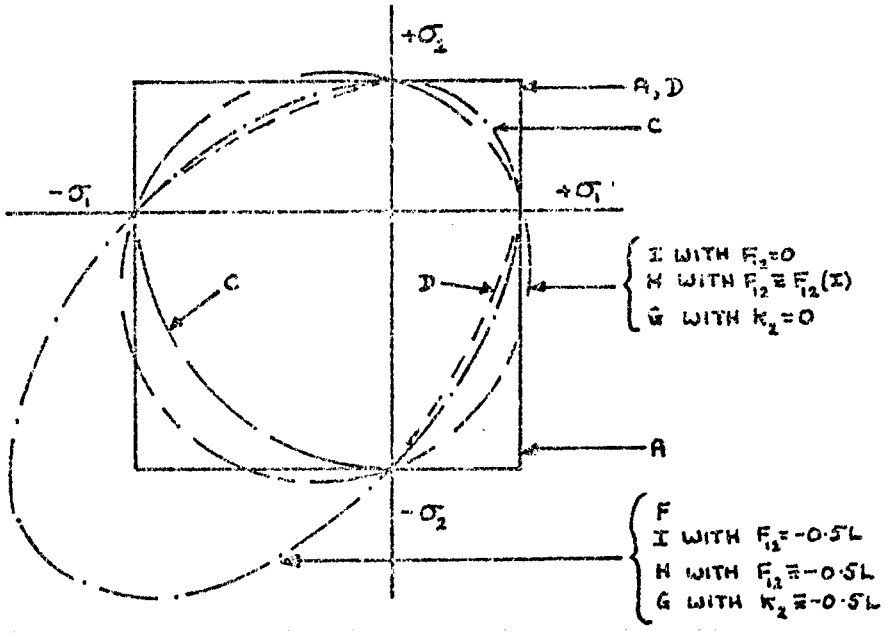

Fig. 8 Comparison of failure envelopes for $X=Y=0.5X'=0.5Y'$ and $\sigma_6=0$.

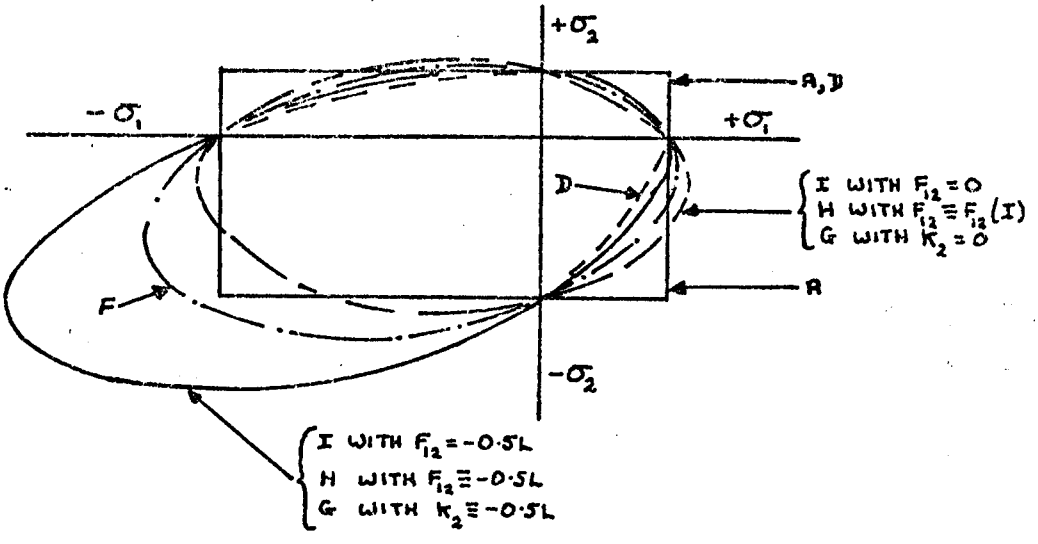

Fig. 9 Comparison of failure envelopes for $X=2Y=0.4X'=0.8Y'$ and $\sigma_6=0$.

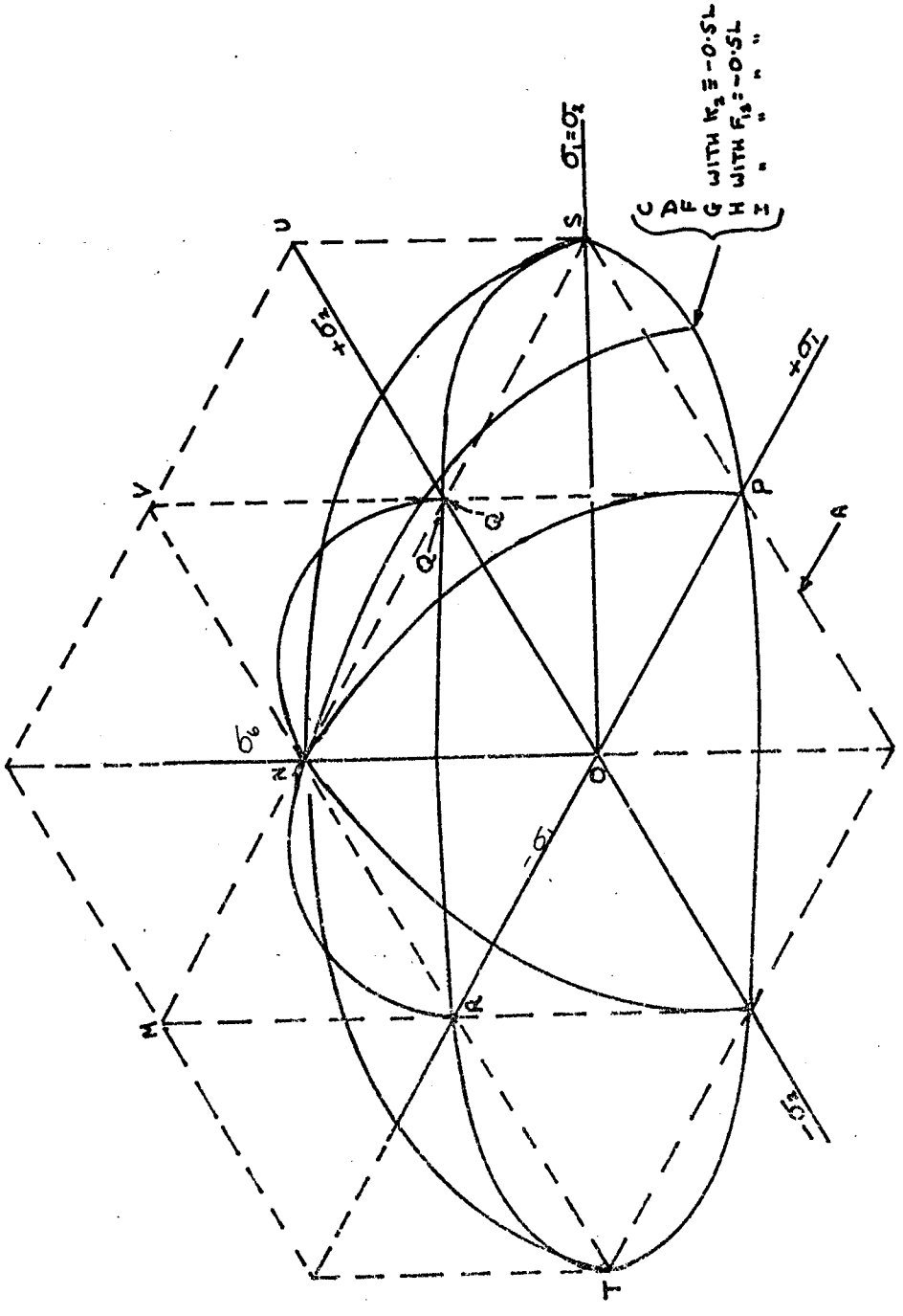

Fig. 10 Plane stress failure surface for X=Y=X'=Y'=S.

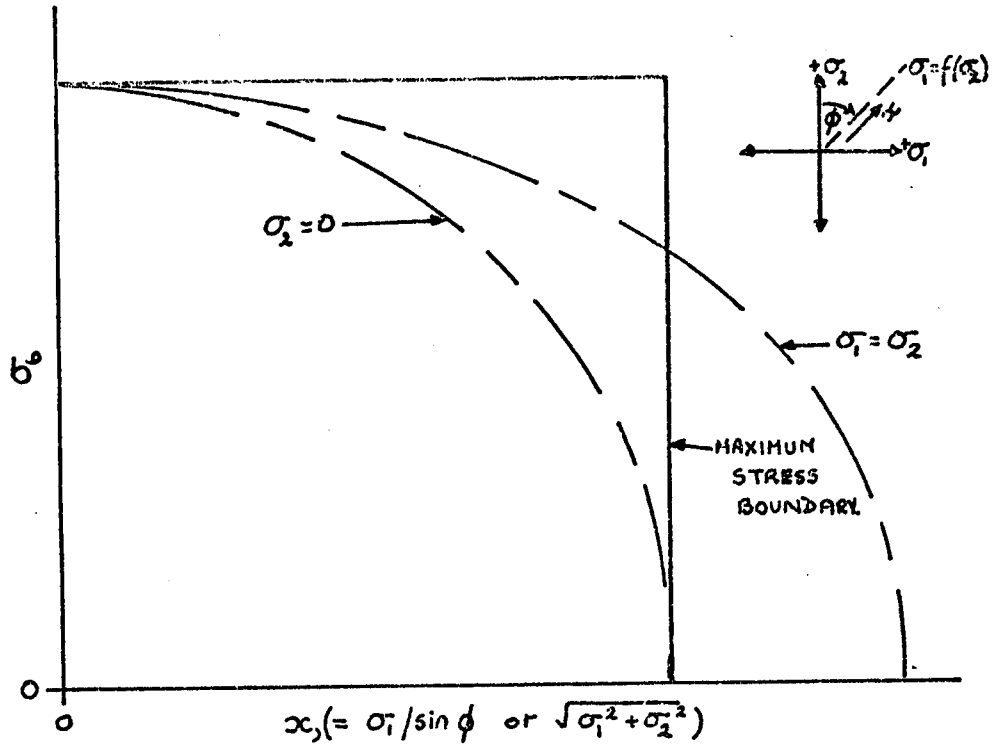

Fig. 11 Section from failure surface of Fig.10.

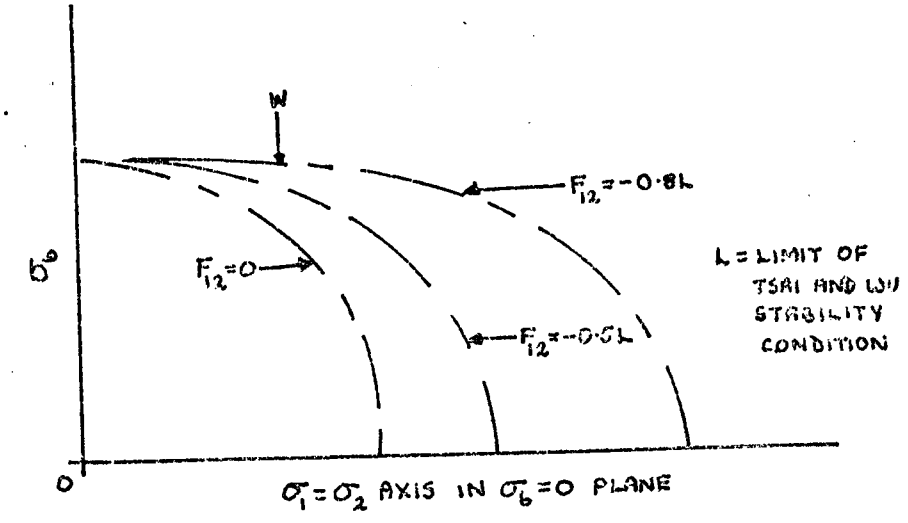

Fig. 12 The effect of F_{12} on the $\sigma_1=\sigma_2$ failure surface profile in σ_1, σ_6 space.

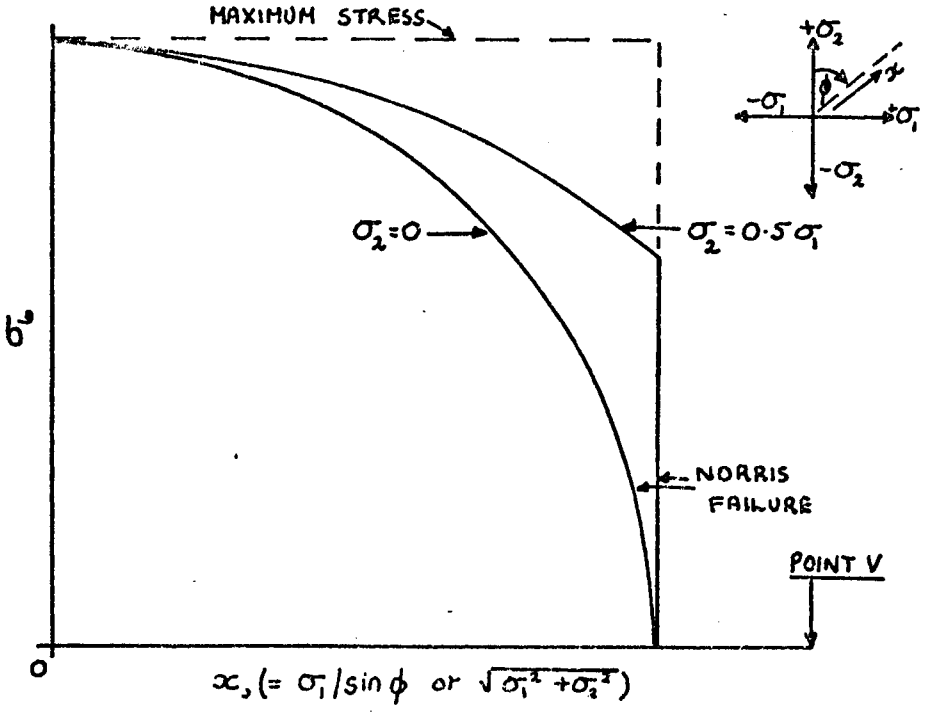

Fig. 13 Section from failure surface of Fig.10 showing the Norris failure theory profile.

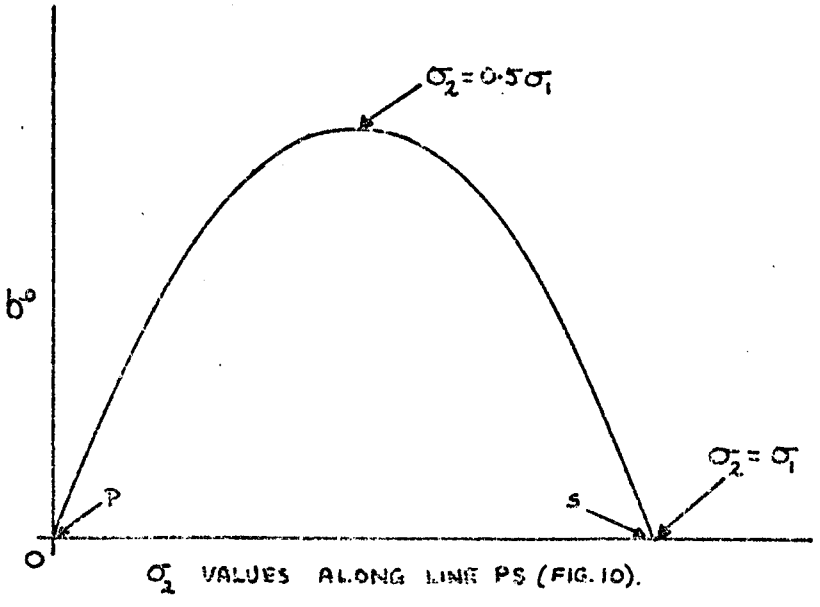

Fig. 14 The Norris failure theory profile seen when looking from point 'V' (Fig.13) towards the σ_6 axis.

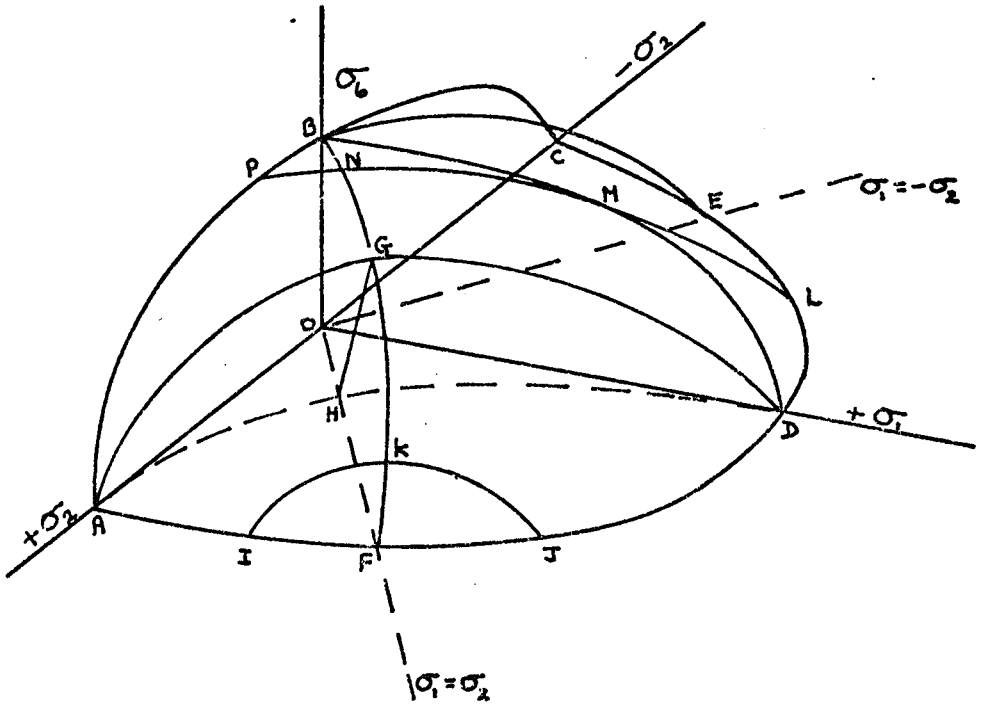

Fig. 15 An experimental failure surface.

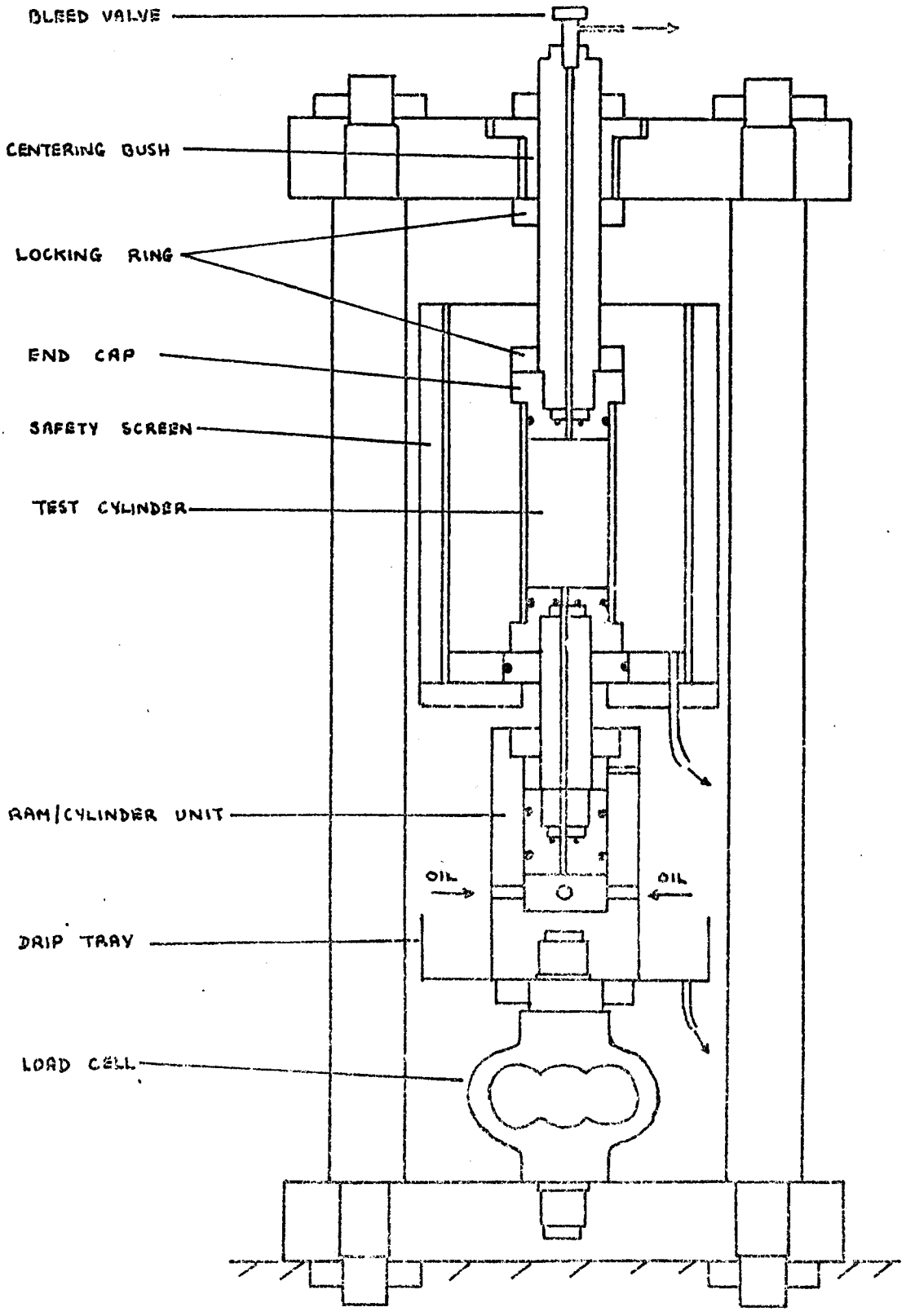

Fig. 16 Section through a loading frame.

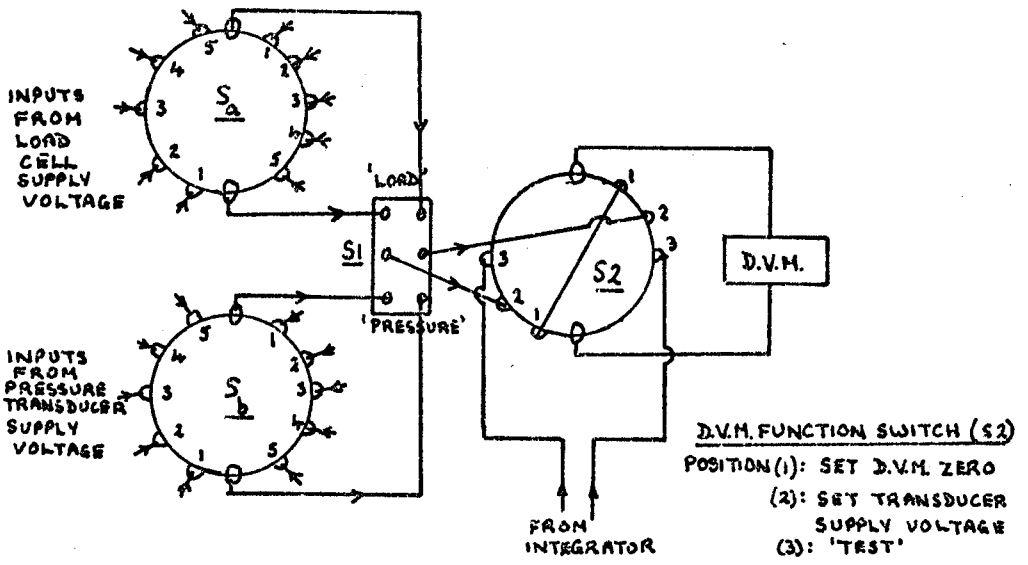

Fig. 17 Electrical modifications to biaxial stress test machine recording frame.

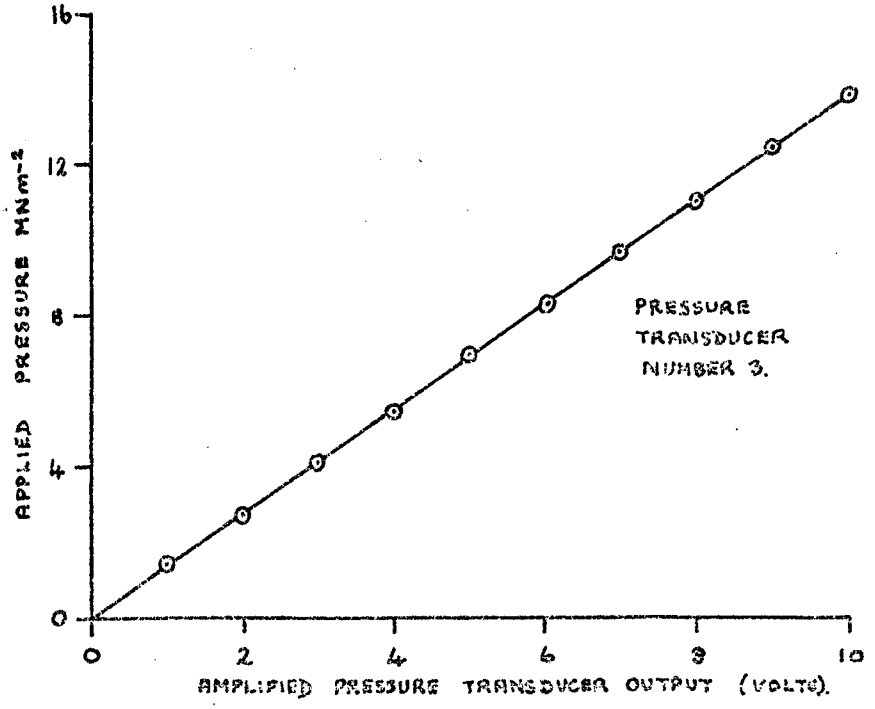

Fig. 18 Typical pressure transducer calibration curve.

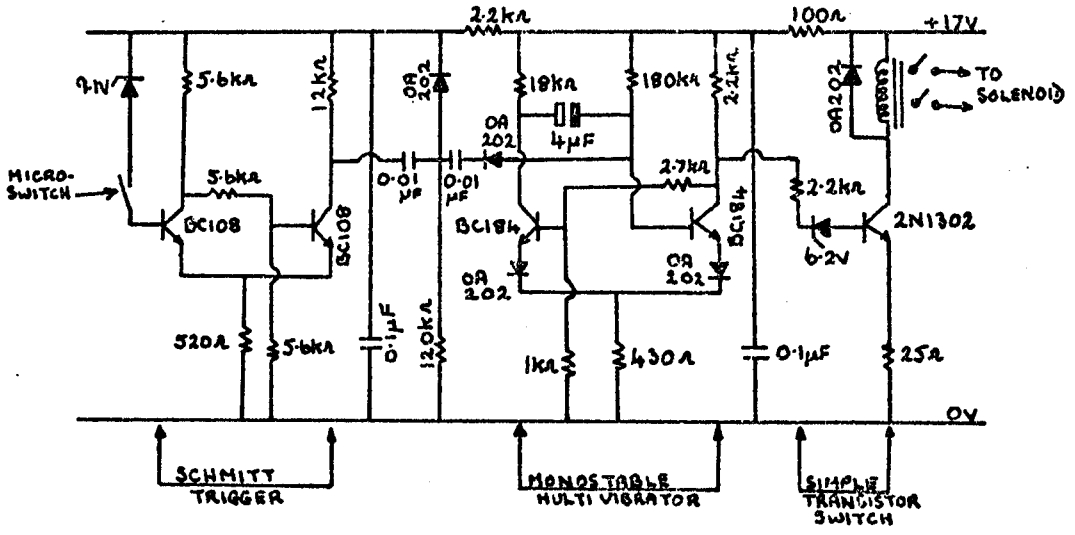

Fig. 19 Torsion fatigue machine trip circuit.

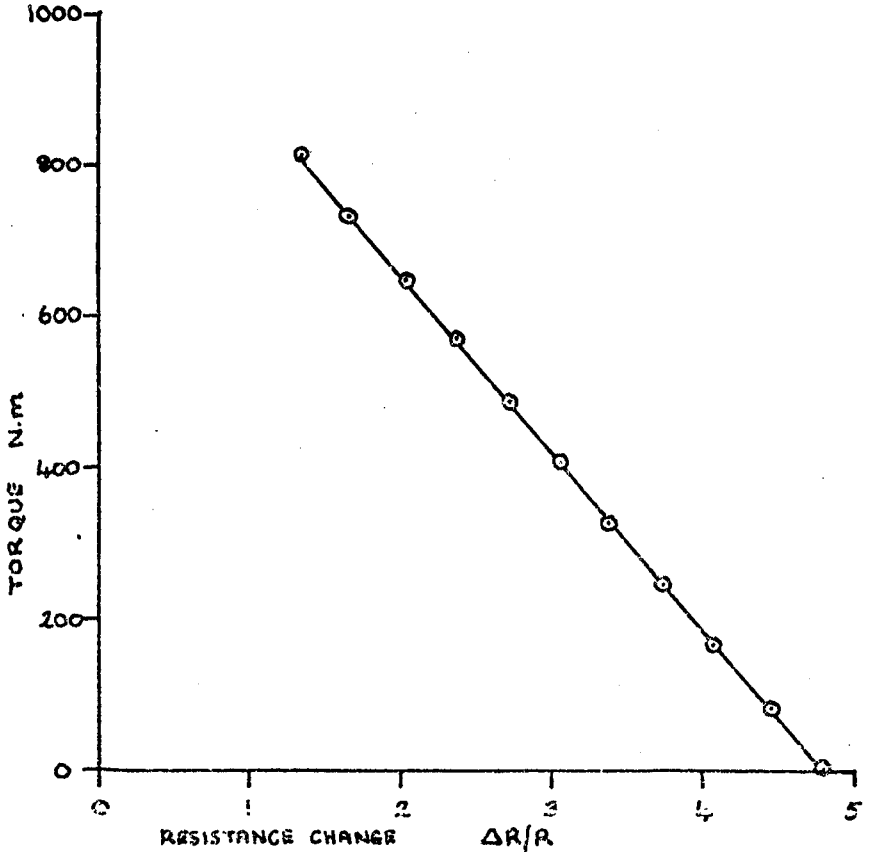

Fig. 20 Torsion bar calibration graph.

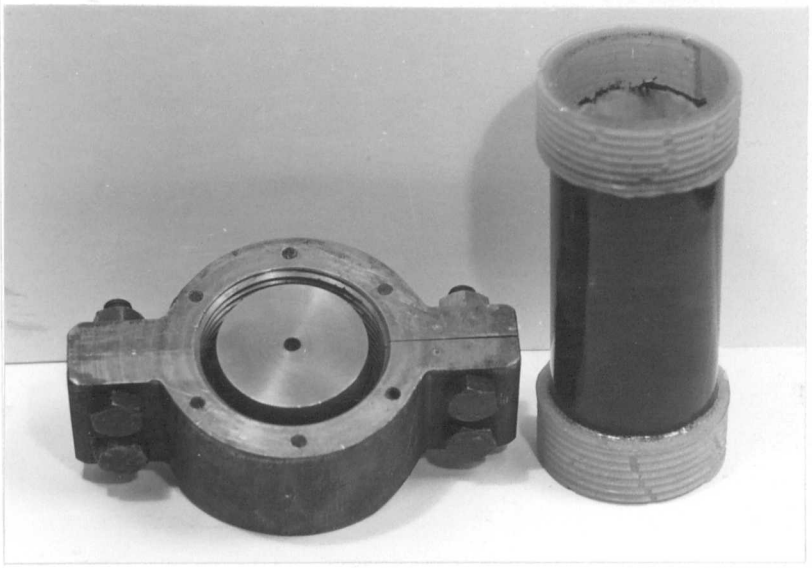

Fig. 21 Tension End Caps

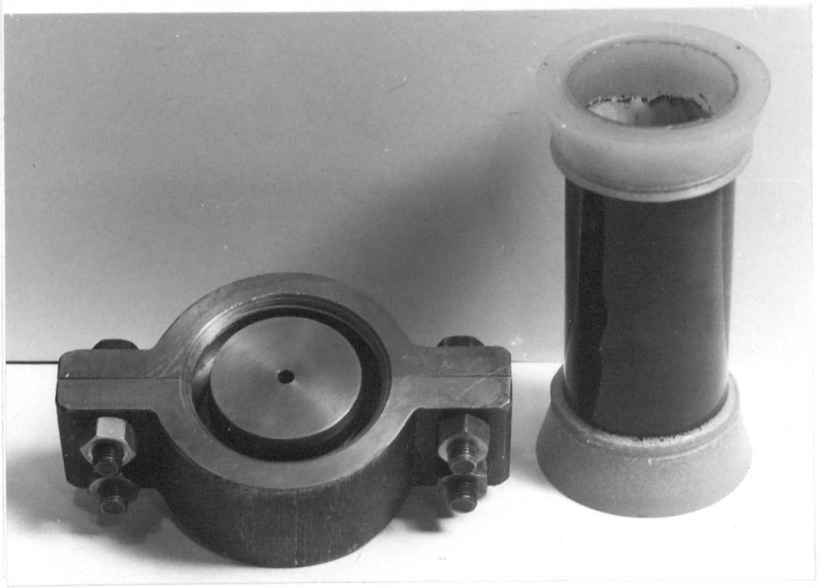

Fig. 22 Tension End Caps

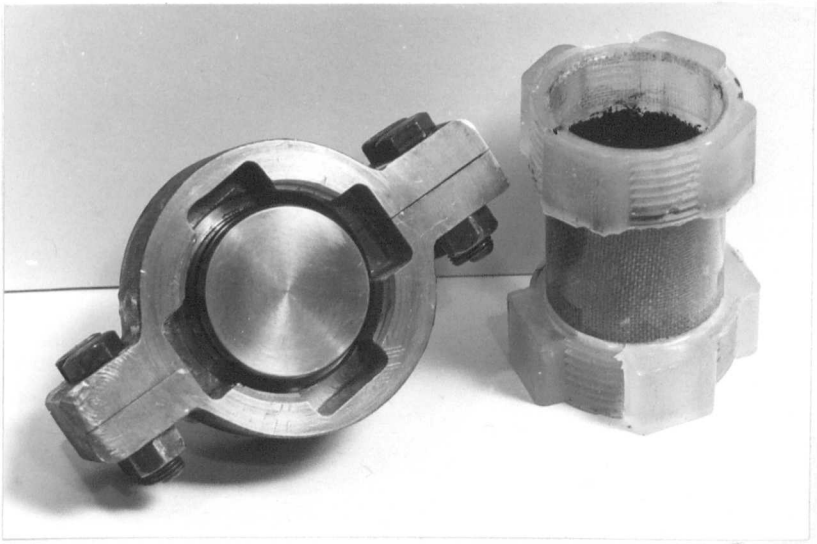

Fig. 23 Torsion Fatigue End Caps

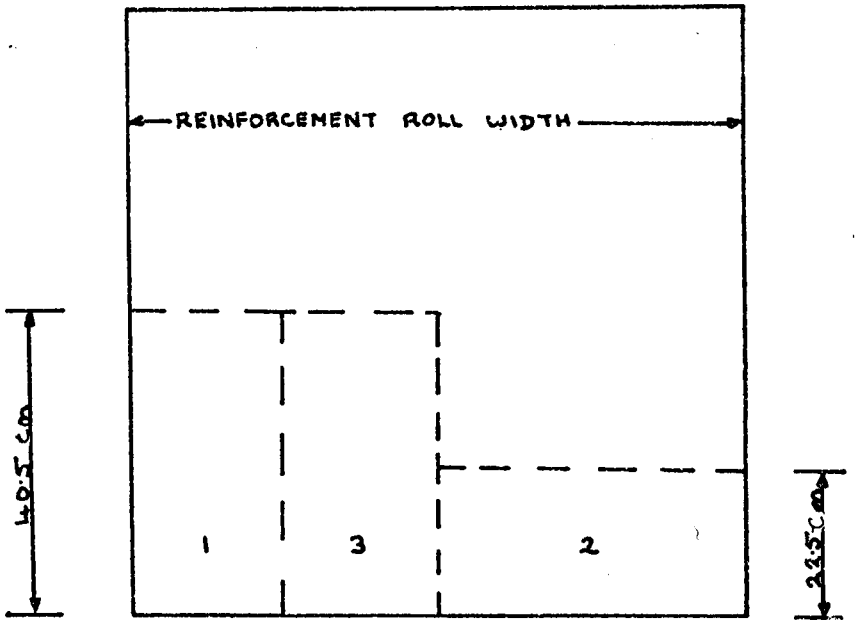

CUTTING PLANS FOR A 3-LAYERED CYLINDER
'2' INDICATES THE MIDDLE LAYER

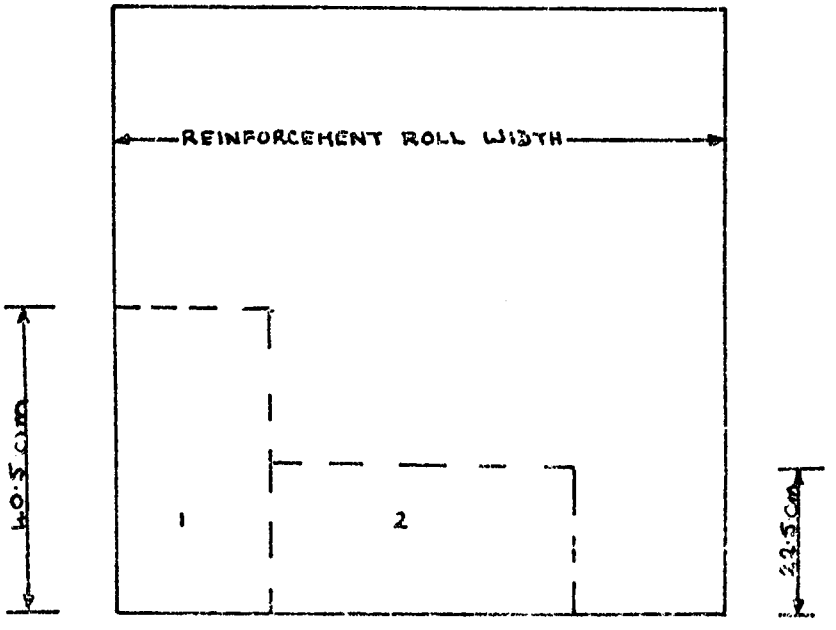

CUTTING PLANS FOR A 2-LAYERED CYLINDER

Fig. 24 Reinforcement cutting plans for C.S.M/Polyester resin cylinders.

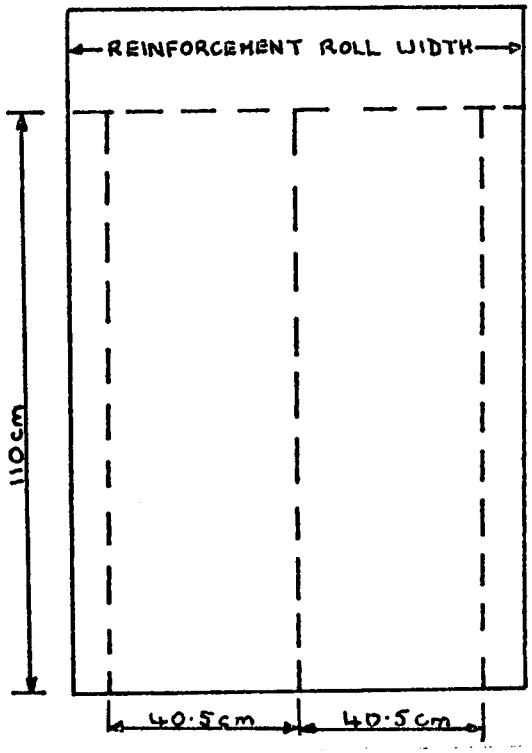

Fig. 25 Cutting plan of Y449 fabric for 0° cylinder manufacture.

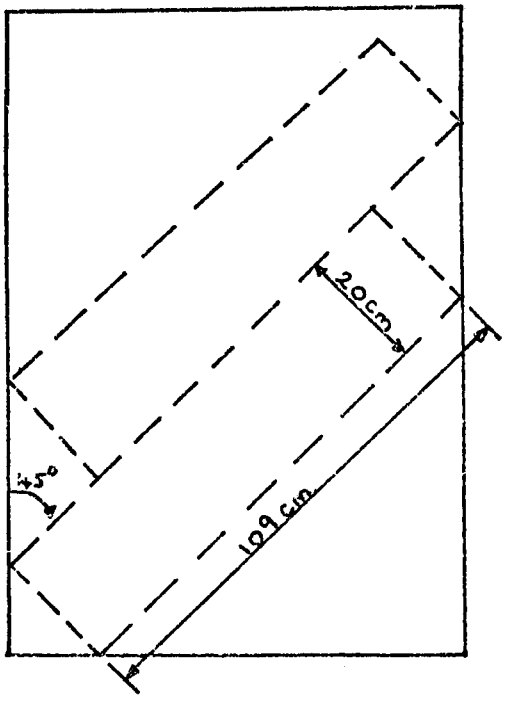

Fig. 26 Cutting plan or Y449 fabric for 45° cylinder manufacture.

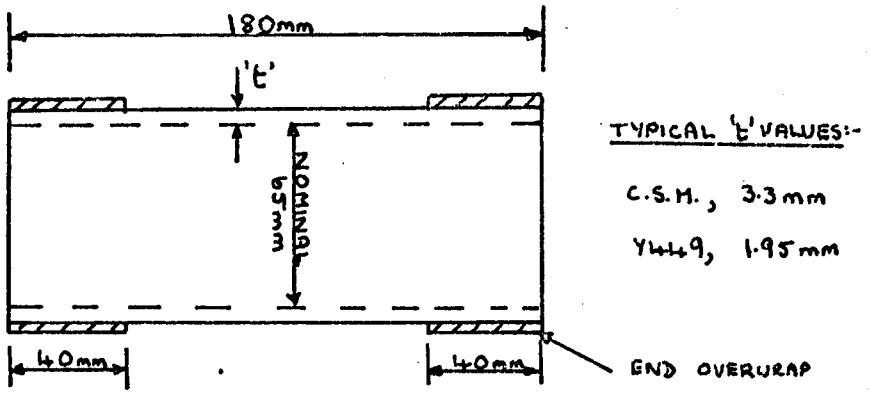

'COMPRESSION' CYLINDER

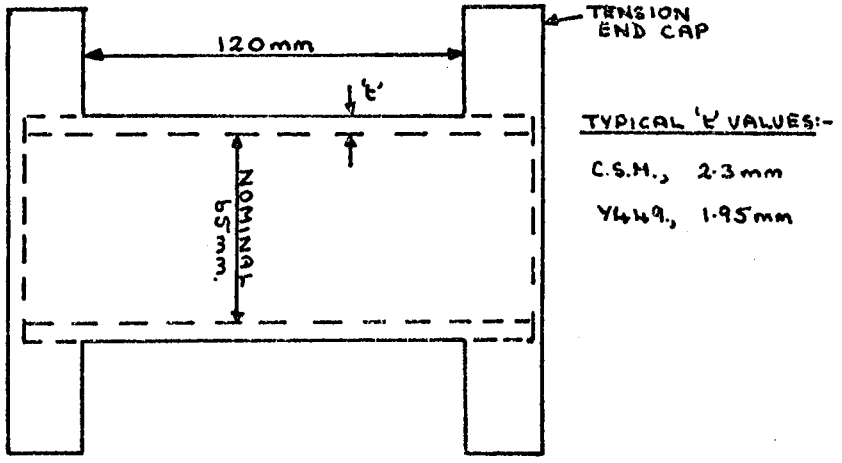

'TENSION' CYLINDER

Fig. 27 Cylinder dimensions.

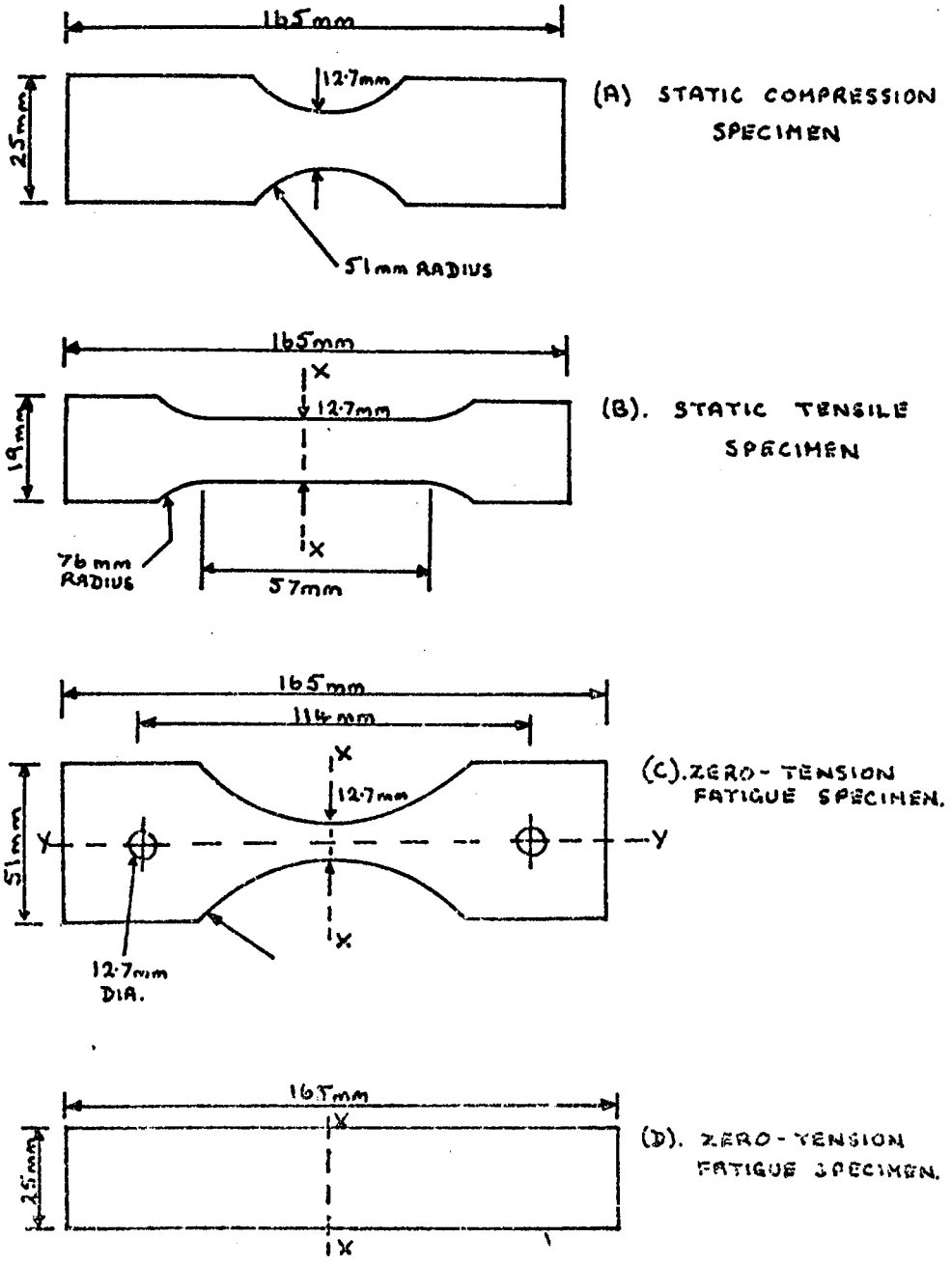

Fig. 28 Uniaxial stress test specimens.

N.B. FOR JOINTED SPECIMENS, JOINT IS LOCATED AT X-X OR Y-Y

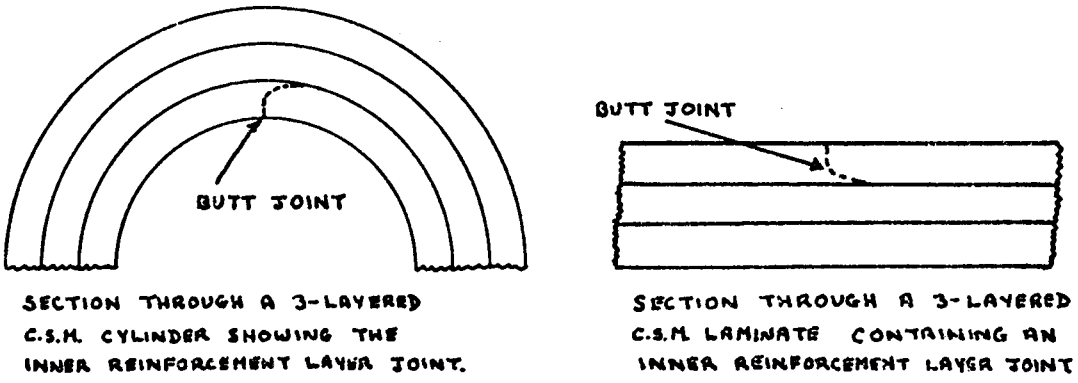

SECTION THROUGH A 3-LAYERED C.S.M. CYLINDER SHOWING THE INNER REINFORCEMENT LAYER JOINT.

SECTION THROUGH A 3-LAYERED C.S.M. LAMINATE CONTAINING AN INNER REINFORCEMENT LAYER JOINT

Fig. 29 Simulation of cylinder construction for C.S.M/ Polyester resin composites.

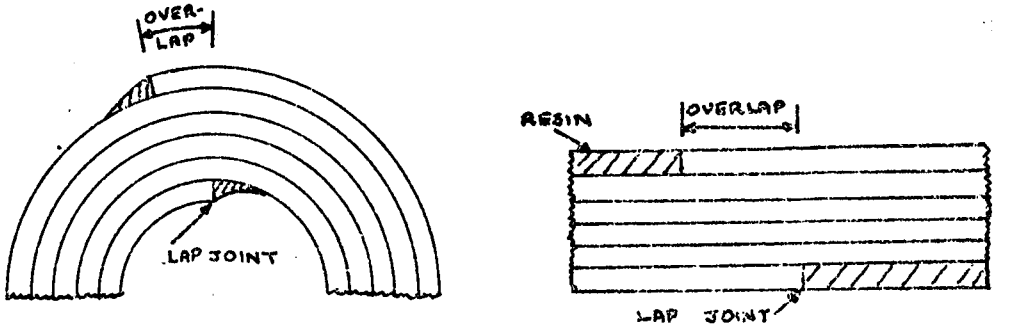

SECTION THROUGH A 5-LAYERED Y449 FABRIC CYLINDER

SECTION THROUGH A 5-LAYERED Y449 FABRIC LAMINATE HAVING A JOINT AND OVERLAP.

Fig. 30 Simulation ofcylinder construction for Y449/ Polyester resin composites.

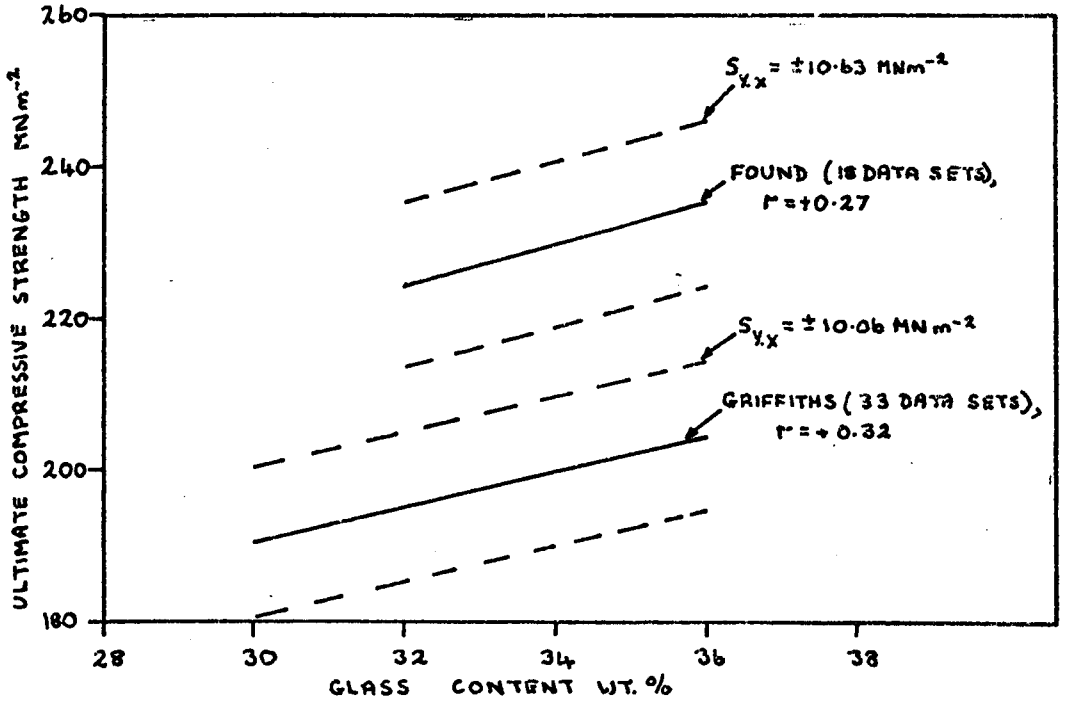

N.B. $S_{Y.X}$ = STANDARD ERROR OF ESTIMATE
r = CORRELATION COEFFICIENT

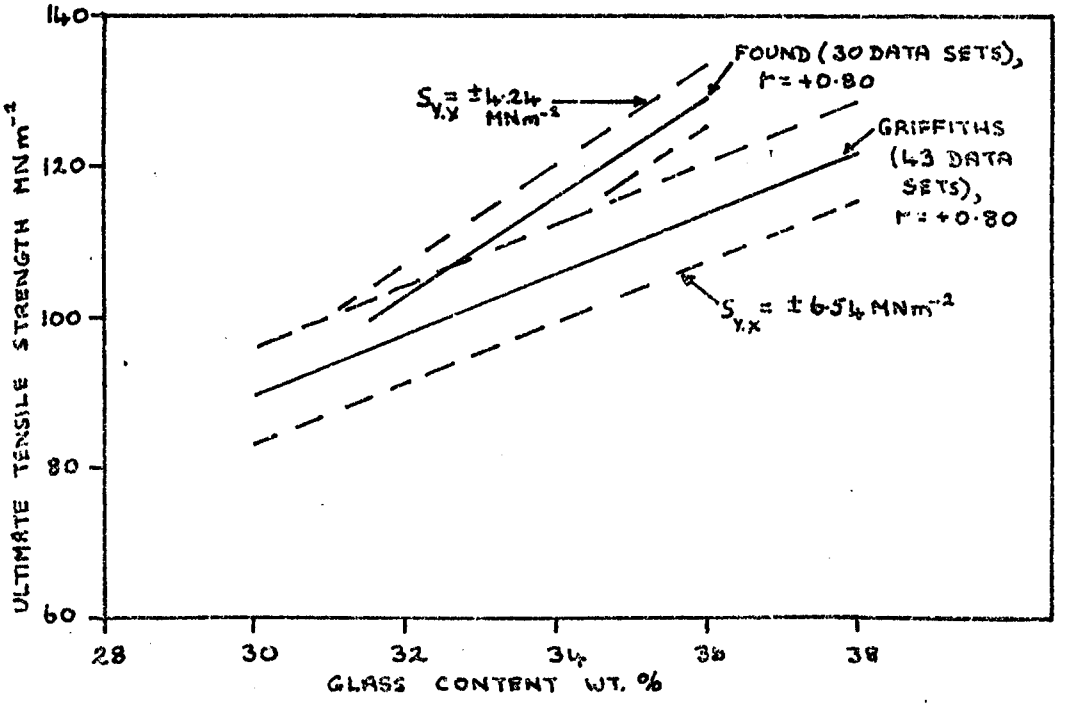

Fig. 31 Variation of strength with glass content for C.S.M/Polyester resin composites.

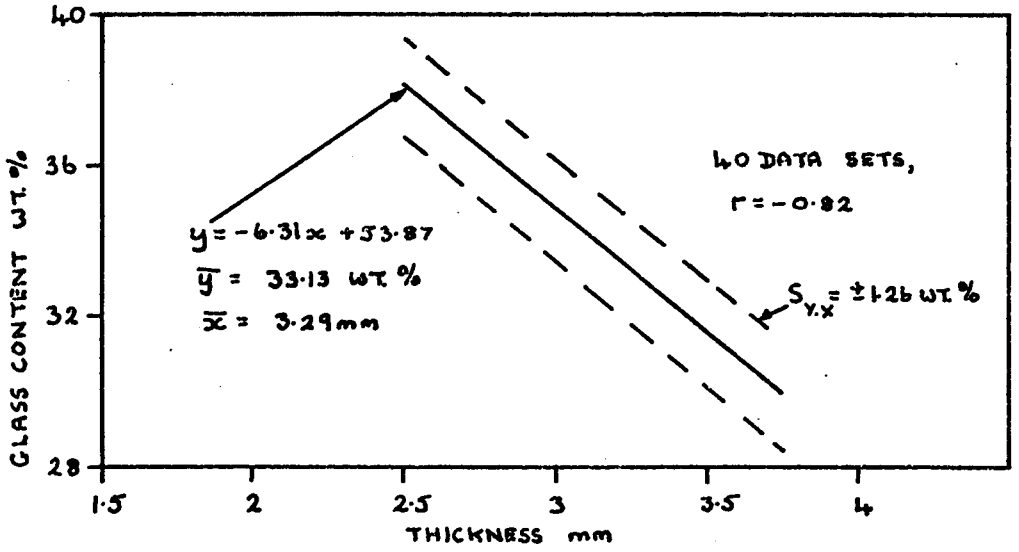

Fig. 32 Variation of glass content with thickness for 3 layered C.S.M/Polyester resin laminates.

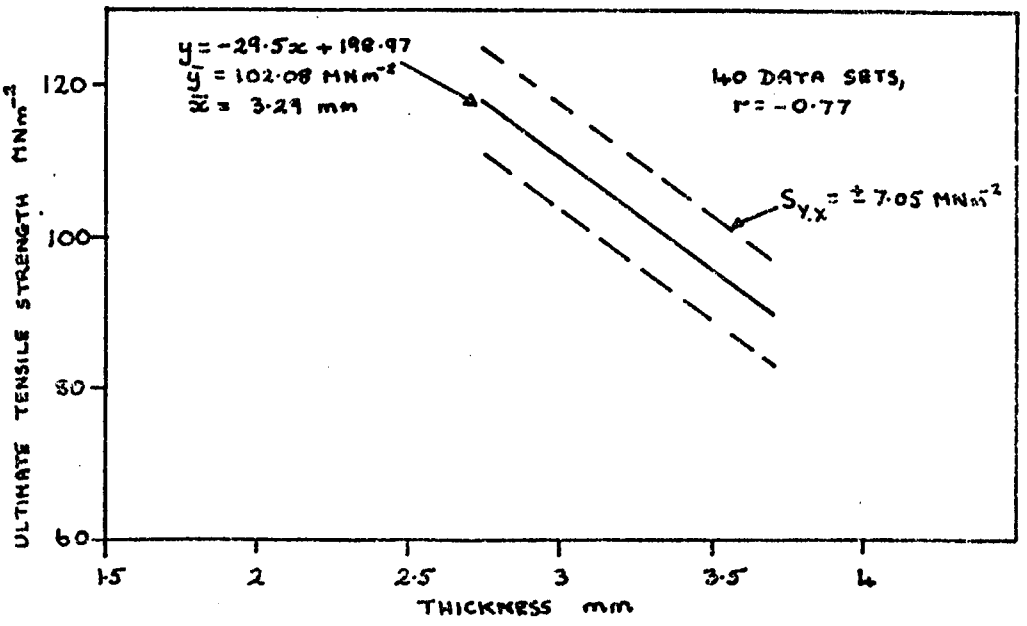

Fig. 33 Relationship between U.T.S. and thickness for 3-layered C.S.M./polyester resin laminates.

UNTESTED SAMPLES GROUND DOWN BY :-

0.5mm	0.5mm	0.5mm	0.3mm
JOINT REGION			
G3	G6	G8	G10

FIG. 34 UNTESTED SAMPLES OF PLAIN AND JOINTED 2,3-LAYERED C.S.M./POLYESTER RESIN LAMINATES

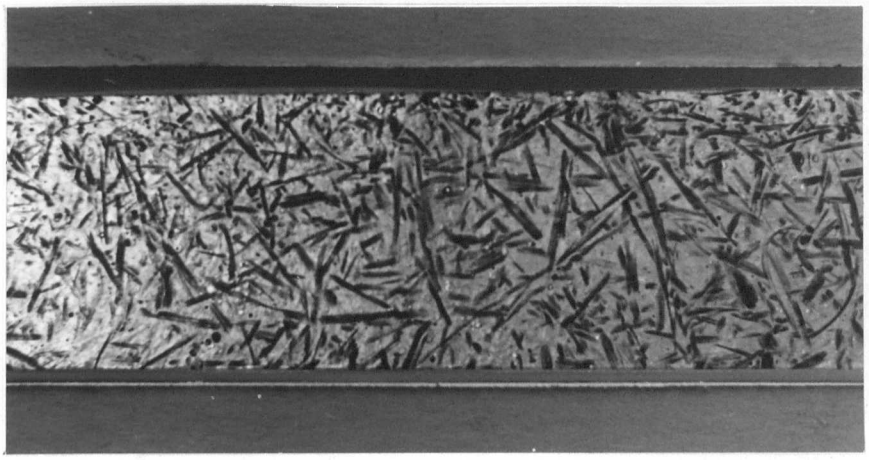

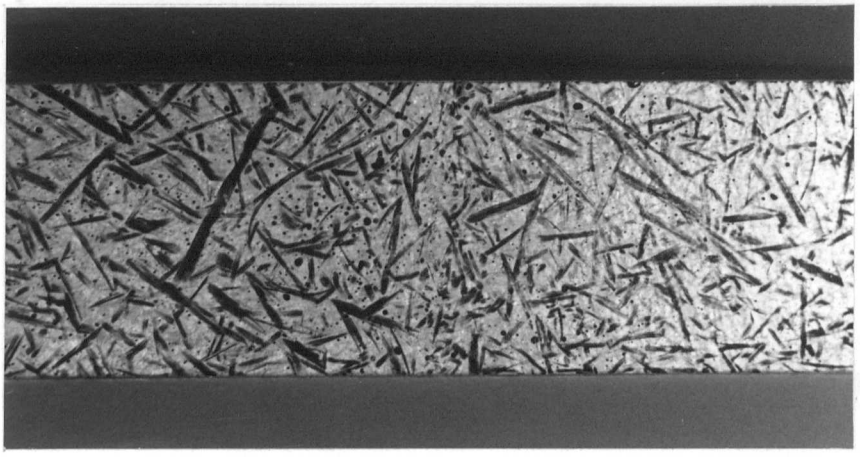

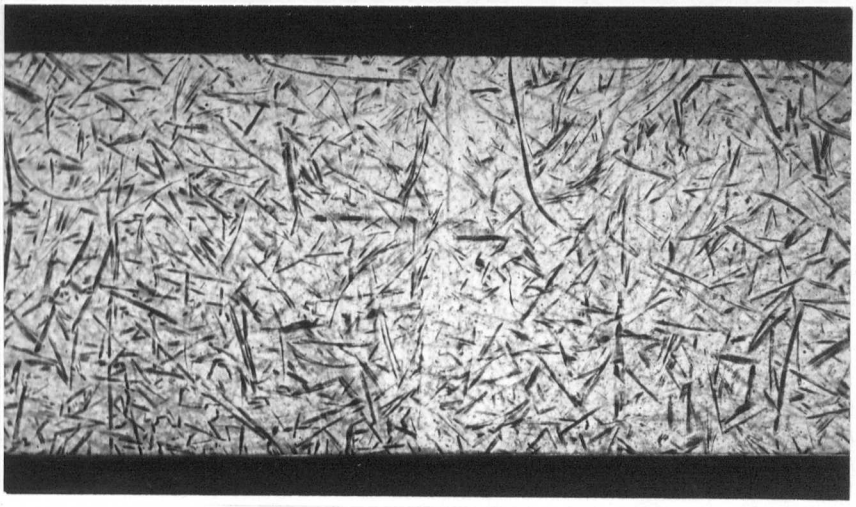

UNTESTED SAMPLES GROUND DOWN BY :-

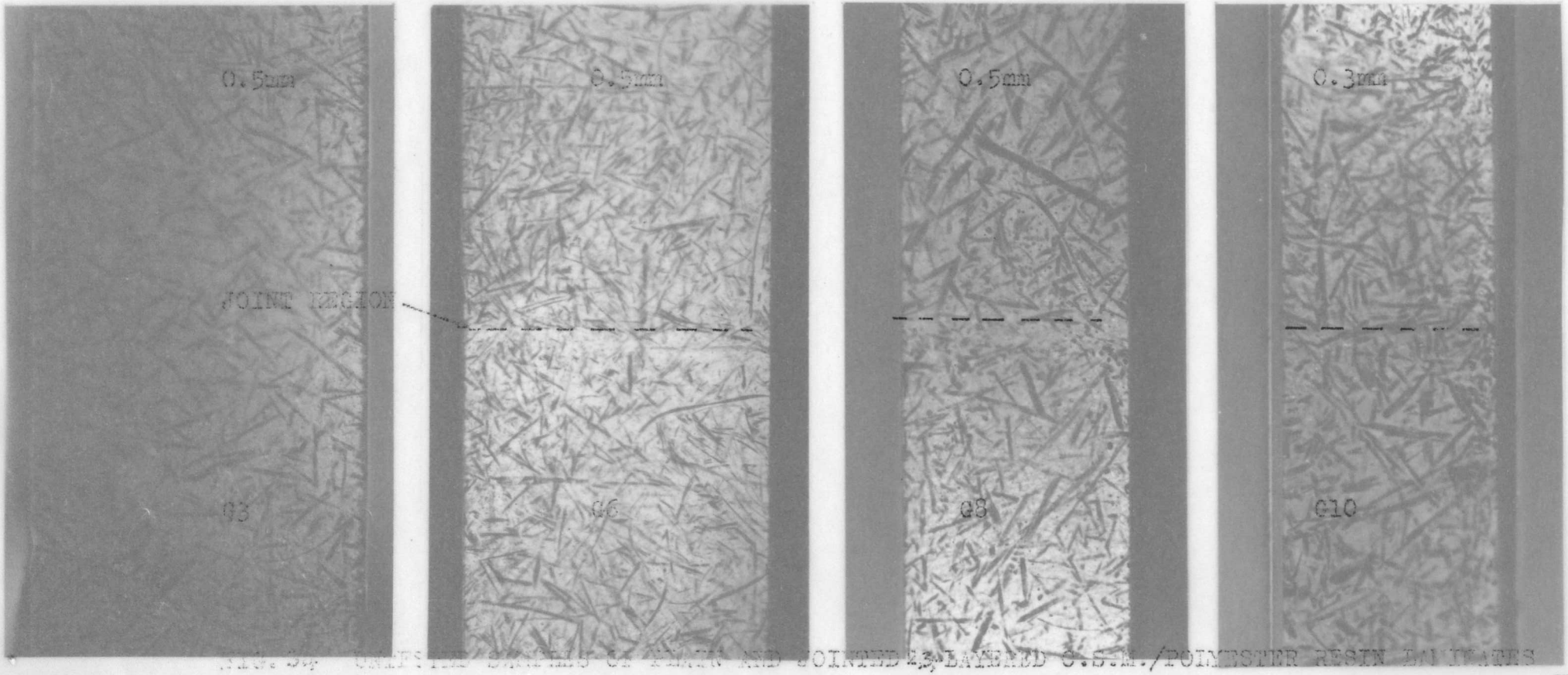

FIG. 3a UNTESTED SAMPLES OF PLAIN AND JOINTED G3, BACKED G.R.P./POLYESTER RESIN LAMINATES

SAMPLES TESTED TO JOINT CRACKING UNDER STATIC TENSION GROUND DOWN BY :-

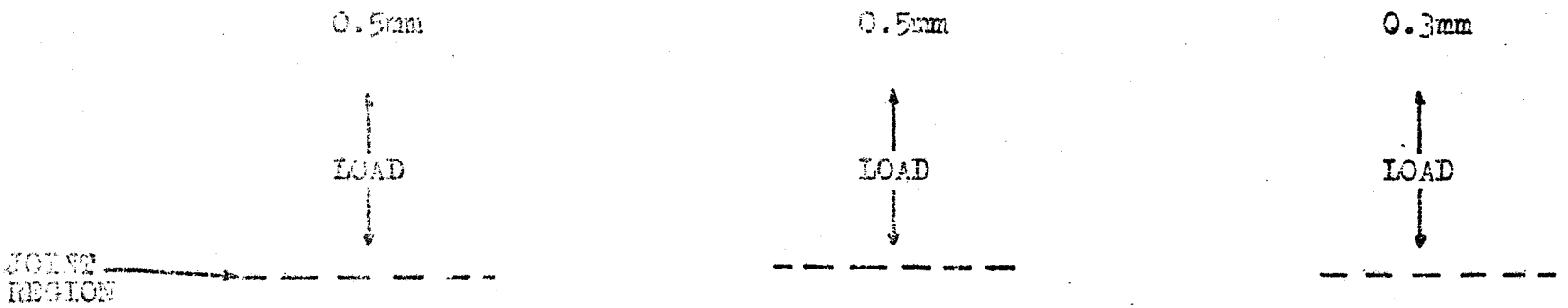

G6 G8 G10

FIG. 35 JOINT CRACKING IN C.S.M./POLYESTER RESIN LAMINATES TESTED UNDER STATIC TENSION.

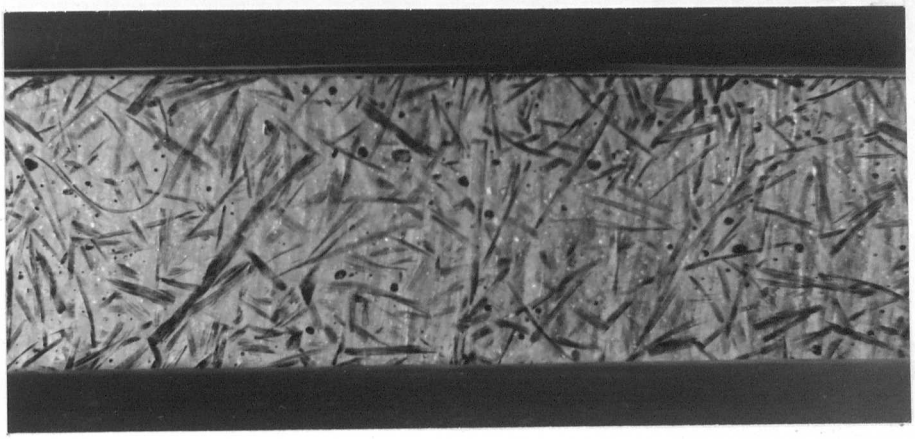

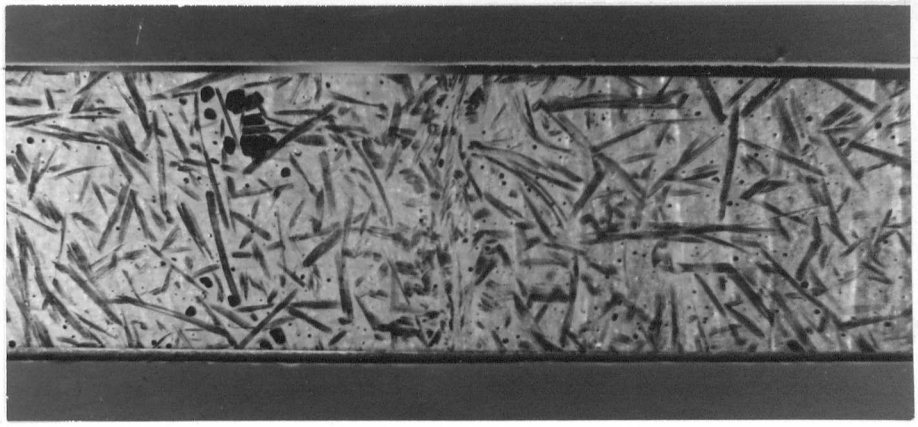

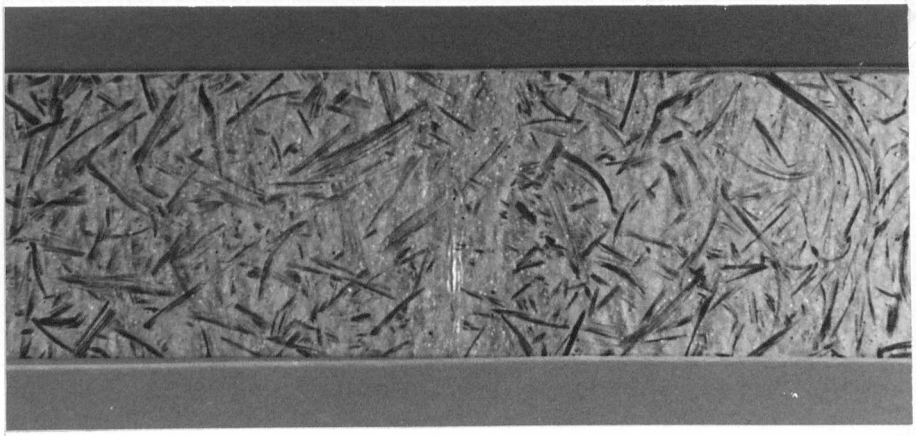

SAMPLES TESTED TO JOINT CRACKING UNDER STATIC TENSION GROUND DOWN BY :-

FIG. 25 JOINT CRACKING IN 0.5 M./2 POLYESTER RESIN LAMINATES TESTED UNDER STATIC TENSION.

UNTESTED SPECIMEN (G17/1), GROUND DOWN BY :-

0.5mm 1.0mm 1.5mm 1.7mm

JOINT REGION

SPECIMEN TESTED TO JOINT CRACKING UNDER STATIC TENSION (G17/2), GROUND DOWN BY:-

0.5mm 1.0mm 1.5mm 1.7mm

LOAD

JOINT CRACKS

FIG. 24 3-LAYERED C.S.M./POLYESTER RESIN LAMINATE (G17) WITH BUTT-JOINT IN THE CENTRE LAYER.

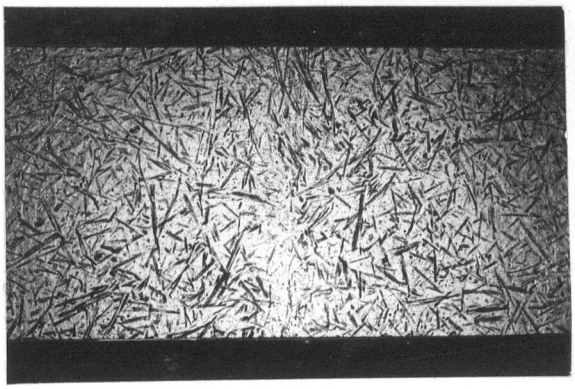

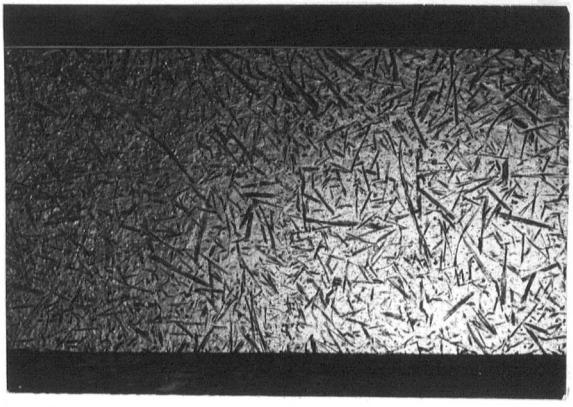

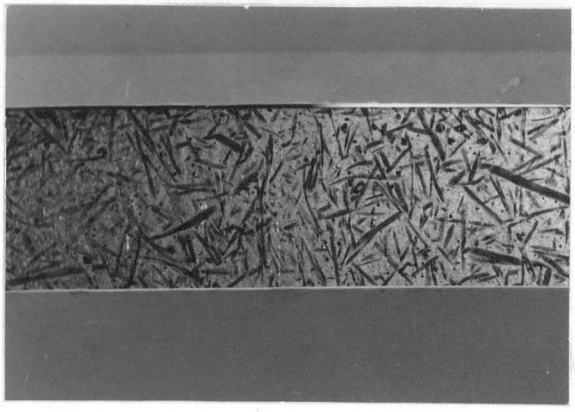

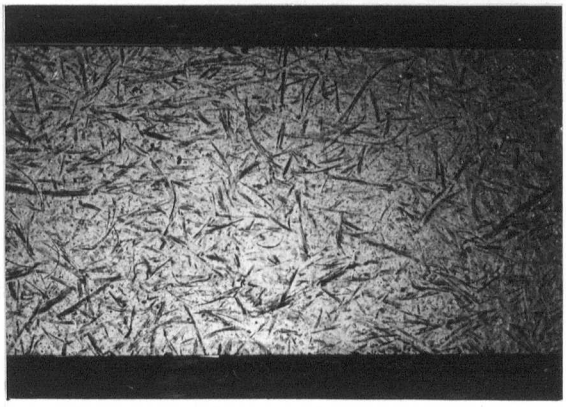

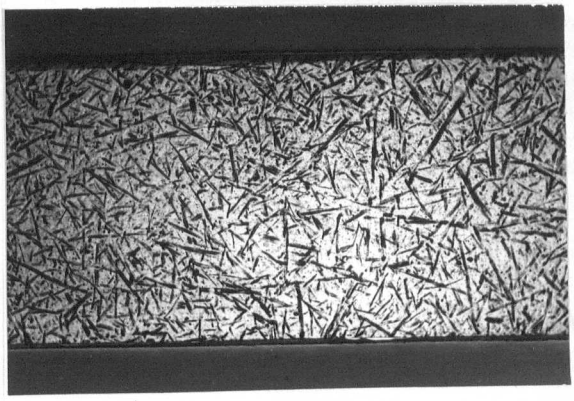

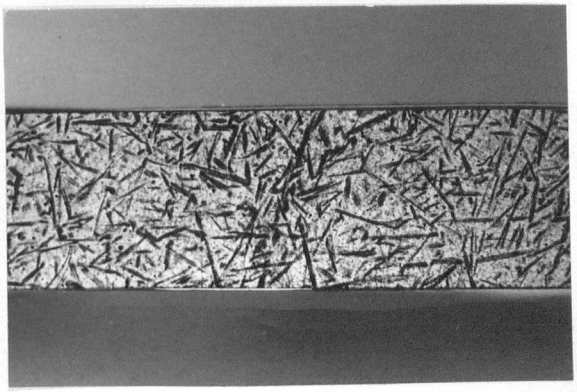

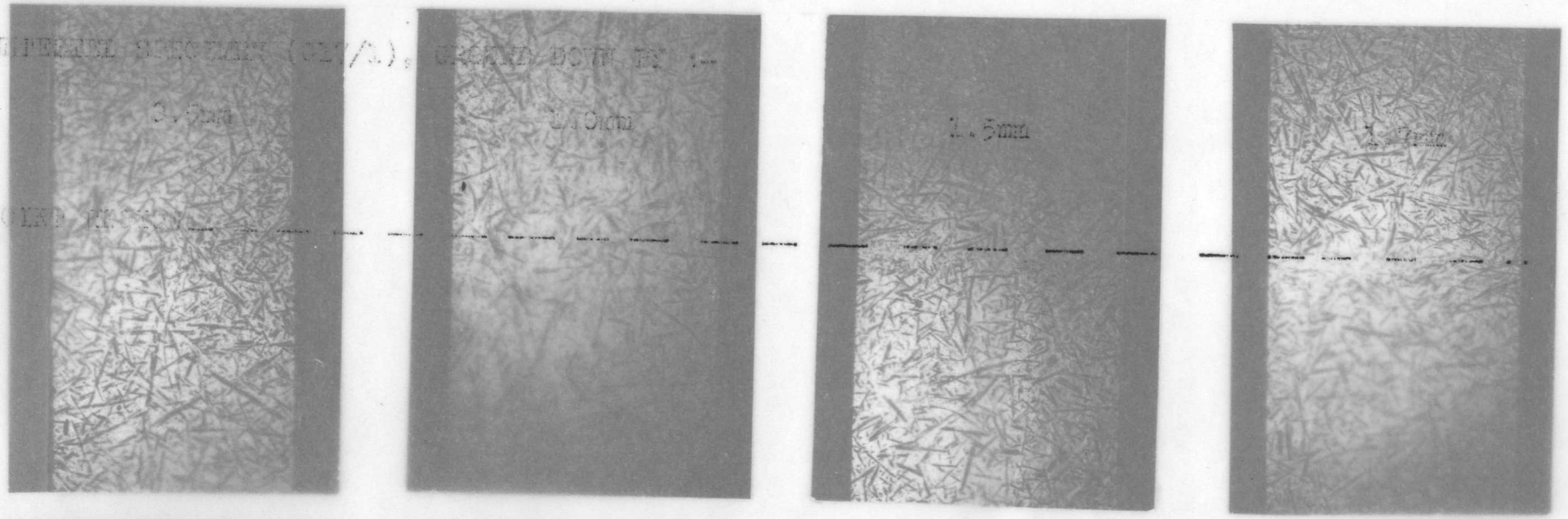

SPECIMEN TESTED TO JOINT CRACKING UNDER STATIC TENSION (G17/2), GROUND DOWN BY:-

JOINT CRACKS

LOAD

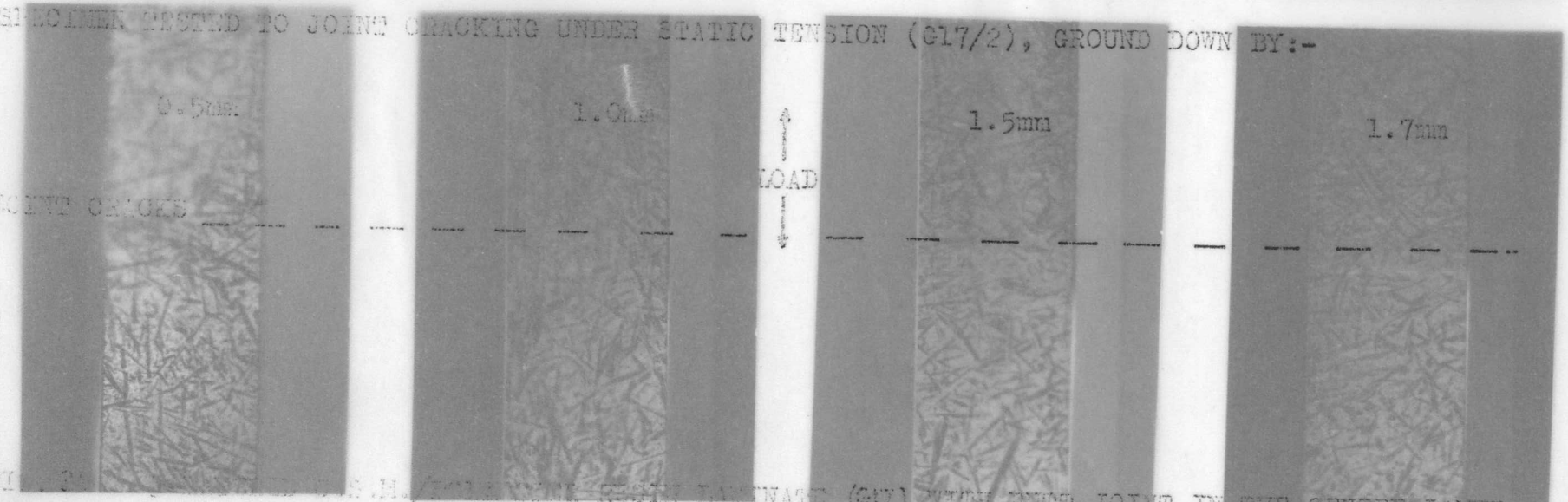

FIG. 3[illegible] S.H./[illegible] STEEL FOIL LAMINATE (G47) WITH BUTT-JOINT IN THE CENTRE LAYER.

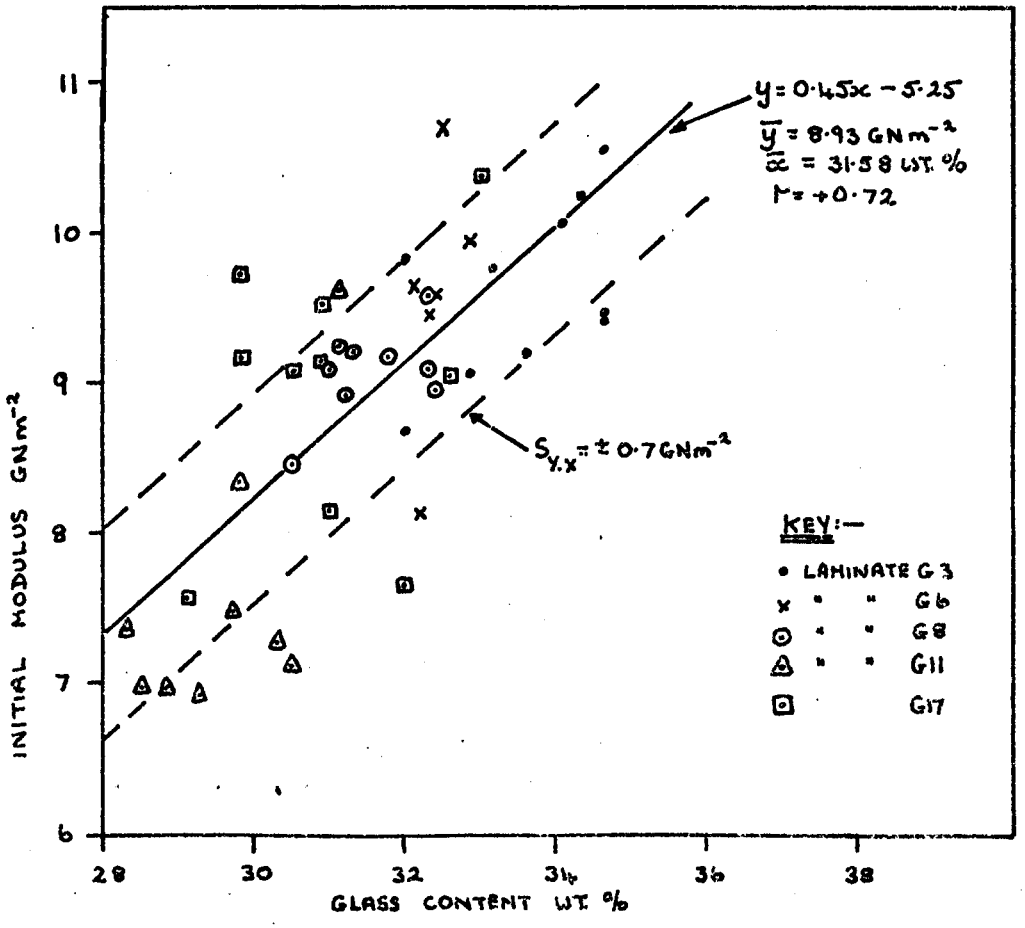

Fig. 37 Variation of initial modulus with estimated glass content for 3 layered C.S.M/Polyester resin laminates.

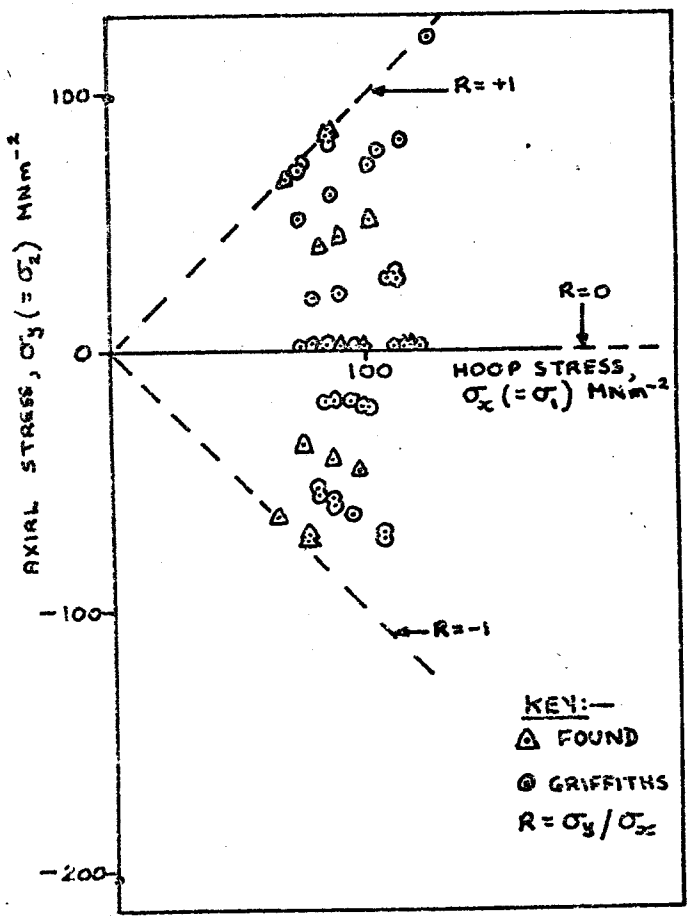

Fig. 38 Biaxial stress static total failure test results for C.S.M./polyester resin cylinders.

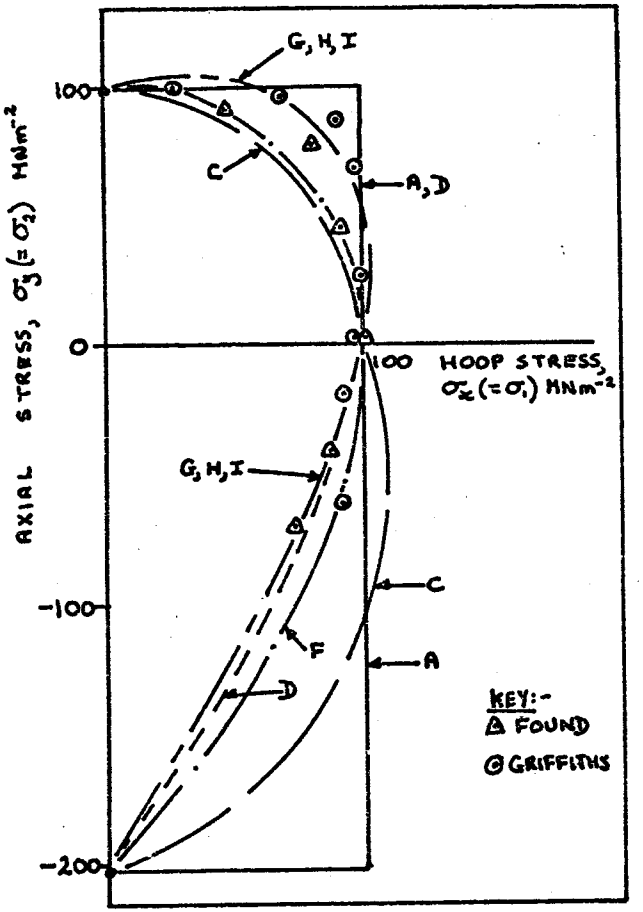

Fig. 39 Comparison between predicted and mean experimental static data for C.S.M./polyester resin cylinders.

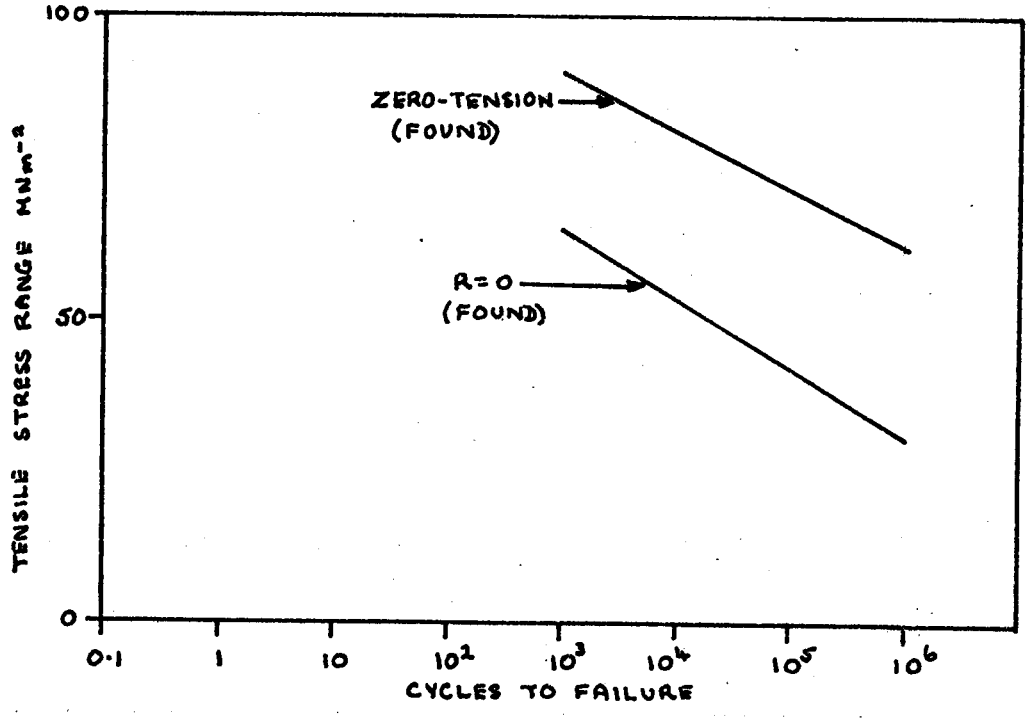

Fig. 40 The fatigue anomaly shown by Found [1,6] for C.S.M/Polyester resin composites.

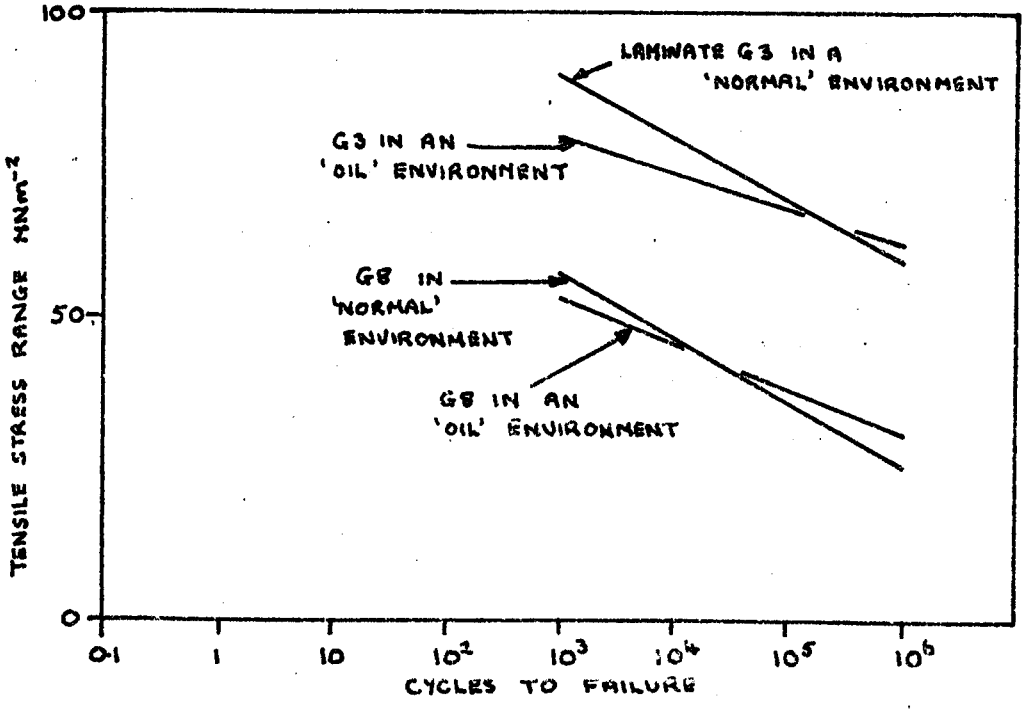

Fig. 41 The effect of Shell 'Tellus 15' mineral oil on the zero-tension fatigue performance of C.S.M/Polyester resin laminates.

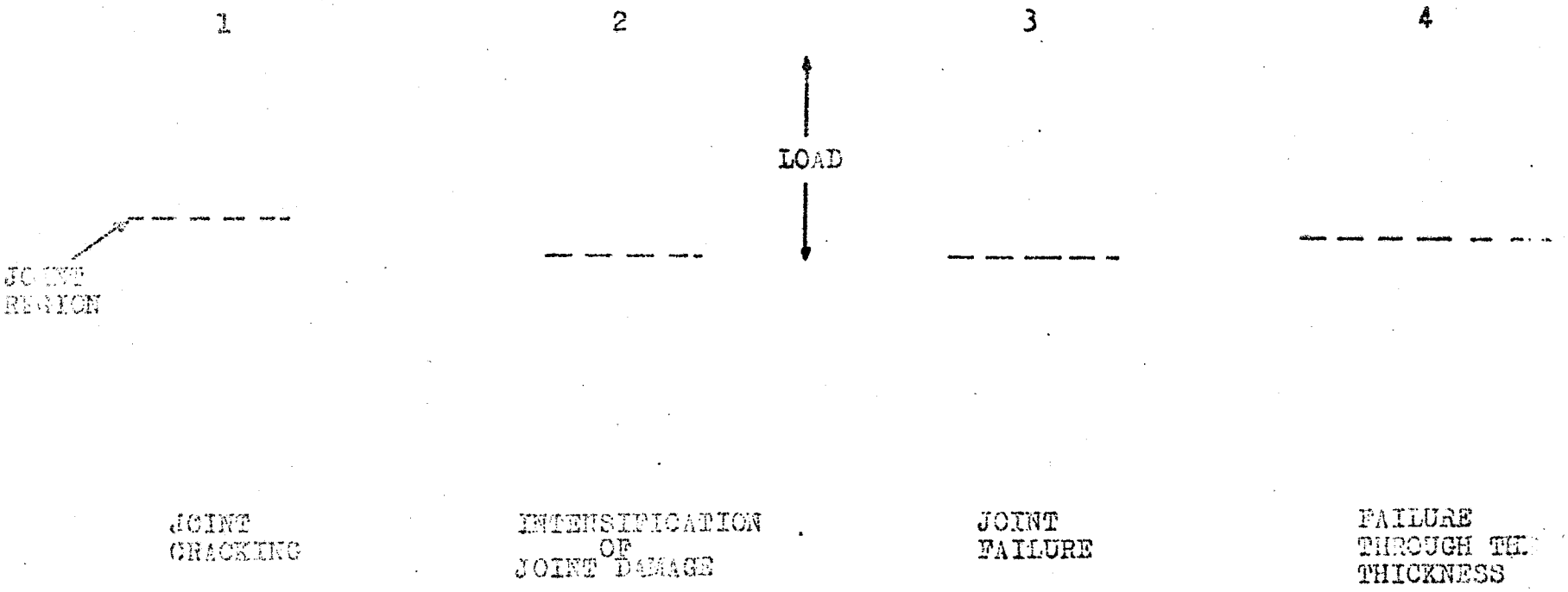

FIG. 42 DAMAGE PROGRESSION IN 3-LAYERED C.S.M. LAMINATES CONTAINING AN INNER REINFORCEMENT LAYER BUTT-JOINT TESTED UNDER ZERO-TENSION FATIGUE LOADING.

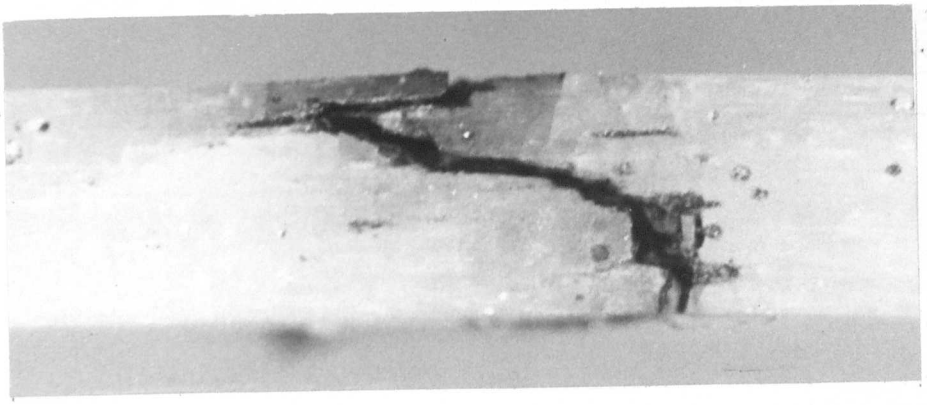

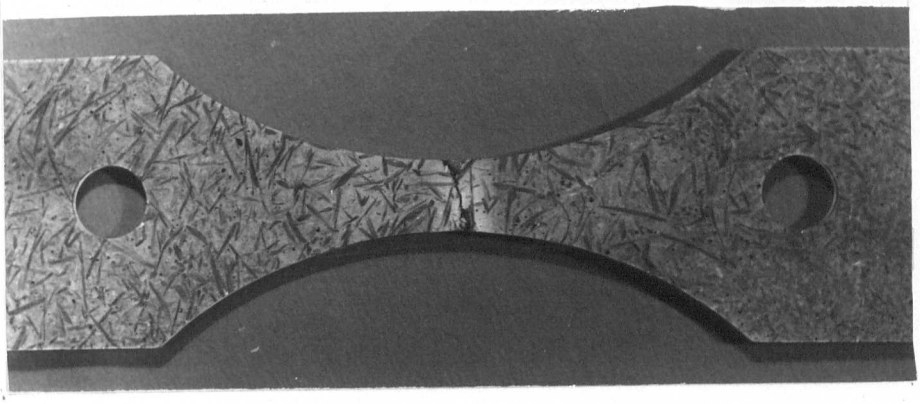

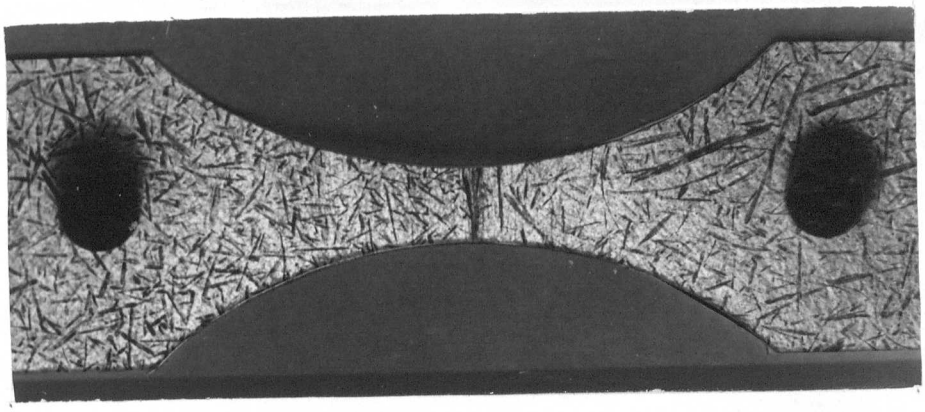

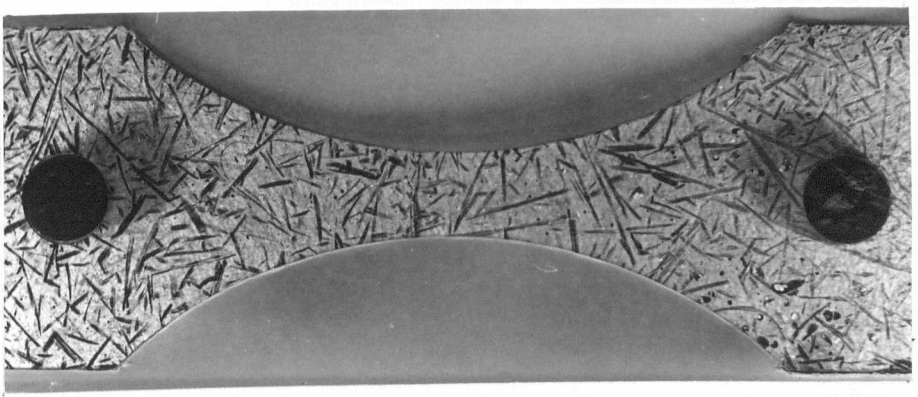

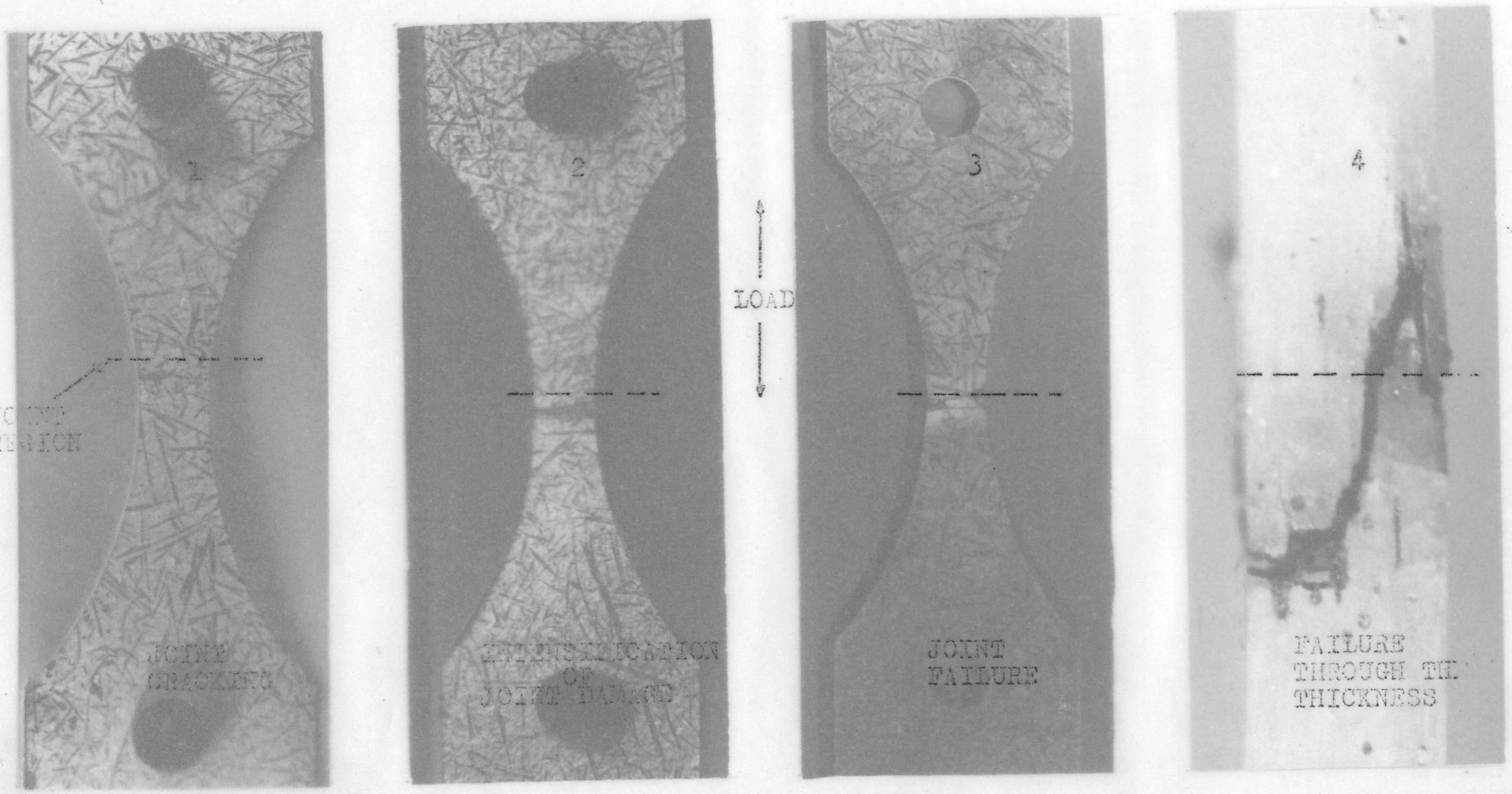

Fig. 42 DAMAGE PROGRESSION IN 3-LAYERED C.S.M. LAMINATES CONTAINING AN INNER REINFORCEMENT LAYER BUTT-JOINT TESTED UNDER ZERO-TENSION FATIGUE LOADING.

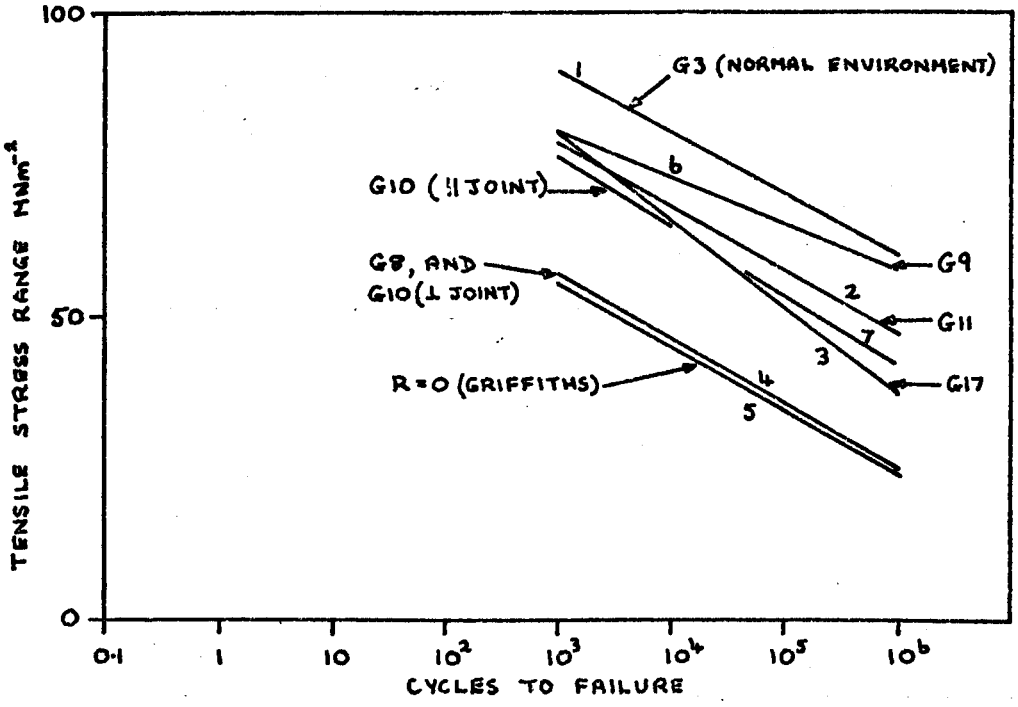

Fig. 43 The effect of a jointed reinforcement layer on the zero-tension fatigue performance of C.S.M/Polyester resin laminates.

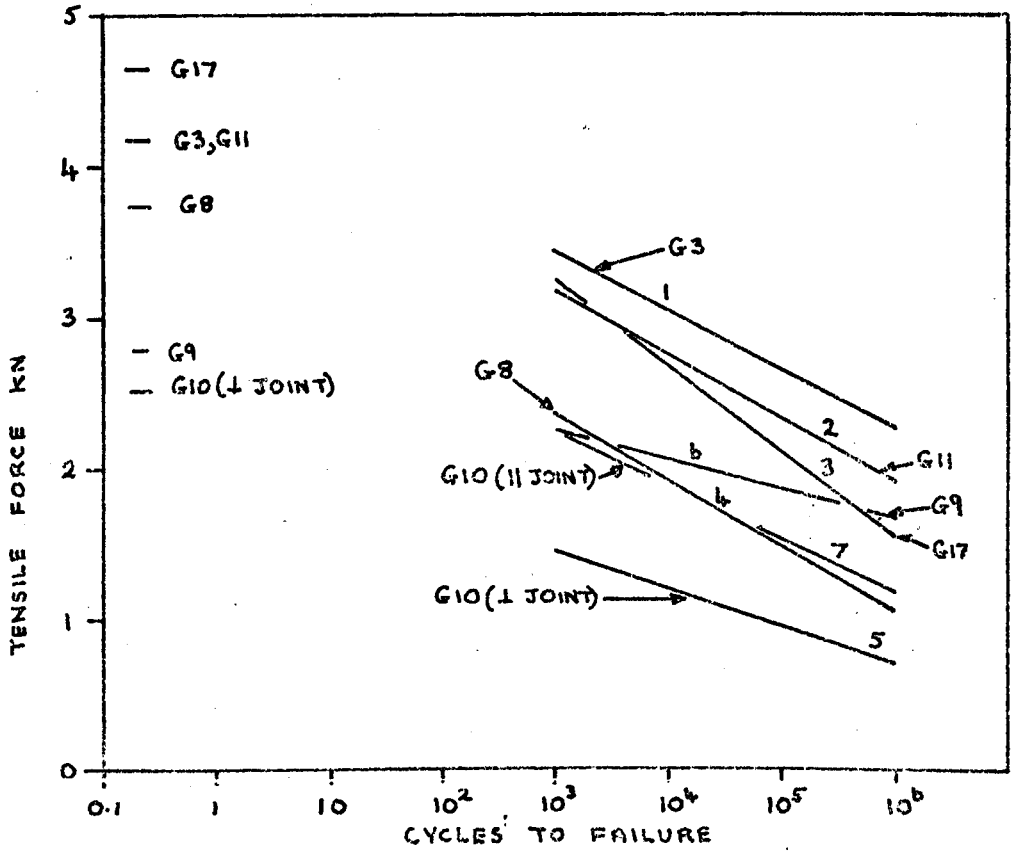

Fig. 44 The effect of a jointed reinforcement layer on the zero-tension fatigue performance of C.S.M/Polyester resin laminates.

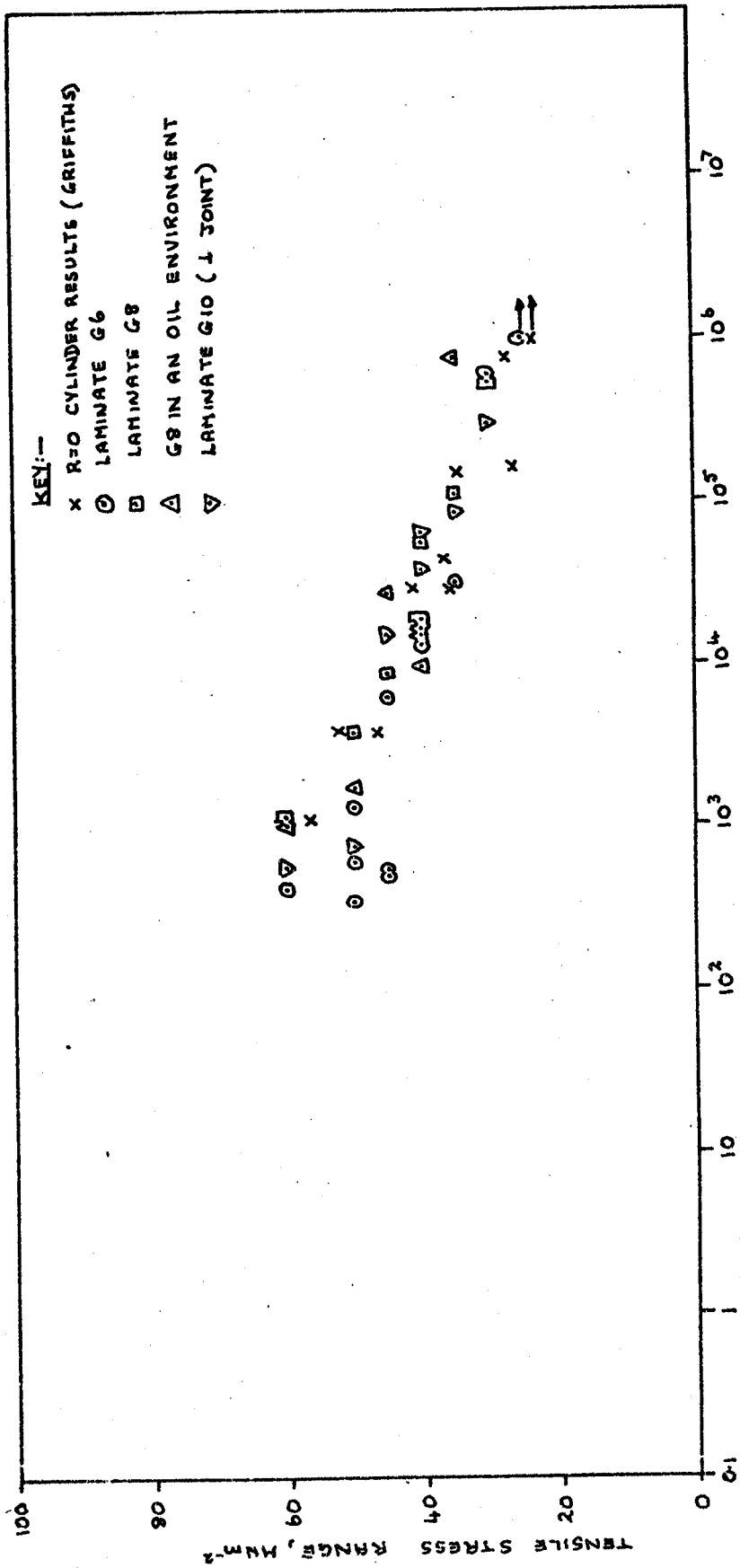

Fig. 45 Comparison of R=0 results with flat specimen results from C.S.M/Polyester resin laminates containing an inner reinforcement layer butt joint perpendicular to the tensile stress axis.

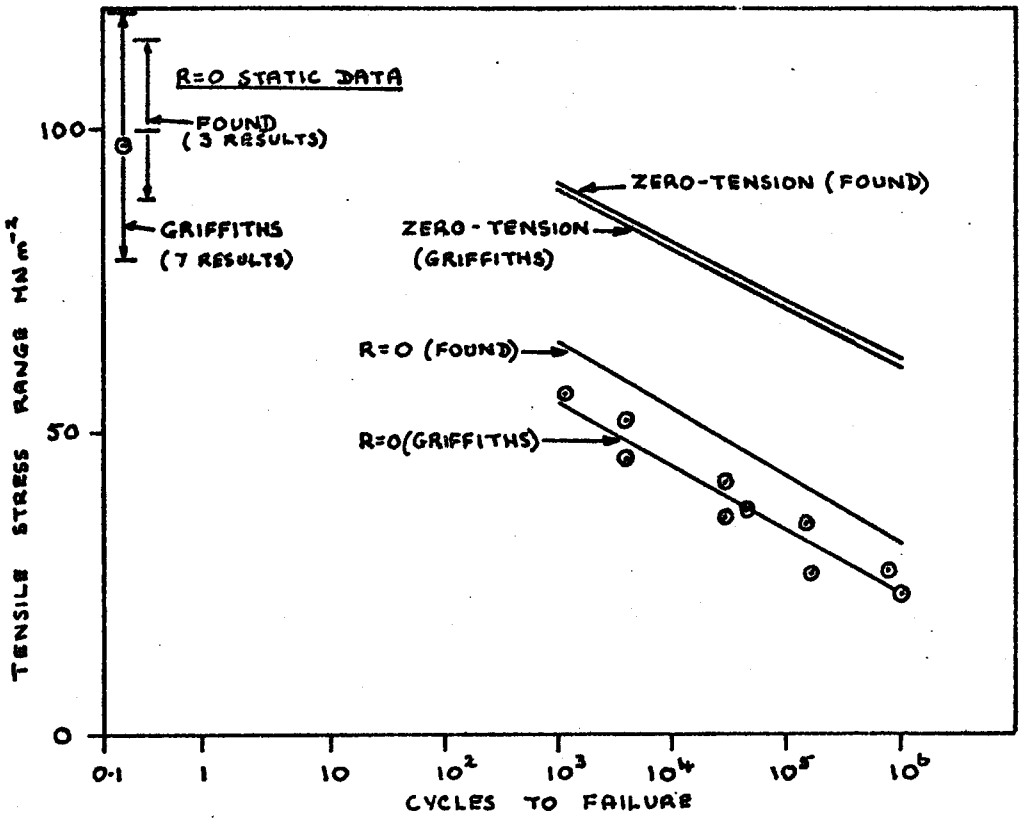

Fig. 46 Comparison between R=0 fatigue data for C.S.M/ Polyester resin cylinders.

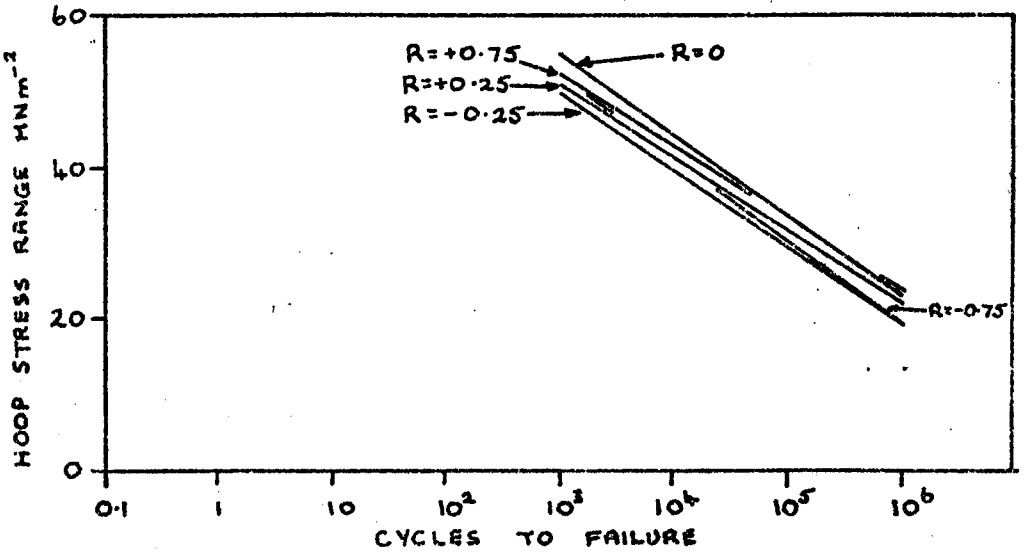

Fig. 47 The effect of biaxial stress ratio on the fatigue behaviour of C.S.M/Polyester resin cylinders.

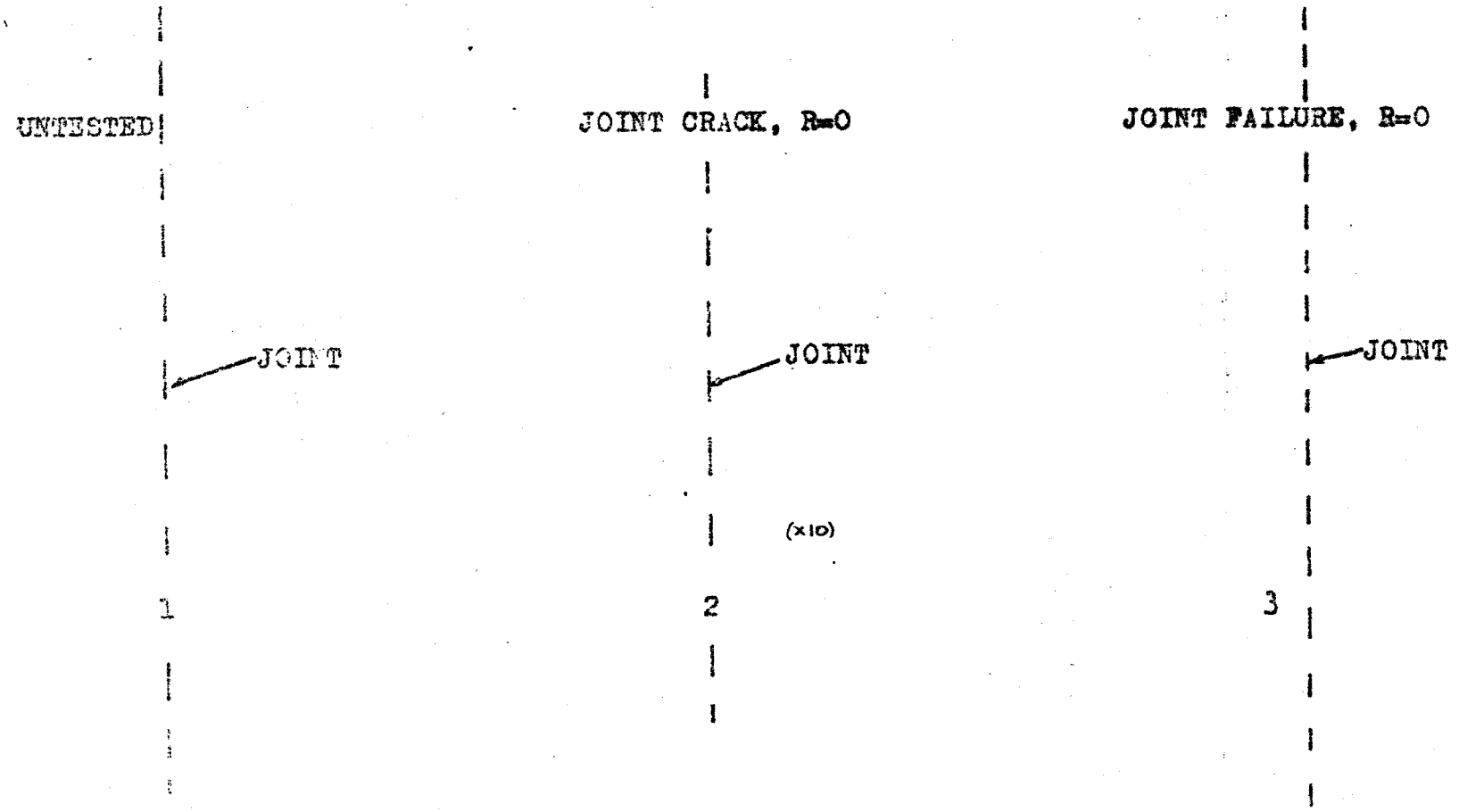

FIG. 48 BUTT-JOINTS IN THE BORE REINFORCEMENT LAYER OF C.S.M./POLYESTER RESIN CYLINDERS

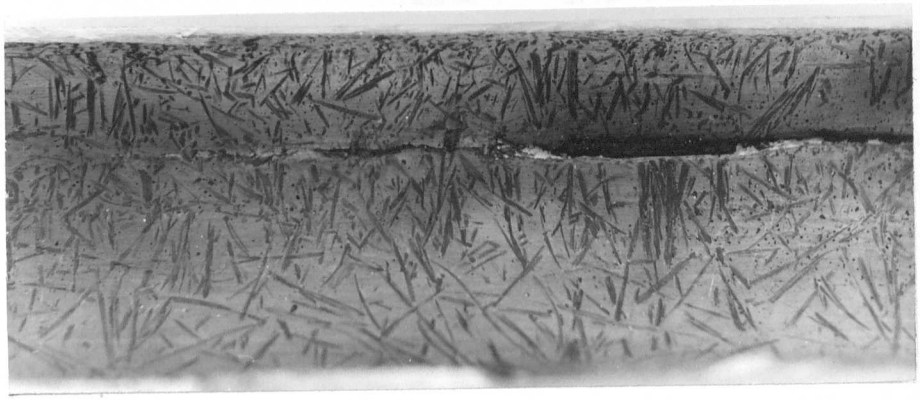

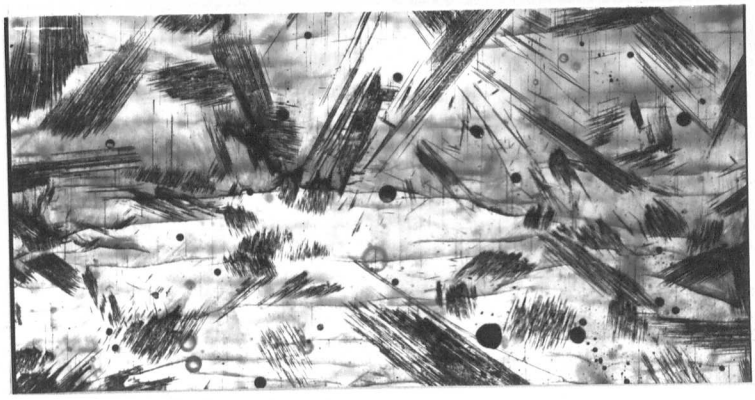

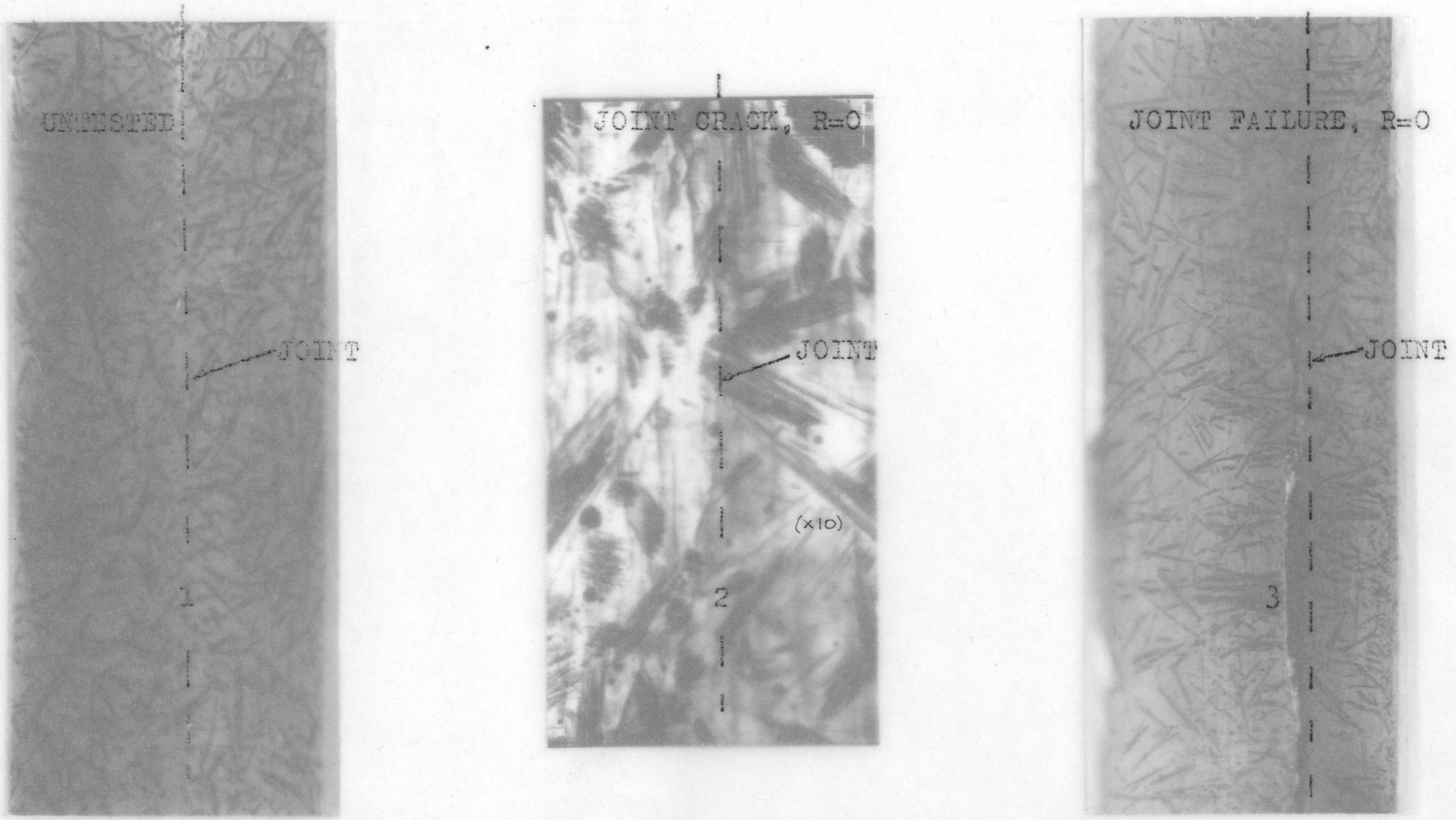

FIG. 48 BUTT-JOINTS IN THE BORE REINFORCEMENT LAYER OF C.S.M./POLYESTER RESIN CYLINDERS

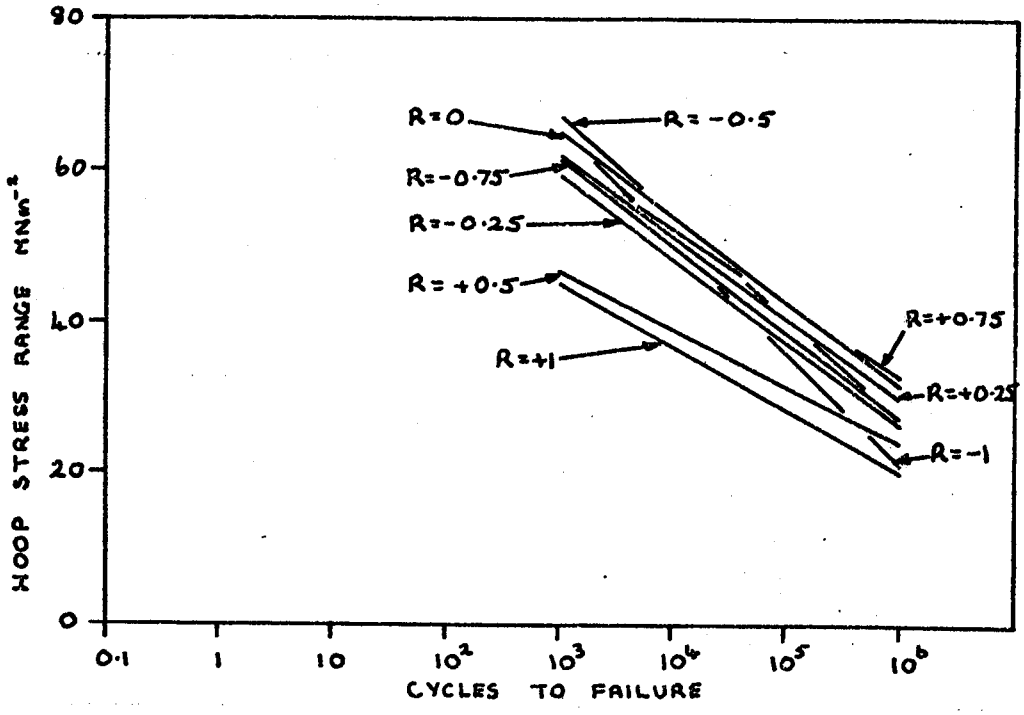

Fig. 49 The effect of biaxial stress ratio on the fatigue behaviour of C.S.M/Polyester resin cylinders.

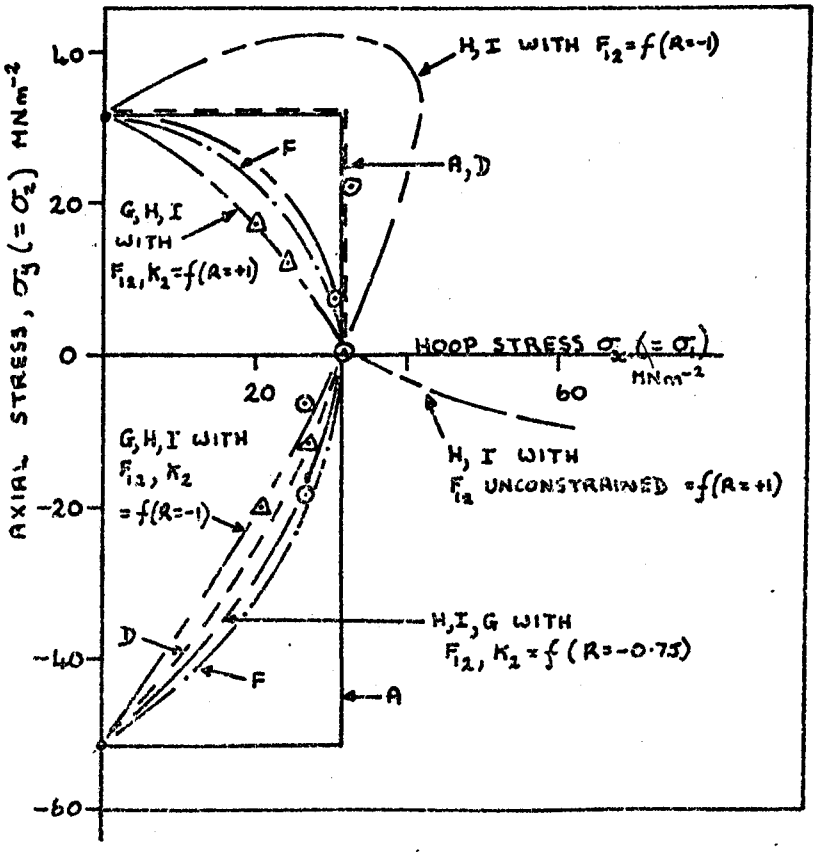

Fig. 50 Comparison between predicted and experimental biaxial stress fatigue data at 10⁶ cycles for C.S.M/Polyester resin composites.

FIG. 51 BIAXIAL STRESS STATIC FAILURES OBSERVED IN C.S.M./POLYESTER RESIN CYLINDERS.

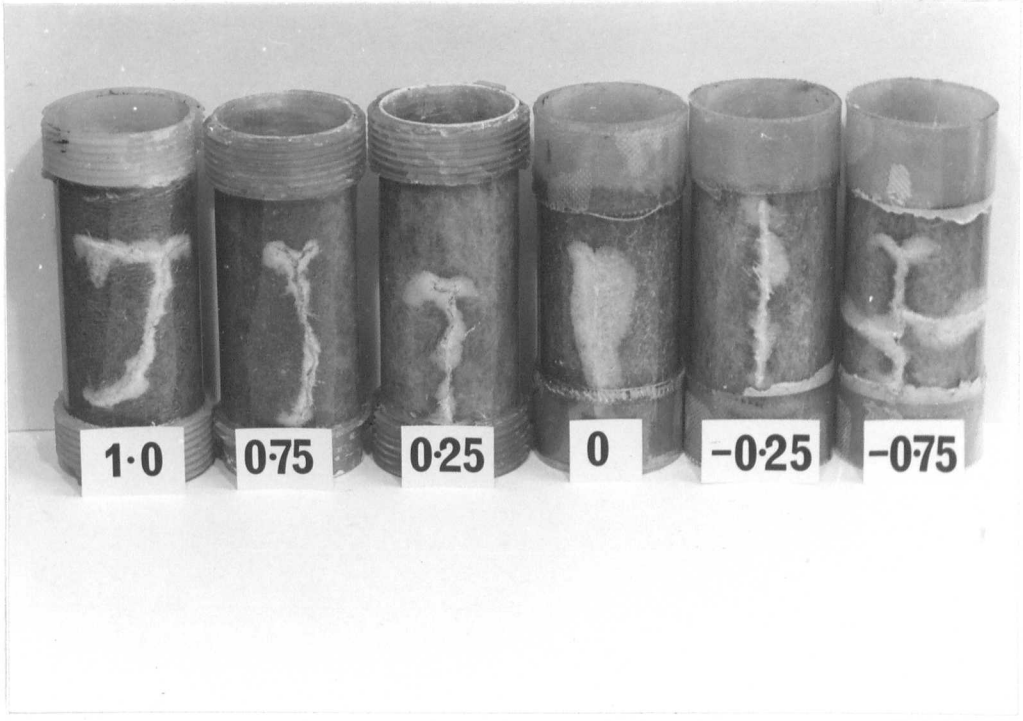
1·0
0·75
0·25
0
−0·25
−0·75

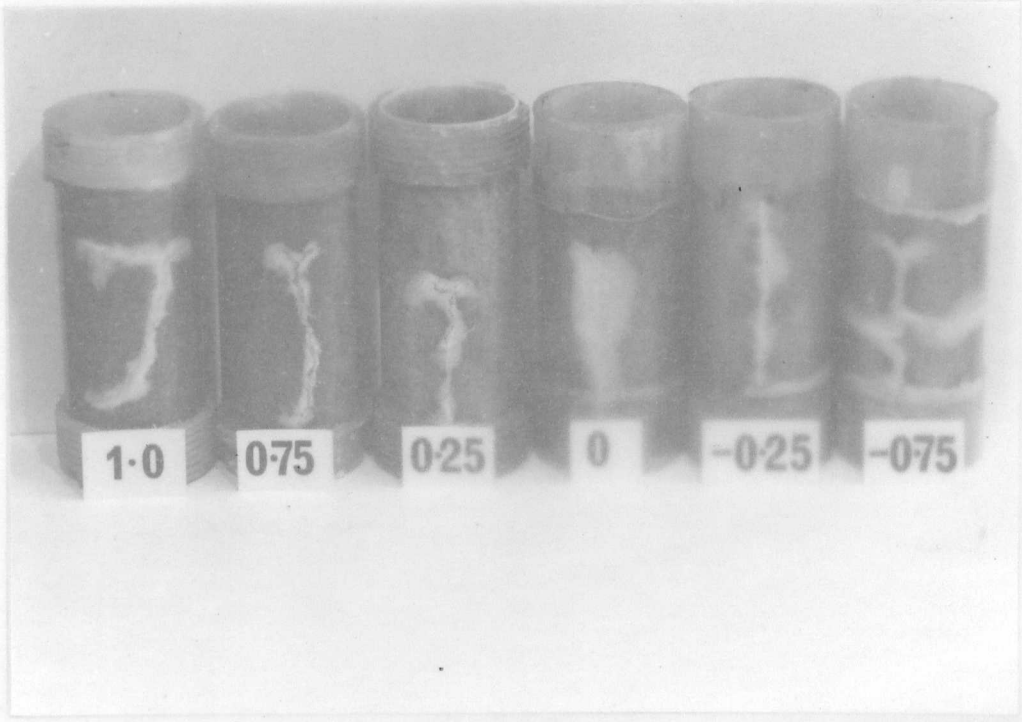

FIG. 51 BIAXIAL STRESS STATIC FAILURES OBSERVED IN C.S.M./POLYESTER RESIN CYLINDERS.

STATIC R = +1 FATIGUE

1  2

STATIC R = 0 FATIGUE

3  4

STATIC R = -1 FATIGUE

5  6

STATIC, R = 0

7 

FIG. 52. STATIC AND FATIGUE DAMAGE OBSERVED IN U.D.R./ POLYESTER RESIN CYLINDERS.

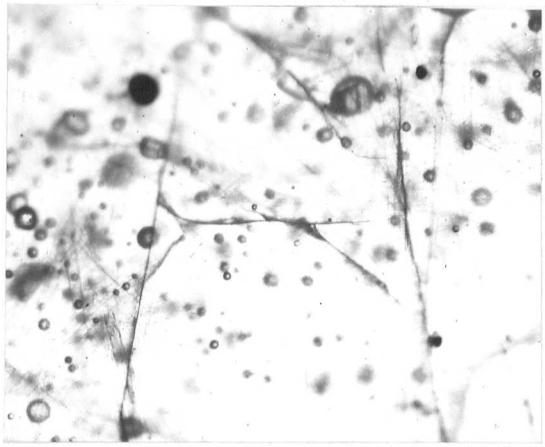

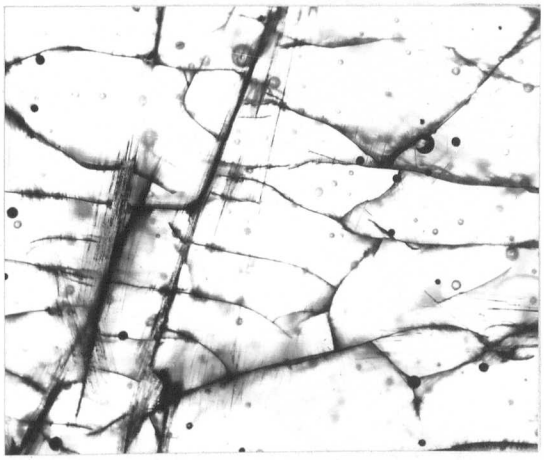

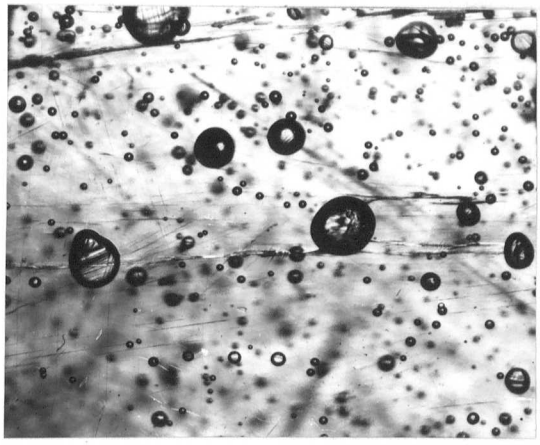

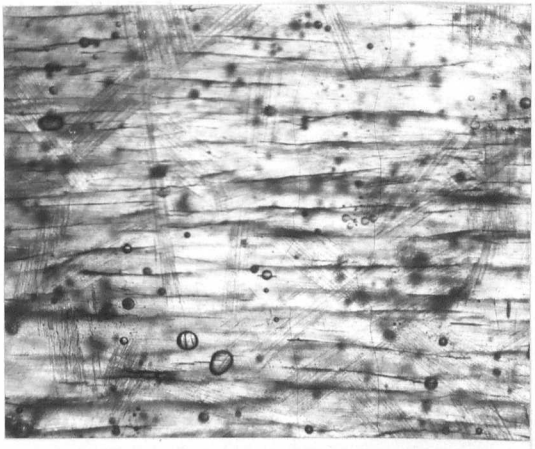

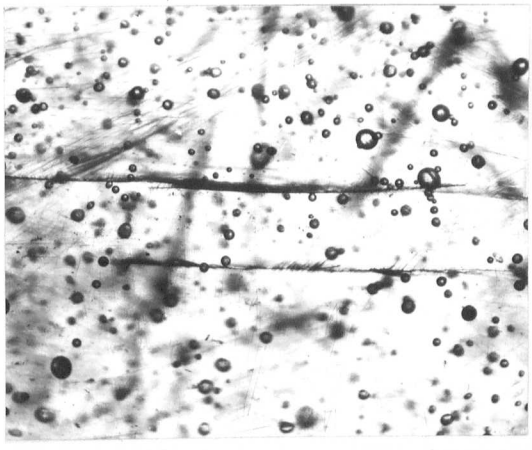

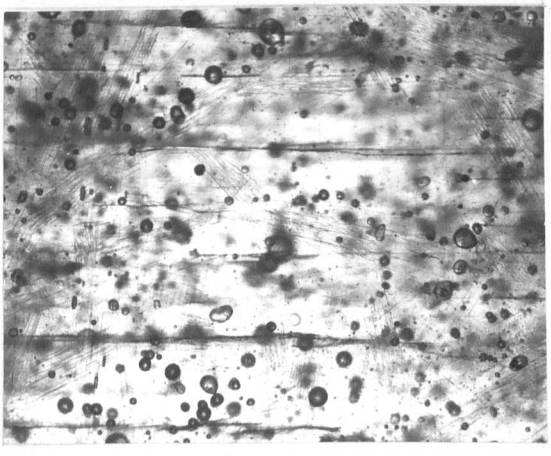

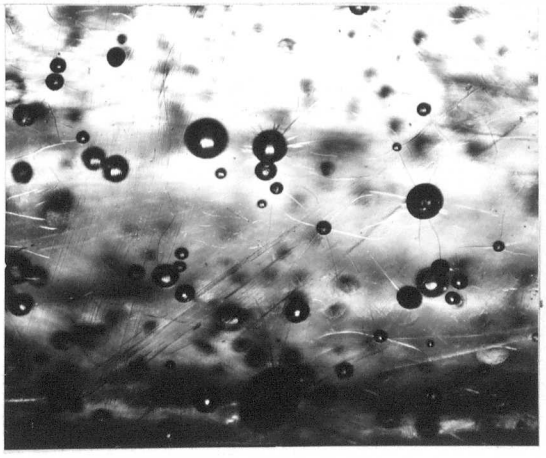

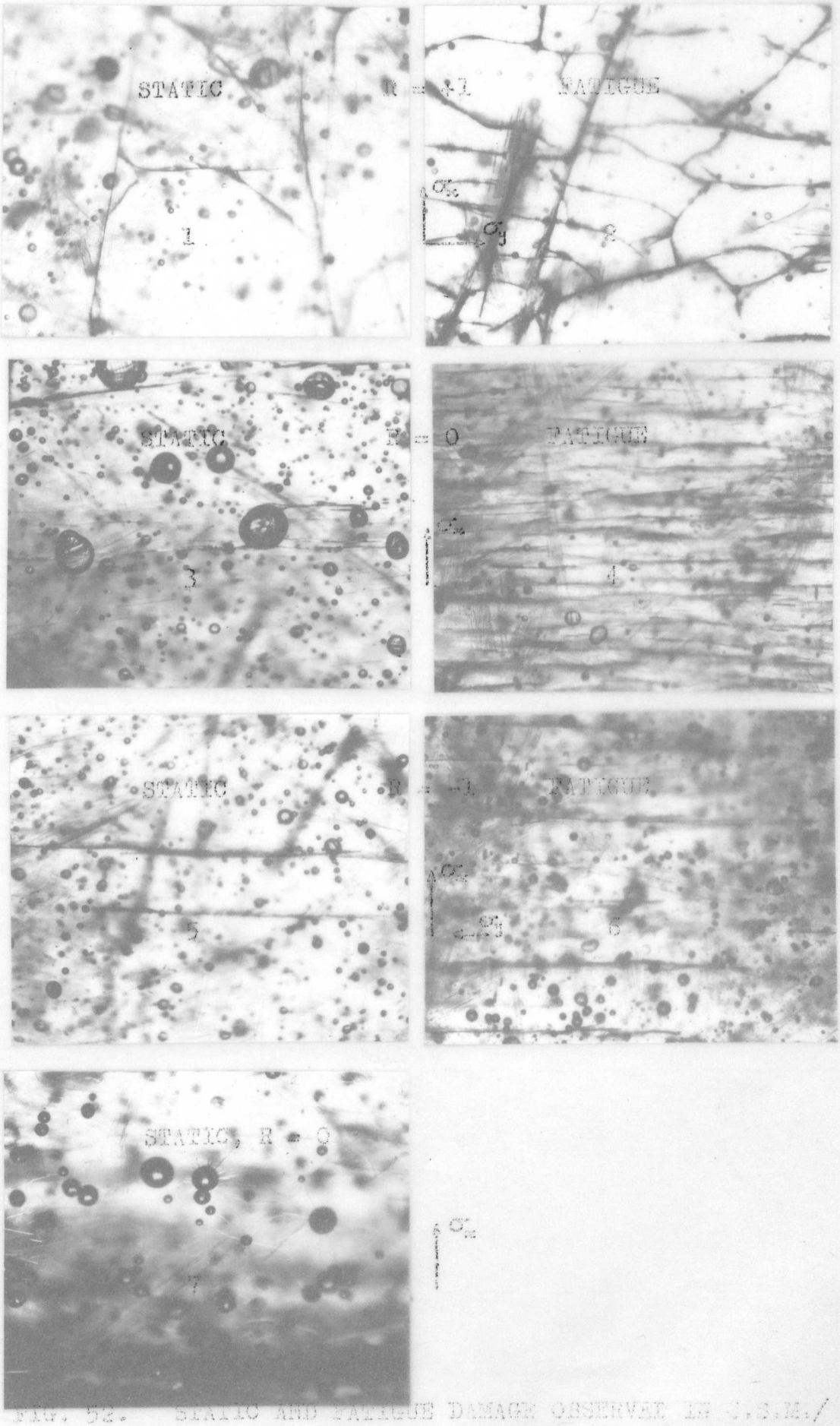

FIG. 52. STATIC AND FATIGUE DAMAGE OBSERVED IN C.S.M./POLYESTER RESIN CYLINDERS.

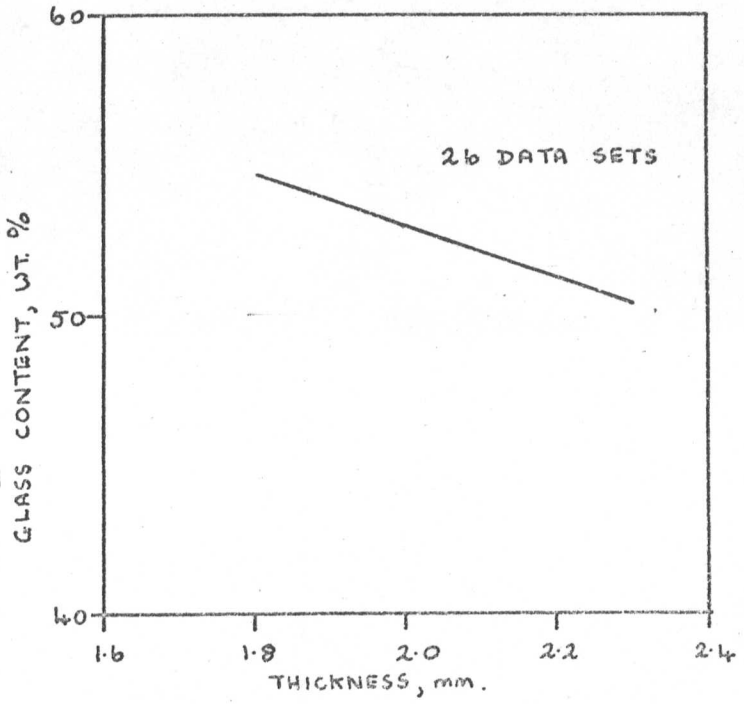

Fig. 53 Relationship between glass content and thickness for 5-layered Y449 fabric reinforced polyester resin laminates.

FIG. 24. SAMPLES OF THREADED-JOINTED X449 FABRIC-REINFORCED POLYESTER RESIN LAMINATE (13)

FIG. 24 - SAMPLE OF FABRIC-REINFORCED POLYESTER RESIN LAMINATE (13)

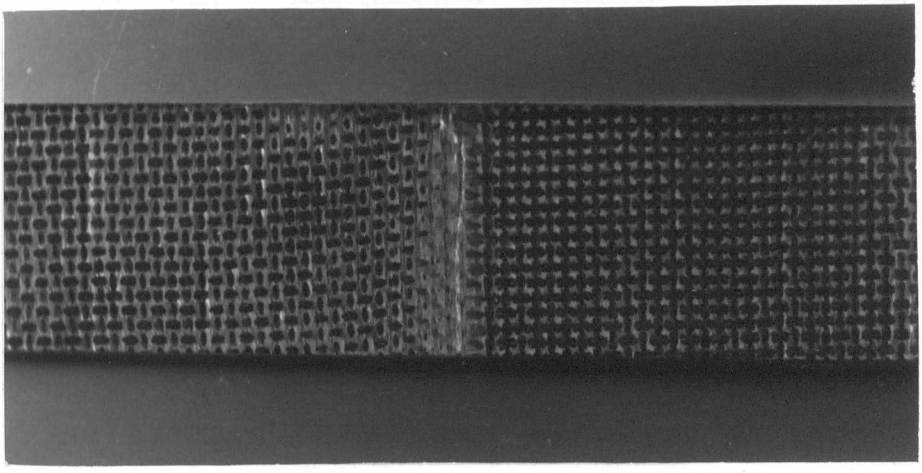

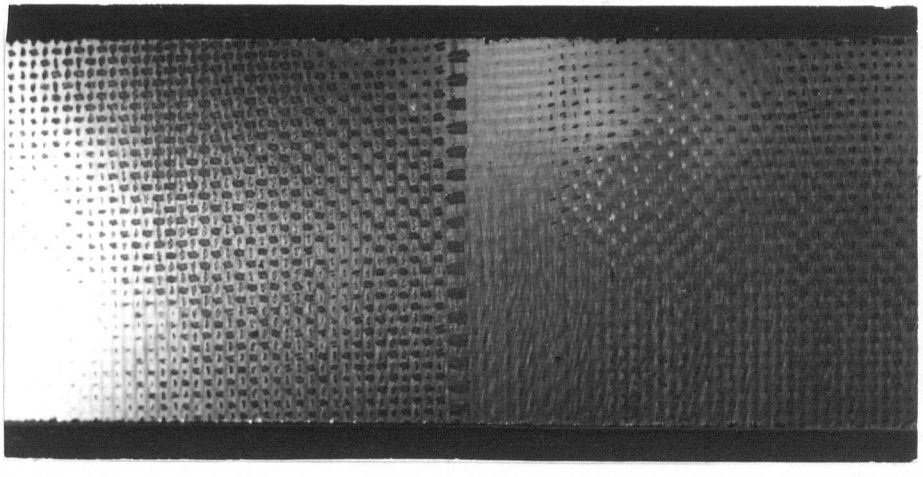

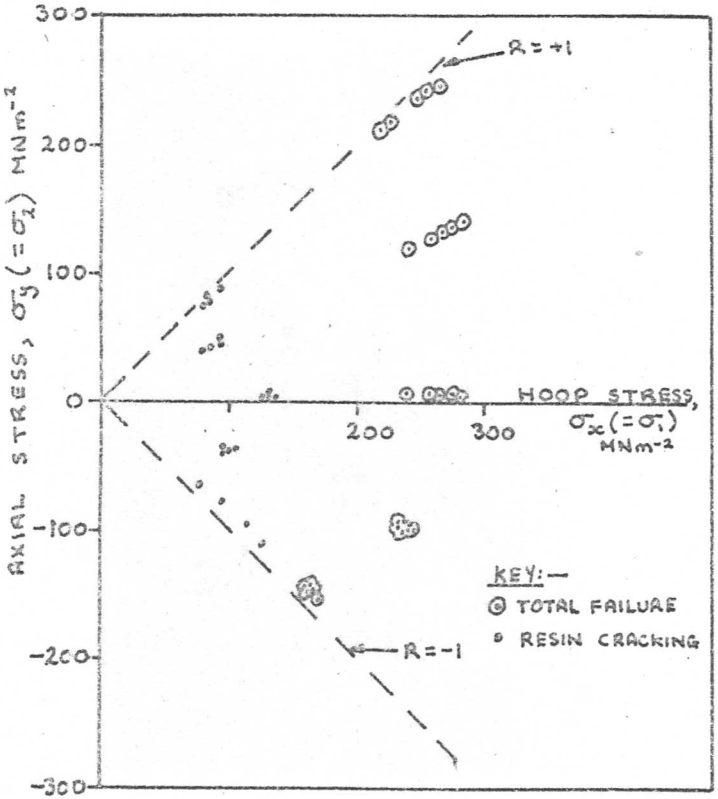

Fig. 55 Biaxial stress static test results from 0^0 Y449 fabric reinforced cylinders.

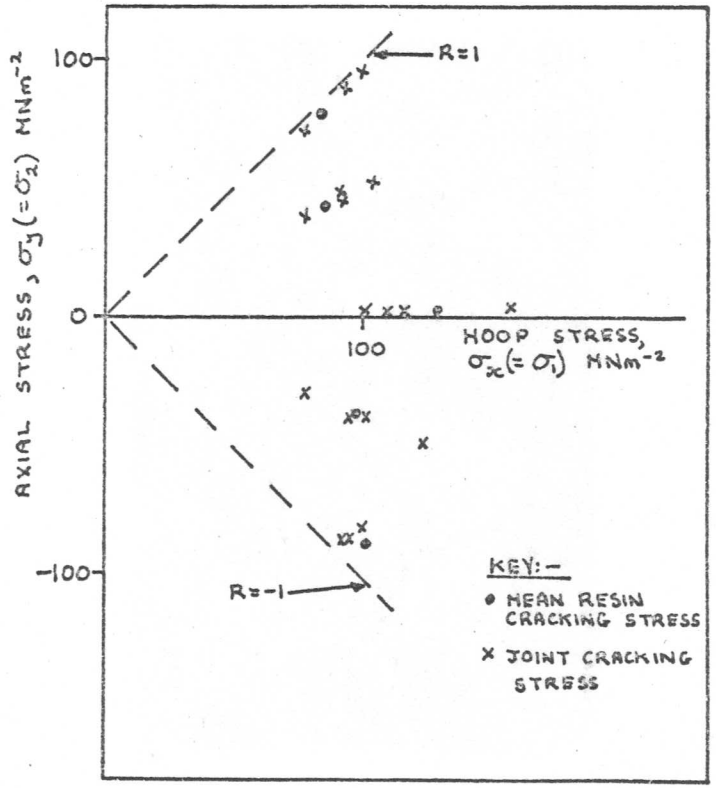

Fig. 56 Biaxial stress damage results from 0^0 Y449 fabric reinforced cylinders.

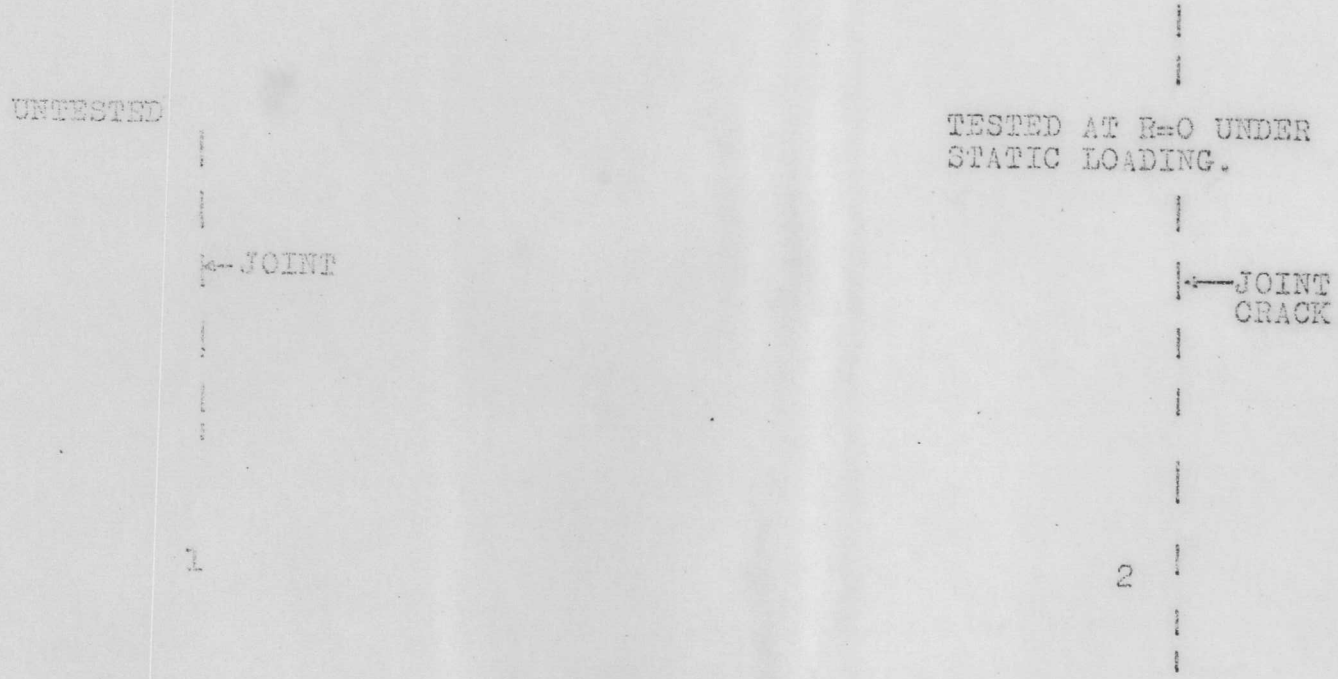

FIG.57 LAP-JOINTS AND JOINT CRACKS IN 0^{o} OFF-AXIS Y449 FABRIC-REINFORCED POLYESTER RESIN CYLINDERS.

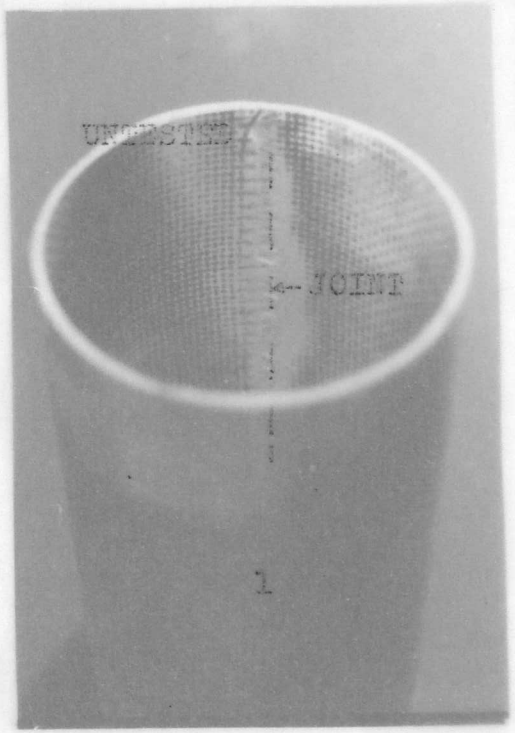

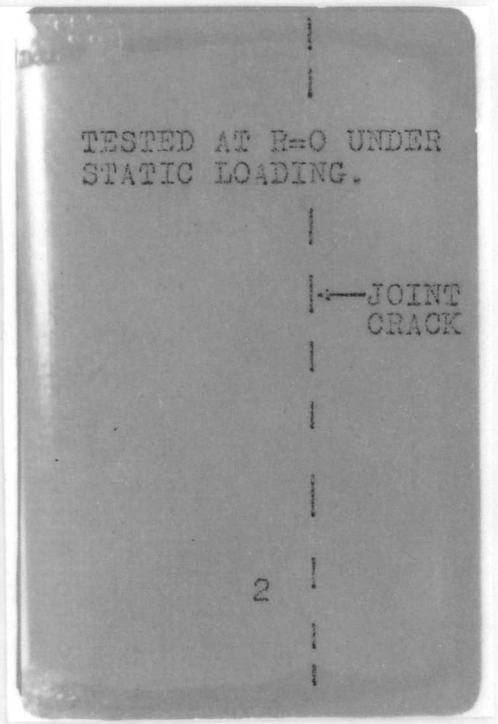

FIG.57 LAP-JOINTS AND JOINT CRACKS IN 0° OFF-AXIS Y449 FABRIC-REINFORCED POLYESTER RESIN CYLINDERS.

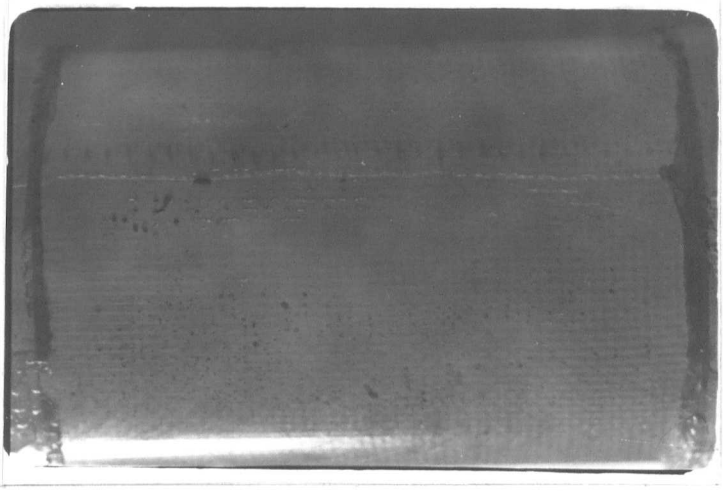

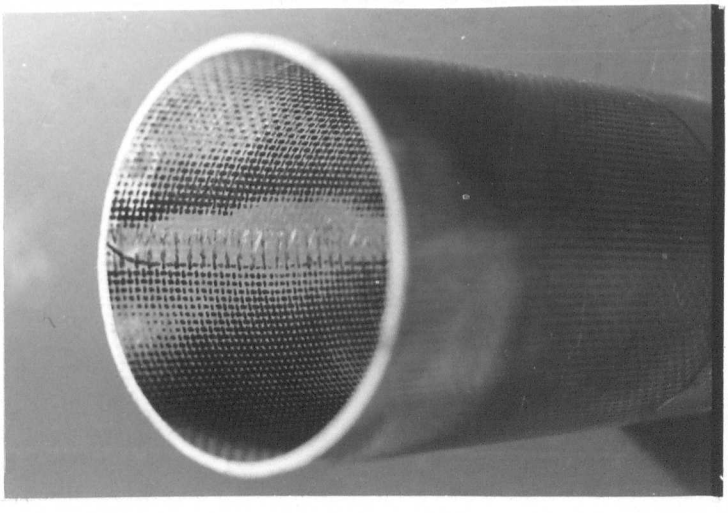

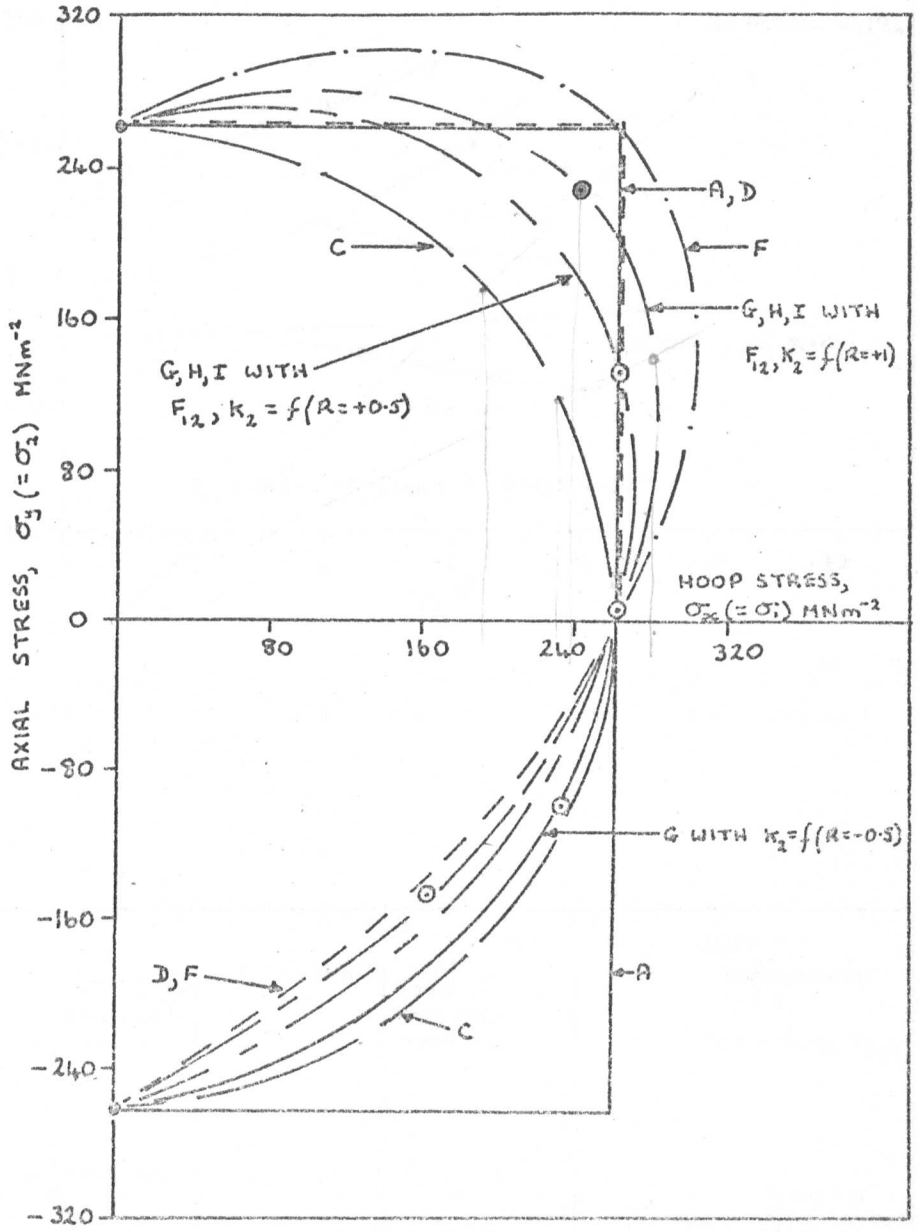

Fig. 58 Comparison of failure theories with mean experimental static burst data from 0° Y449/Polyester resin cylinders.

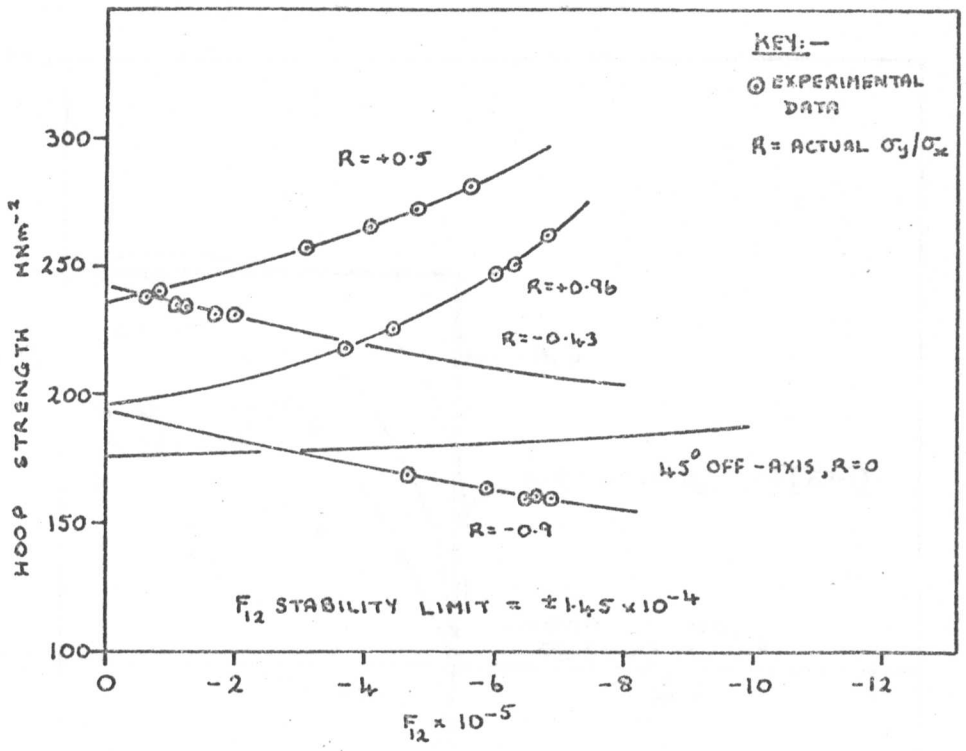

Fig. 59 Variation of F_{12} with failure strength of 0° Y449/ Polyester resin cylinders at different biaxial stress ratios.

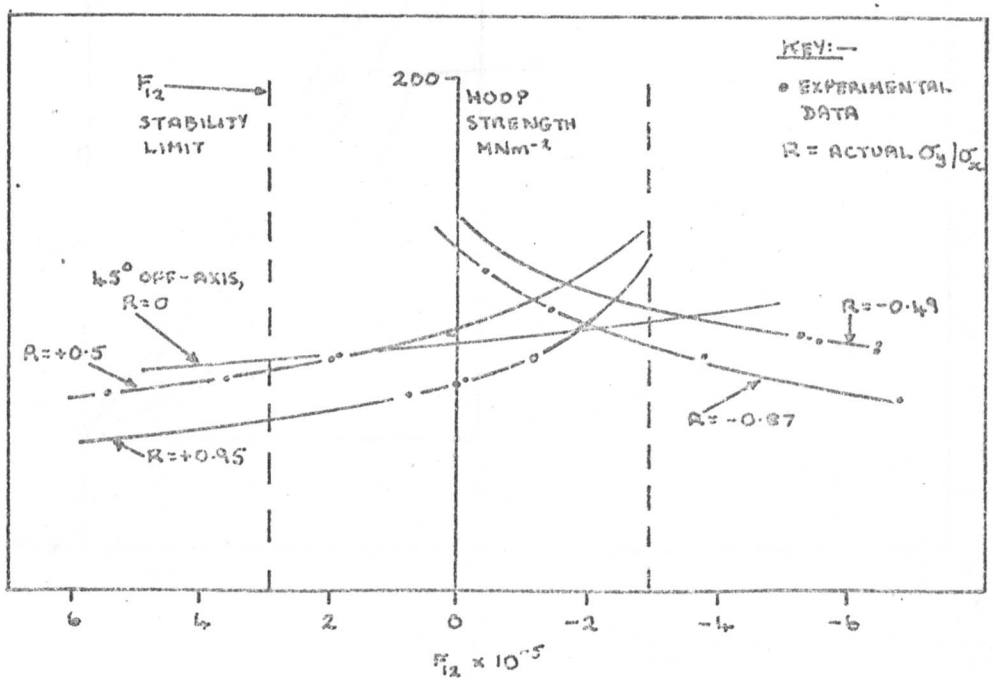

Fig. 60 Variation of F_{12} with resin cracking stress of 0° Y449/Polyester resin cylinders at different biaxial stress ratios.

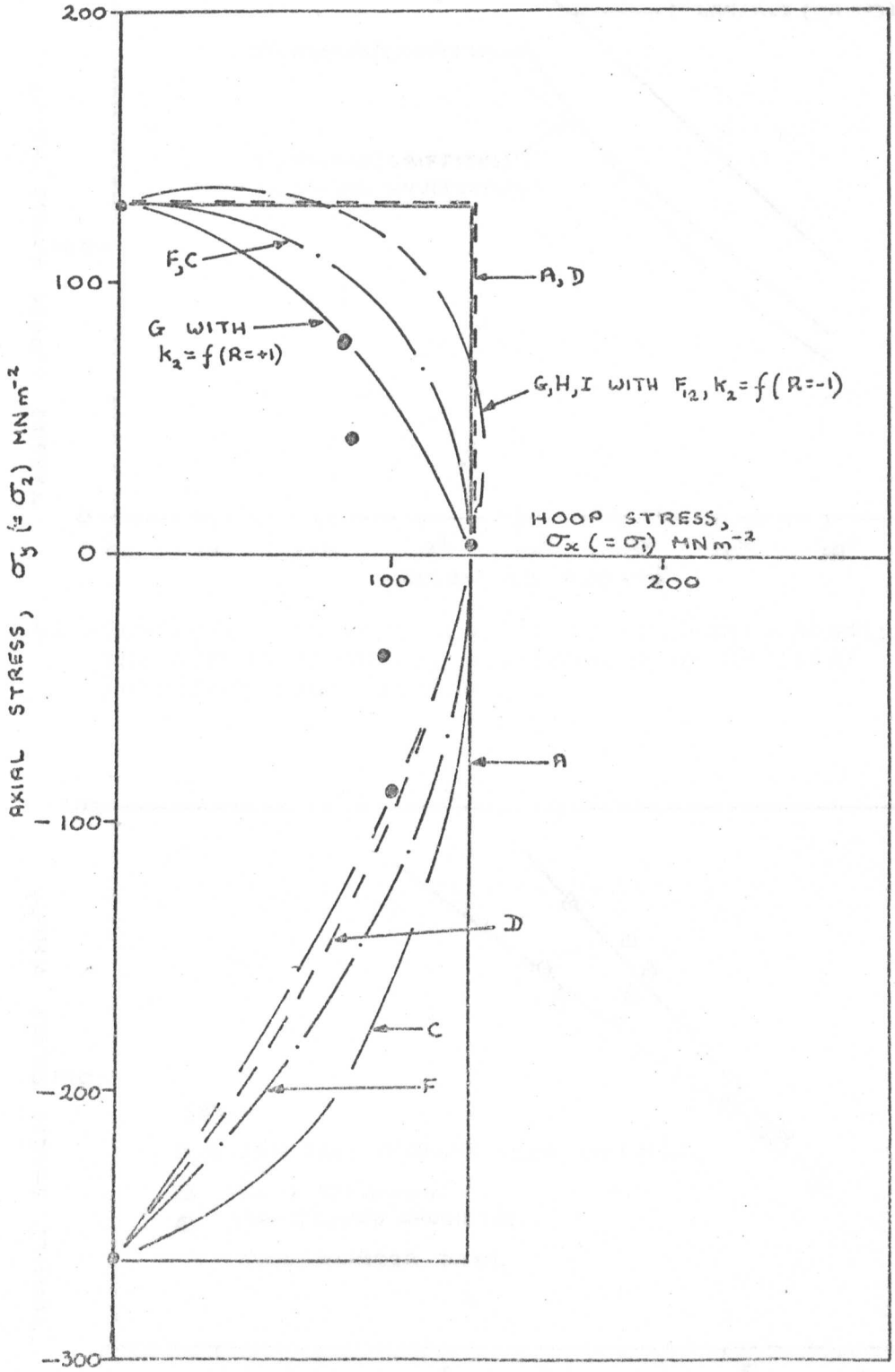

Fig. 61 Comparison of failure theories with mean experimental static resin cracking data from 0° Y449/Polyester resin cylinders.

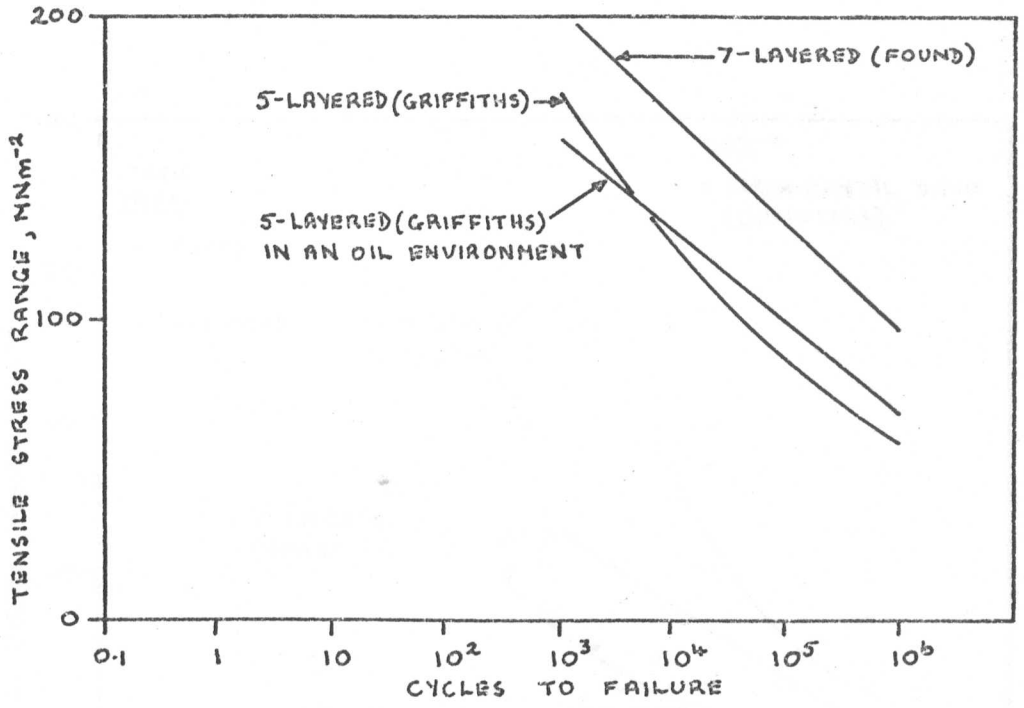

Fig. 62 Comparison of zero-tension fatigue data showing the effect of an oil environment on 0° Y449/ Polyester resin laminates.

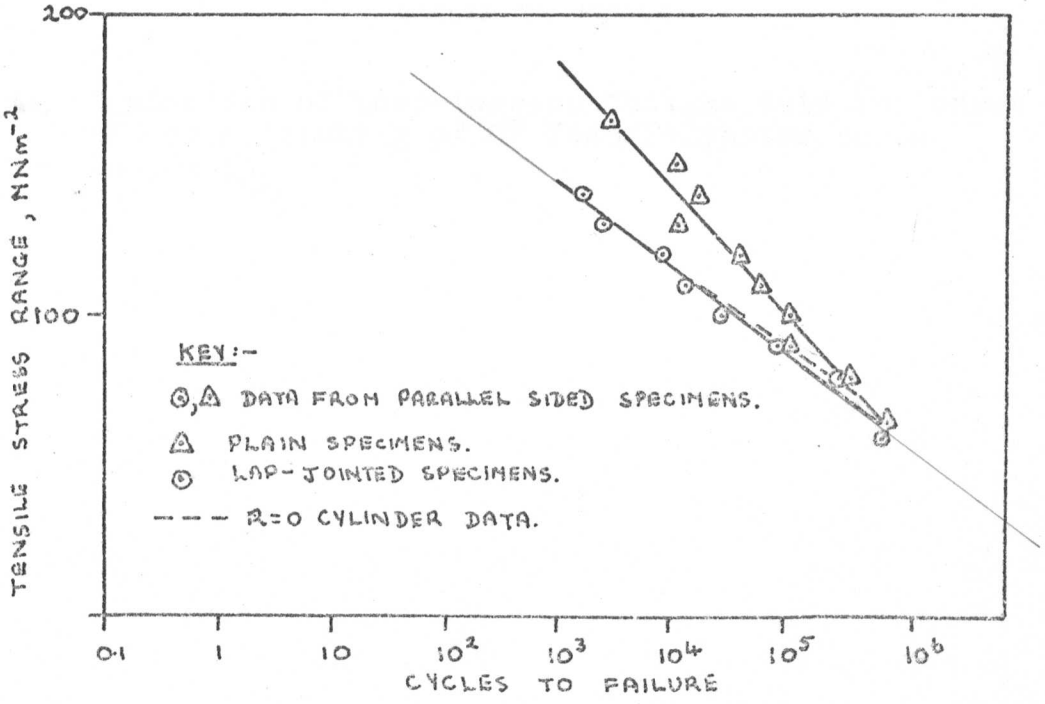

Fig. 63 The effect of a lap joint on the zero-tension fatigue behaviour of 0° Y449/Polyester Resin laminates.

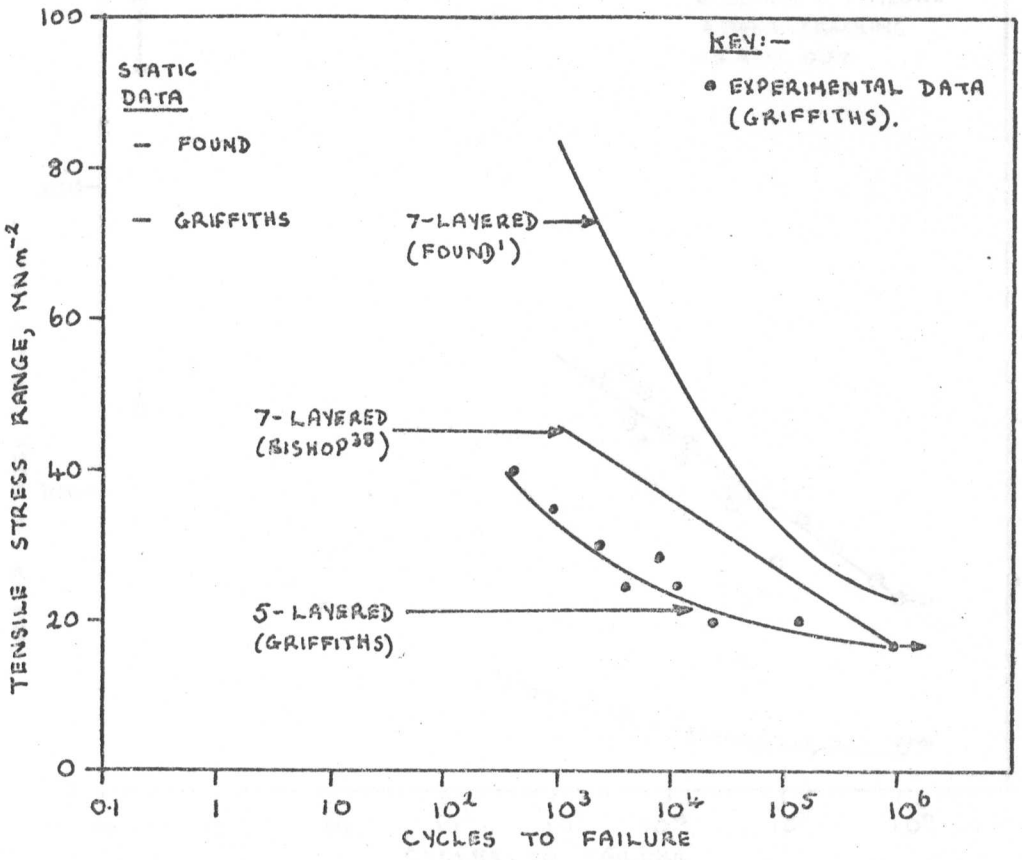

Fig. 64 Comparison of zero-tension fatigue data for onset of resin cracking of 0^{o} Y449/Polyester resin laminates.

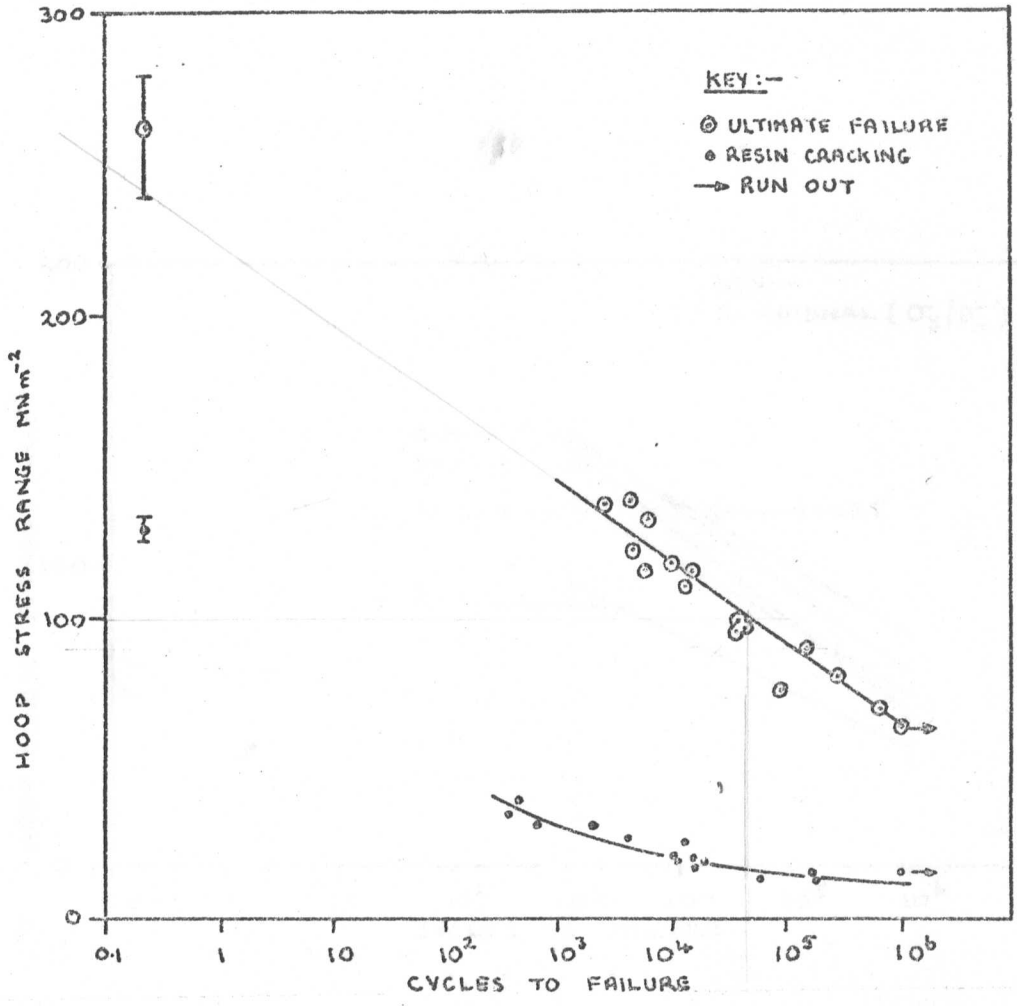

Fig. 65 R = 0 Fatigue data for 0° Y449/Polyester resin cylinders.

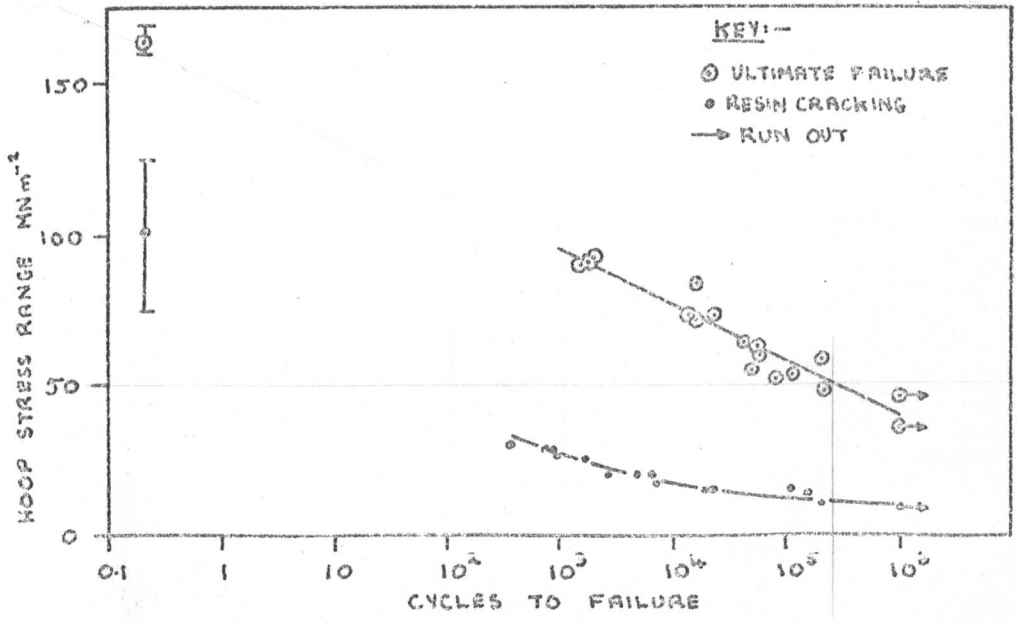

Fig. 66 R=-1.0 Fatigue data for 0° Y449/Polyester resin cylinders.

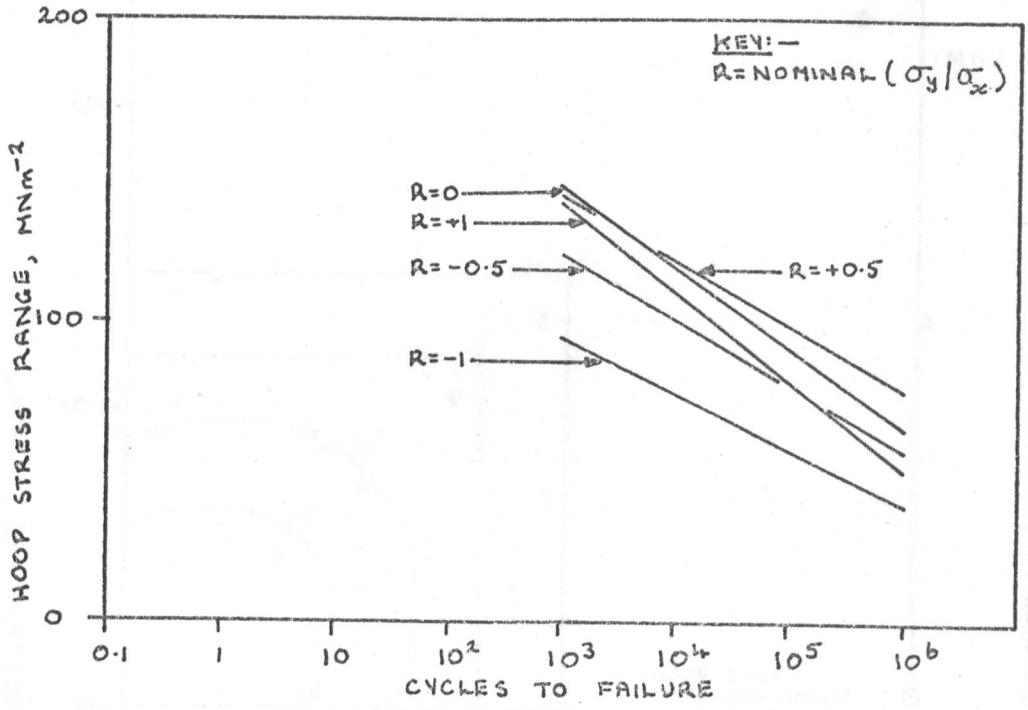

Fig. 67 The effect of 'R' on the total failure fatigue behaviour of 0° Y449/Polyester resin cylinders.

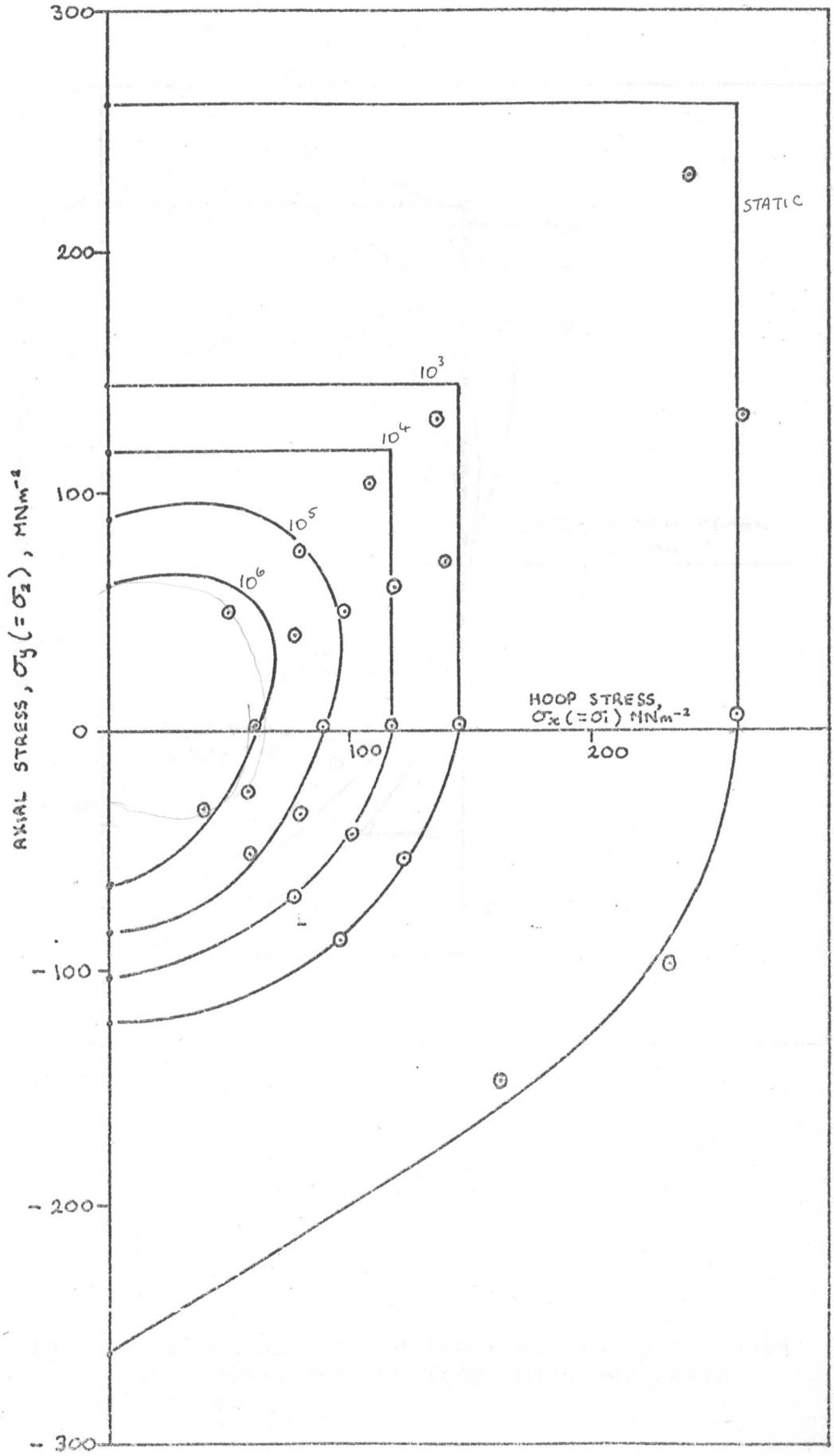

Fig. 69 Constant life diagram for total failure of 0° Y449/Polyester Resin cylinders.

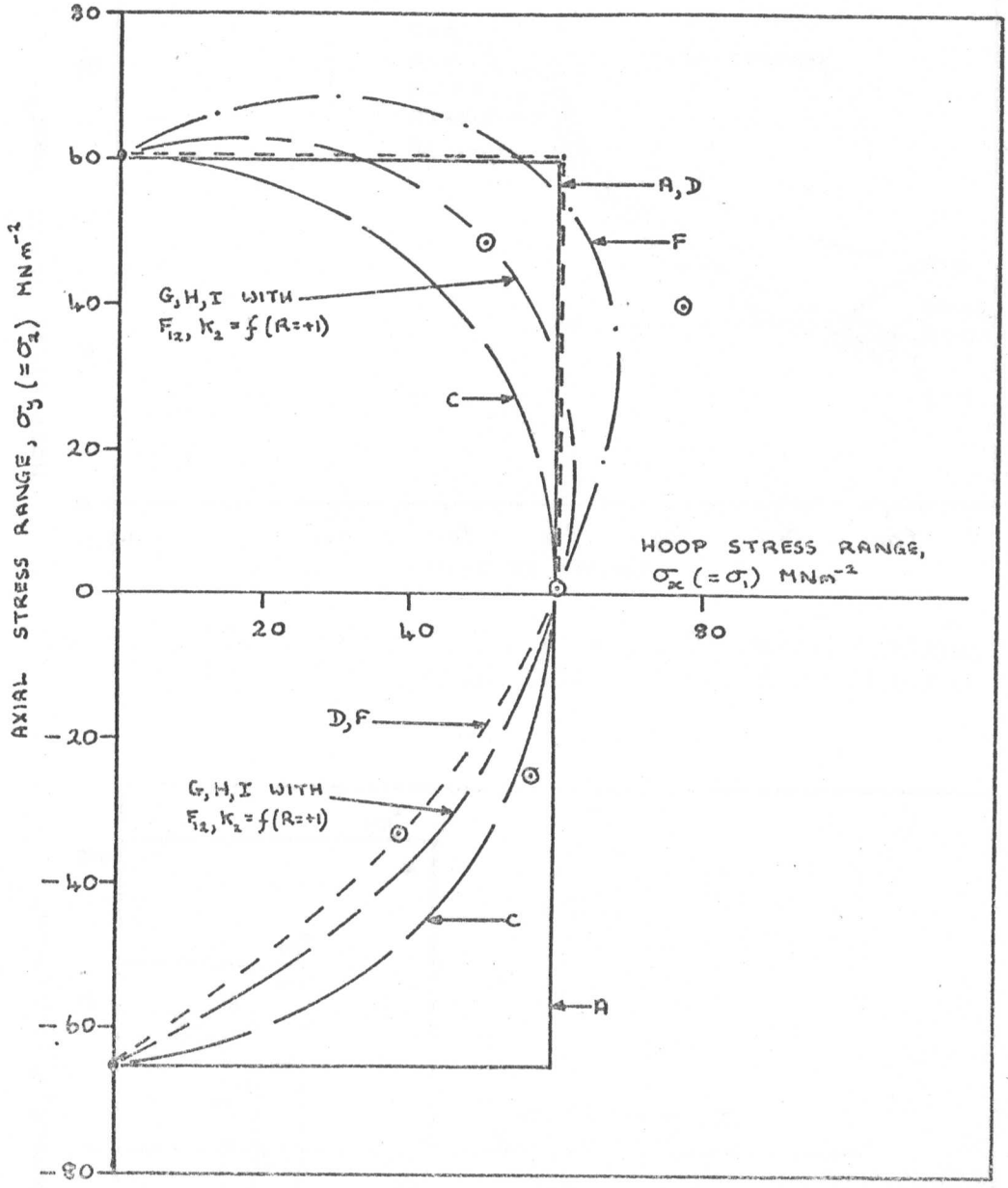

Fig. 69 Comparison of failure theories with burst data at 10^6 cycles from 0° Y449/Polyester resin cylinders.

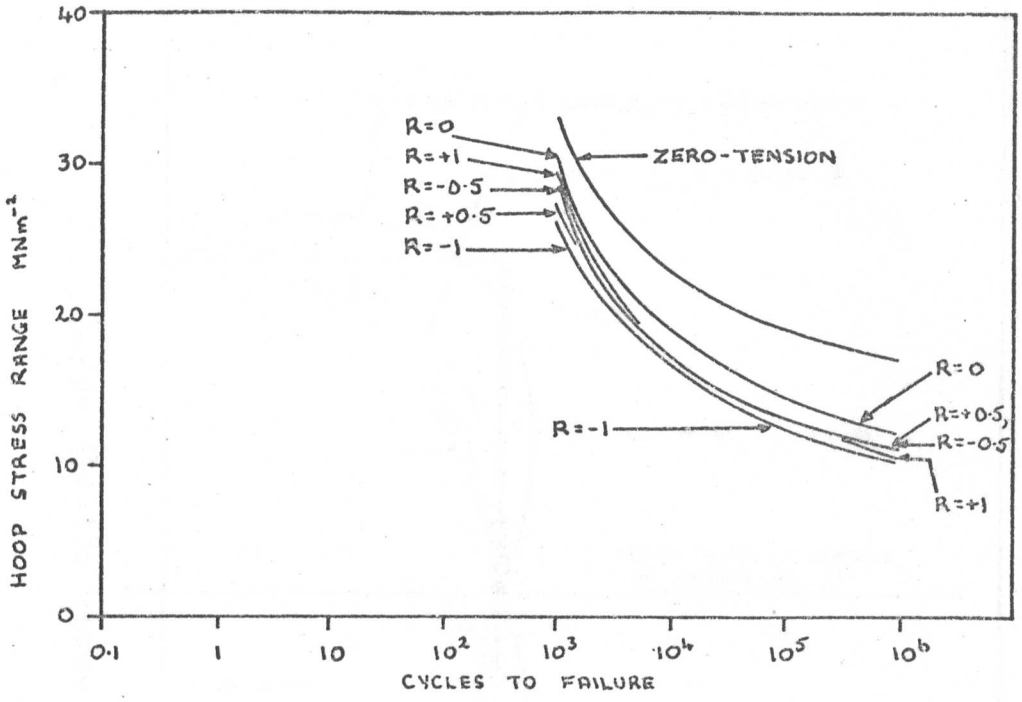

Fig. 70 The effect of 'R' on the resin cracking fatigue behaviour of 0° Y449/Polyester resin cylinders.

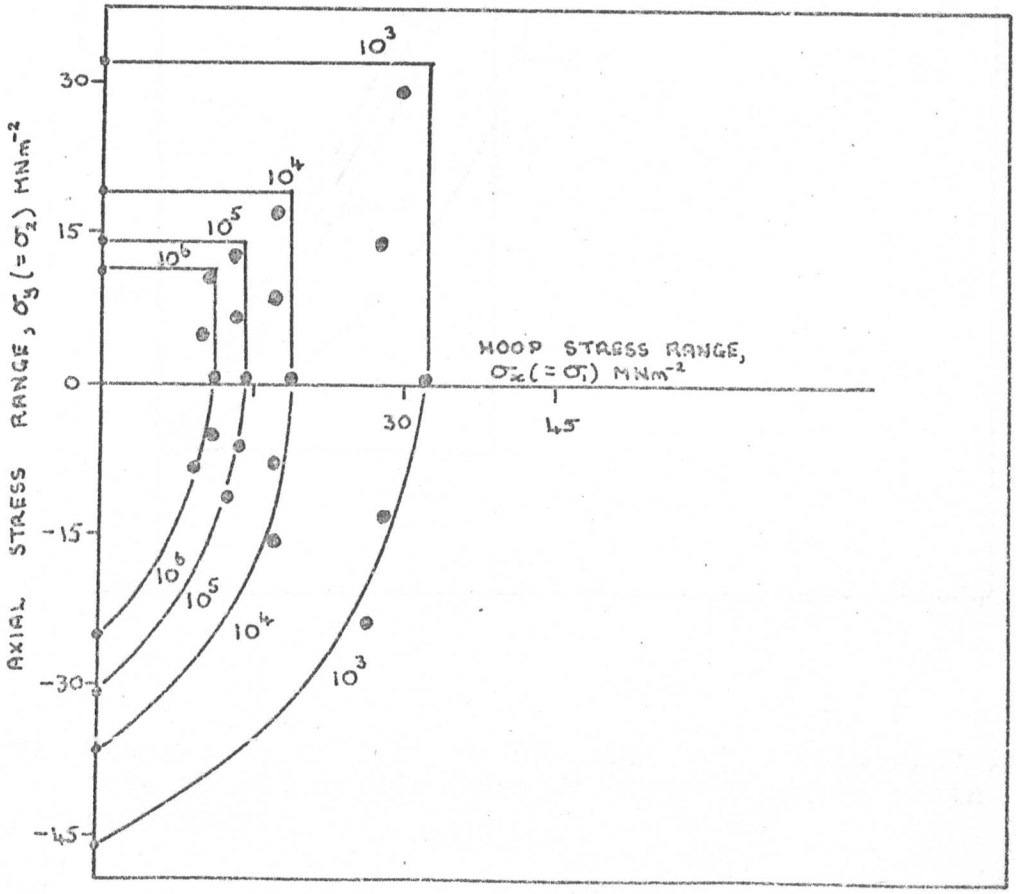

Fig. 71 Constant life diagram for resin cracking of 0° Y449/Polyester resin cylinders.

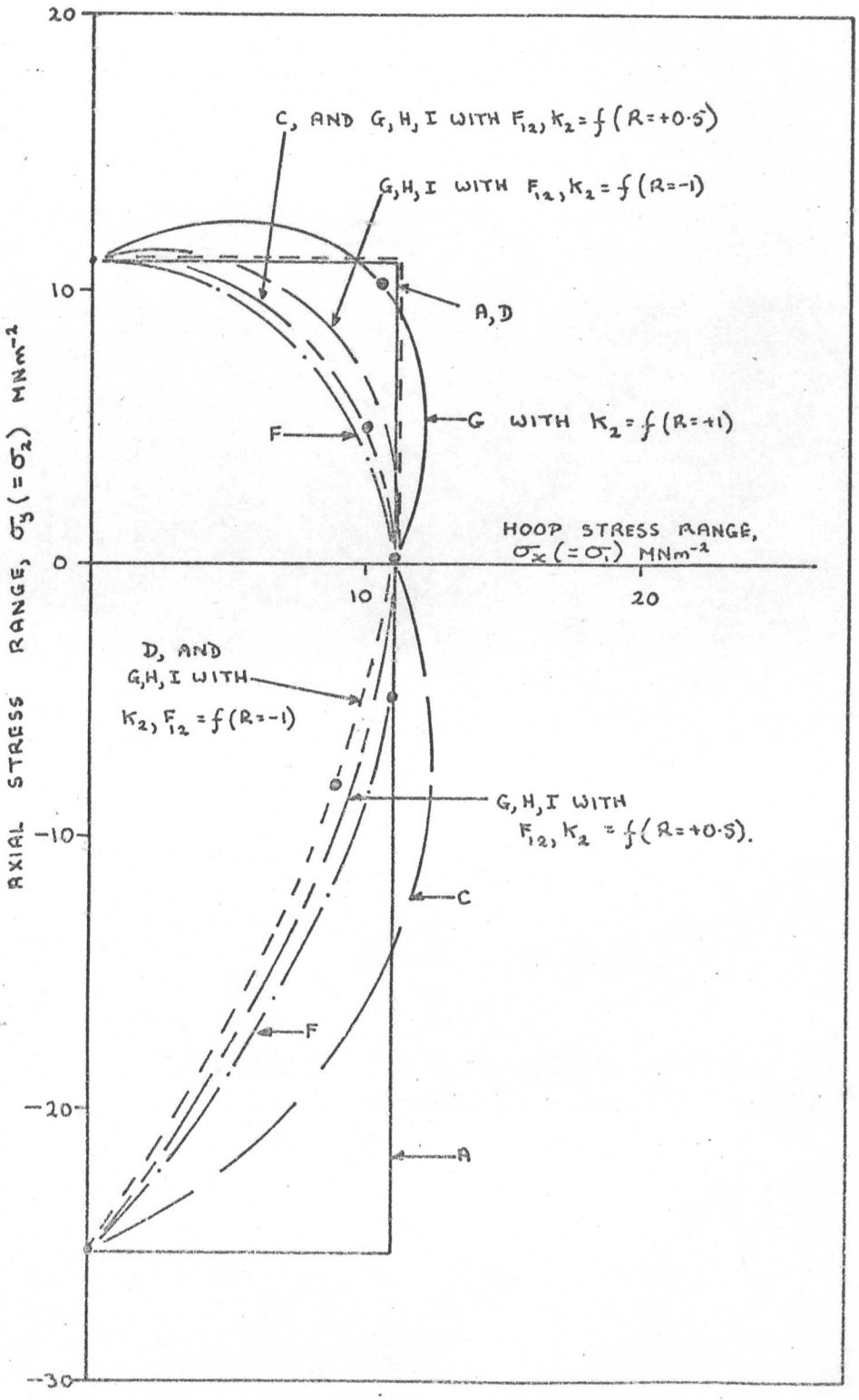

Fig. 72 Comparison of failure theories with resin cracking data at 10^6 cycles from 0° Y449/Polyester resin cylinders.

FIG. 73 BIAXIAL STRESS STATIC FAILURES OBSERVED IN 0° OFF-AXIS Y449 FABRIC-REINFORCED POLYESTER RESIN CYLINDERS.

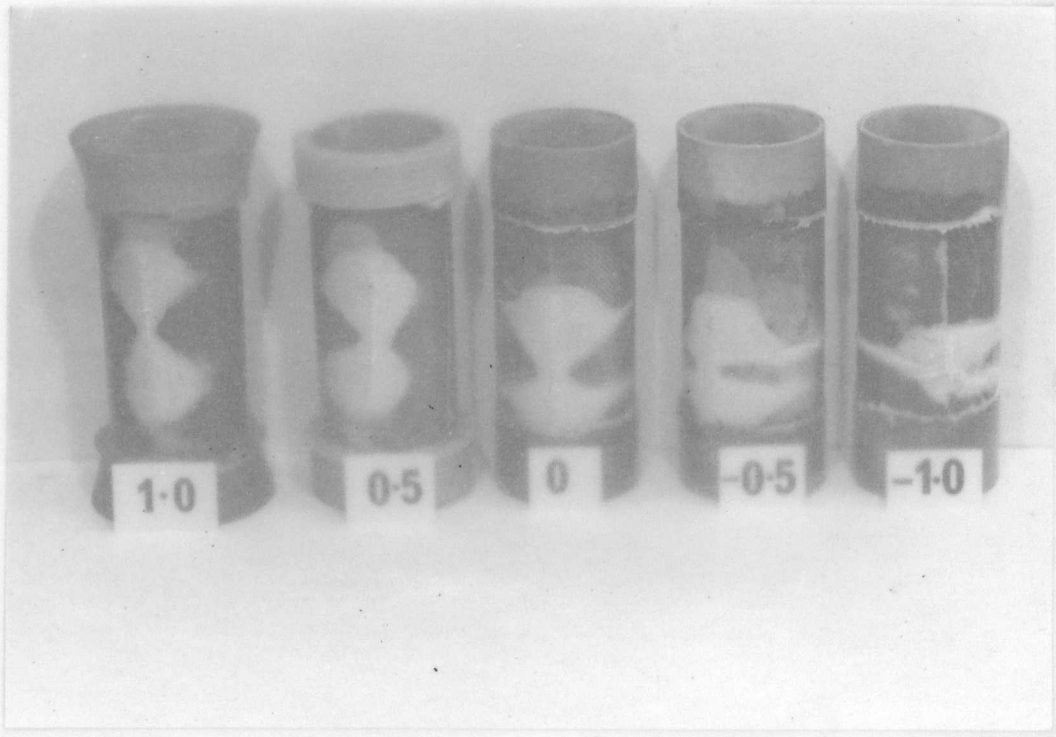

FIG. 73 BIAXIAL STRESS STATIC FAILURES OBSERVED IN 0^{o} OFF-AXIS Y449 FABRIC-REINFORCED POLYESTER RESIN CYLINDERS.

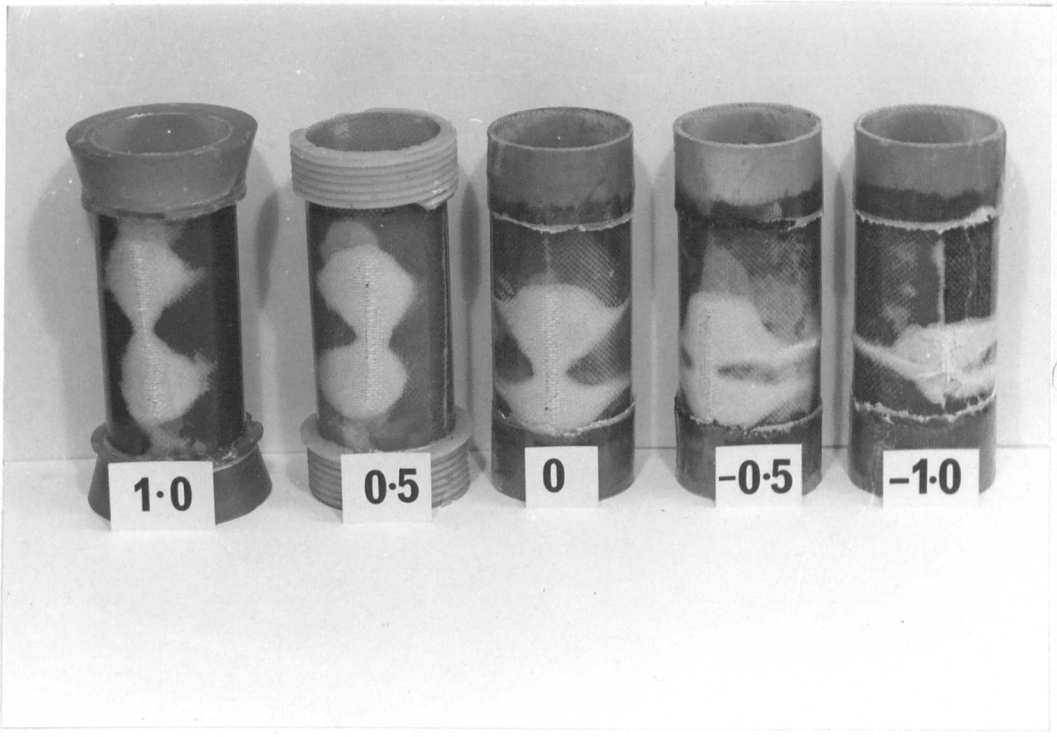
1·0
0·5
0
-0·5
-1·0

STATIC	R= +1	FATIGUE
1		2

STATIC	R = 0	FATIGUE
3		4

STATIC	R = -1	FATIGUE
5		6

FIG. 74. STATIC AND FATIGUE DAMAGE OBSERVED IN 0° OFF-AXIS X440 FABRIC-REINFORCED POLYESTER RESIN CYLINDERS.

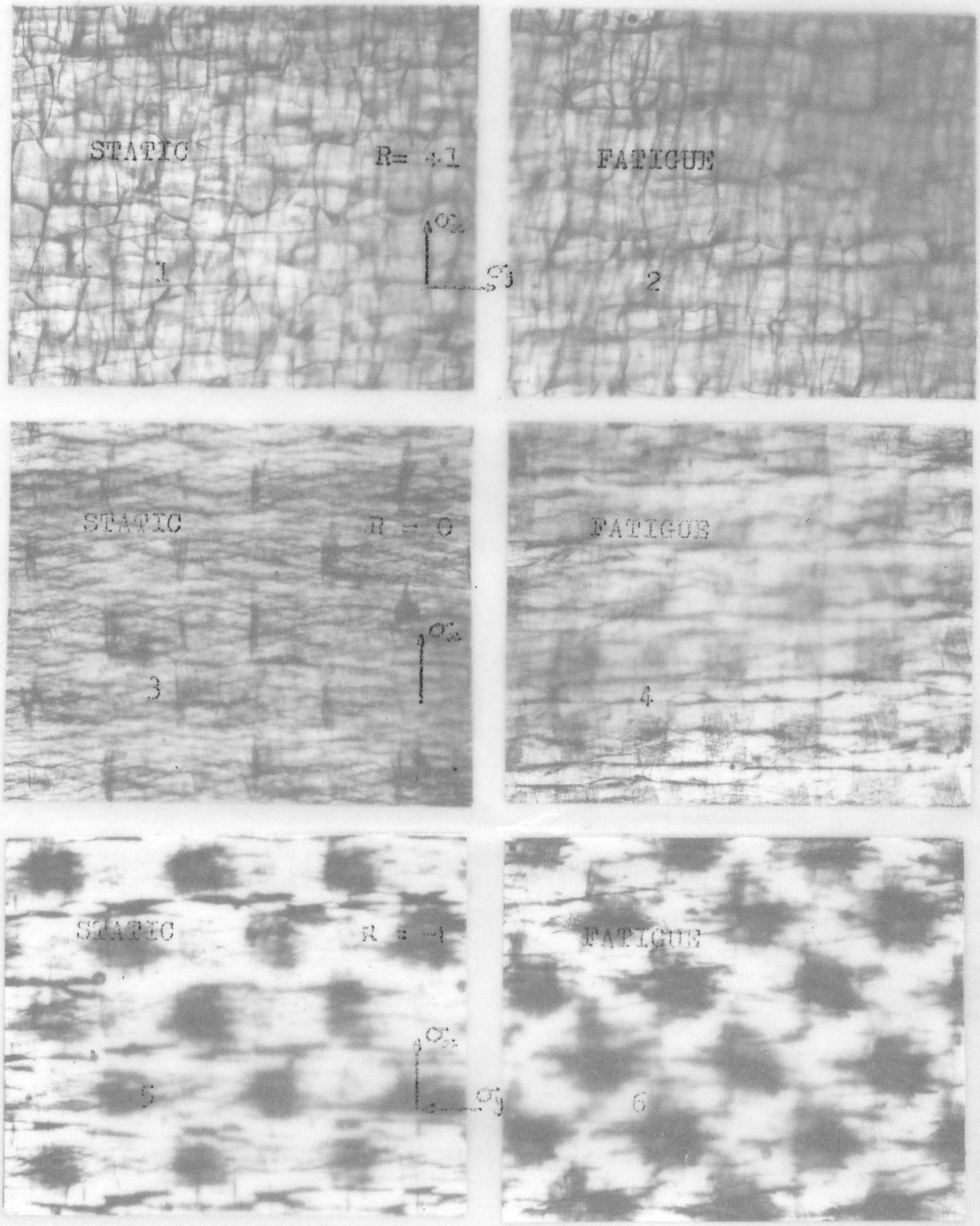

FIG. 74. STATIC AND FATIGUE DAMAGE OBSERVED IN 0° OFF-AXIS Y449 FABRIC-REINFORCED POLYESTER RESIN CYLINDERS.

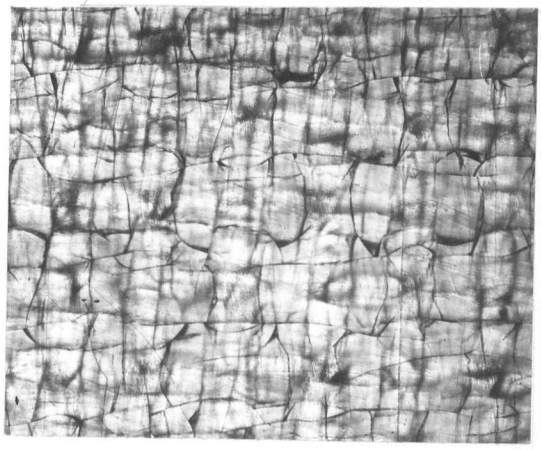

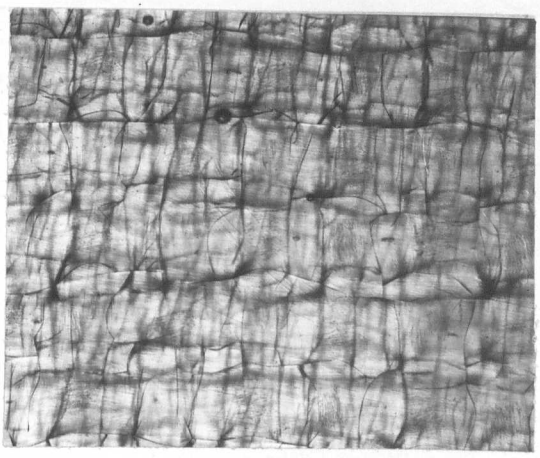

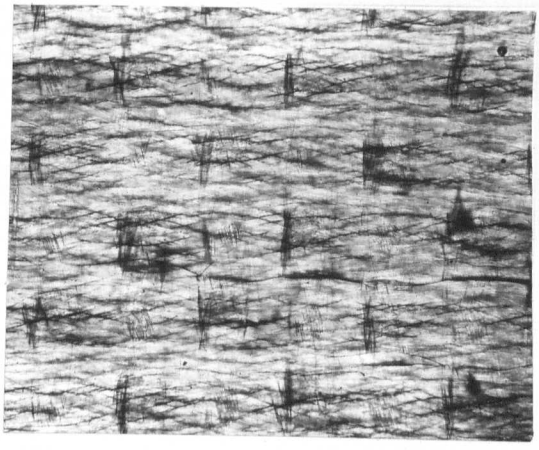

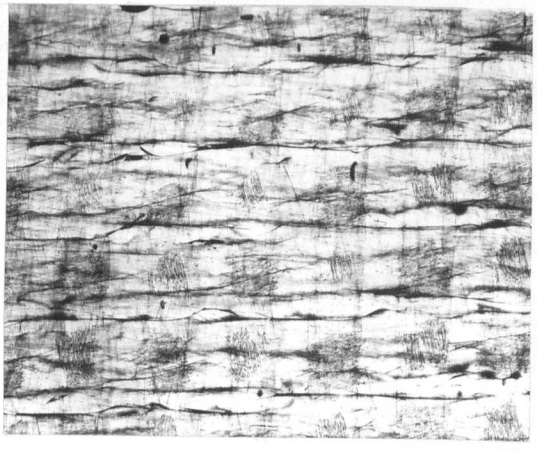

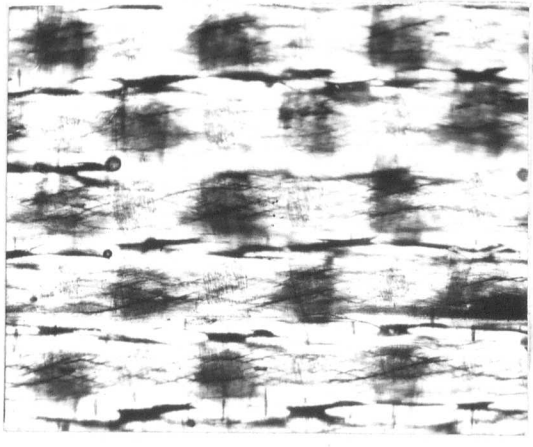

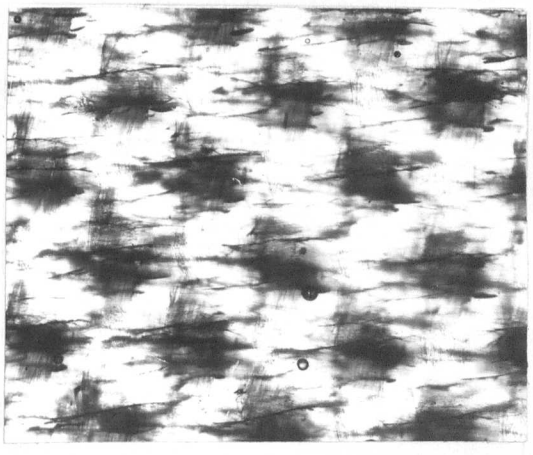

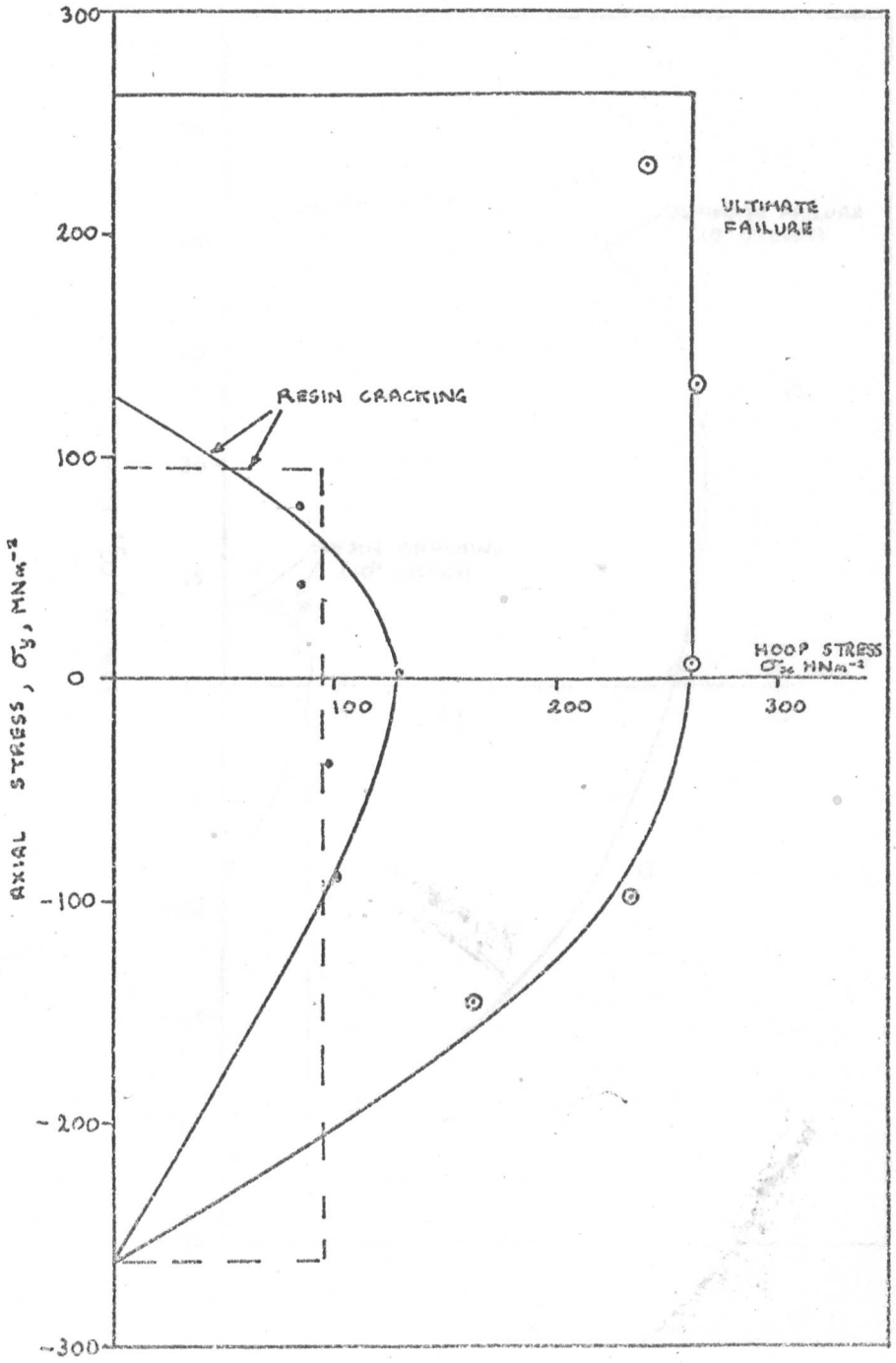

Fig. 75 Ultimate strength and damage failure envelopes for fabric reinforced cylinders under static loading.

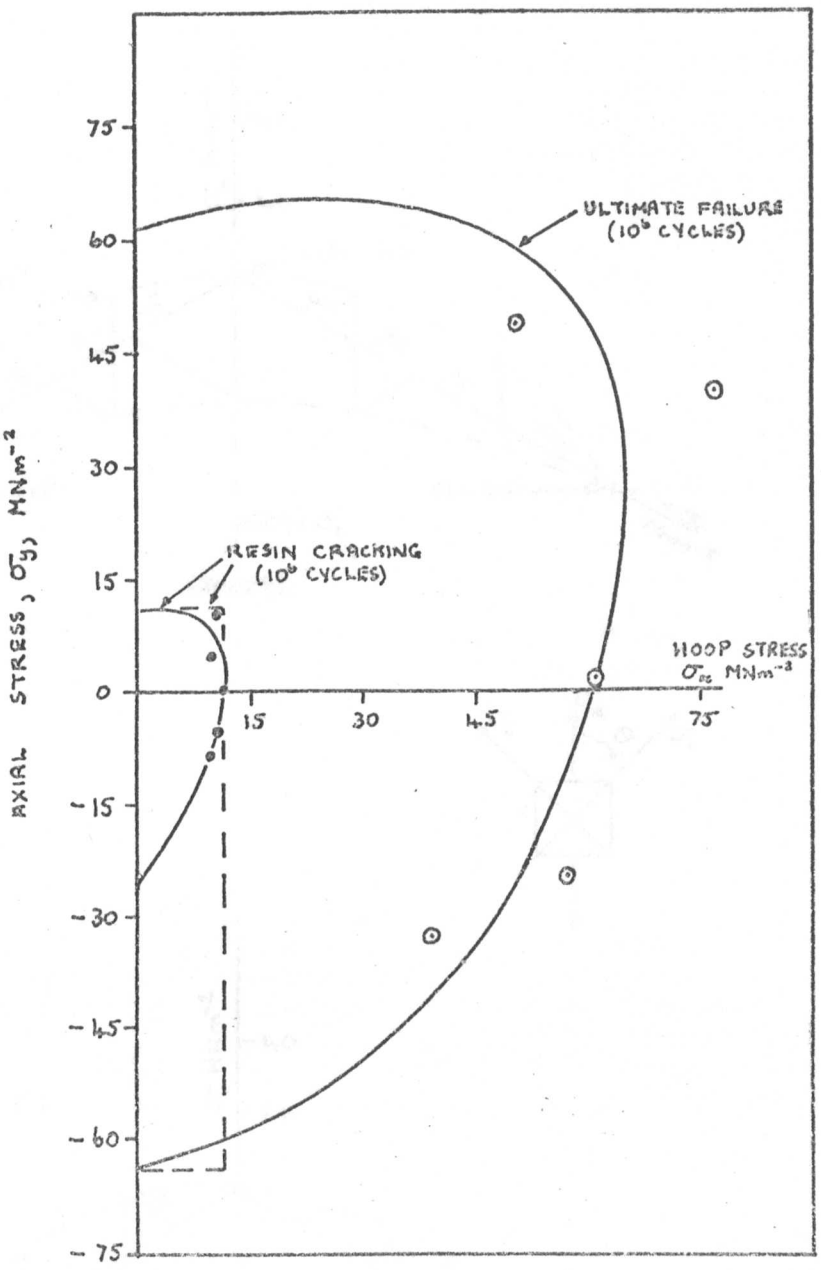

Fig. 76 Ultimate strength and damage failure envelopes for fabric reinforced cylinders at 10^6 cycles under fatigue loading.

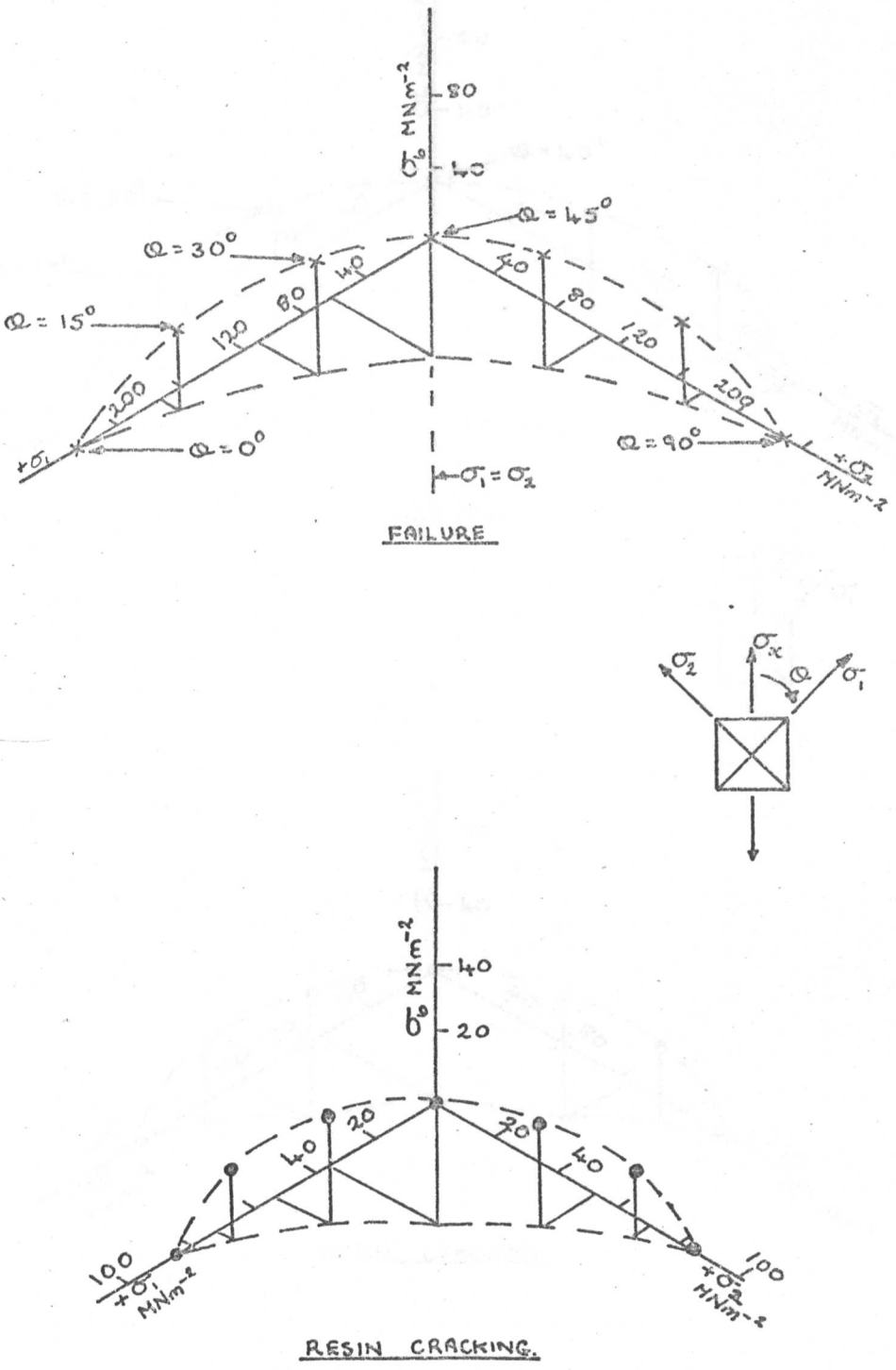

Fig. 77 Uniaxial off-axis tension results (Found[1]), from 7 layered Y449/Polyester resin laminates, plotted in 3-D.

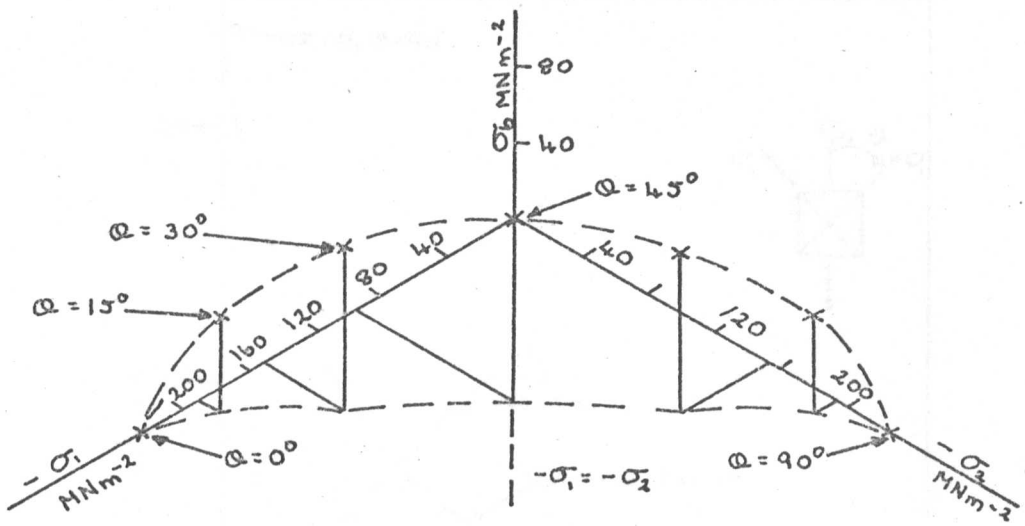

FAILURE

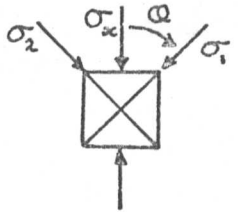

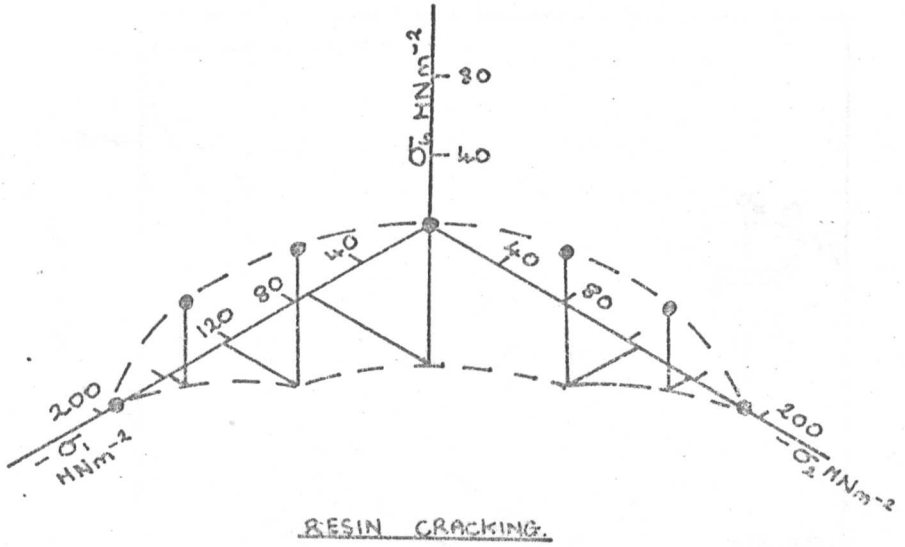

RESIN CRACKING.

Fig. 78 Uniaxial off-axis compression results (Found[1]), from 7 layered Y449/Polyester resin laminates, plotted in 3-D.

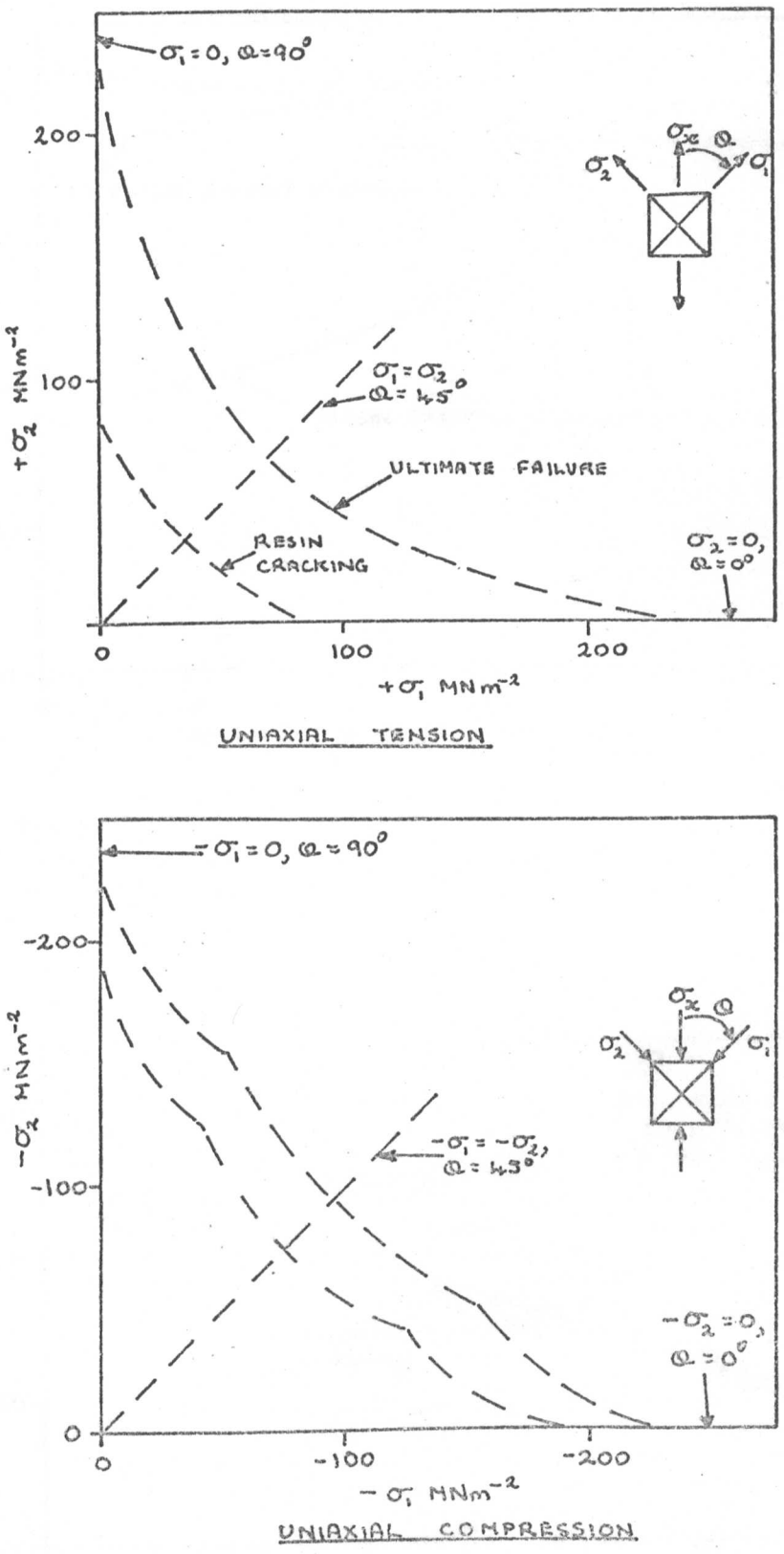

Fig. 79 The profile described by Found's uniaxial off-axis test results in the $\sigma_6 = 0$ plane.

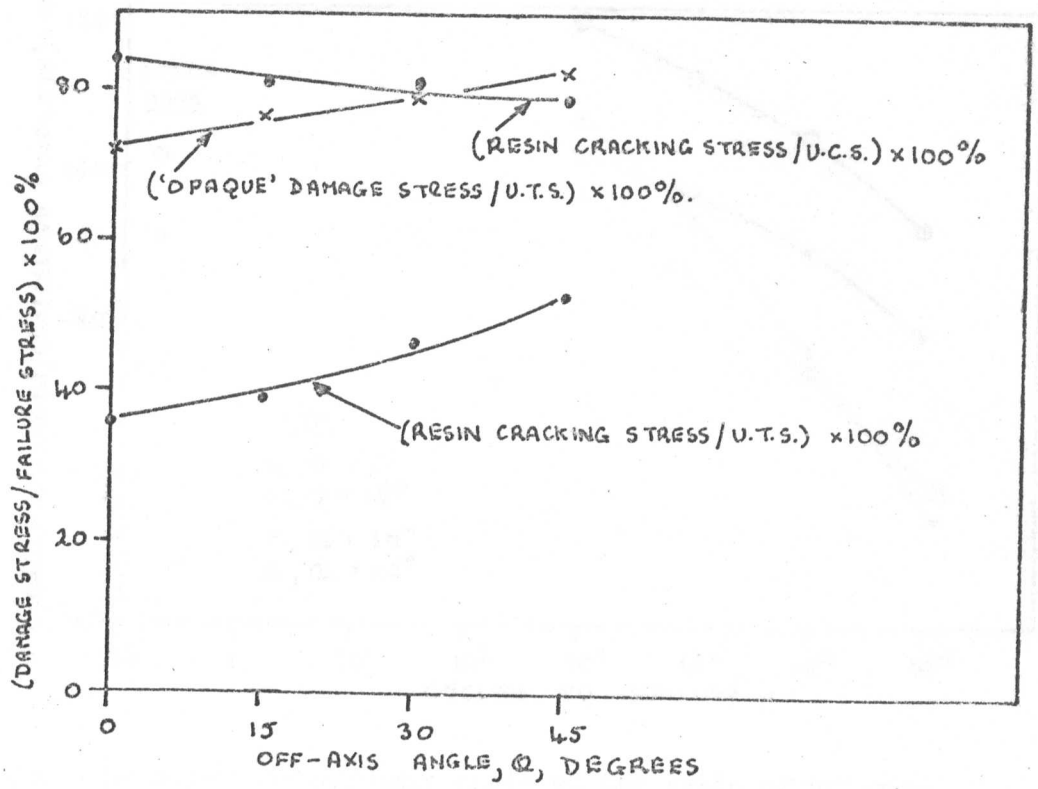

Fig. 80 The effect of off-axis angle on the static damage stress to ultimate strength ratio of 7-layered Y449 fabric reinforced laminates.

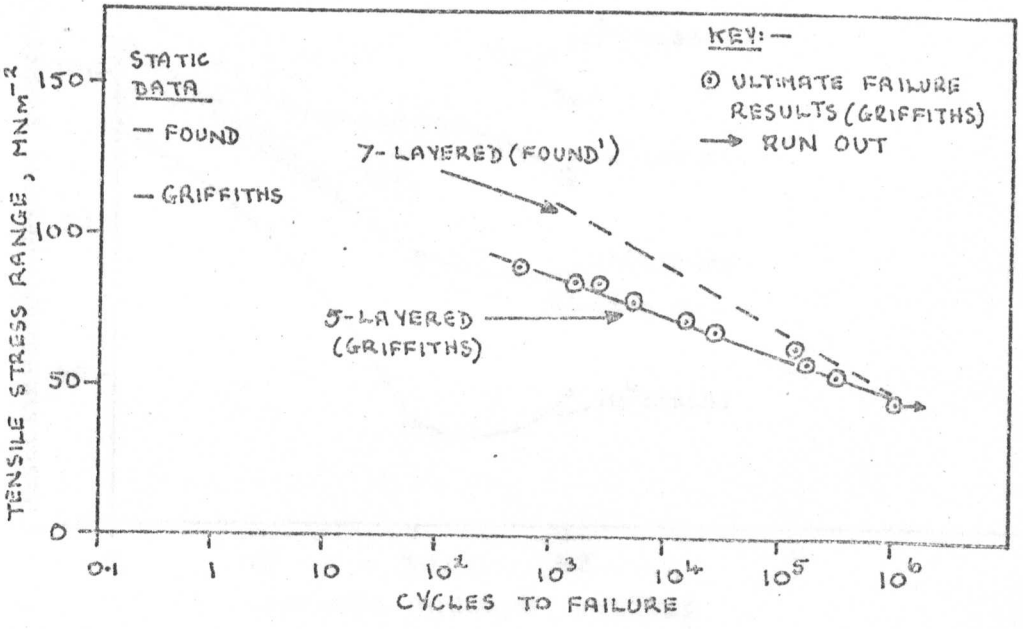

Fig. 81 Comparison between zero-tension fatigue data from Y449 fabric reinforced laminates.

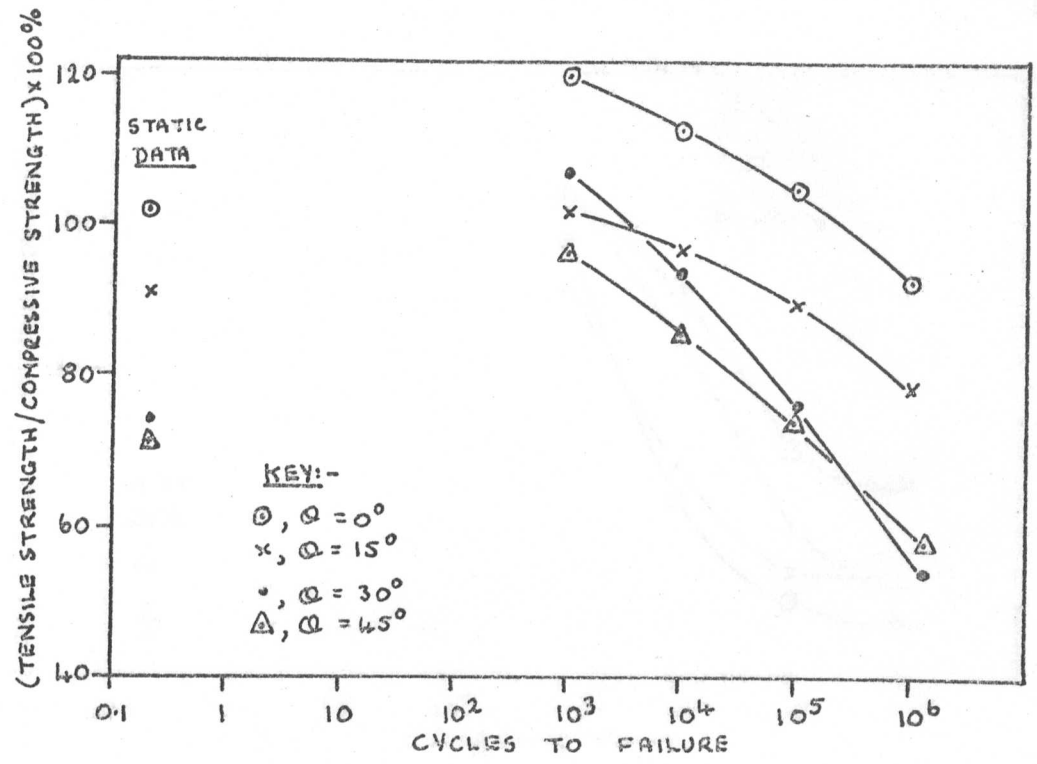

Fig. 82 The effect of off-axis angle on the ratio of uniaxial tensile to compressive fatigue strength of 7-layered Y449 fabric reinforced laminates.

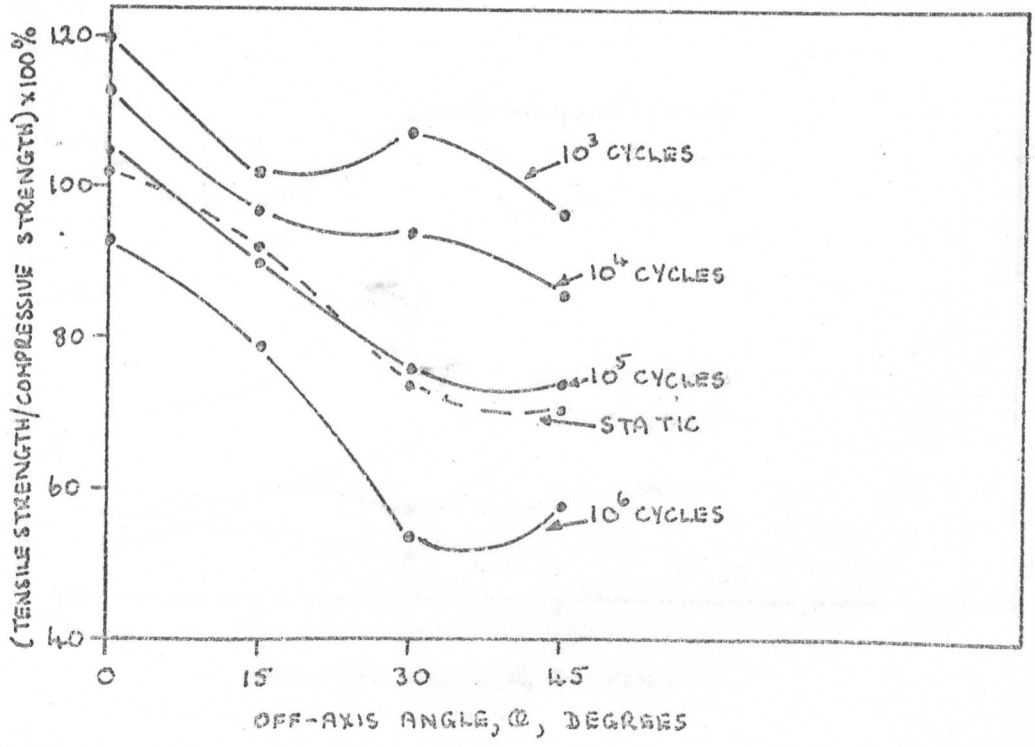

Fig. 83 The effect of off-axis angle on the ratio of uniaxial tensile to compressive fatigue strength of 7-layered Y449 fabric reinforced laminates.

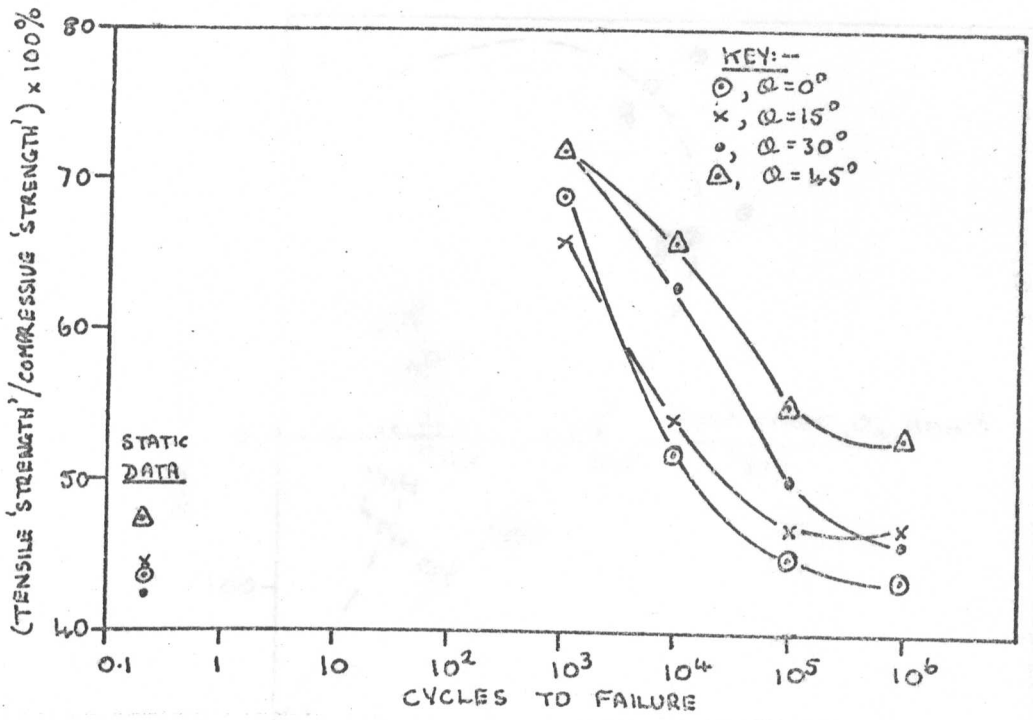

Fig. 84 The effect of off-axis angle on the ratio of uniaxial tensile to compressive damage fatigue strength of 7-layered Y449 fabric reinforced laminates.

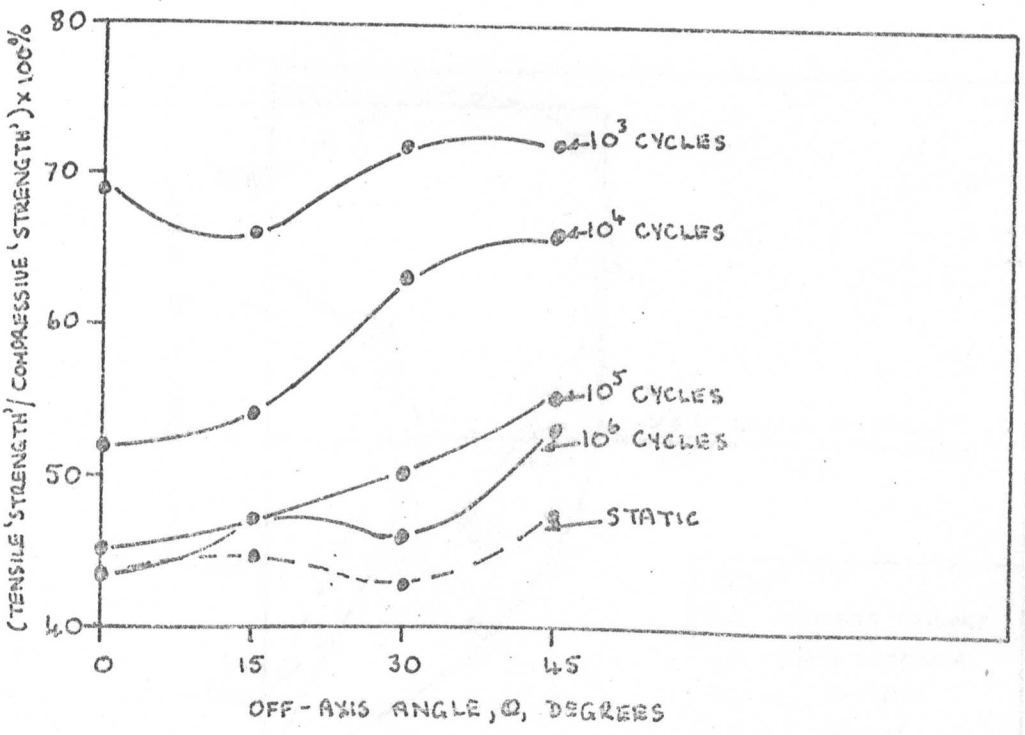

Fig. 85 The effect of off-axis angle on the ratio of uniaxial tensile to compressive damage fatigue strength of 7-layered Y449 fabric reinforced laminates.

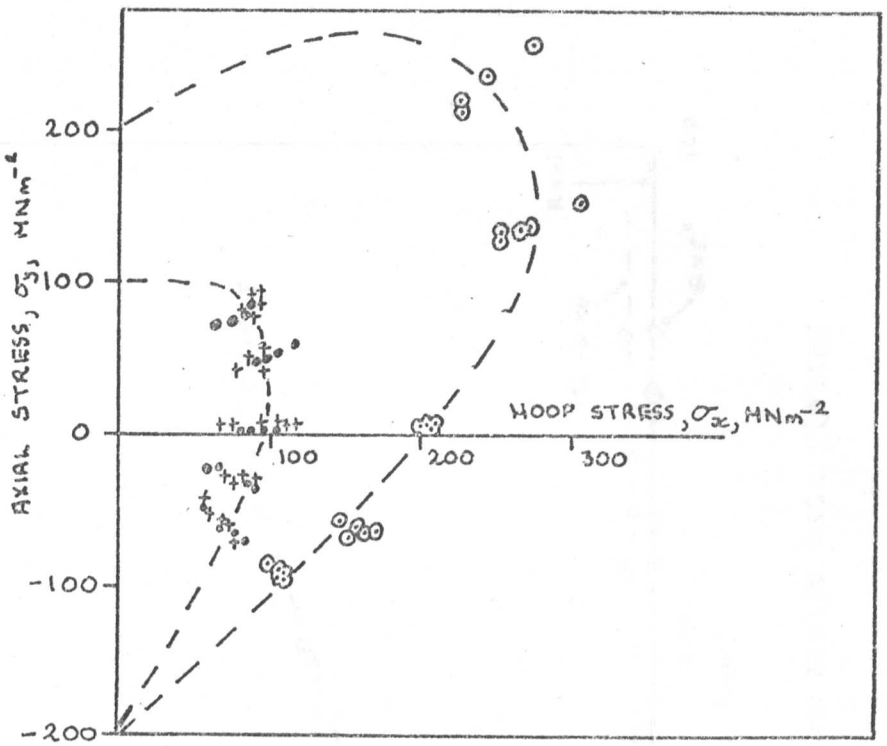

Fig. 86 45^0 off-axis biaxial stress static test data from Y449 fabric reinforced cylinders plotted in terms of principal stresses.

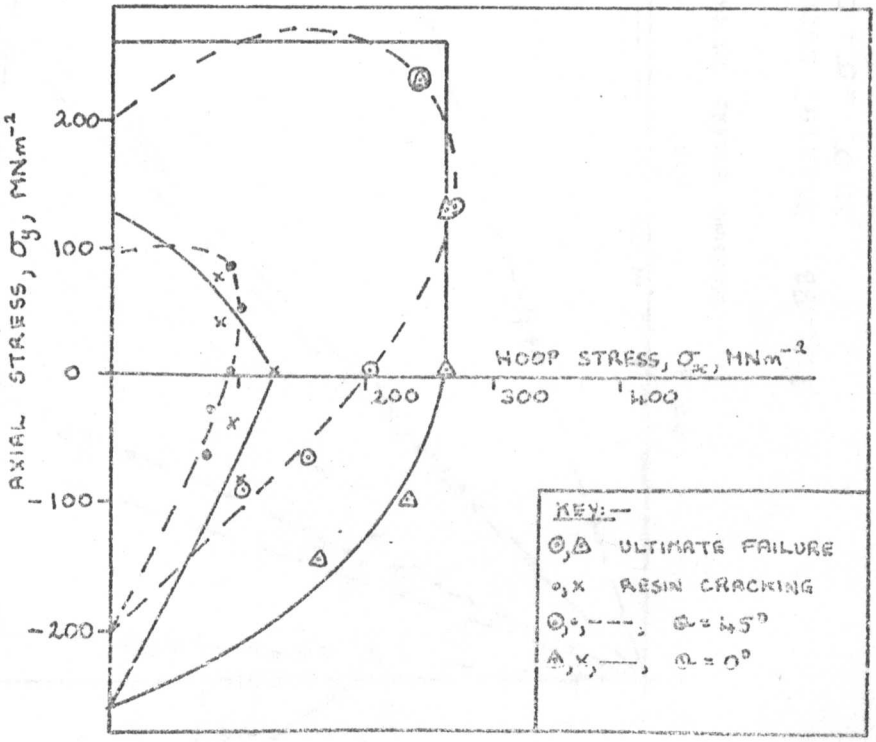

Fig. 87 Comparison between 0^0 and 45^0 off-axis biaxial stress static data from Y449 fabric reinforced cylinders.

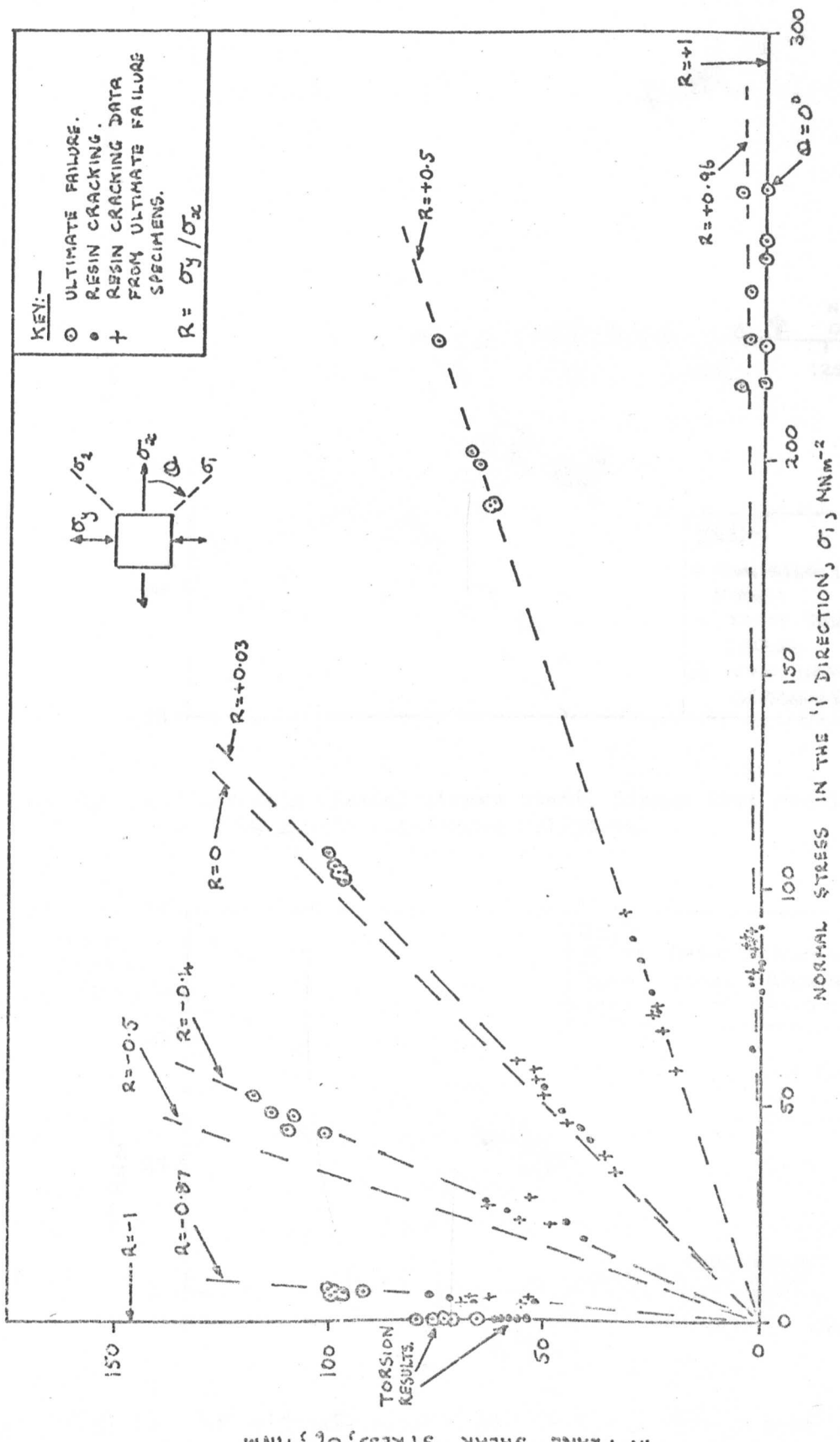

Fig. 88 Biaxial stress 45° off-axis static data plotted in $\sigma_1 = \sigma_2$, σ_6 plane.

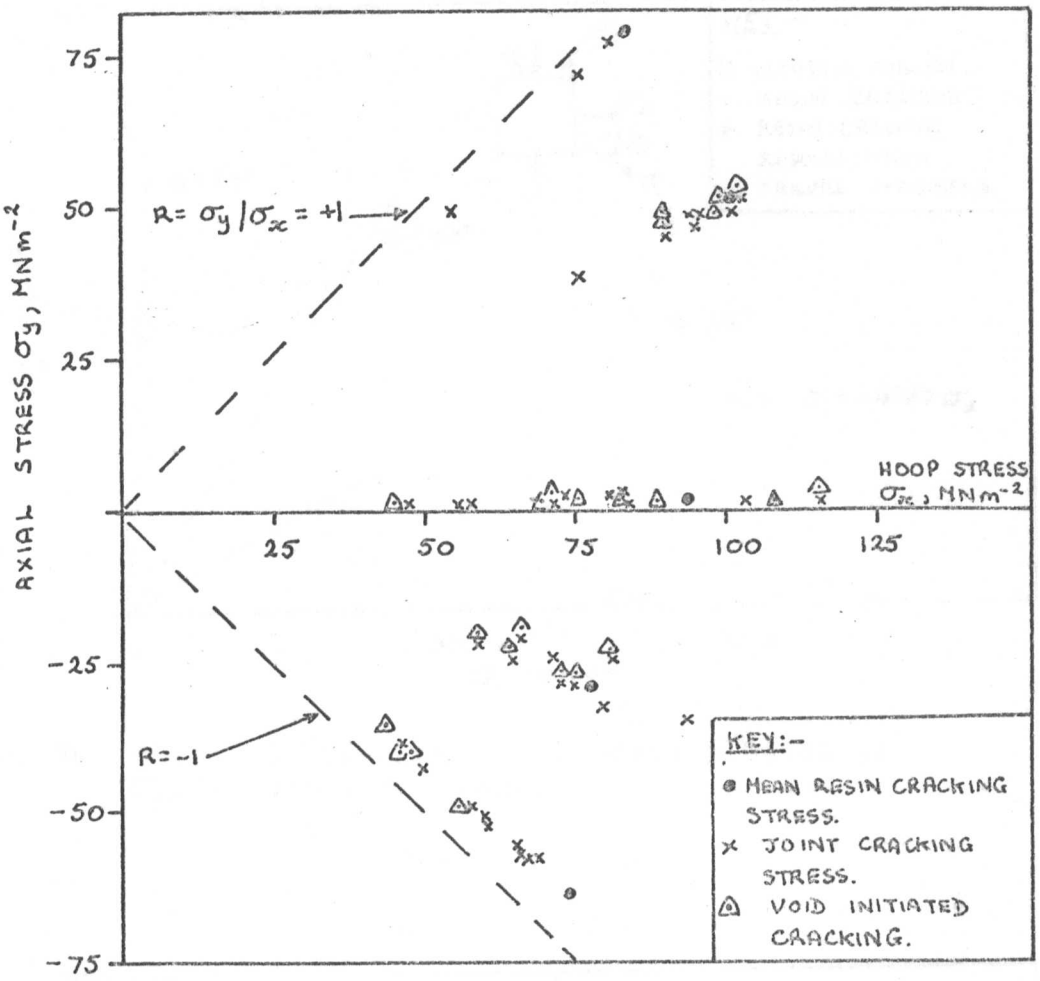

Fig. 89 45^0 off-axis biaxial stress static damage test results from Y449 fabric reinforced cylinders.

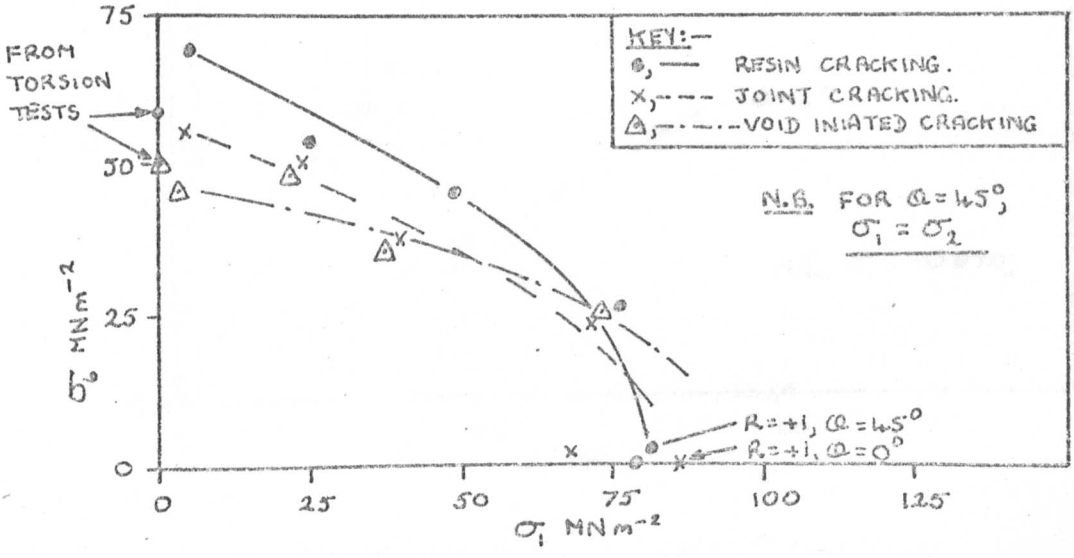

Fig. 90 45^0 off-axis biaxial stress static damage test results from Y449 fabric reinforced cylinders.

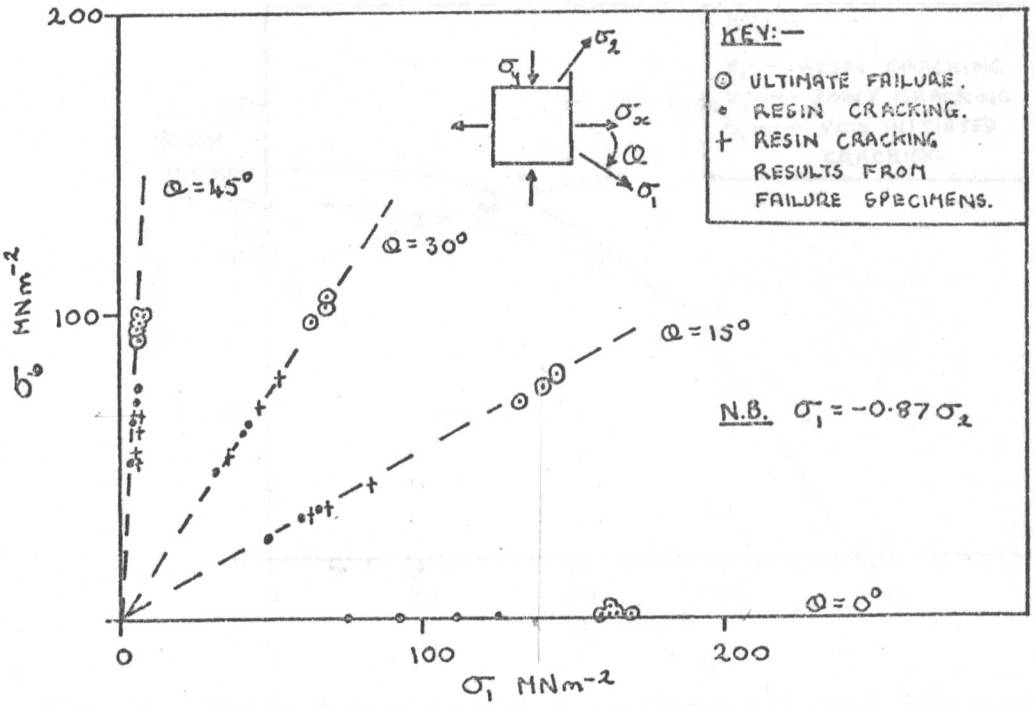

Fig. 91 R = -1.0 off-axis static data plotted in $\sigma_2 = -0.87\sigma_1$, σ_6 plane.

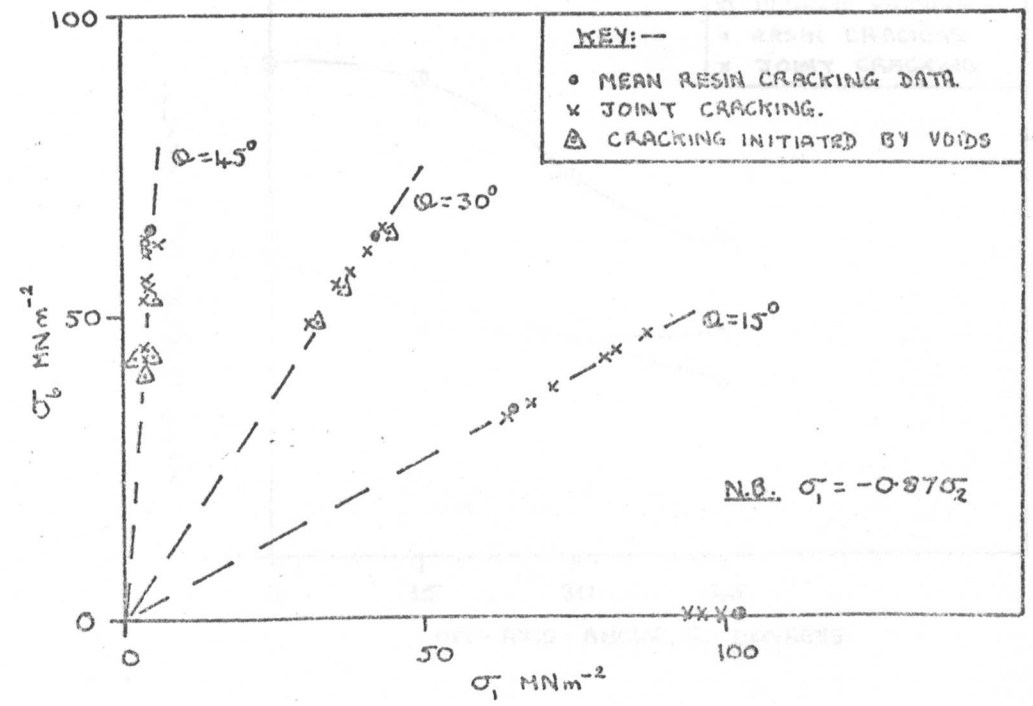

Fig. 92 Static damage data at R = -1(nominal) from Y449 fabric reinforced cylinders.

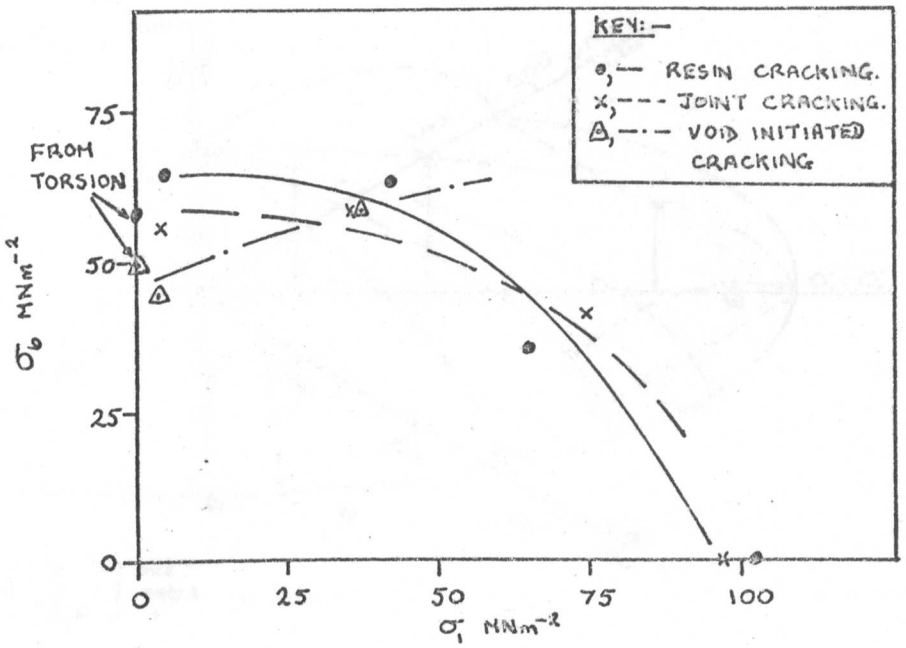

Fig. 93 Static damage data at R = -1(nominal) from Y449 fabric reinforced cylinders.

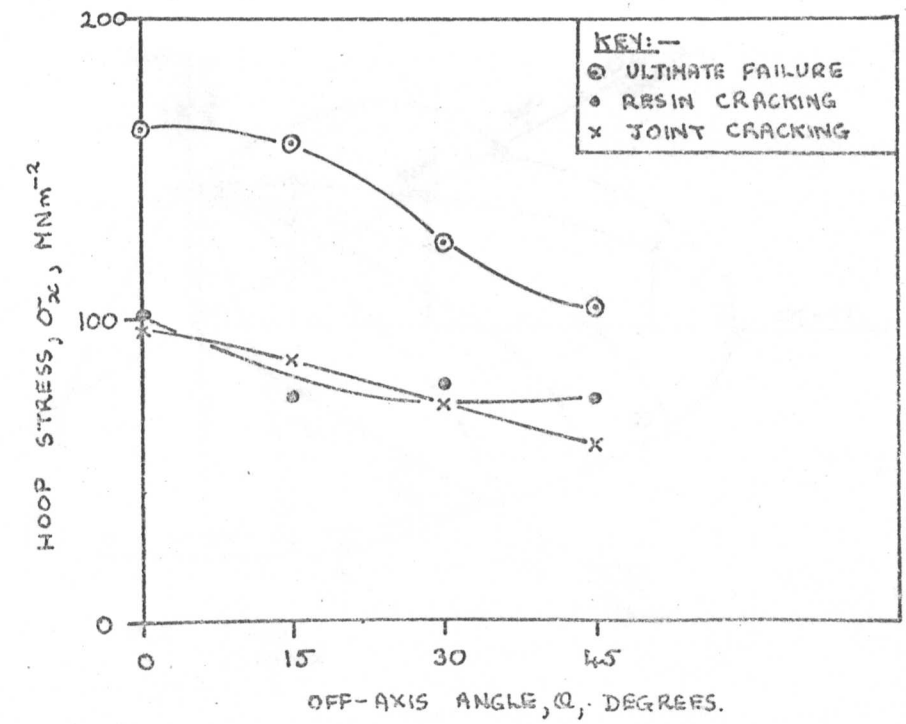

Fig. 94 Variation in hoop strength with off-axis angle at R = -1(nominal) for Y449 fabric reinforced cylinders.

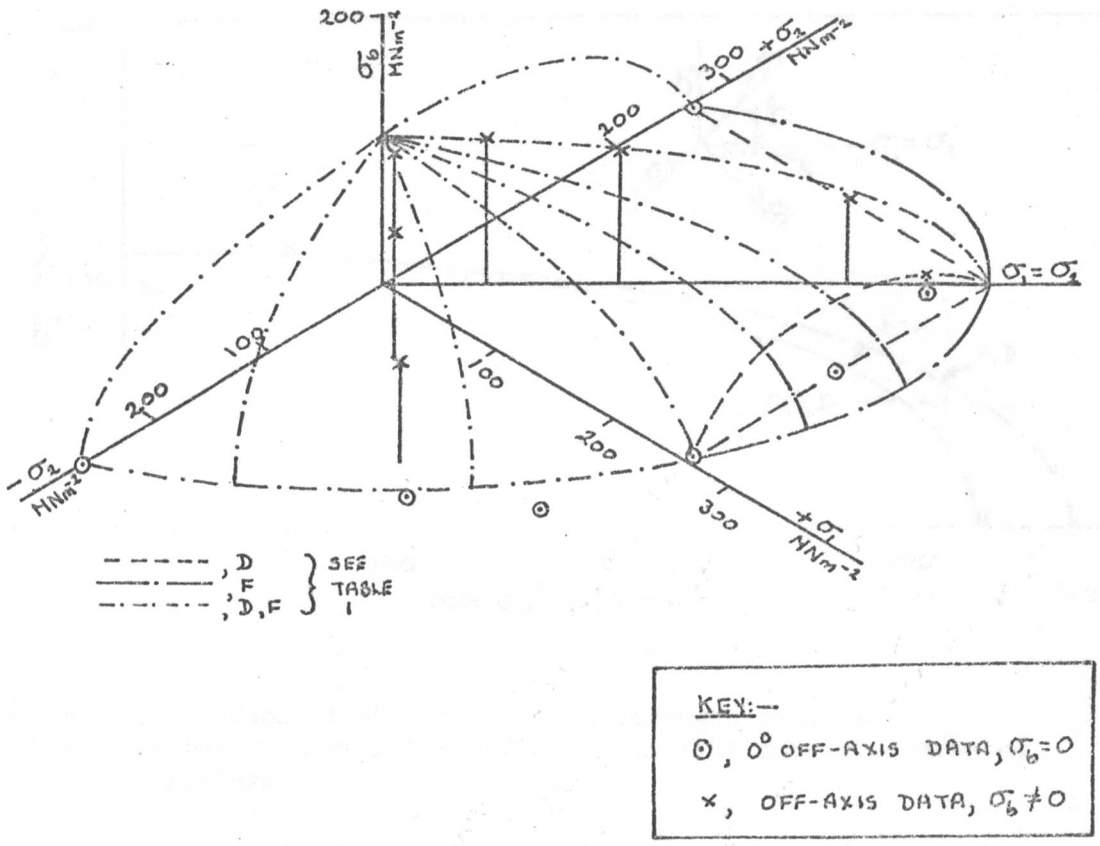

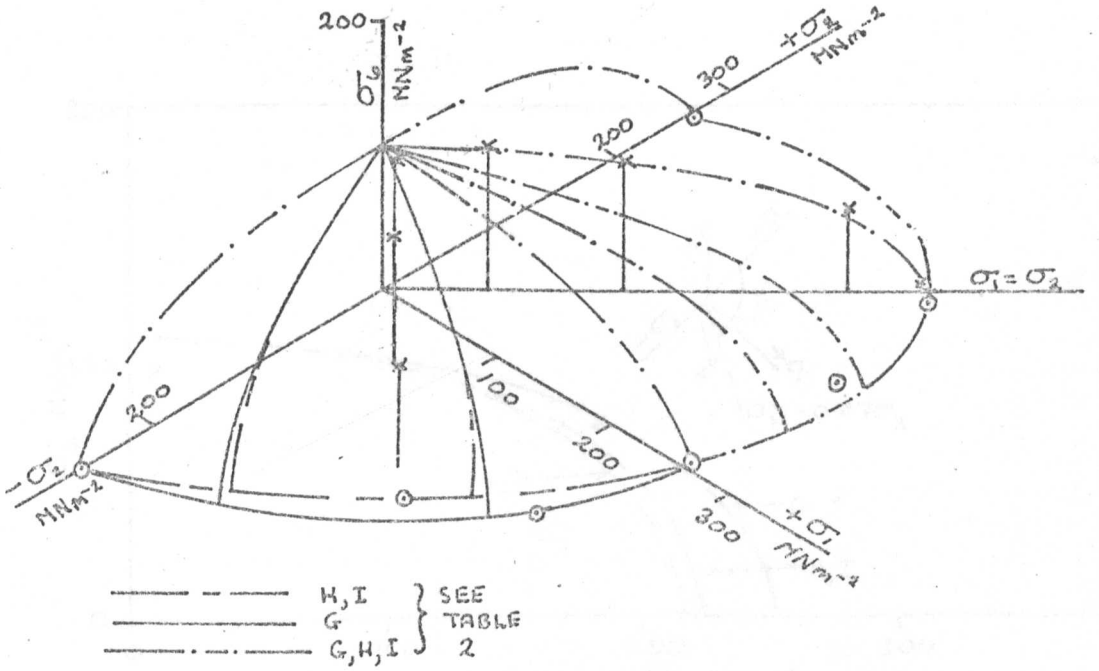

Fig. 95 Comparison of static ultimate strength data with failure theories for Y449 fabric reinforced cylinders.

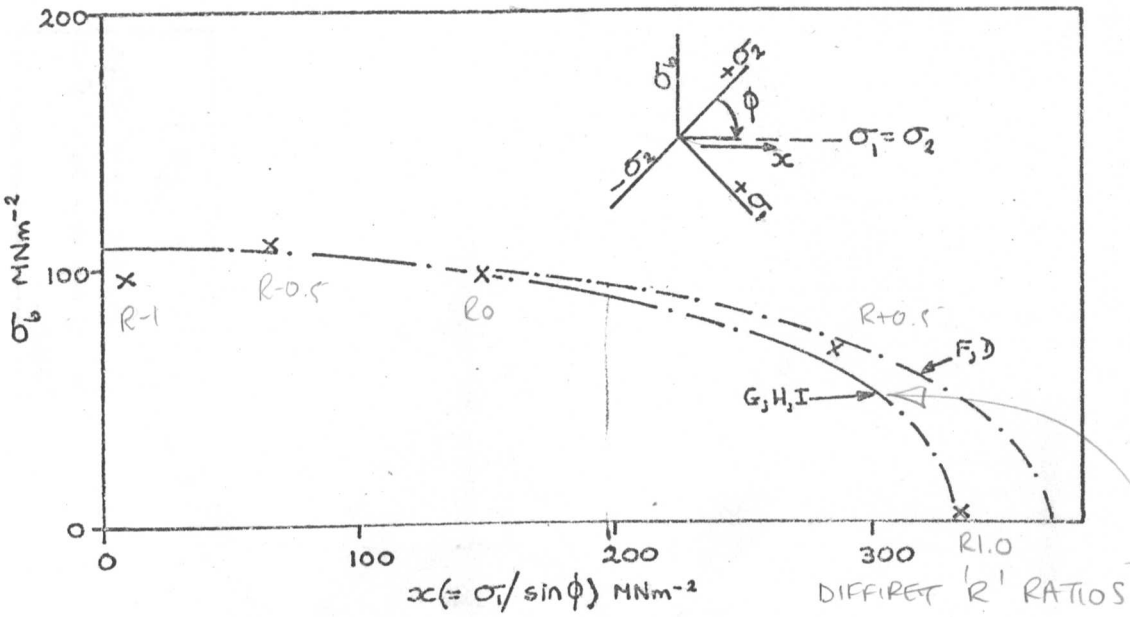

Fig. 96 Comparison of static ultimate strength data with failure theories for 45^0 off-axis Y449 fabric reinforced cylinders.

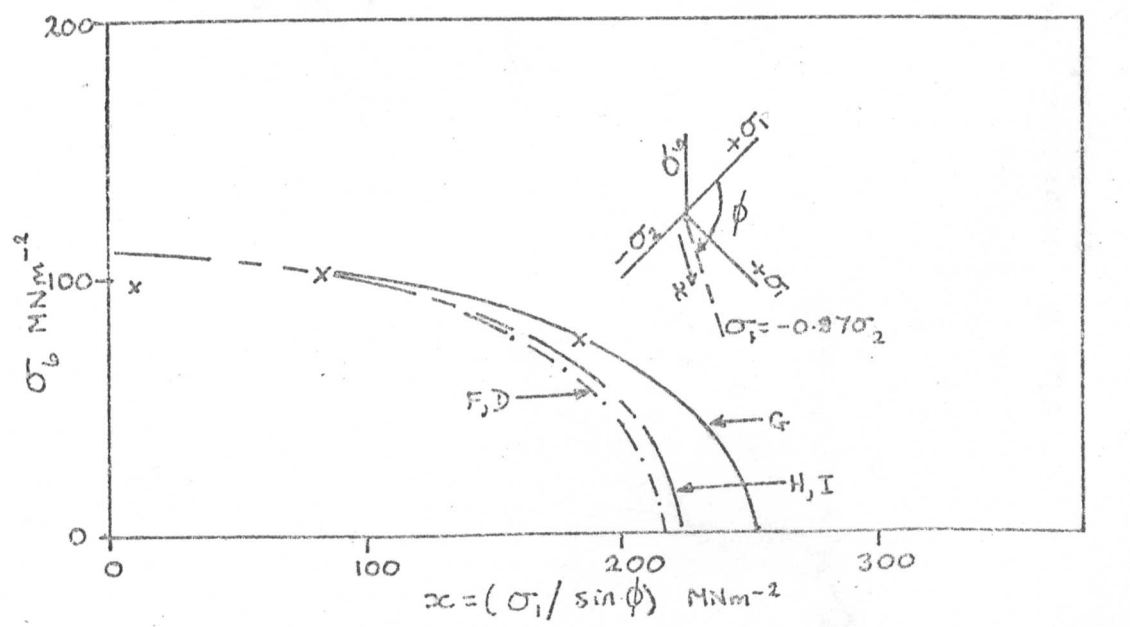

Fig. 97 Comparison of static ultimate strength data at R = -1 (nominal) with failure theories for Y449 fabric reinforced cylinders.

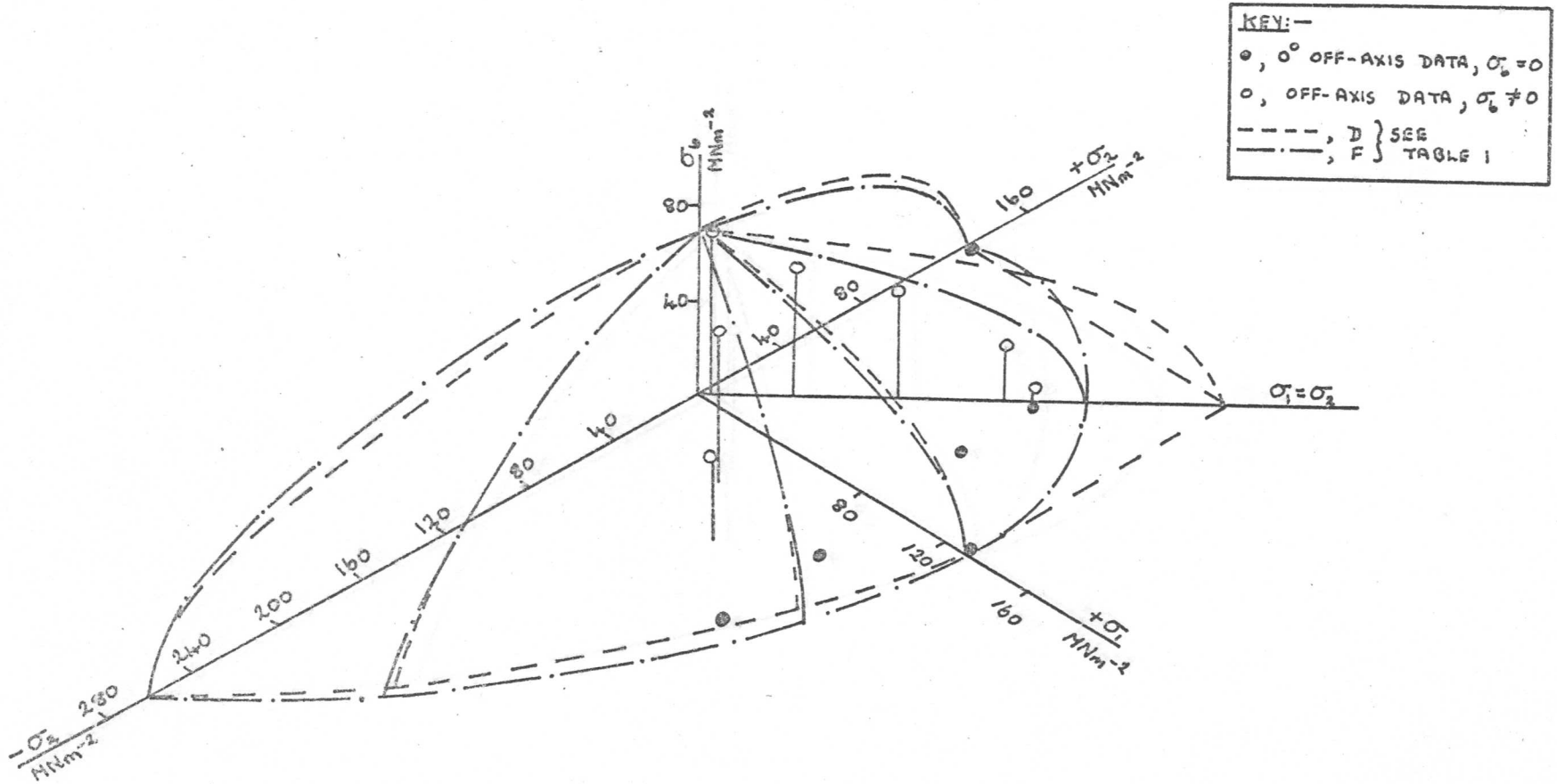

Fig. 98 Comparison of resin cracking data with failure theories for Y449 fabric reinforced cylinders.

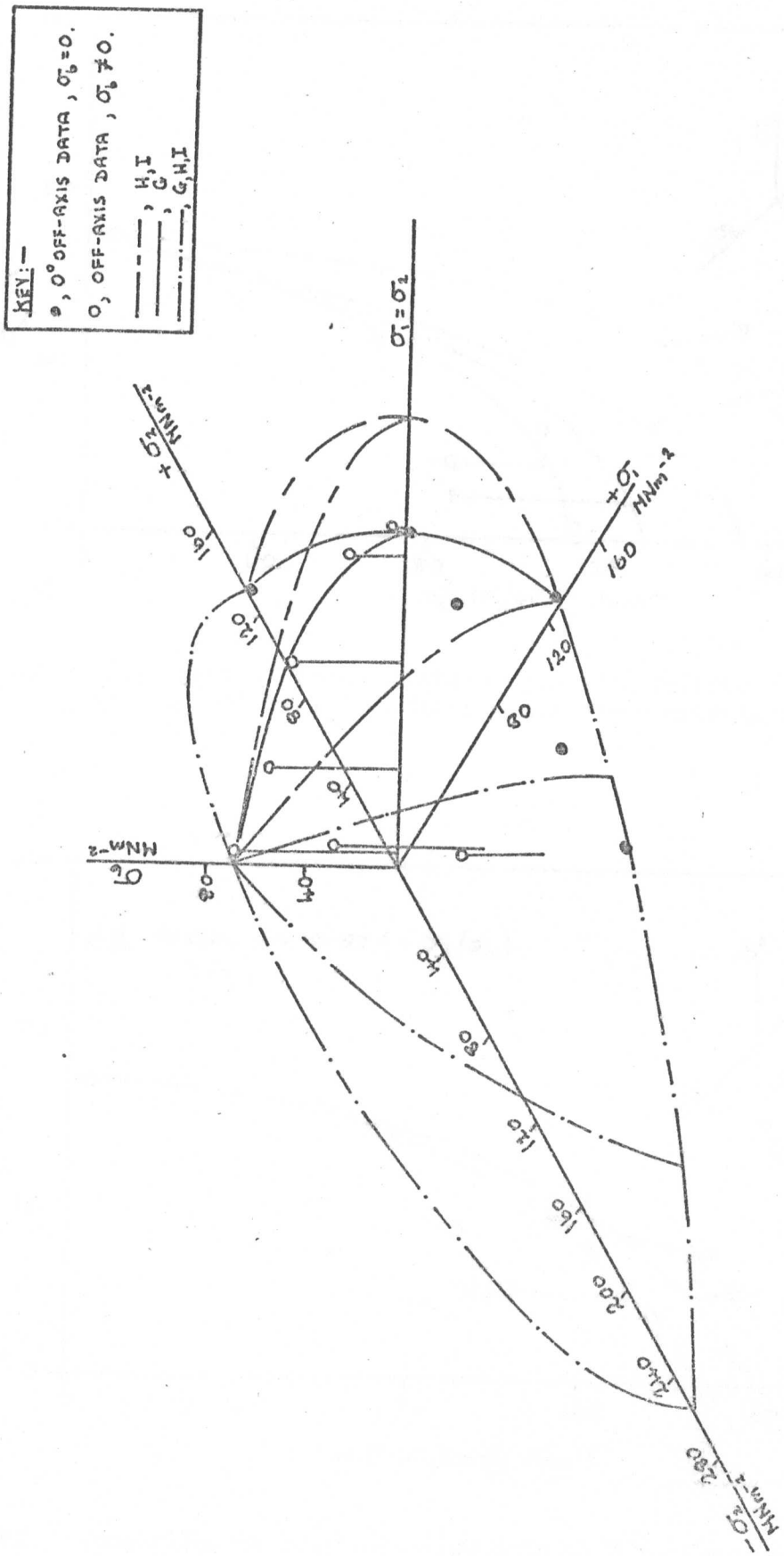

Fig. 99 Comparison of resin cracking data with failure theories for Y449 fabric reinforced cylinders.

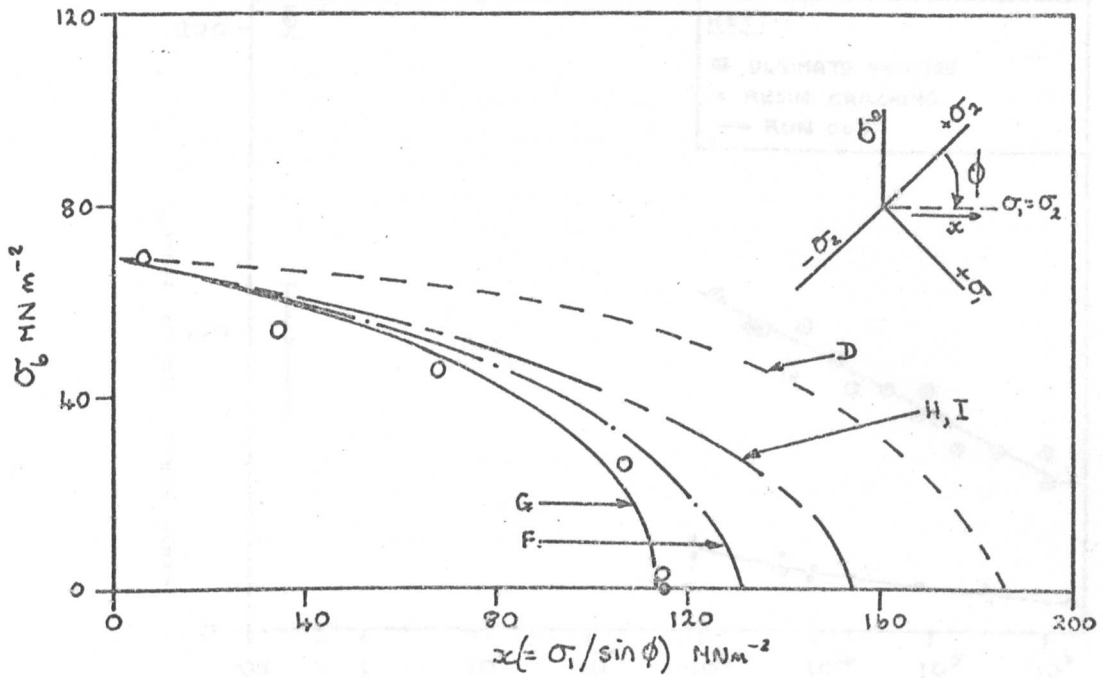

Fig. 100 Comparison of resin cracking data with failure theories for 45^0 off-axis Y449 fabric reinforced cylinders.

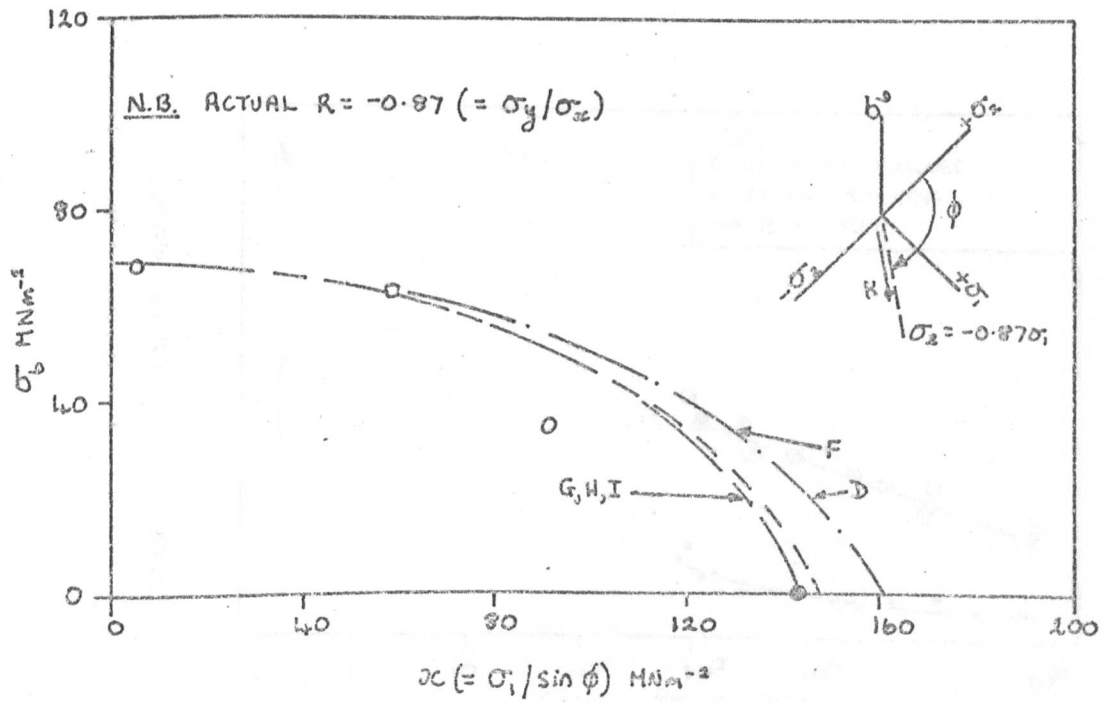

Fig. 101 Comparison of resin cracking data at R = -1(nominal) with failure theories for Y449 fabric reinforced cylinders.

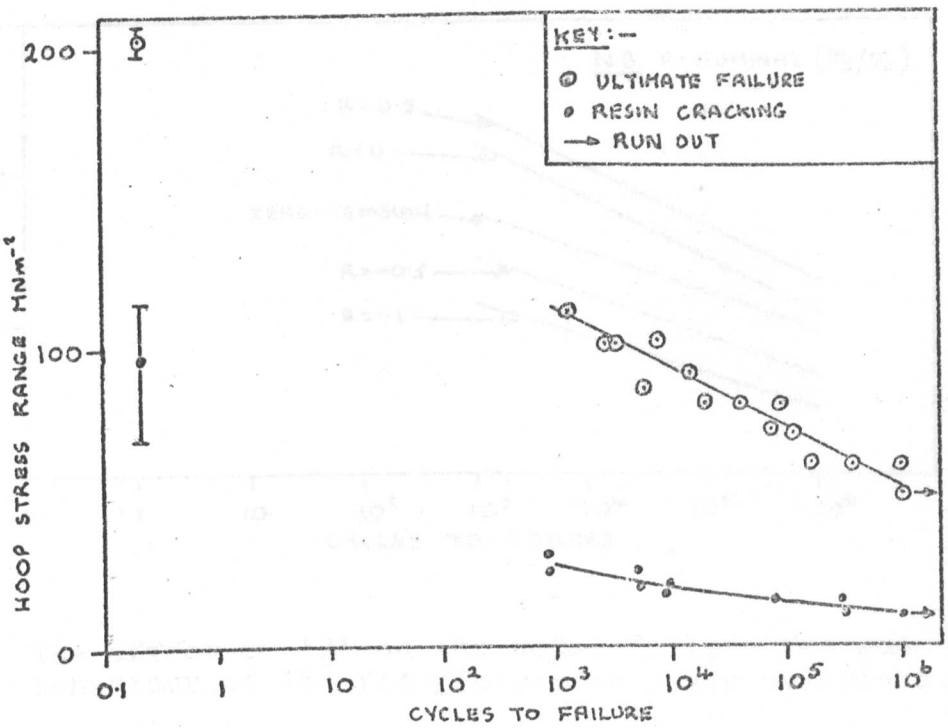

Fig. 102 R=0 fatigue data for 45° Y449/Polyester resin cylinders.

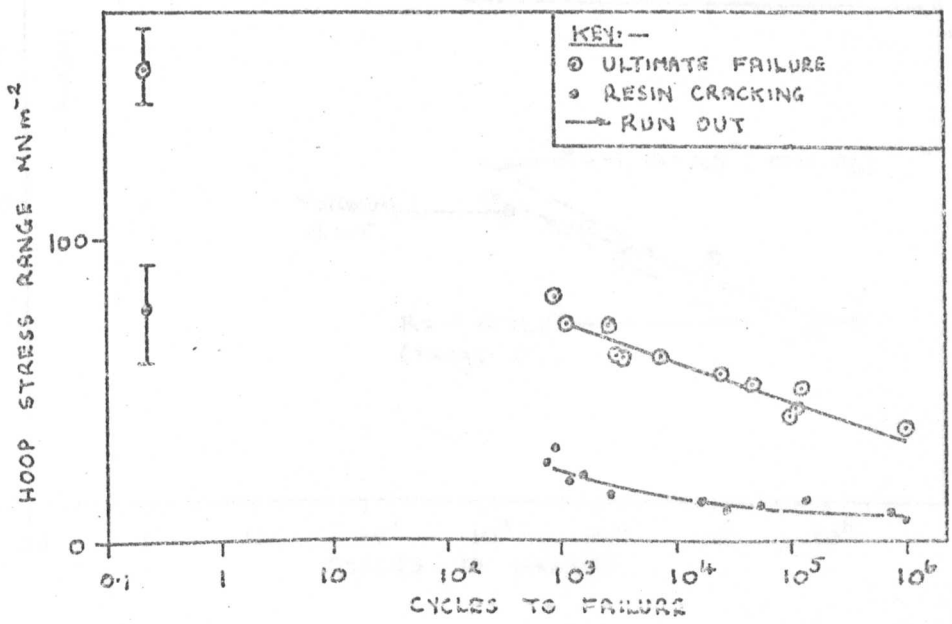

Fig. 103 R= -0.5 fatigue results from 45° Y449/Polyester resin cylinders.

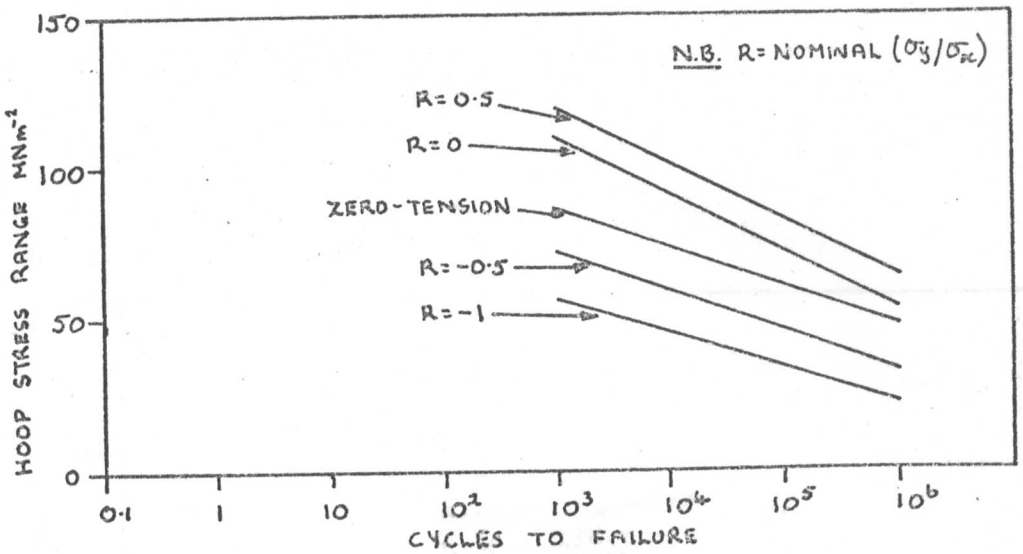

Fig. 104 The effect of 'R' on the total failure fatigue behaviour of 45° Y449/Polyester resin cylinders.

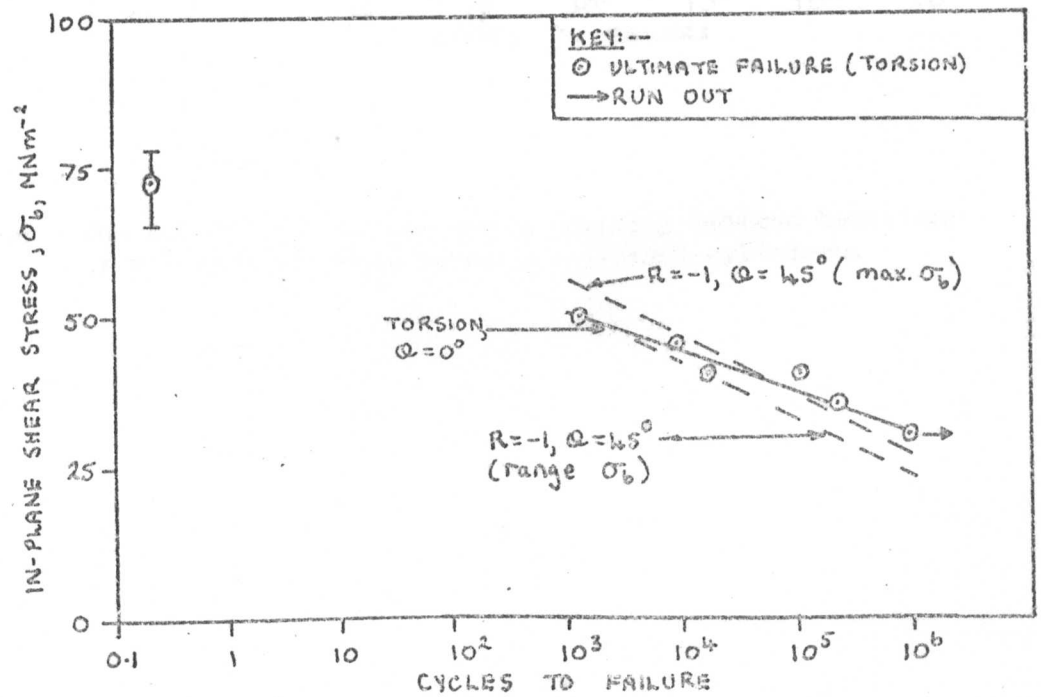

Fig. 105 In-plane shear fatigue results from Y449 fabric reinforced cylinders.

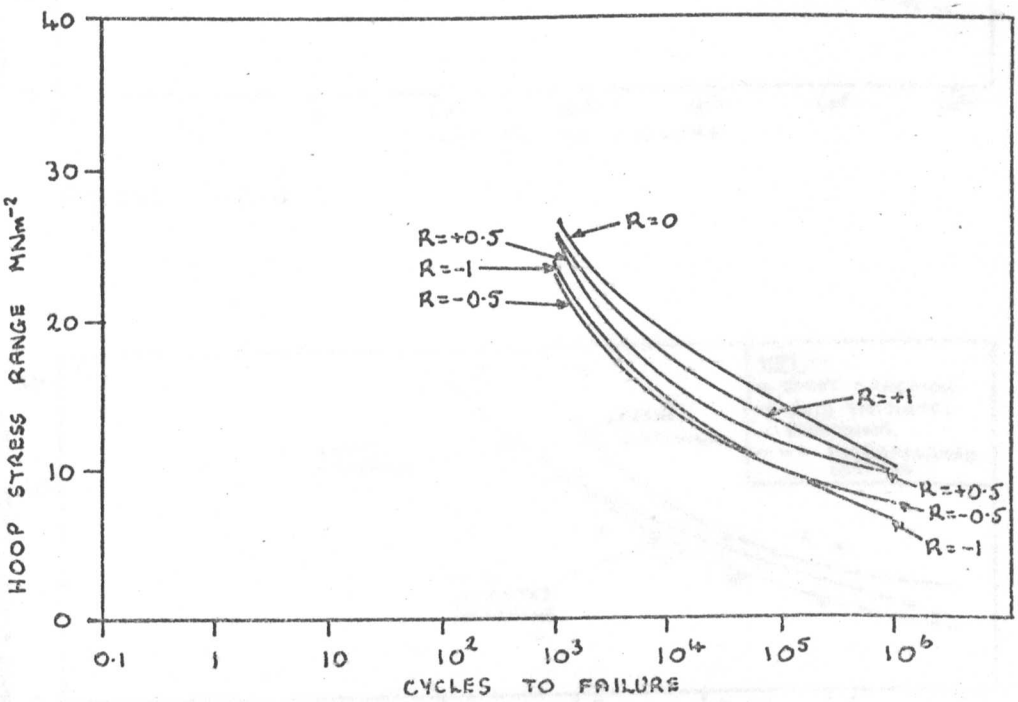

Fig. 106 The effect of R on the resin cracking fatigue behaviour of 45^0 off-axis Y449 fabric reinforced cylinders.

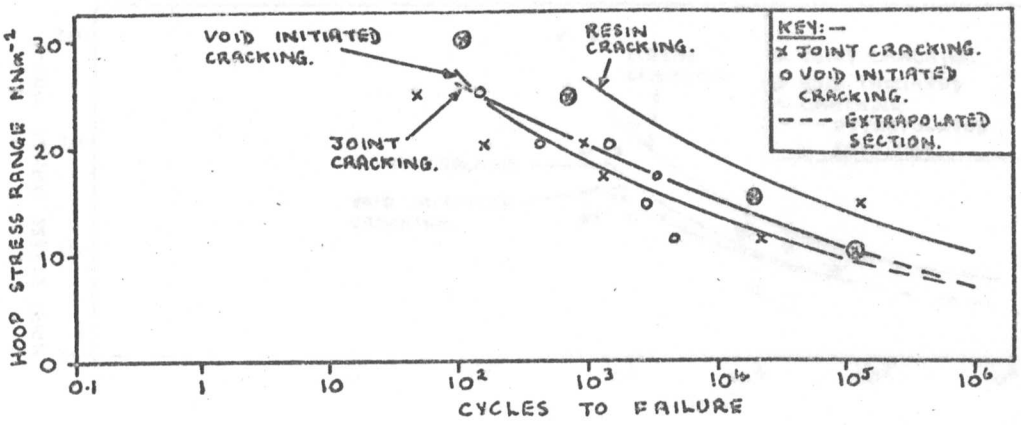

FIG. 107 R=0

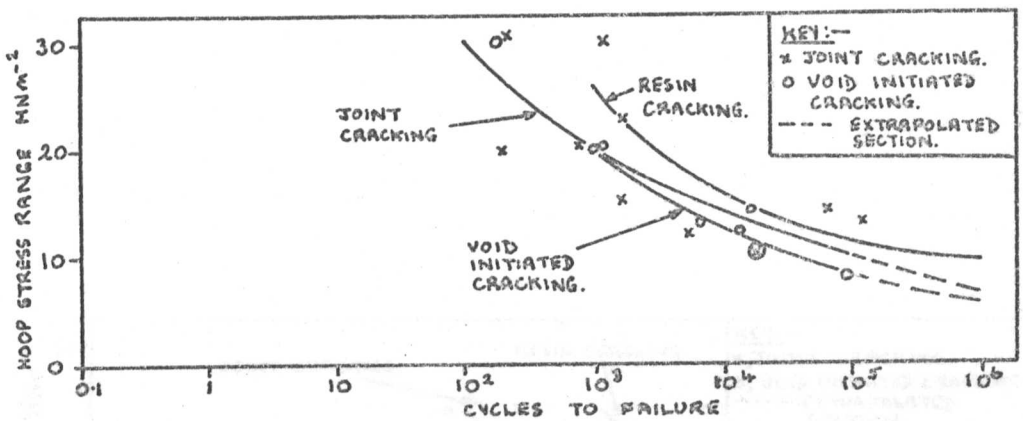

FIG. 108 R= +0·5

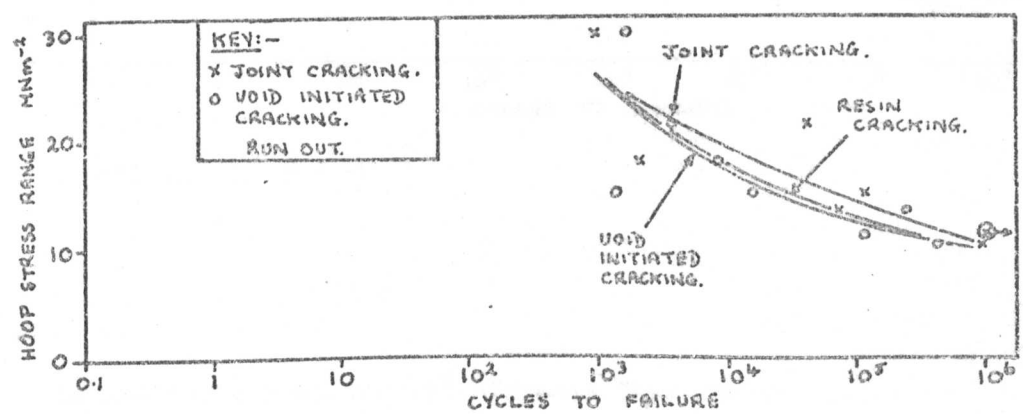

FIG. 109 R= +1

Damage S-N curves for 45^0 off-axis Y449 fabric reinforced cylinders.

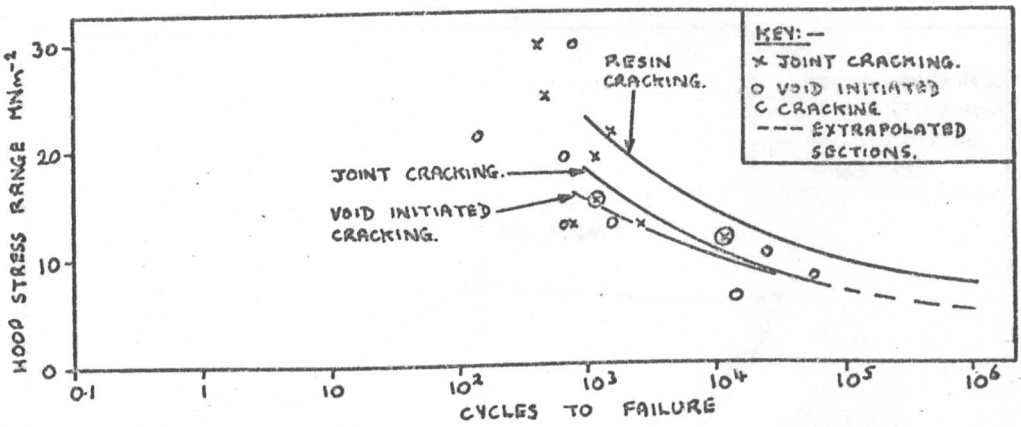

FIG. 110 R = -0·5

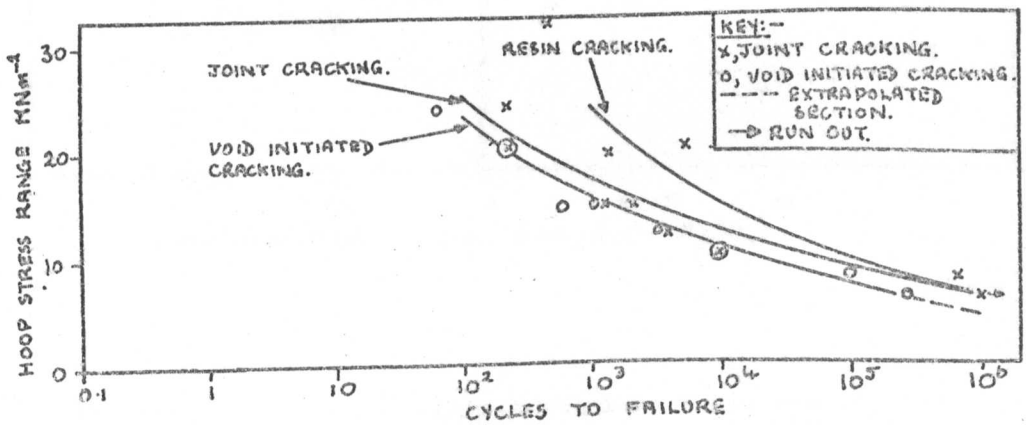

FIG. 111 R = -1

Damage S-N curves for 45^0 off-axis Y449 fabric reinforced cylinders.

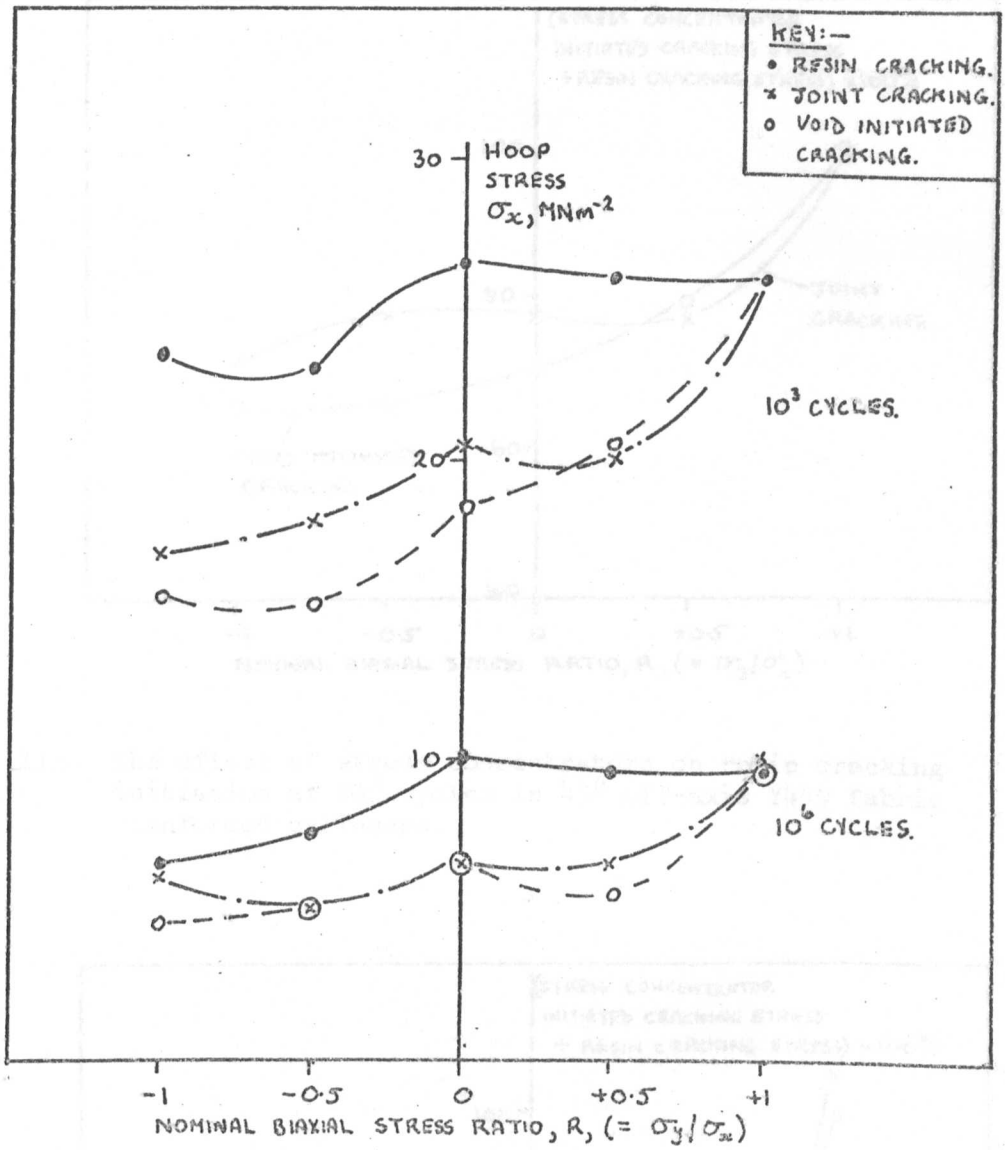

Fig. 112 The effect of stress concentrators on resin cracking initiation in 45^0 off-axis Y449 fabric reinforced cylinders.

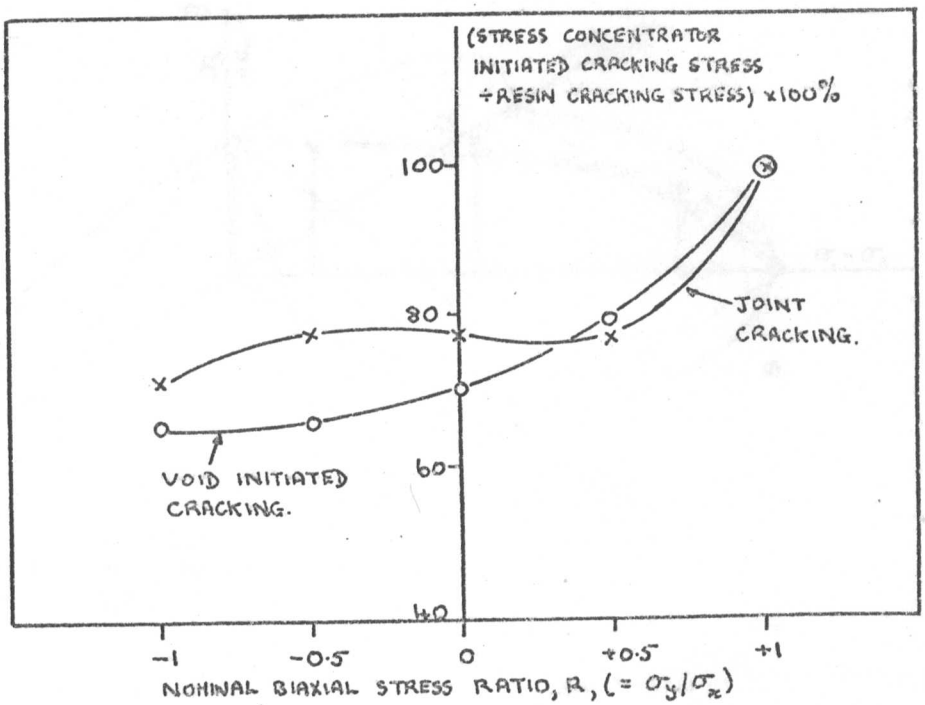

Fig. 113 The effect of stress concentrators on resin cracking initiation at 10^3 cycles in 45^0 off-axis Y449 fabric reinforced cylinders.

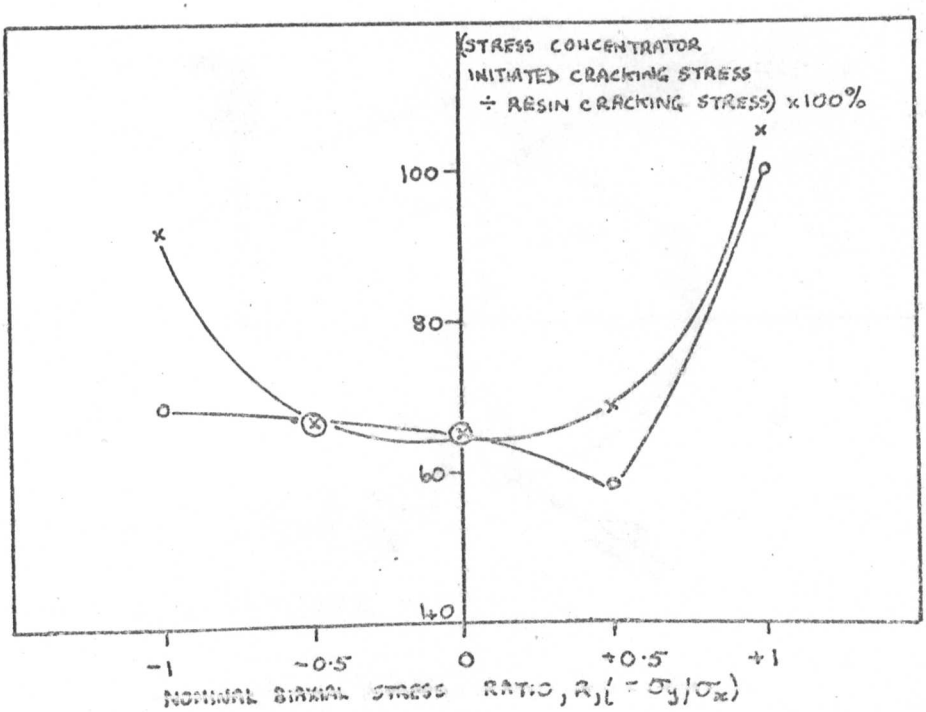

Fig. 114 As Fig. 113 but at 10^6 cycles.

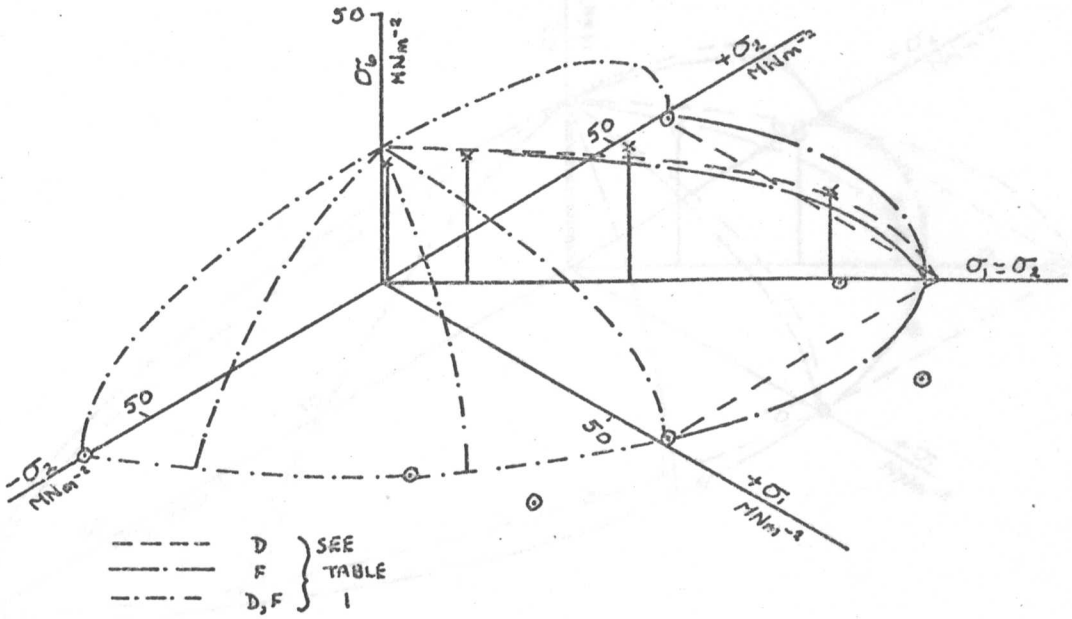

KEY:-

⊙, 0° OFF-AXIS DATA, $\sigma_6 = 0$.

×, OFF-AXIS DATA, $\sigma_6 \neq 0$.

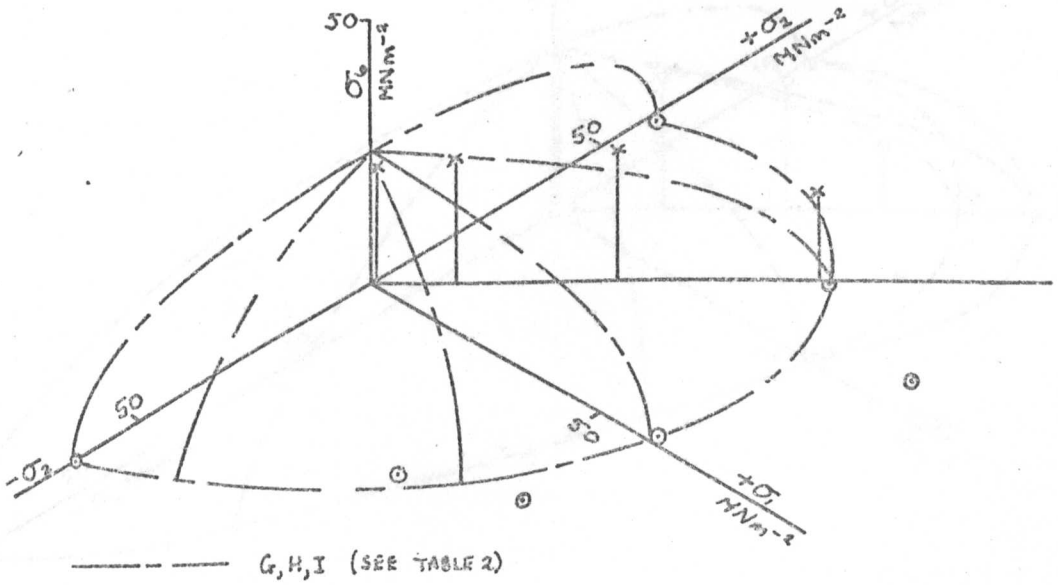

Fig. 115 Comparison between ultimate strength data at 10^6 cycles and failure theories for Y449 fabric reinforced cylinders.

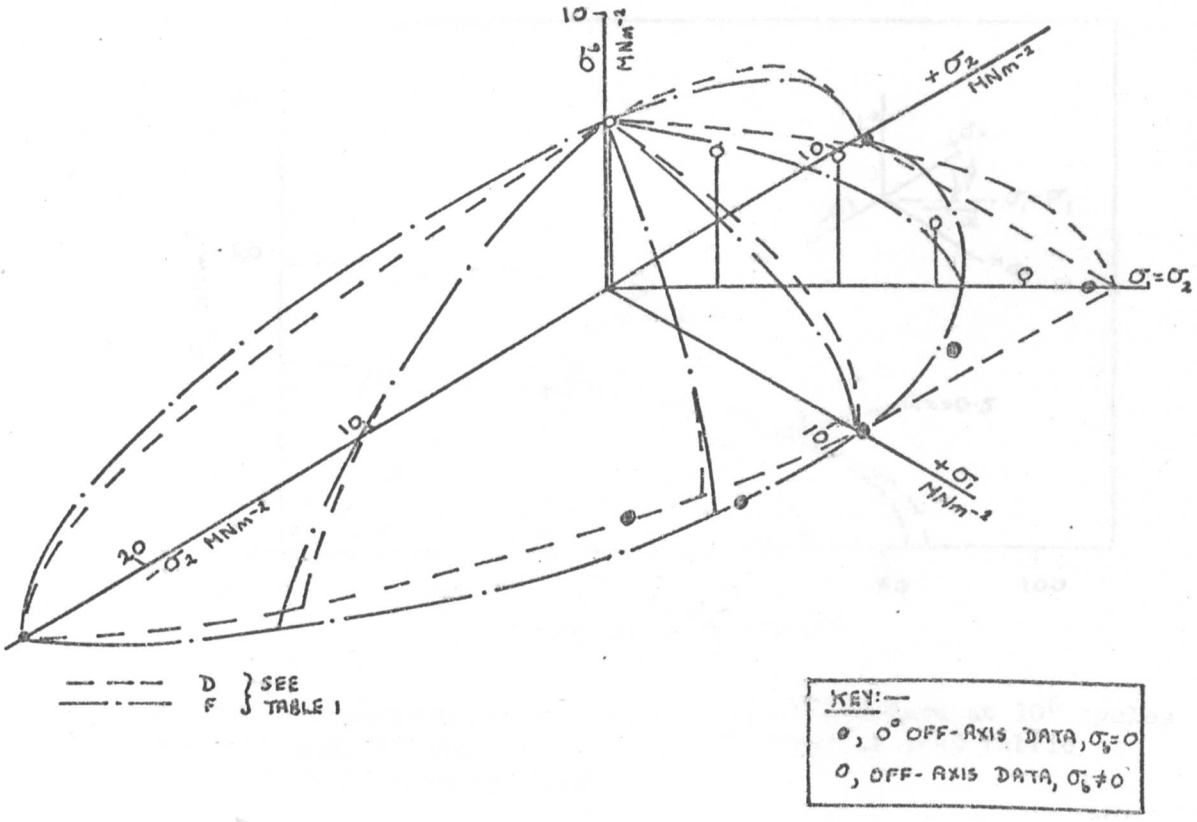

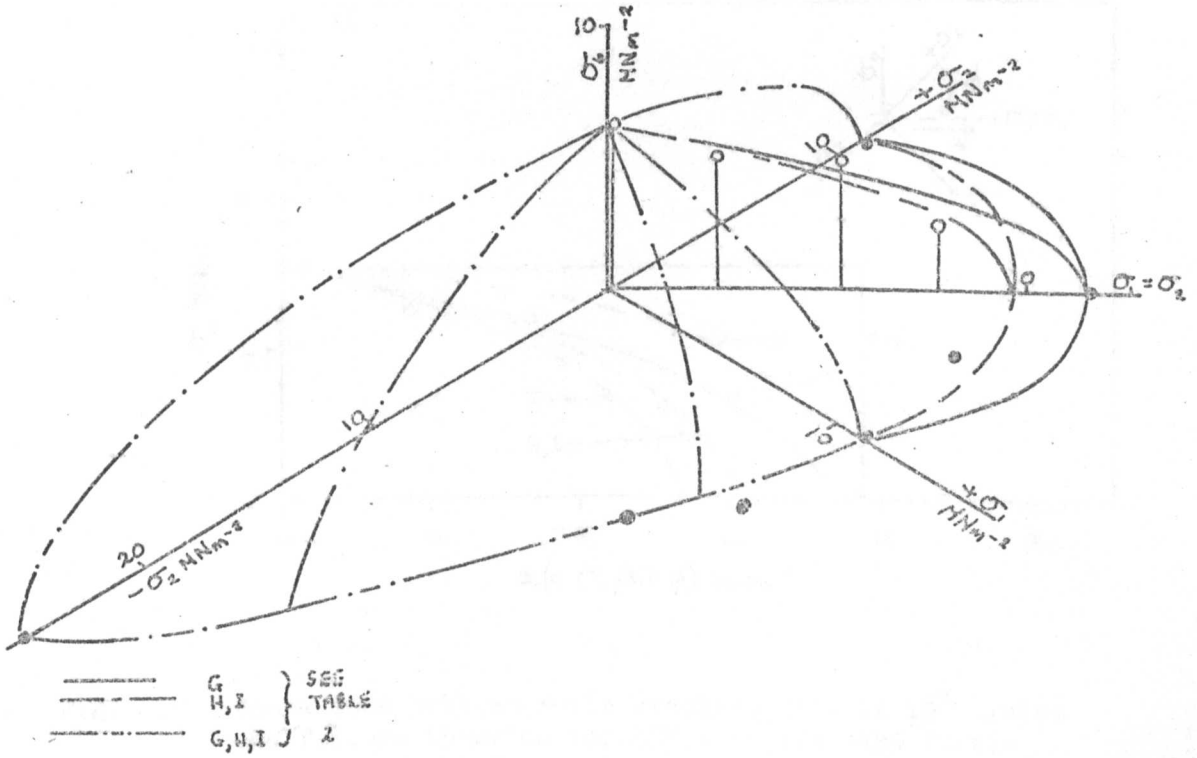

Fig. 116 Comparison between resin cracking data at 10^6 cycles and failure theories for Y449 fabric reinforced cylinders.

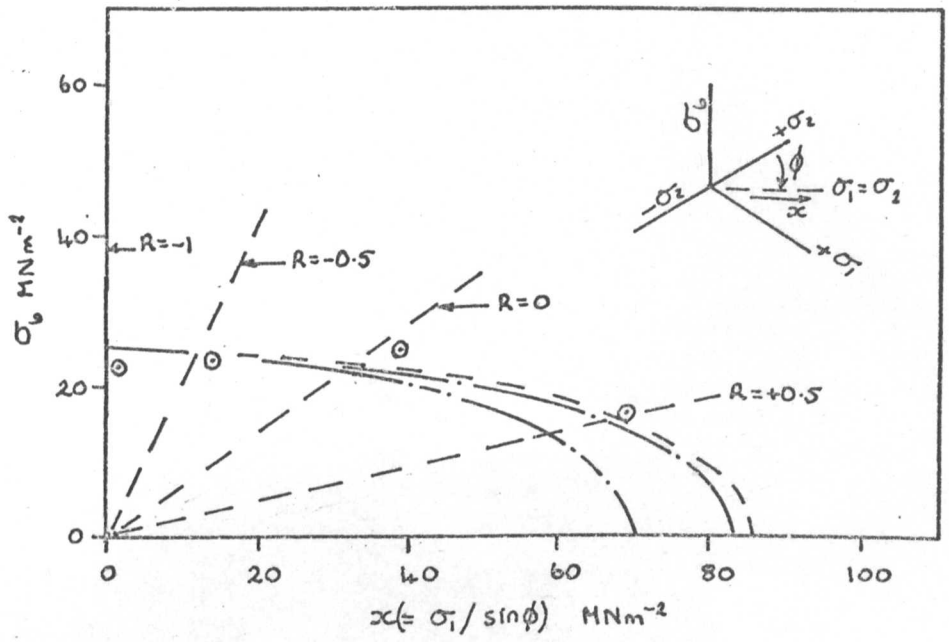

Fig. 117 Comparison between ultimate strength data at 10^6 cycles and failure theories for 45^0 off-axis Y449 fabric reinforced cylinders.

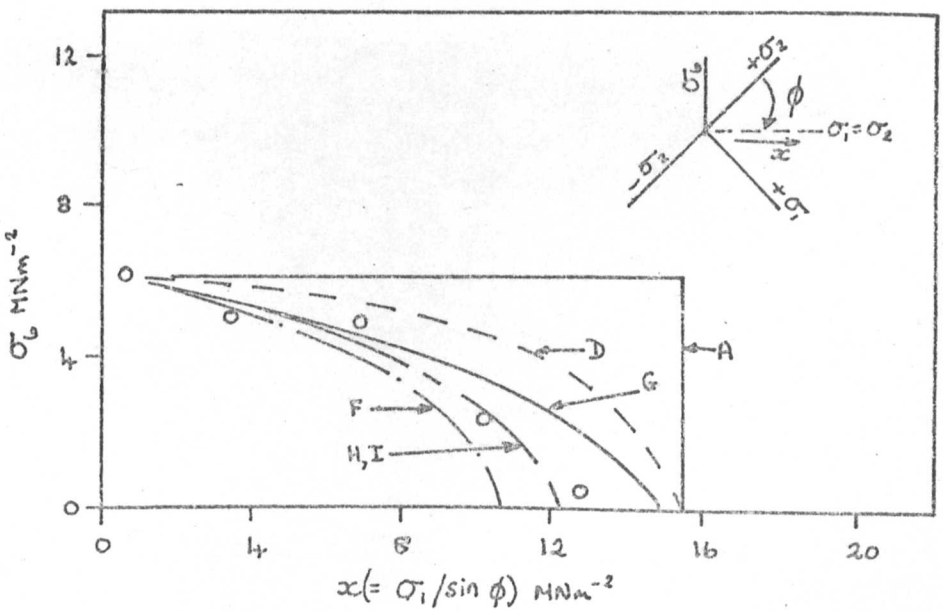

Fig. 118 Comparison between resin cracking data at 10^6 cycles and failure theories for 45^0 off-axis Y449 fabric reinforced cylinders.

FIG. 119. FATIGUE FAILURE IN A 45° OFF-AXIS Y-9 FABRIC-REINFORCED POLYESTER RESIN CYLINDER TESTED AT R = -1.

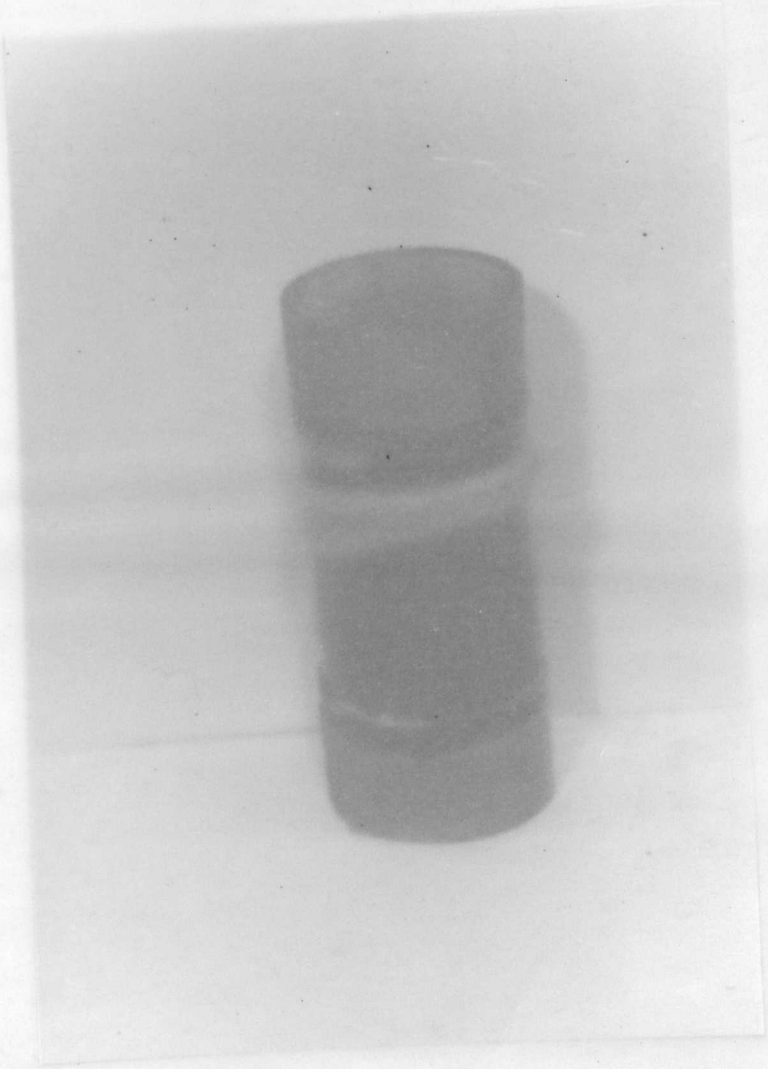

FIG. 119. FATIGUE FAILURE IN A 45° OFF-AXIS Y4-9 FABRIC-REINFORCED POLYESTER RESIN CYLINDER TESTED AT R = -1.

FIG. 120. BIAXIAL STRESS STATIC FAILURES OBSERVED IN 45° OFF-AXIS Y449 FABRIC-REINFORCED POLYESTER RESIN CYLINDERS.

FIG. 121. STATIC TORSION FAILURES OBSERVED IN Y449 FABRIC REINFORCED POLYESTER RESIN CYLINDERS.

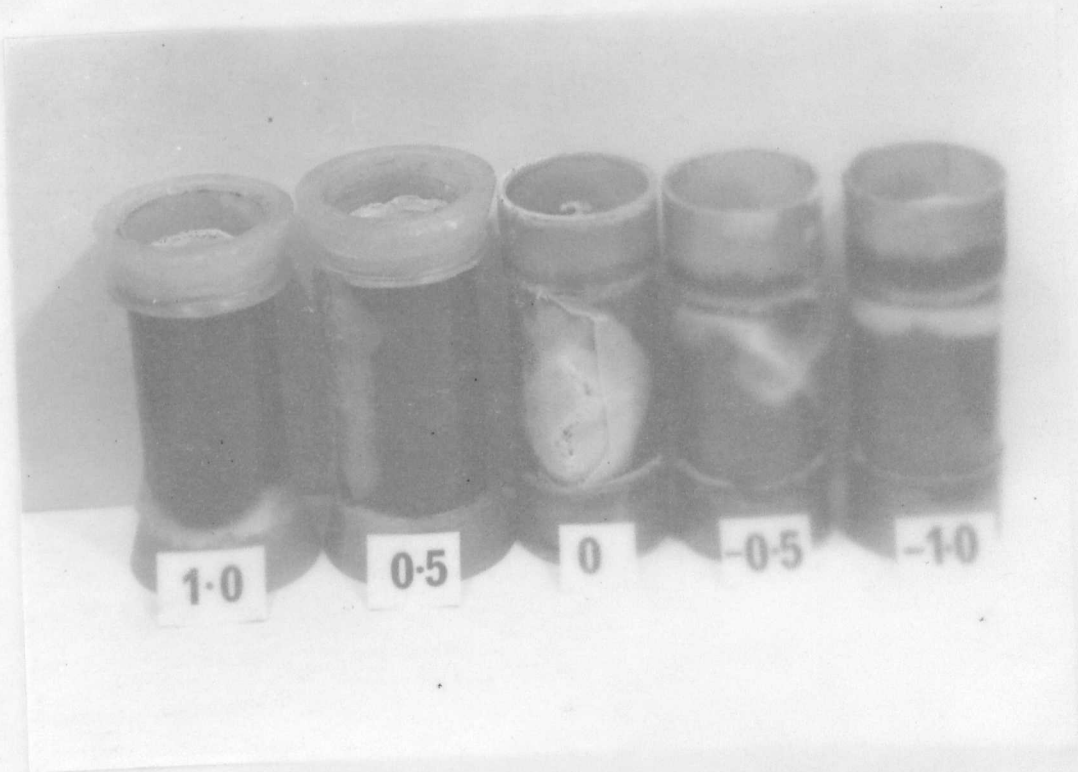

FIG. 120. BIAXIAL STRESS STATIC FAILURES OBSERVED IN 45° OFF-AXIS Y449 FABRIC-REINFORCED POLYESTER RESIN CYLINDERS.

FIG. 121. STATIC TORSION FAILURES OBSERVED IN Y449 FABRIC REINFORCED POLYESTER RESIN CYLINDERS.

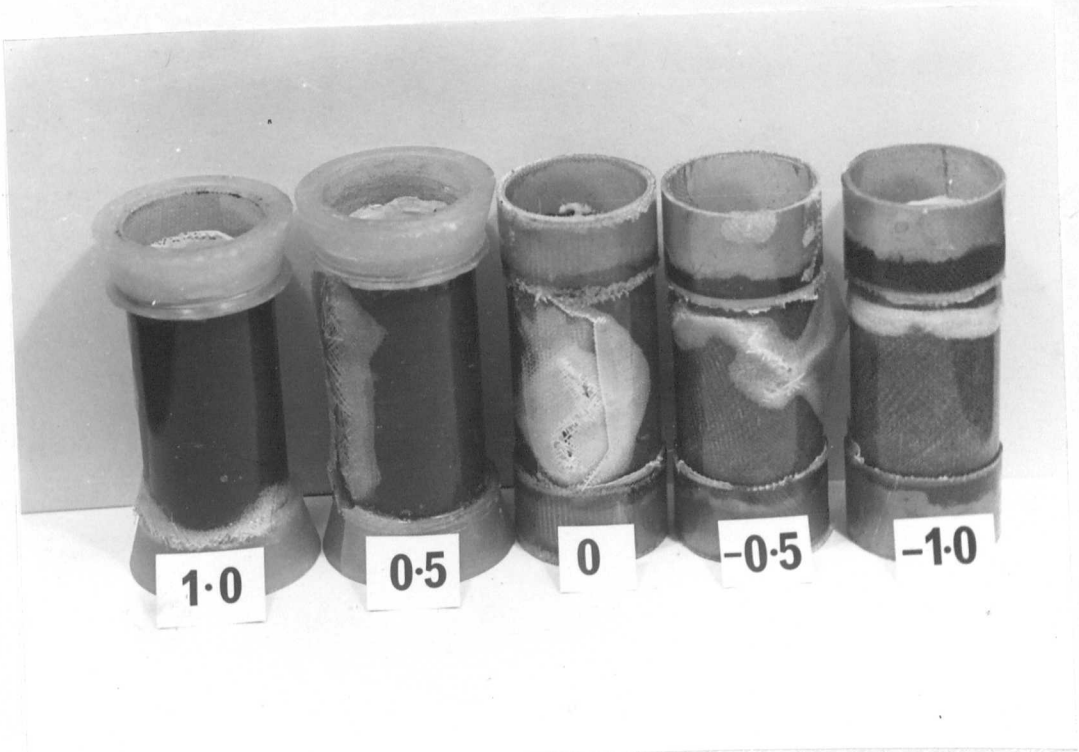
1·0
0·5
0
-0·5
-1·0

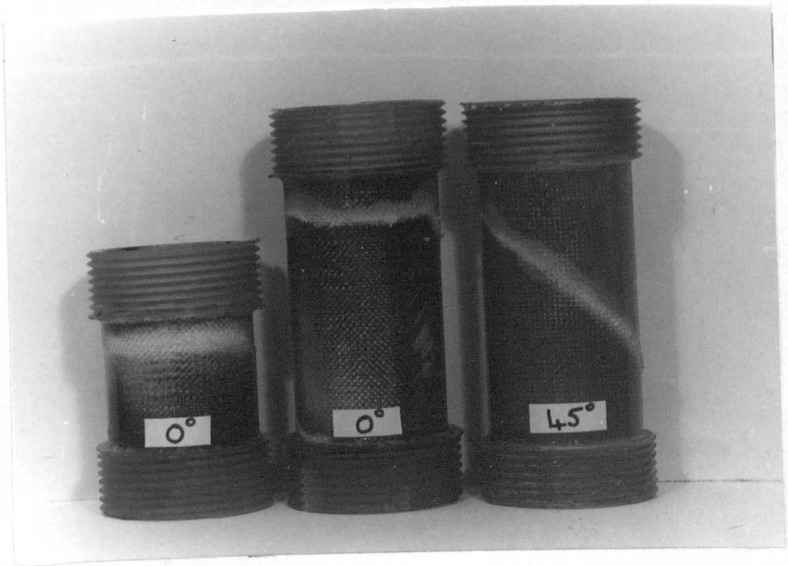
0°
0°
45°

STATIC, R = +1

1

STATIC R= +0.5 FATIGUE

2

3

STATIC R = 0 FATIGUE

4

5

STATIC R = -1 FATIGUE

6

7

FIG. 122 STATIC AND FATIGUE DAMAGE OBSERVED IN 45° ORIENTED Y449 FABRIC-REINFORCED POLYESTER RESIN CYLINDERS.

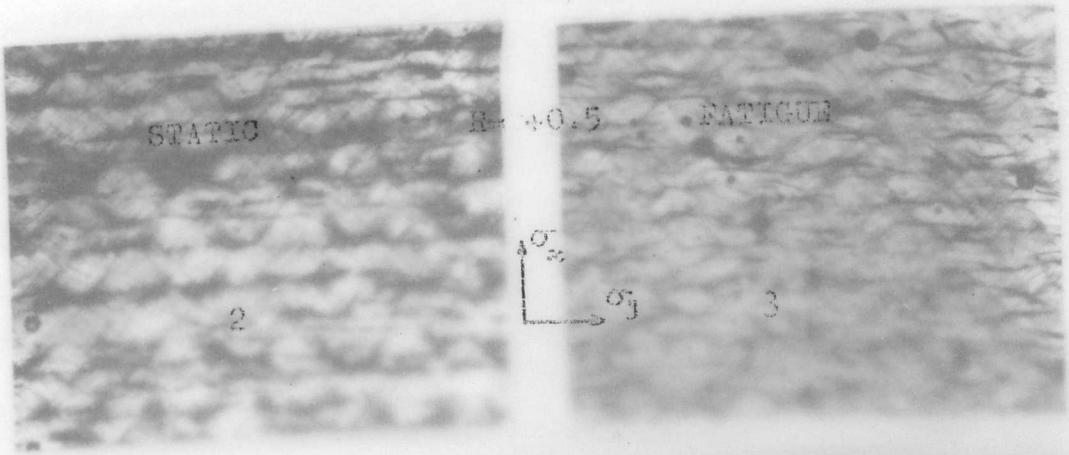

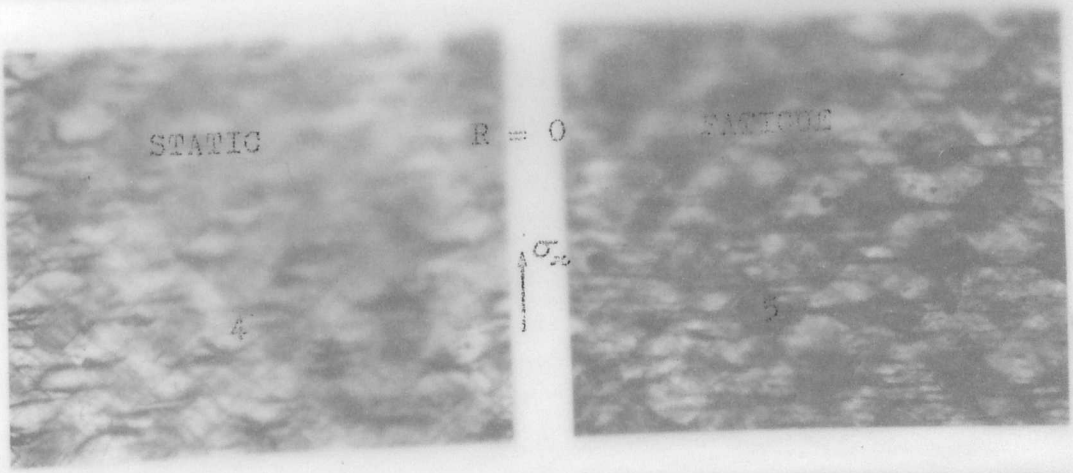

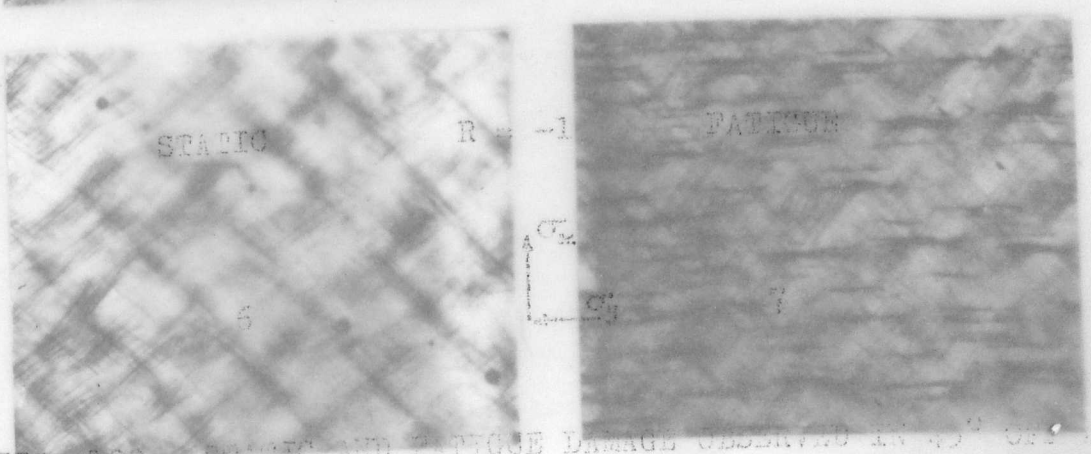

FIG. 122 STATIC AND FATIGUE DAMAGE OBSERVED IN 45° OFF-AXIS Y449 FABRIC-REINFORCED POLYESTER RESIN CYLINDERS.

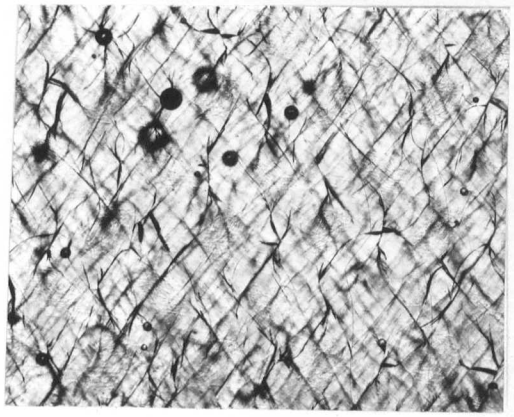

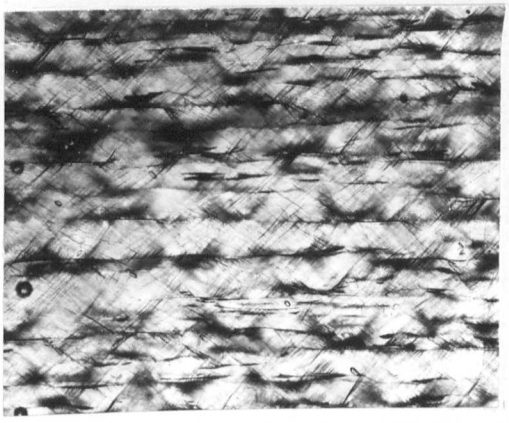

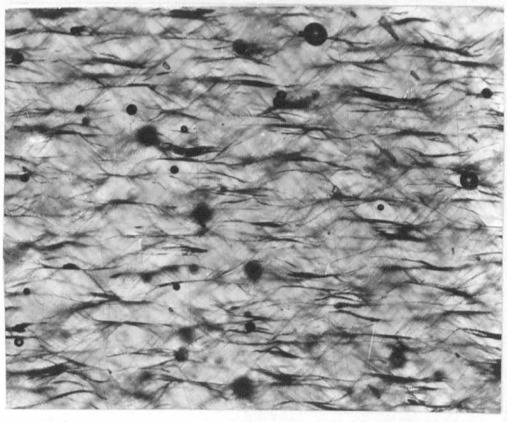

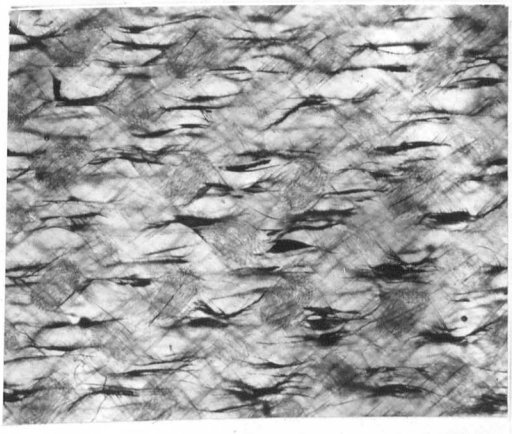

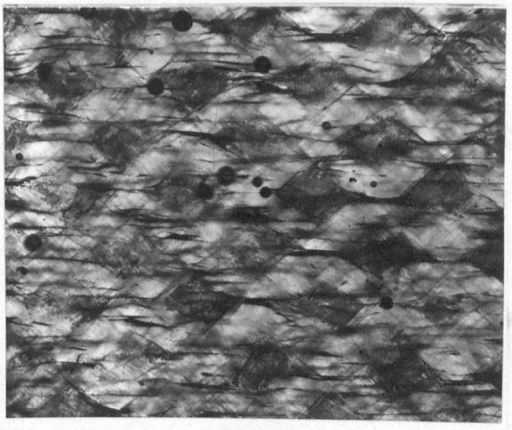

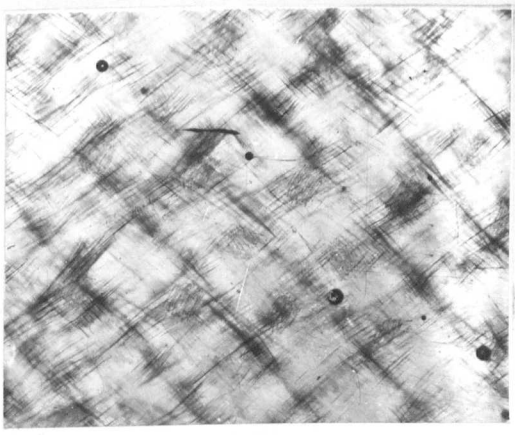

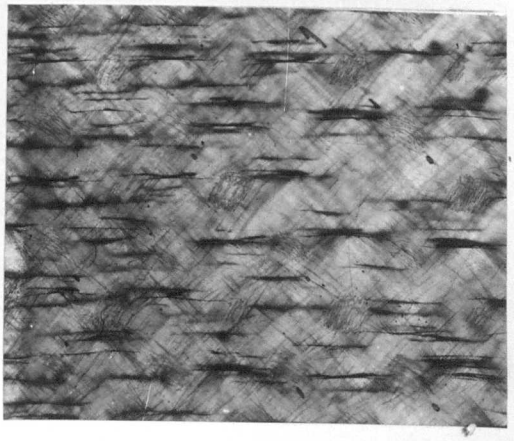

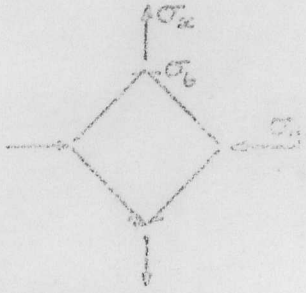

STATIC $R = -1$ FATIGUE
$\Phi = 45^\circ$

STATIC TORSION FATIGUE
$\Phi = 0^\circ$

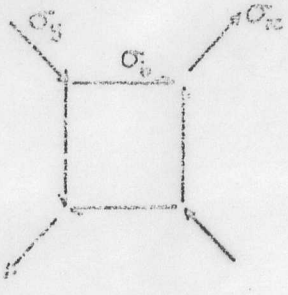

FIG. 123. COMPARISON OF STATIC AND FATIGUE DAMAGE OBSERVED IN Y449 FABRIC-REINFORCED POLYESTER RESIN CYLINDERS TESTED UNDER EQUIVALENT LOADING CONDITIONS.

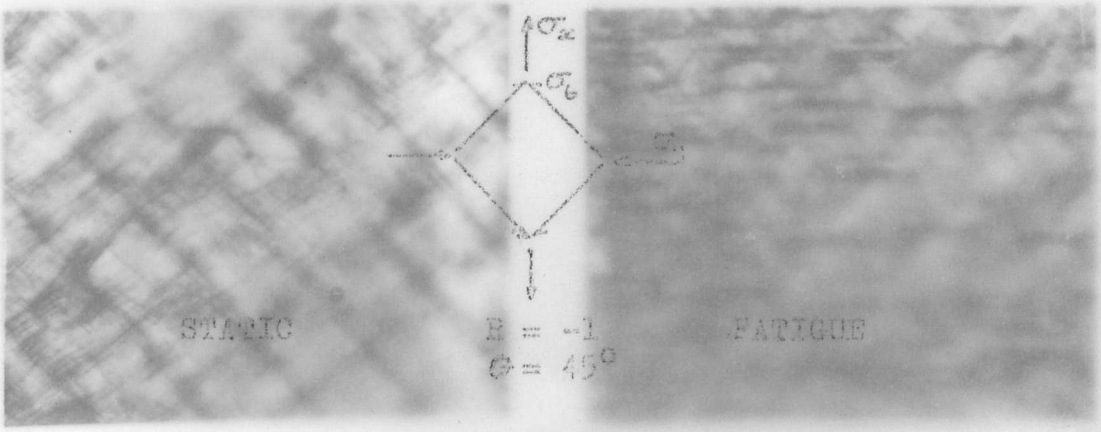

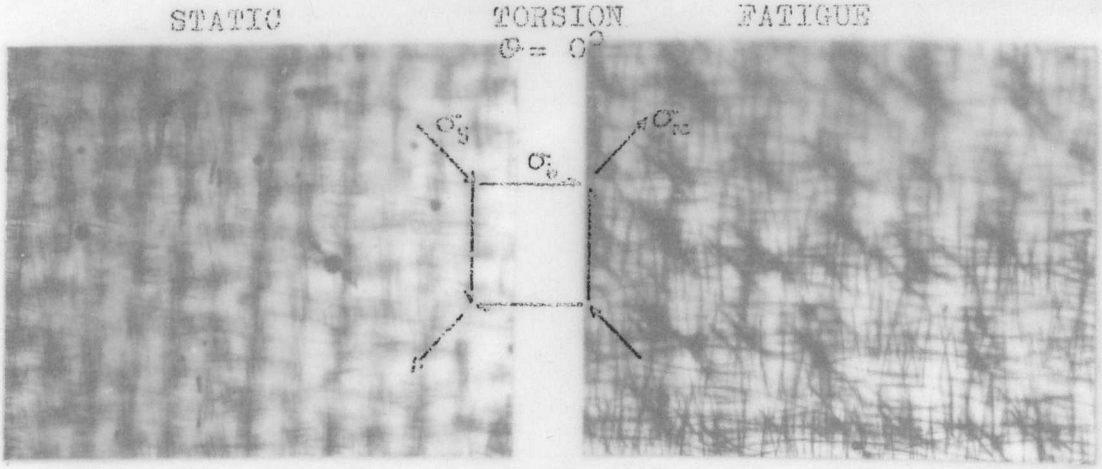

FIG. 123. COMPARISON OF STATIC AND FATIGUE DAMAGE OBSERVED IN Y449 FABRIC-REINFORCED POLYESTER RESIN CYLINDERS TESTED UNDER EQUIVALENT LOADING CONDITIONS.

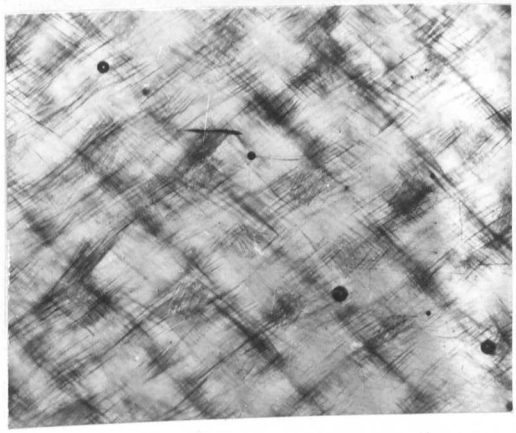

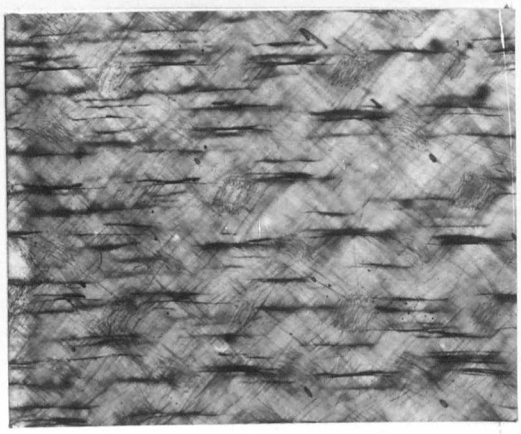

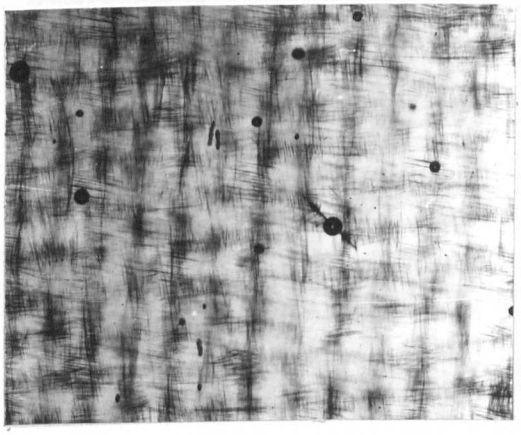

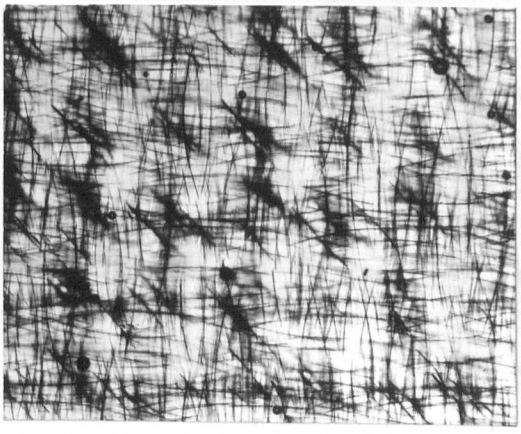

APPENDICES

Hill

$$H(\sigma_1-\sigma_2)^2+F(\sigma_2-\sigma_3)^2+G(\sigma_3-\sigma_1)^2+2N\sigma_6^2+2L\sigma_4^2+2M\sigma_5^2=1$$

H, F, G, N, L, M are evaluated from principal strengths e.g.:-

$$2H=\left(\frac{1}{X^2}+\frac{1}{Y^2}-\frac{1}{Z^2}\right),\quad 2F=\left(\frac{1}{Y^2}+\frac{1}{Z^2}-\frac{1}{X^2}\right),\quad 2G=\left(\frac{1}{X^2}+\frac{1}{Z^2}-\frac{1}{Y^2}\right),$$

$$2N=\frac{1}{S^2}\quad \text{etc.}$$

Norris Failure

$$\left(\frac{\sigma_1}{X}\right)^2+\left(\frac{\sigma_2}{Y}\right)^2-\frac{\sigma_1\sigma_2}{XY}+\left(\frac{\sigma_6}{S}\right)^2=1$$

$$\left(\frac{\sigma_2}{Y}\right)^2+\left(\frac{\sigma_3}{Z}\right)^2-\frac{\sigma_2\sigma_3}{YZ}+\left(\frac{\sigma_4}{S_4}\right)^2=1$$

$$\left(\frac{\sigma_3}{Z}\right)^2+\left(\frac{\sigma_1}{X}\right)^2-\frac{\sigma_3\sigma_1}{XZ}+\left(\frac{\sigma_5}{S_5}\right)^2=1$$

S_4, S_5 are transverse shear strengths.

Hoffman

$$C_1(\sigma_2-\sigma_3)^2+C_2(\sigma_3-\sigma_1)^2+C_3(\sigma_1-\sigma_2)^2+C_4\sigma_1+C_5\sigma_2+C_6\sigma_3+C_7\sigma_4^2$$
$$+C_8\sigma_5^2+C_9\sigma_6^2=1$$

Constants C_i evaluated similar to Hill e.g. :-

$$C_1=\frac{1}{2}\left(\frac{1}{YY'}+\frac{1}{ZZ'}-\frac{1}{XX'}\right),\quad C_2=\frac{1}{2}\left(\frac{1}{ZZ'}+\frac{1}{XX'}-\frac{1}{YY'}\right),\quad C_3=\frac{1}{2}\left(\frac{1}{XX'}+\frac{1}{YY'}-\frac{1}{ZZ'}\right)$$

$$C_4=\frac{1}{X}-\frac{1}{X'},\quad C_5=\frac{1}{Y}-\frac{1}{Y'},\quad C_9=\frac{1}{S^2}\quad \text{etc.}$$

Caddell et al

$$H(\sigma_1-\sigma_2)^2+F(\sigma_2-\sigma_3)^2+G(\sigma_3-\sigma_1)^2+2N\sigma_6^2+2L\sigma_4^2+2M\sigma_5^2$$
$$+k_1\sigma_1+k_2\sigma_2+k_3\sigma_3=1 \qquad \ldots\ldots\ldots\ldots\ldots\ldots\ldots\ldots\ldots\ldots (1)$$

Constants evaluated as from Hoffman e.g. $2H \equiv C_3$.

Substituting stress transformation equations,

$$\sigma_1=\sigma_x\cos^2\Theta,\quad \sigma_2=\sigma_x\sin^2\Theta,\quad \sigma_6=-\sigma_x\sin\Theta\cos\Theta,$$

where σ_x = off-axis uniaxial strength, Θ = off-axis angle, into equation (1) gives (for plane stress) :-

$$\sigma_x^2\left[(G+H)\cos^4\Theta+(H+F)\sin^4\Theta+2(N-H)\sin^2\Theta\cos^2\Theta\right]+\sigma_x\left[k_1\cos^2\Theta+k_2\sin^2\Theta\right]=1 \quad \ldots (2)$$

Table A1 Failure Theories (General cases).

Gol'denblat and Kopnov

$$(F_i \sigma_i)^{\alpha} + (F_{ij} \sigma_i \sigma_j)^{\beta} + (F_{ijk} \sigma_i \sigma_j \sigma_k)^{\gamma} + \ldots\ldots = 1$$

They investigated case where $\alpha = 1, \beta = 1/2, \gamma = -\infty$ above can be re-arranged to give :-

$$2 F_i \sigma_i + F_{ij} \sigma_i \sigma_j - (F_i \sigma_i)^2 = 1$$

where F_i = 2nd rank tensor

F_{ij} = 4th rank tensor

i,j = 1,2....6, contracted notation

Tsai and Wu

$$f(\sigma_k) = F_i \sigma_i + F_{ij} \sigma_i \sigma_j = 1 \quad \ldots\ldots\ldots\ldots\ldots (1)$$

F_i = 2nd rank tensor

F_{ij} = 4th rank tensor

i,j = 1,2....6, contracted notation

stability limit :- $F_{ii} F_{jj} > F_{ij}^2$

Assuming plane stress, $\sigma_3 = \sigma_4 = \sigma_5 = 0$, and expanding(1):-

$$F_1 \sigma_1 + F_2 \sigma_2 + F_6 \sigma_6 + F_{11} \sigma_1^2 + 2F_{12} \sigma_1 \sigma_2 + 2F_{16} \sigma_1 \sigma_6 + F_{22} \sigma_2^2 + 2F_{26} \sigma_2 \sigma_6 + F_{66} \sigma_6^2 = 1$$

if assume that shear stress sign does not change shear strength then :- $F_6 = F_{16} = F_{26} = 0$

Thus, for special orthotropy :-

$$F_1 \sigma_1 + F_2 \sigma_2 + F_{11} \sigma_1^2 + F_{22} \sigma_2^2 + 2F_{12} \sigma_1 \sigma_2 + F_{66} \sigma_6^2 = 1$$

where :- $F_1 = \frac{1}{X} - \frac{1}{X'}$, $F_2 = \frac{1}{Y} - \frac{1}{Y'}$, $F_{11} = \frac{1}{XX'}$, $F_{22} = \frac{1}{YY'}$, $F_6 = \frac{1}{S^2}$

Table A2 Failure Theories (General cases).

(A) Combined Internal Pressure and Axial Force

L = section length

p = internal pressure

r = radius

t = wall thickness

σ_x = hoop stress

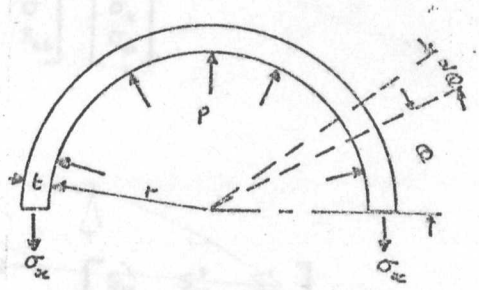

in vertical direction, equilibrium equation :-

$$-2\sigma_x tL + \int_0^{\pi} pr(d\theta)(\sin\theta)L = 0$$

intergrating :-

$$2\sigma_x tL = -prL\left[\cos\theta\right]_0^{\pi}$$

$$\therefore \quad \sigma_x = \frac{pr}{t}$$

similarly, for axial stress σ_y :-

$$2\pi rt\,\sigma_y = \pm F + p\pi r^2$$

$$\therefore \quad \sigma_y = \frac{\pm F}{2\pi rt} + \frac{\sigma_x}{2}$$

where F = axial force

for internal pressure only, F = 0 :-

$$\therefore \quad \sigma_y = \frac{\sigma_x}{2}$$

(B) Torsion

$$\tau = \frac{16 M_T D_1}{\pi(D_1^4 - D_2^4)}$$

where τ = shear stress on outer surface

M_T = torsional moment

D_1 = outside diameter of cylinder

D_2 = inside diameter of cylinder

Table A3 Thin Cylinder Relationships.

Special Orthotropy :-

$$\begin{bmatrix} \epsilon_1 \\ \epsilon_2 \\ \epsilon_6 \end{bmatrix} = \begin{bmatrix} S_{11} & S_{12} & 0 \\ S_{12} & S_{22} & 0 \\ 0 & 0 & S_{66} \end{bmatrix} \begin{bmatrix} \sigma_1 \\ \sigma_2 \\ \sigma_6 \end{bmatrix}$$

General Orthotropy :-

The transformed matrix is :- $\begin{bmatrix} S'_{11} & S'_{12} & S'_{16} \\ S'_{12} & S'_{22} & S'_{26} \\ S'_{16} & S'_{26} & S'_{66} \end{bmatrix}$

where :-

$$S'_{16} = -2\cos^3\theta\sin\theta S_{11} + 2\cos\theta\sin^3\theta S_{22} + 2S_{12}(\cos^3\theta\sin\theta - \cos\theta\sin^3\theta) + S_{16}(\cos^4\theta - 3\cos^2\theta\sin^2\theta) + S_{26}(3\cos^2\theta\sin^2\theta - \sin^4\theta) + S_{66}(\cos^3\theta\sin\theta - \cos\theta\sin^3\theta).$$

$$S'_{26} = -2\cos\theta\sin^3\theta S_{11} + 2\cos^3\theta\sin\theta S_{22} + 2S_{12}(\cos\theta\sin^3\theta - \cos^3\theta\sin\theta) + S_{16}(3\cos^2\theta\sin^2\theta - \sin^4\theta) + S_{26}(\cos^4\theta - 3\cos^2\theta\sin^2\theta) + S_{66}(\cos\theta\sin^3\theta - \cos^3\theta\sin\theta).$$

if $\theta = 45^\circ$ and $S_{11} = S_{22}$, $S_{16} = S_{26}$ (as for Y449) then:-

$$S'_{16} = S'_{26} = 0$$

and the S_{ij} matrix becomes :-

$$S'_{ij} = \begin{bmatrix} S'_{11} & S'_{12} & 0 \\ S'_{12} & S'_{22} & 0 \\ 0 & 0 & S'_{66} \end{bmatrix}$$

Table A4 Compliance Matrices (contracted notation) For Plane Stress.

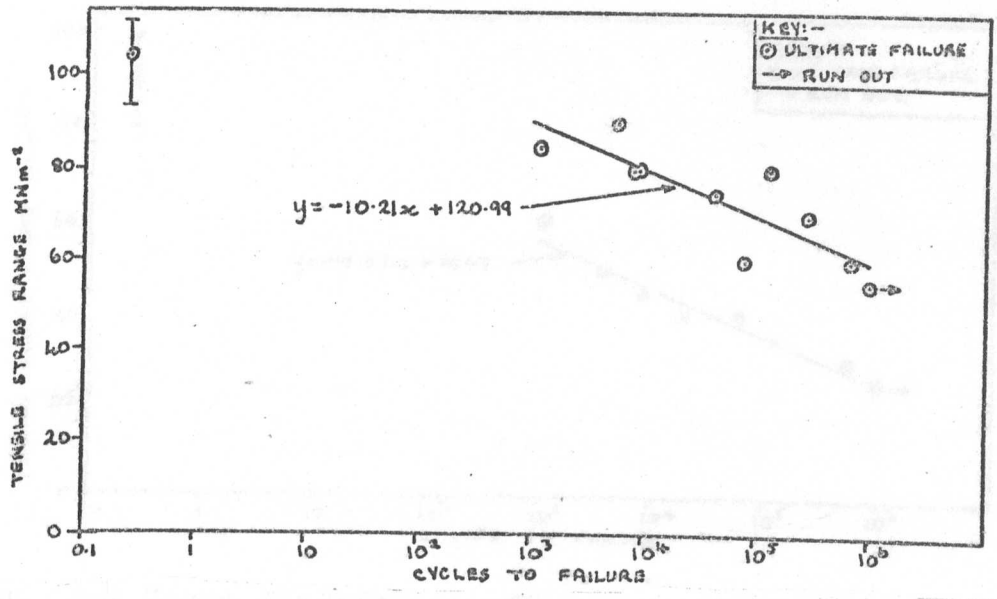

Fig. A1 S-N curve for laminate G3 (see table 9).

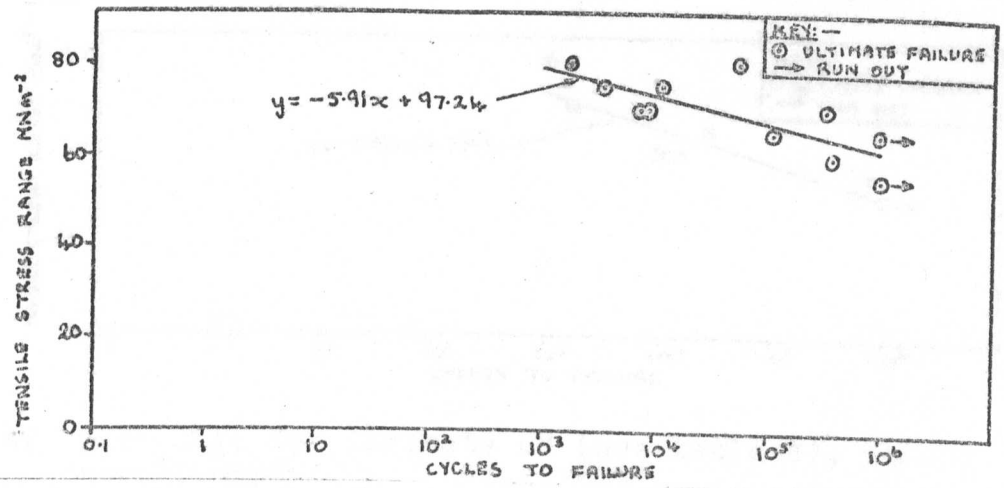

Fig. A2 S-N curve for laminate G3 (see table 9), in oil environment.

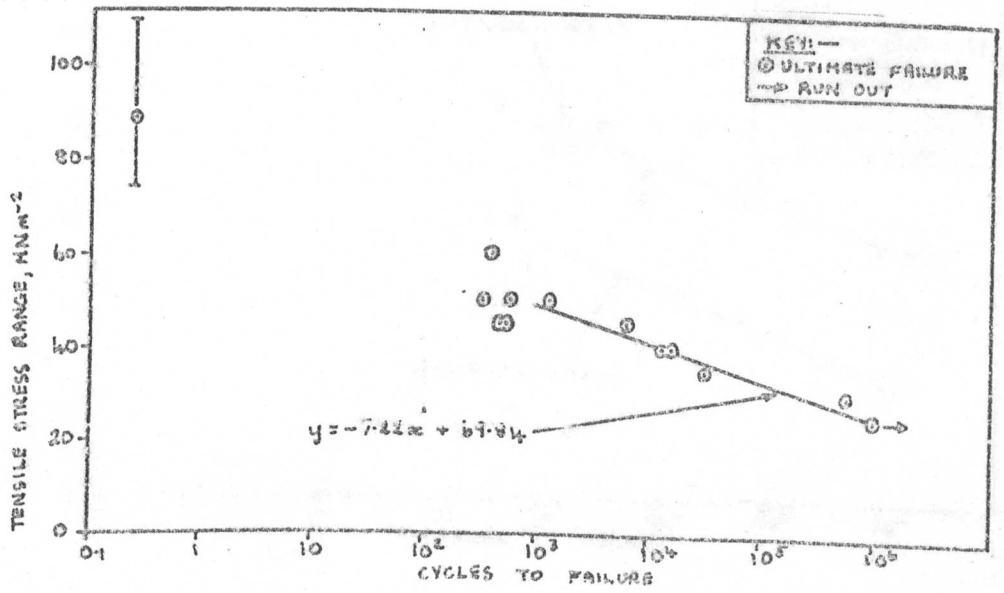

Fig. A3 S-N curve for laminate G6 (see table 9).

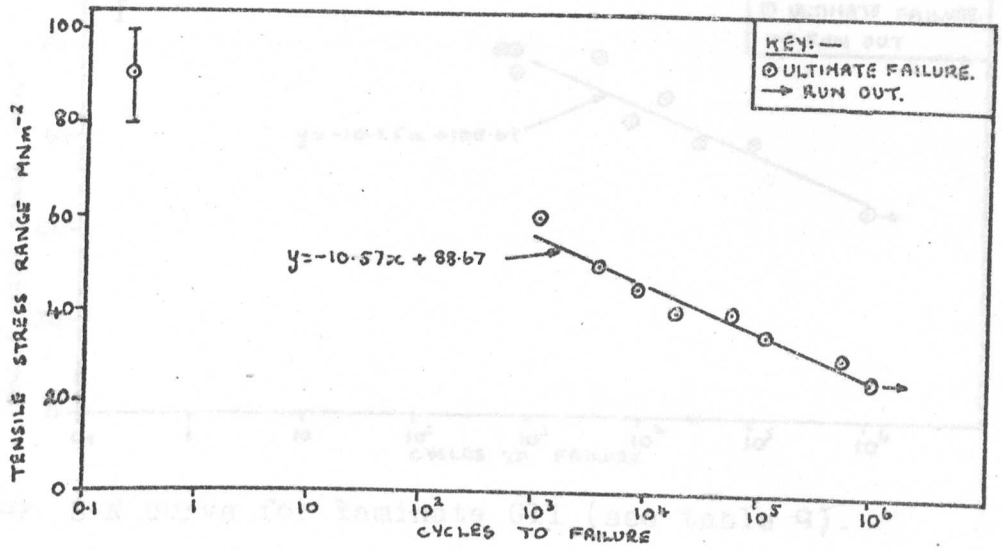

Fig. A4 S-N Curve for laminate G8 (see table 9).

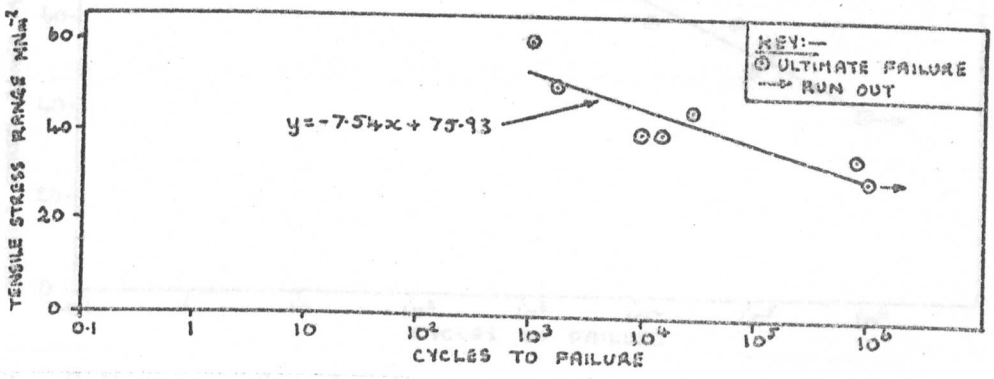

Fig. A5 S-N curve for laminate G8 (see table 9), in oil environment.

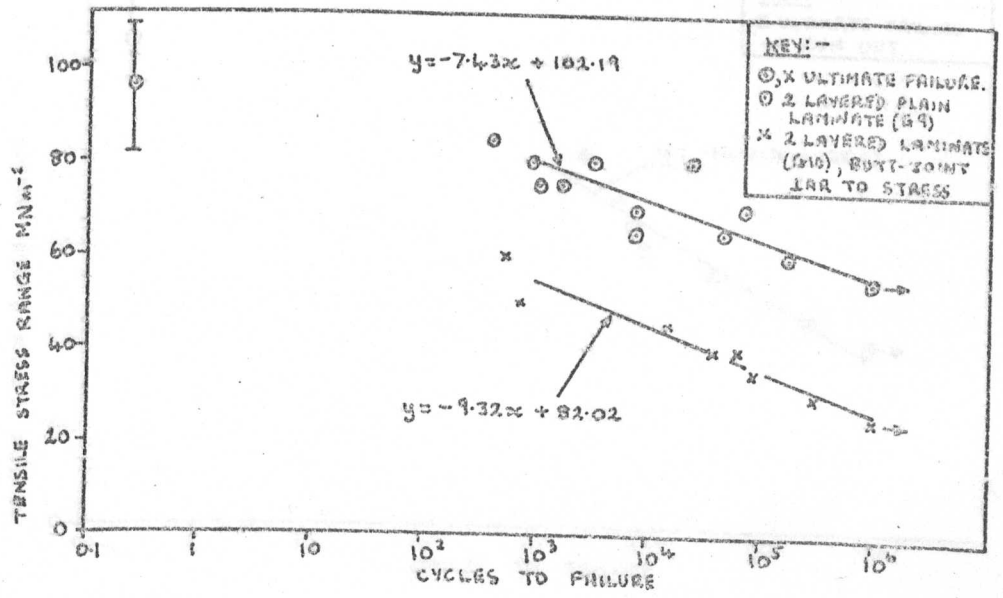

Fig. A6 The effect of a jointed layer on the zero-tension fatigue of 2 layered C.S.M. laminates.

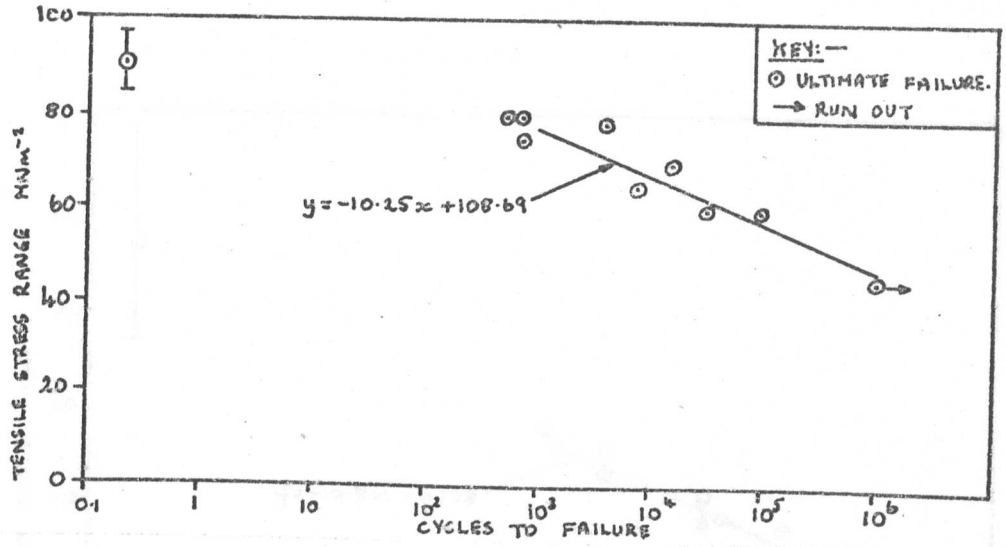

Fig. A7 S-N curve for laminate G11 (see table 9).

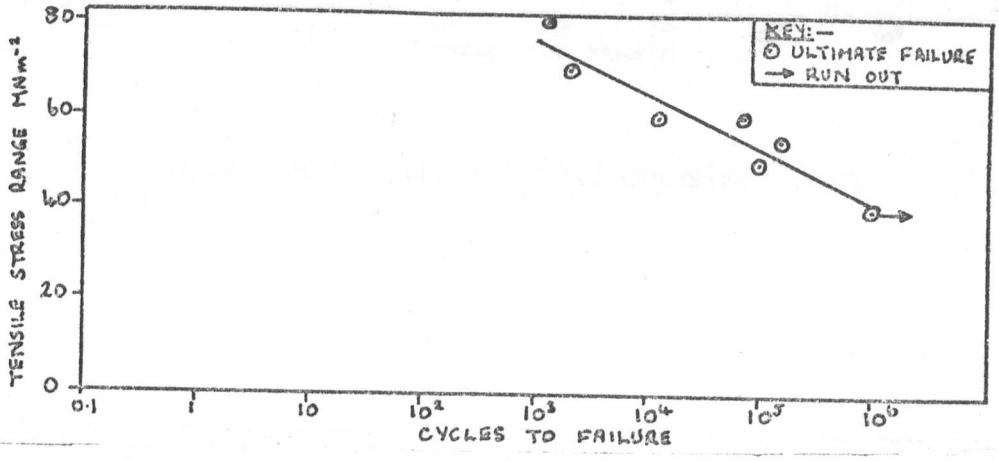

Fig. A8 S-N curve for laminate G10 (see table 9), joint // axis.

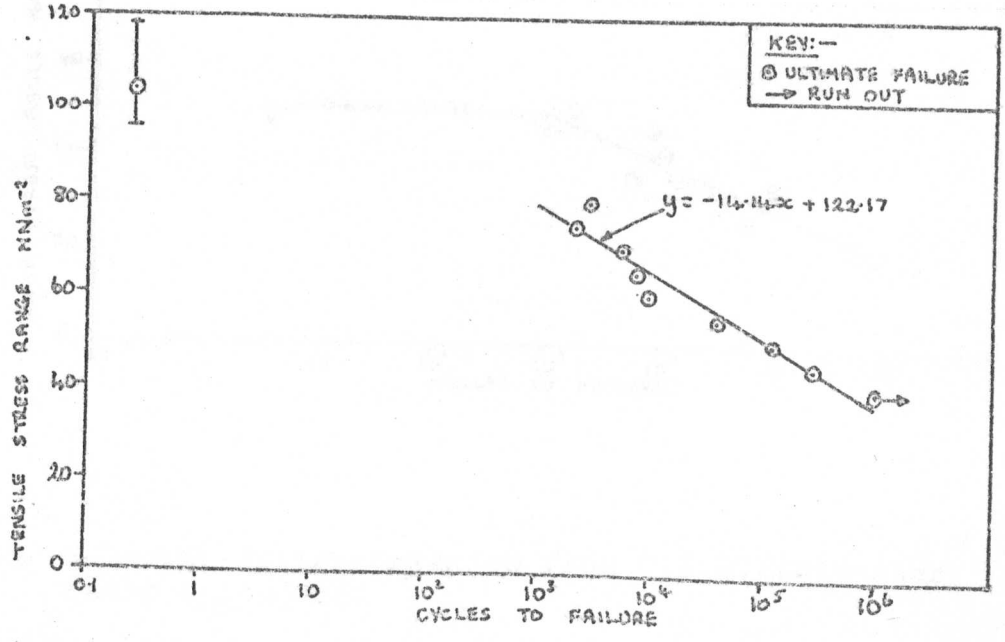

Fig. A9 S-N curve for laminate G17 (see table 9).

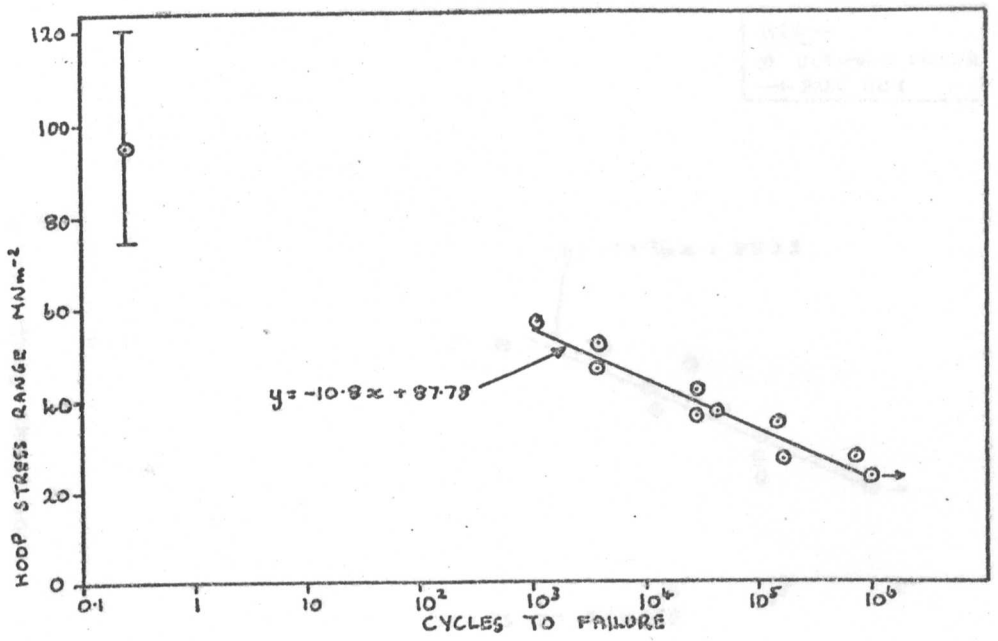

Fig. A10 $R = 0$ fatigue results from C.S.M./polyester resin cylinders

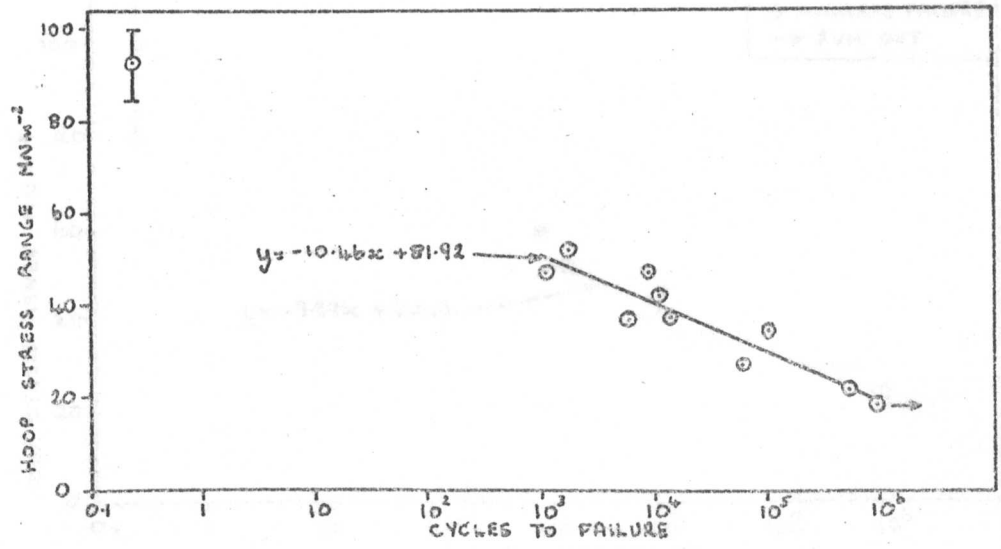

Fig. A11 R= -0.25 fatigue results from C.S.M./Polyester resin cylinders.

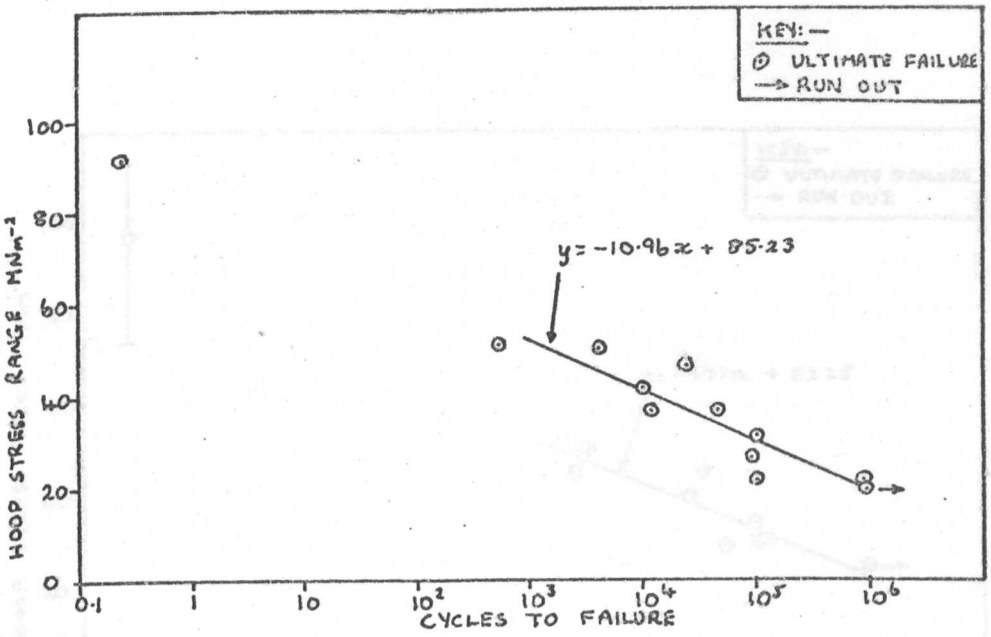

Fig. A12 R= -0.75 fatigue results from C.S.M./Polyester resin cylinders.

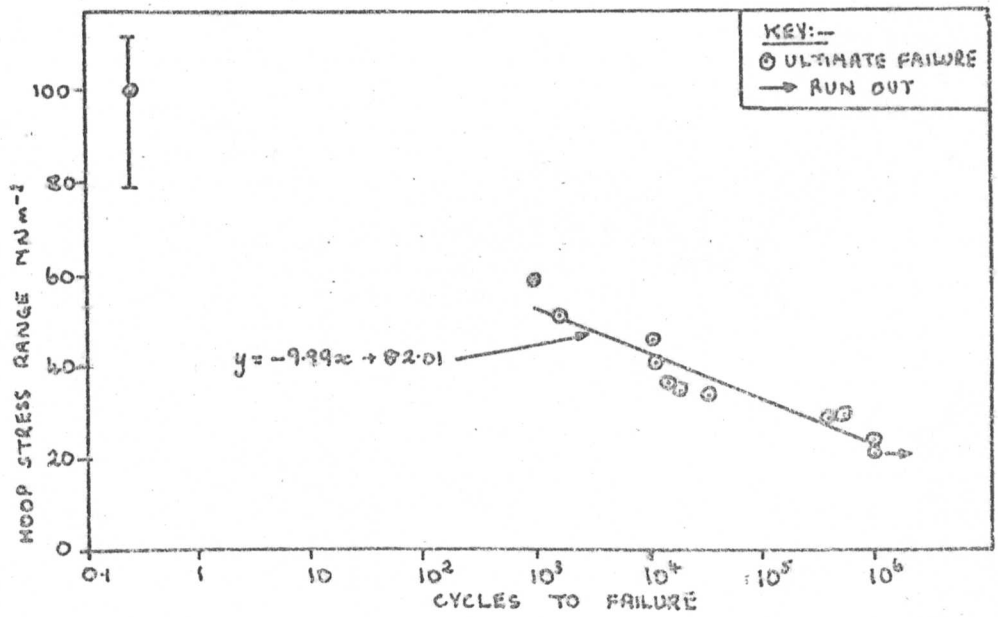

Fig. A13 R= +0.25 fatigue results from C.S.M./Polyester resin cylinders.

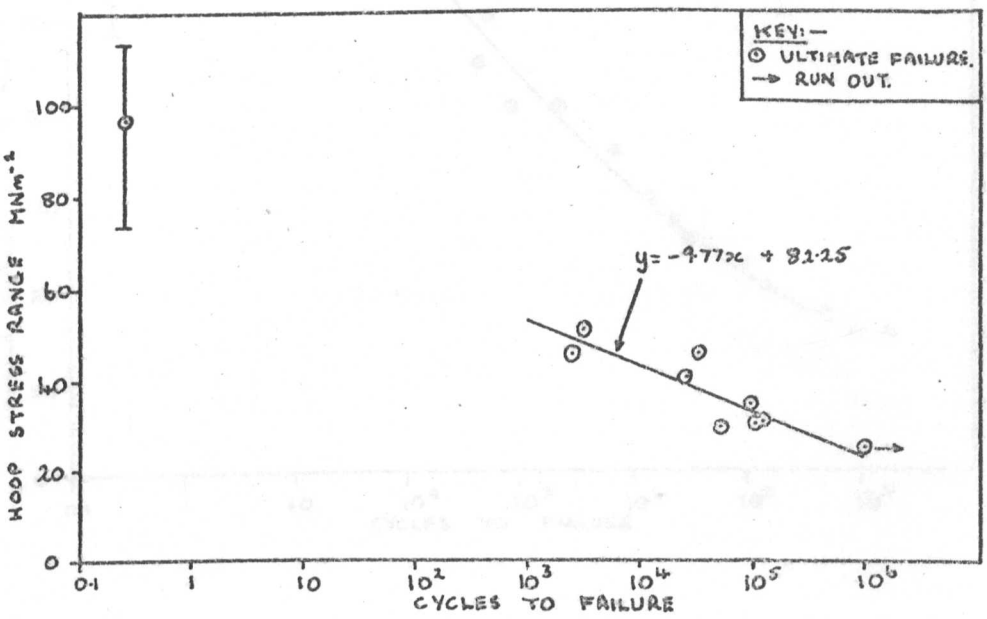

Fig. A14 R= +0.75 fatigue results from C.S.M./Polyester resin cylinders.

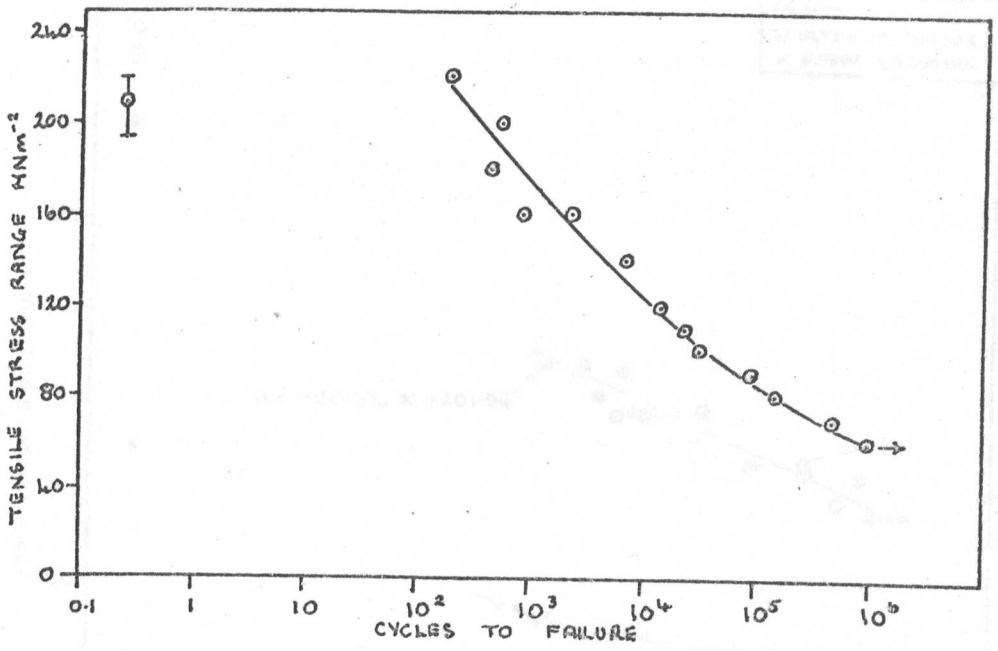

Fig. A15 S-N curve for laminate G12 (see table 12) type C specimens.

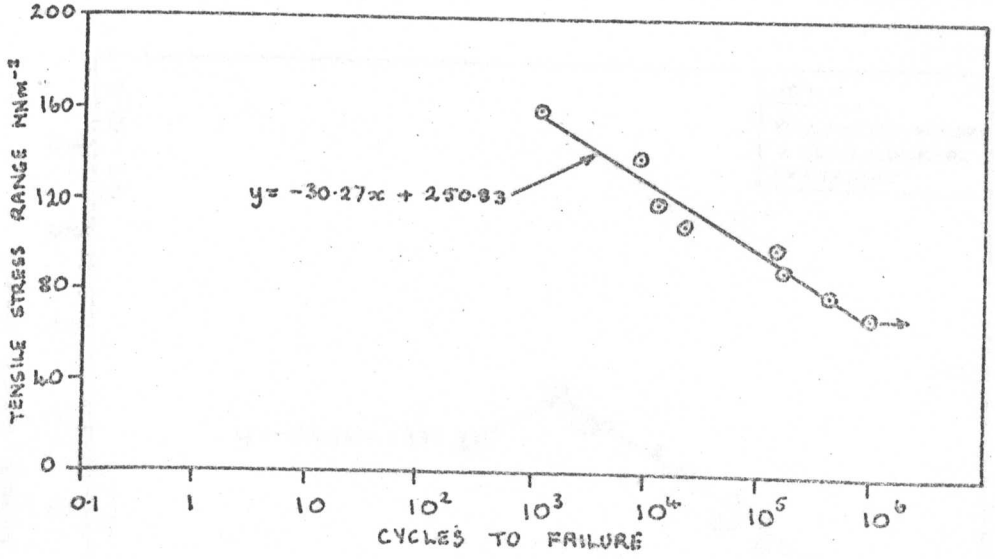

Fig. A16 S-N curve for laminate G12 (see table 12) in oil environment.

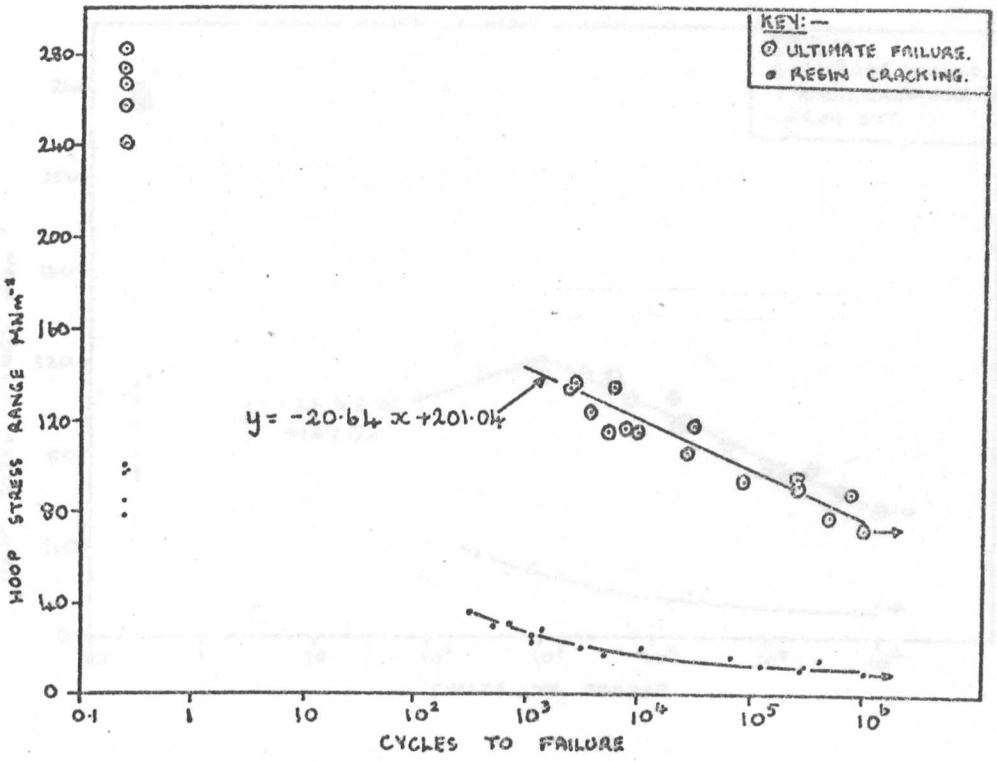

Fig. A17 R= +0.5 fatigue results from 0° Y449/Polyester resin cylinders.

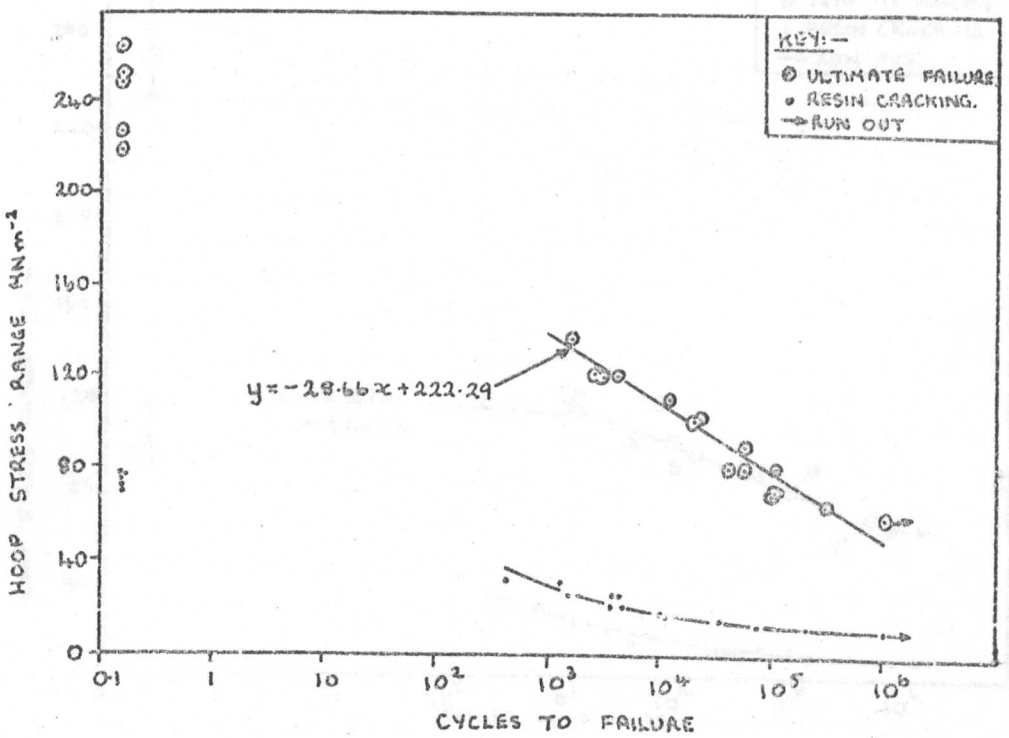

Fig. A18 R= +1.0 fatigue results from 0° Y449/Polyester resin cylinders.

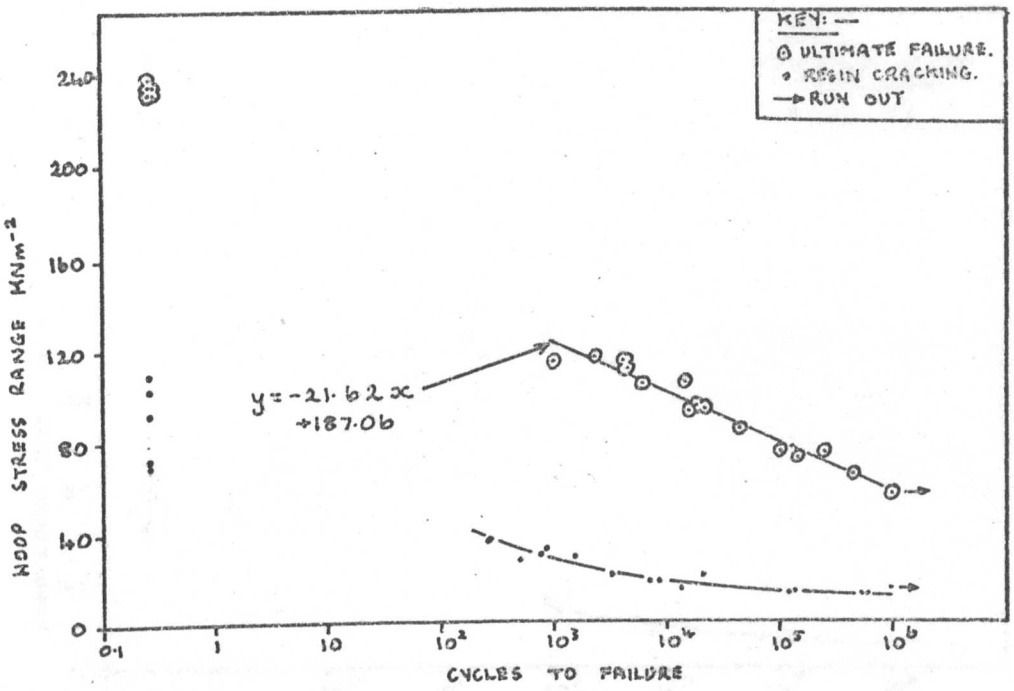

Fig. A19 R= -0.5 fatigue results from 0° Y449/Polyester resin cylinders.

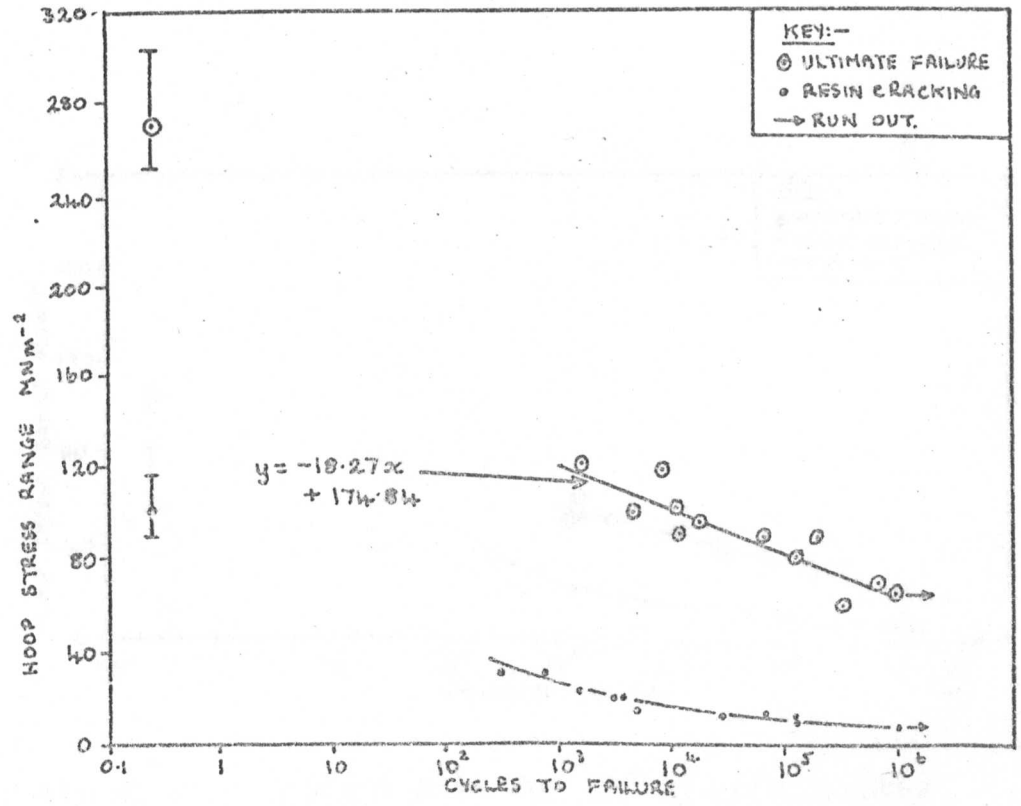

Fig. A20 R= +0.5 fatigue results from 45° Y449/Polyester resin cylinders.

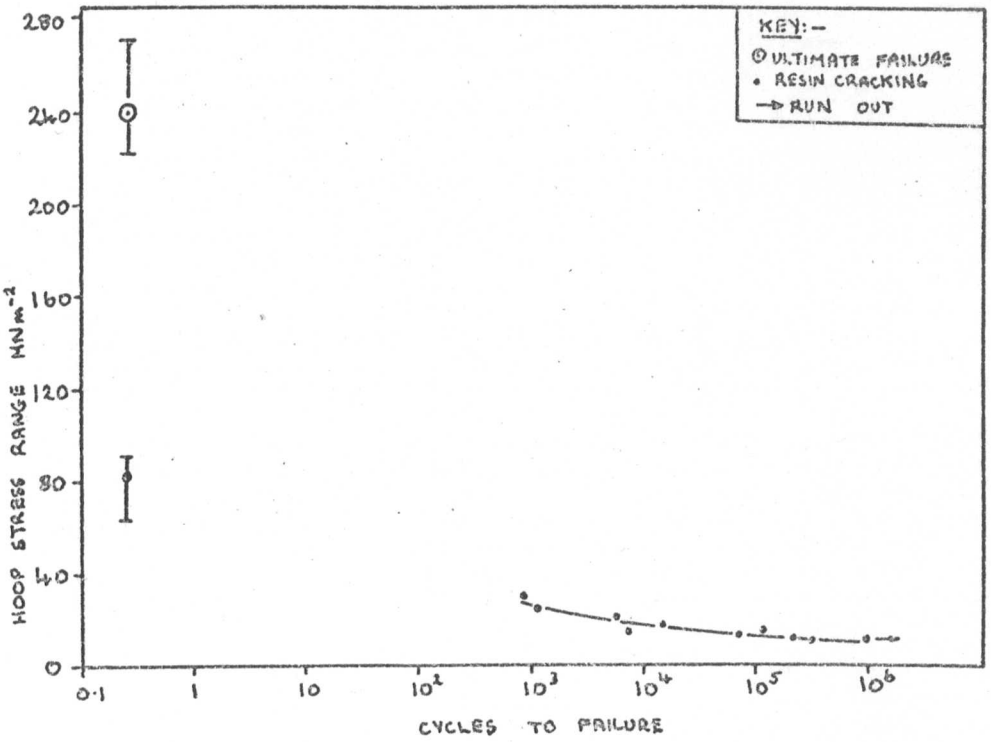

Fig. A21 R= +1.0 fatigue results from 45° Y449/Polyester resin cylinders.

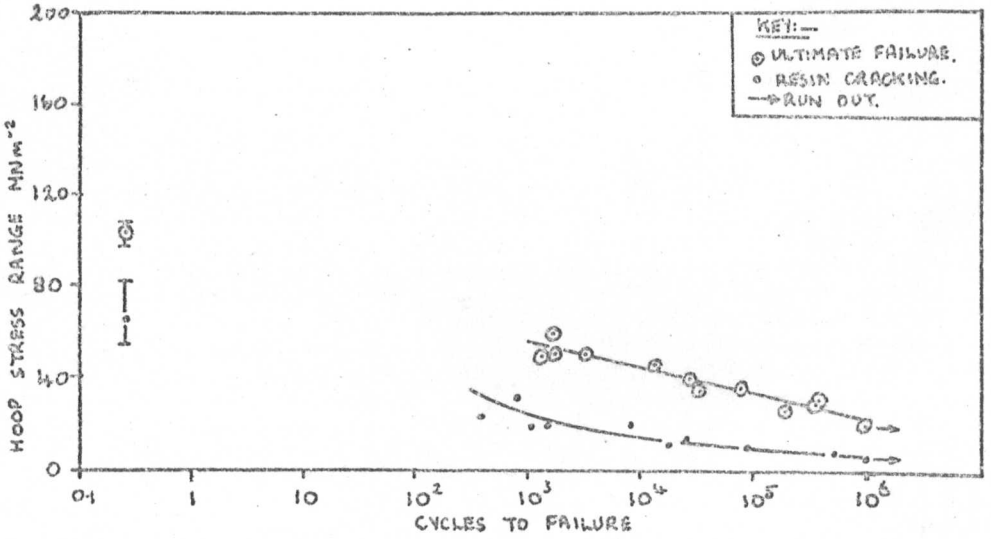

Fig. A22 R= -1.0 fatigue data for 45° Y449/Polyester resin cylinders.